FUNDAMENTAL ANALYSIS FOR THE PROCESSING

OF SEARCH AND RESCUE SATELLITE-AIDED

TRACKING (SARSAT) SIGNALS AT BASEBAND

By

MOAWAD IBRAHIEM MOAWAD DESSOUKY, B.Sc., M.Sc.

A Thesis

Submitted to the School of Graduate Studies

in Partial Fulfilment of the Requirements

for the Degree

Doctor of Philosophy

FUNDAMENTAL ANALYSIS FOR THE PROCESSING

OF SARSAT SIGNALS

DOCTOR OF PHILOSOPHY (1986)
Electrical and Computer Engineering

McMaster University
Hamilton, Ontario, Canada

TITLE: Fundamental Analysis for the Processing of Search and Rescue Satellite - Aided Tracking (SARSAT) Signals at Baseband.

AUTHOR: Moawad Ibrahiem Moawad Dessouky, B.Sc. (Menoufia University)
M.Sc. (Menoufia University)

SUPERVISOR: Professor C.R. Carter

NUMBER OF PAGES: xxiii, 287

ABSTRACT

Search and rescue satellite aided tracking (SARSAT) is a method of employing satellites in low polar orbits to relay the emergency signals of distressed aircraft and marine vessels to an earth station. At the earth station, the signals are processed using spectral estimation techniques which permit the calculation of the location of the distressed vehicle. Of considerable importance are the characteristics of the spectrum of the emergency locator transmitter (ELT) signal since the probability of locating the downed aircraft is closely related to the quality of the ELT signal itself.

This thesis analyses and investigates the ELT signal spectra for ranges of different parameter values. A mathematical representation for the variation of the pulse duration across the sweep period for actual real ELT signals has been developed and verified. New models are proposed with nearly ideal spectral properties.

The matched filter performance for detection of the ELT signals has been calculated. Also, the periodogram and averaged periodogram performances for detection of the ELT signals are calculated and verified by computer simulation.

A new processor, called the complex baseband processor, which employs both the periodogram and the maximum entropy method (MEM) is developed. Baseband processing has many advantages over bandpass processing.

This thesis examines the processing of simulated ELT signals, real testbed ELT signals and actual data received from satellite passes using this new baseband processor. It is shown theoretically and by computer simulation that the minimum detectable carrier-to-noise density ratio (CNDR) is approximately 21 dB-Hz when the 512 complex-point FFT is applied to 50 blocks comprising 1 second of data.

A new technique called rate reduction filtering is developed. By applying this technique to the data sequence, improved frequency resolution is obtained along with an increase in signal-to-noise ratio. Further, a new algorithm called "ELT Tracking Algorithm" based on using rate reduction filtering is developed and analysed.

ACKNOWLEDGEMENTS

I wish to express my sincere gratitude to Professor Charles R. Carter for his guidance, assistance, continued encouragement and support during the course of this study and preparation of this thesis. I wish him success in all his future endeavors.

I am also grateful to the members of my supervisory committee, Professors S. Haykin and P.C. Yip for their valuable suggestions and guidance at various stages of this investigation.

I would like to take this opportunity to thank the Communication Research Center, Ottawa for providing us real SARSAT data and for their continued interest in the research. I wish to thank the Engineering Word Processing Centre for the excellent typing of this thesis.

Last but not the least I would deeply like to thank my parents and my dear wife, without their help and cooperation, this thesis could never have been written. I would also like to thank my son Mohammed, and my daughter Bassma, for being patient during this work.

Finally, I would like to thank my Lord.

TABLE OF CONTENTS

LIST OF FIGURES

CHAPTER 1

INTRODUCTION

1.1   Search and Rescue (SAR)

Search and rescue satellite aided tracking (SARSAT) employs satellites in 850 km polar orbits to relay the emergency locator transmitter (ELT) signals of distressed aircraft and the emergency position indicating radio beacon (EPIRB) signals from marine vessels in difficulty to an earth station [1-8]. At the earth station, the signals are processed using spectral estimation techniques and the location of the distressed platform is deduced. The system involving the United States, Canada and France, became operational in 1982 and has had a significant number of rescues to date which would otherwise have been difficult using only search aircraft. Currently, there are five satellites in orbit; three launched by the Soviet Union which has a parallel system called COSPAS and two by the United States. The developing world interest in the COSPAS-SARSAT system has been demonstrated by countries such as Norway, Sweden, and the United Kingdom, while Finland and Bulgaria will be involved soon. More countries are expected to join as the project progresses.

Search and Rescue (SAR) operations in remote areas can be costly and time consuming since location of a distressed platform may take a month or more. In a country such as Canada with large areas in the north which are sparsely populated, the SAR problem becomes even more significant. Also, the harsh environment in these areas makes SAR operation particularly difficult in winter. A blanket of snow can easily hide a crash site. This leads to a reduction in the probability of survival.

The main difficulty facing a distressed aircraft is survival. The United States Department of Transportation studies [1] have shown that survival probability is less than a

1

10% chance when the rescue extends beyond two days after aircraft crash. In contrast, if the rescue can be accomplished within eight hours, the survival rate is over 50%. Thus rapid detection and location of an aircraft crash is of paramount importance in terms of survival. It is evident that in order to improve the efficiency of the SAR program, the delay in rescue must be kept to a minimum. This delay stems from two sources:

1)   Excessive delay in notification or no notification at all.

2)·   Long search times caused by inaccurate position information.

The use of ELT units became mandatory for all general aviation aircraft in the U.S.A. in July 1974 and for aircraft in Canada in January 1975 [1-5]. In addition, in the maritime area, there is also a growing trend for vessels to carry emergency beacons. These devices, commonly called EPIRBs are extensively carried by many vessels on a voluntary basis.

The first rescue involving a small aircraft occurred in northern British Columbia in September 1982. All three persons on board survived. The first marine rescue using COSPAS-SARSAT data occurred in October 1982. Again, three persons were rescued. From September 1982 to May 1983, a total of 14 incidents occurred involving 40 people, of which 36 survived, making an auspicious beginning for the COSPAS-SARSAT System [6].

1.2   System Considerations

1.2.1   SARSAT Requirements

The SARSAT requirements can be summarized as follows [4]:

(a)   The system must provide coverage of the whole search and rescue region.

(b)   The system must provide the alert and location functions for existing ELT or EPIRB units operating at 121.5 and 243 MHz.

(c)   The system location accuracy must be, with a high probability, within home-in

range to an ELT by a search aircraft.

(d)   The system must detect and locate the transmitting ELT signal within six hours of

an emergency incident.

1.2.2   Orbit Choices

Two orbit types have been considered for use in a SARSAT system; these orbits are

the geostationary and the polar orbit. It is a well-known fact that northern coverage from a

geostationary orbit is limited and this orbit does not provide coverage for the full search and

rescue region. In addition, the distance from the earth's surface to geosynchronous orbit

requires the development of a new, higher-powered ELT.

The polar orbiting satellite, while providing intermittent coverage, does in fact

.cover the whole search and rescue region after about five passes. Multiple satellites are

required to reduce maximum waiting time to an acceptable value. For example, two satellites

will provide full earth coverage every six hours, three satellites every four hour, and so on.

The shorter ELT-to-satellite range for a polar orbit is also compatible with the current low-

powered ELT units.

1.3   SARSAT System Concept

In concept, the system operates as shown in Fig. 1.1 [1-8]. While we describe

operation with the ELT unit, the operation with the EPIRB is similar. When an aircraft is in

distress, the emergency locator transmitter unit is activated either manually or by the

deceleration switch in the unit which is tripped during the aircraft crash. The signal radiated

by the ELT unit is received by the moving satellite, and then transponded by this satellite to

the earth station called a local user terminal (LUT). An HP1000 computer with an FPS array
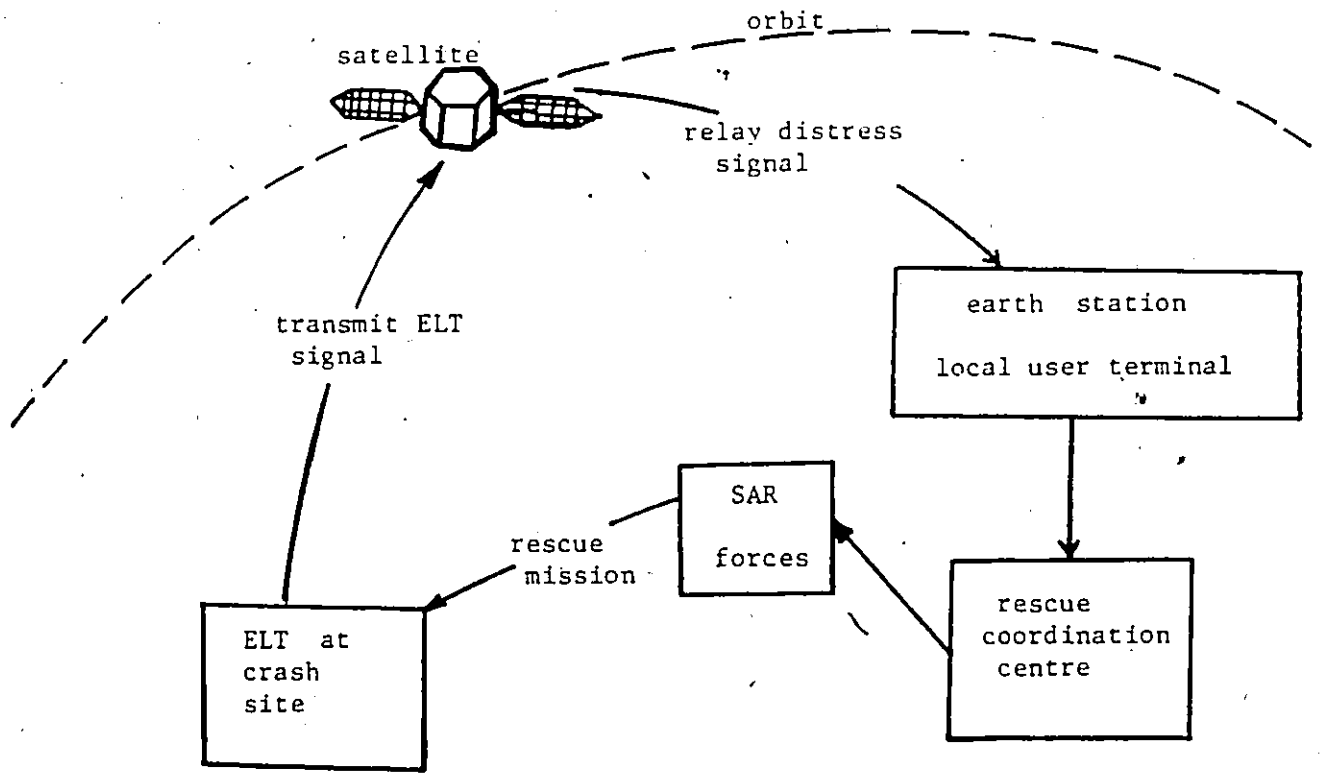
Fig. 1.1   SARSAT system diagram.

processor in the LUT measures the Doppler shifted frequencies of the ELT signals and, knowing the orbit of the satellite, is able to calculate the location of the crash site, i.e. the sources of the ELT unit.

A repeater on board the satellite relays the ELT signal to an earth station where the signal is analysed to extract an ELT position. The main problem is to determine with as much accuracy as possible the zero Doppler point or point of closest approach of the satellite to the ELT unit. The time of closest approach and the slope of the Doppler curve at this point are used to estimate the location of the ELT source. This estimate is passed to a Rescue Coordination Centre (RCC) which speedily dispatches search aircraft to the emergency site. The search aircraft then uses conventional "homing" techniques to pinpoint the exact ELT location.

1.4   The Doppler-Curve

The estimate of ELT Position is based on information extraced from the doppler-time curve. When a satellite in low polar orbit (850 km above earth) receives a distress signal from an ELT source, a Doppler frequency shift occurs due to the relative motion of the satellite with respect to the transmitter, i.e. movement of the satellite over the face of the earth affects a change in the radial velocity along the line joining the satellite and the ELT.

A plot of Doppler versus time produces an S-shaped curve, as shown in Fig. 1.2 [9]. As the satellite approaches the emergency site, the Doppler shift becomes less until the minimum distance is reached where the Doppler shift is zero. Beyond this point, a negative Doppler shift occurs. This Doppler curve leads to a measure of ELT position with respect to the known position of the satellite. The measure of the range to the crash site is based on the calculation of the slope of the curve at the point of inflection, which represents the zero Doppler shift. Assuming an accurate satellite orbit model, the accuracy of the estimated

Fig. 1.2   Doppler curve.

Fig. 1.3   Flat earth model of the SARSAT geometry.
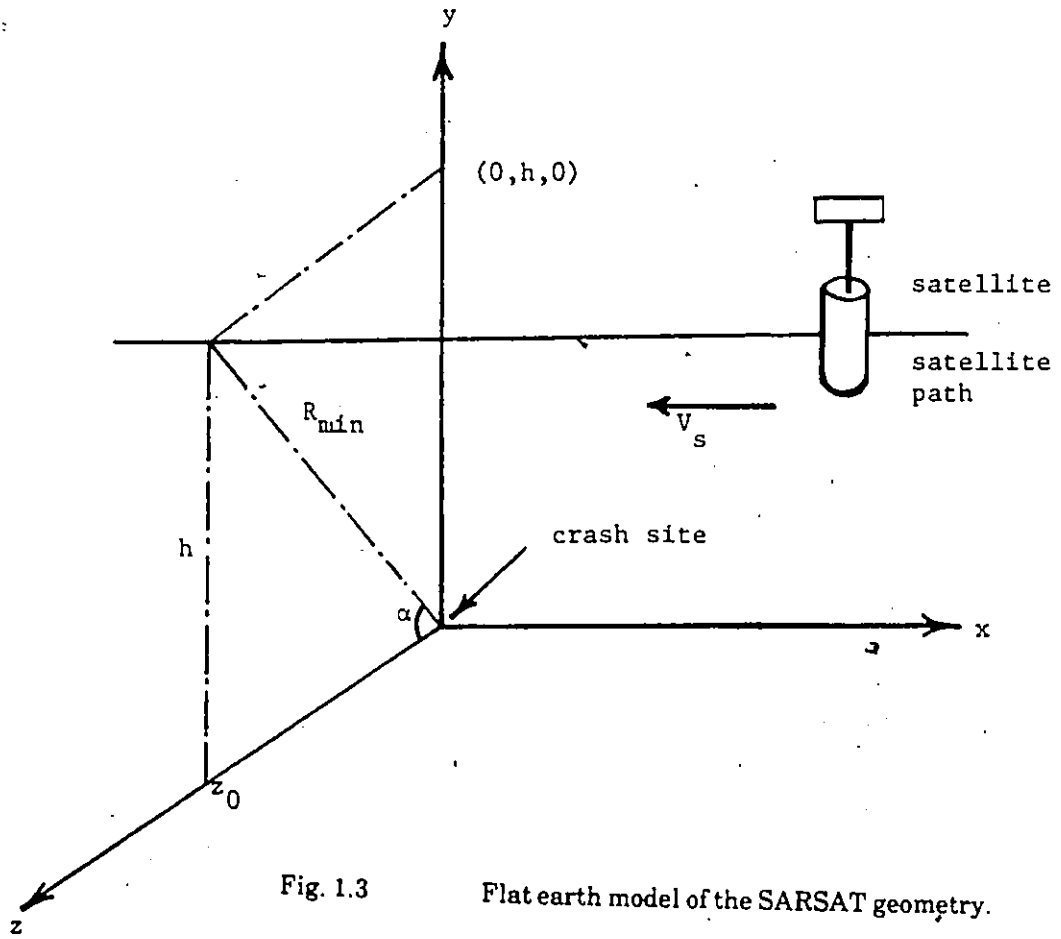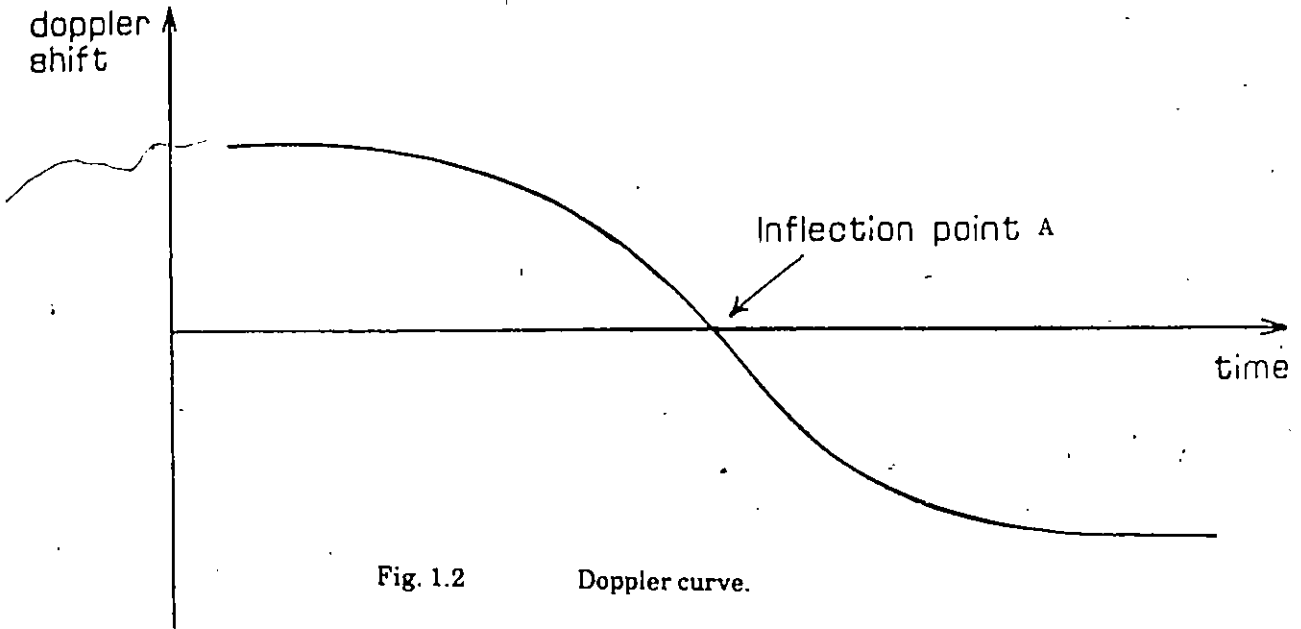
position is mainly dependent on the accuracy of the estimated Doppler and hence on the choice of signal processing method.

1.5 Location Estimation by Satellite

The estimate of aircraft location can be derived by assuming the flat earth model of Fig. 1.3. As the satellite approaches the crash site, the ELT signal is received, and the carrier frequency of the signal at the satellite is given by [10]:

$$f = f_c + f_d \frac{x}{(x^2 + h^2 + z_0^2)^{1/2}} \qquad (1.1)$$

where:

f : received frequency at the satellite.

f_c : transmitted carrier frequency from the ELT.

f_d : Constant Doppler shift of the signal.

x : distance along the flight path.

h : altitude of the satellite.

z_0 : displacement of unknown magnitude of direction.

The signal is relayed from the satellite to a local user terminal (LUT) where the frequency is plotted as a function of time resulting in the graph of Fig. 1.2. Now, calculating the first derivative of Eq. (1.1) (with respect to time) yields:

$$\therefore \frac{df}{dt} = -V_s f_d \left[\frac{h^2 + h^2 \cot^2 a}{(x^2 + h^2 + h^2 \cot^2 a)^{3/2}} \right] \qquad (1.2)$$

where

$$V_s = \text{velocity of the satellite}$$

$$= -dx/dt.$$

and from Fig. 1.3, $z_0 = h \cot a$.

The satellite is closest to the crash site when $x = 0$, this gives

$$\therefore \quad R\text{min} = - \frac{V_s f_d}{\left.\dfrac{df}{dt}\right|_{R\text{min}}} \quad\quad\quad (1.3)$$

From Fig. 1.2 $df/dt|_{R\text{min}}$ occurs at the point of inflection (A) on the curve; hence, this is measured. Where Rmin is the shortest distance between the spacecraft and the ELT source. Also the parameters V_s and f_d are known for any satellite orbit. In order to have an accurate estimation of the crash site, it is important to measure the Doppler shift information on the ELT carrier frequency. There are always two possible locations for the crash site. This requires two passes of the satellite in order to eliminate the erroneous position.

1.6   Scope of Thesis

In Chapter 2, we examine the characteristics of the ELT spectrum and investigate the spectral properties of the ELT signal. This chapter gives an exhaustive study of the effect of each parameter in the ELT signal spectral analysis.

Chapter 3 is devoted to describing and reviewing the theories of different methods of signal processing employed. These methods are: First, linear spectral estimation methods, including, the matched filtering, the periodogram and the average periodogram. Second, the non-linear spectral estimation methods which include, the maximum entropy method (MEM) and the averaged MEM. In this chapter, the description of the complex baseband system is given. The description of the computer simulation results of a single ELT signal in the absence of noise is given here. The comparison between the periodogram and matched filtering method is presented and the theoretical bound of minimum carrier-to-noise density ratio (CNDR) is evaluated in this chapter. A complete discussion of the results of a single ELT signal in the presence of noise with different levels of CNDR is also given.

Chapter 4 develops a new approach called Rate Reduction Filtering technique which is one of the main advantages of the baseband processing system. By using this method

the frequency error is reduced, the signal-to-noise ratio is increased and the frequency resolution is improved which consequently improves the detection of ELT signal at low CNDR level using both linear and non-linear spectral estimation methods. Furthermore, a new method called "ELT Tracking Method" is described and analysed theoretically and verified using simulation results.

Chapter 5 deals with processing the multiple ELT signals using the complex baseband system. It describes the computer simulation results for multiple ELT signals with equal power levels using linear and non-linear spectral estimation methods. A complete discussion of the results for multiple ELT signals with different strengths is covered here. At the end of this chapter, we describe the detection of the weak ELT signal using the periodogram and MEM as applied with Rate Reduction Filtering technique.

Chapter 6 examines the processing of real ELT signals using the complex baseband system. The spectral estimation results for single real ELT signal (Pointer ELT signals, Garrett ELT signals and Narco ELT signals) using the linear and non-linear spectral estimation methods are described here. A complete discussion of the results for multiple real ELT signals (two ELT signals, three ELT signals and five ELT signals) is covered in this chapter. In addition, this chapter shows that rate reduction filtering technique gives excellent detection for the Narco ELT signal and this method can be used as an identification technique for all ELT signals.

Chapter 7 examines satellite pass data using the complex baseband system. A detailed analysis of the results of spectral estimations of the real ELT signals received from two different satellite passes is covered in this chapter.

The final chapter gives the conclusions and suggestions for further research.

CHAPTER 2

SPECTRAL ANALYSIS OF ELT

SIGNAL MODELS

2.1 Introduction

The estimate of the location of a downed aircraft or stranded marine vessel using the search and rescue satellite aided tracking (SARSAT) system relies heavily on the spectral properties of the emergency locator transmitter (ELT) on-board the aircraft or the emergency position indicating radio beacon (EPIRB) on the vessel. Since the processing of ELT signals is identical to that of processing EPIRB signals, reference is made only to the former. Normally, the signal is processed using the periodogram and averaging, which is near-optimal when the ELT signal is coherent and has constant carrier frequency.

In this chapter, we provide a general analysis of the spectrum produced by ELT signals. By separating the amplitude modulation portion of the signal from the phase and frequency portions of the signal, it is possible to analyze the effects of the two characteristics independently. Finally, a new modulation scheme for ELT signals is proposed which provides signals with greatly improved spectral characteristics.

2.2 ELT Signal Sweep

The typical ELT signal may be represented as an amplitude modulated sinusoidal carrier, as shown in Fig. 2.1.

The signal power is about 100 mW with a carrier frequency of 121.5 MHz or optionally 243 MHz. The carrier is modulated by a pulse train having increasing pulse period

10
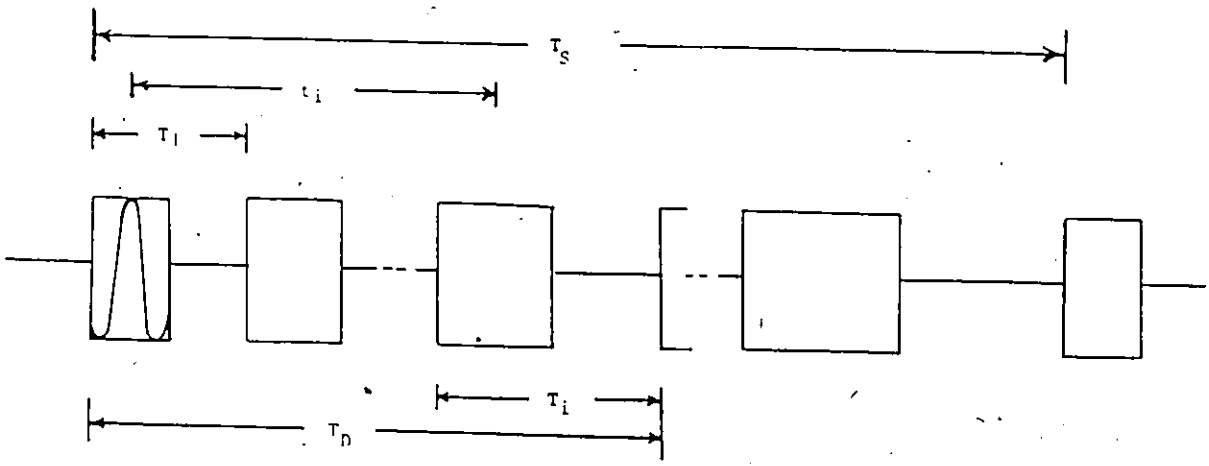
Fig. 2.1   ELT signal comprisisng N_p pulse-null pairs of carrier.
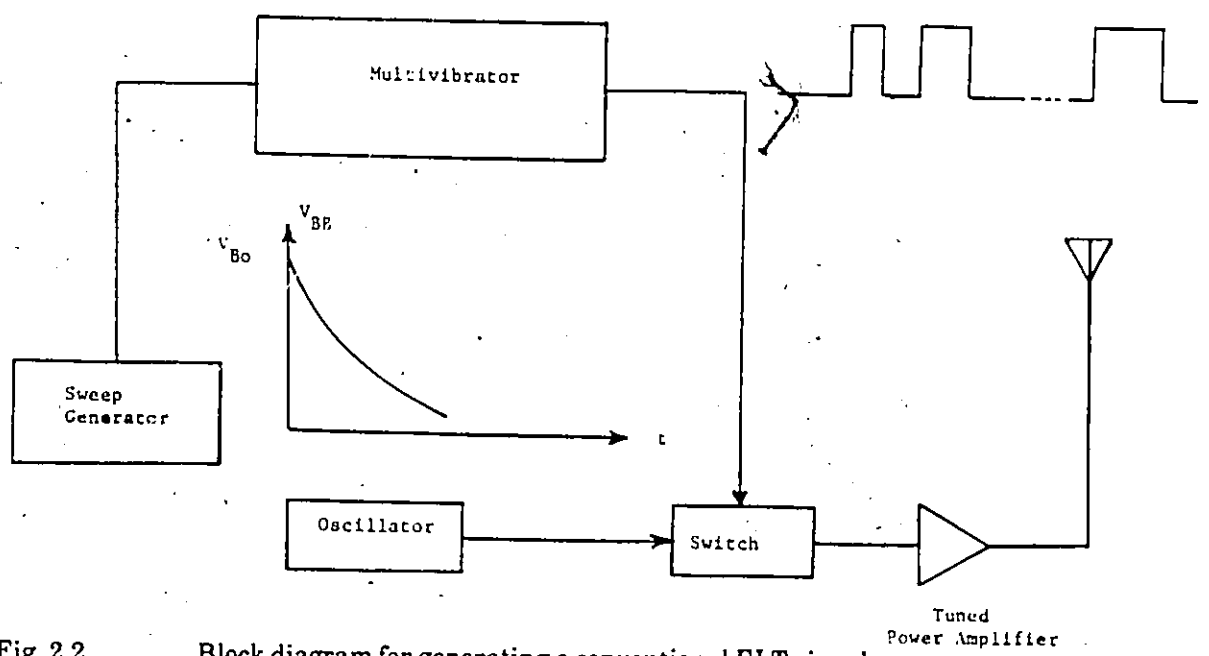
Fig. 2.2   Block diagram for generating a conventional ELT signal.

with time and a total sweep between 0.25 s and 0.5 s repeating continuously. Table 2.1 lists the pertinent specifications.

Of considerable interest is the variation of the pulse-null duration across the sweep period T_S for the actual real ELT signal. For many ELT units, the modulation is produced by employing a sweep generator that creates an exponentially decaying waveform, as illustrated in Fig. 2.2, with a period equal to the sweep period T_S. This signal is then used to control the voltage feeding the base resistors of a multivibrator circuit.

For any standard multivibrator, the period of oscillation is given by

$$T = RC \, \ell n \left[\frac{1 + \dfrac{V_{CC}}{V_{BB}}}{1 - \dfrac{0.7}{V_{BB}}} \right] \qquad (2.1)$$

where V_{CC} is the power supply voltage, V_{BB} is the sweep voltage feeding the base resistors R, and C is the capacitance.

Now, the base voltage generated by the sweep generator is given by

$$V_{BB} = V_{BO} \, e^{-t/T_s} \qquad (2.2)$$

where V_{BO} is a constant voltage.

Substituting Eq. (2.2) into Eq. (2.1) yields

$$T = RC \, \ell n \left[\frac{1 + \dfrac{V_{CC}}{V_{BO}} e^{t/T_S}}{1 - \dfrac{0.7}{V_{BO}} e^{t/T_S}} \right] \qquad (2.3)$$

Consider

$$T_o = RC$$

and

$$\lambda = \frac{V_{CC}}{V_{BO}} \qquad (2.4)$$

Normally, $0.7 \, V_{CC} < V_{BO} < V_{CC}$ and V_{CC} is approximately 10V.

Table 2.1

carrier frequency	121.5 MHz (optional 243 MHz)
frequency tolerance	$\pm$ 50 ppm
power output	approximately 100 mW
modulation type	pulse
pulse duration	33% to 55%
percentage modulation	> 85%
modulation frequency	downward swept
sweep rate	2 to 4 sweeps/second
modulation frequency change	700 Hz minimum
modulation frequency limits	300-1600 Hz

Then, substituting from Eq. (2.4) into Eq. (2.3) yields

$$T = T_0 \ell n \left[\frac{1 + \lambda e^{t/T_s}}{1 - 0.07 \lambda e^{t/T_s}} \right]$$

(2.5)

The change in T along the sweep can be evaluated by simply differentiating Eq. (2.5) to give [11]

$$\frac{dT}{dt} = \frac{T_0}{T_S} \lambda e^{t/T_s} \left[\frac{1}{1 + \lambda e^{t/T_s}} + \frac{\frac{0.7}{V_{CC}}}{1 - \frac{0.7}{V_{CC}} \lambda e^{t/T_s}} \right]$$

(2.6)

Spectral plots for three different ELT signals are presented in Fig. 2.3, 2.4, and 2.5 for a Pointer ELT, a Garrett ELT and a Narco ELT [12]. It is shown later in this chapter that the frequency of the first upper and lower sidebands relative to the carrier frequency is exactly the inverse of the duration of the pulse-null pair or for the lower sideband,

$$f_C - f_A = \frac{1}{T}$$

(2.7)

Using this relation, the pulse-null durations for these three signals has been measured at three different locations along the sweep; namely, $t = 0$, $t = T_S/2$ and $t = T_S$. The results are presented in Table 2.2. Values are also given in the Table for the change in pulse-null duration at the same three locations.

Substituting the measured values at $t = 0$ and $t = T_S$ into eq. (2.5), the value for T can be calculated at $t = T_S/2$ and compared with the measured values. In addition, the values of (dT/dt) are calculated and presented. It is clear from this comparison that the variation in pulse-null pair duration is well represented by eq. (2.5) [11].

2.3 Generalized ELT Signal Spectrum

For a window length T_D of the signal, we have

$$s(t) = a(t) \cdot w(t) \cdot \cos[\omega(t) \cdot t + \theta(t)]$$

(2.8)
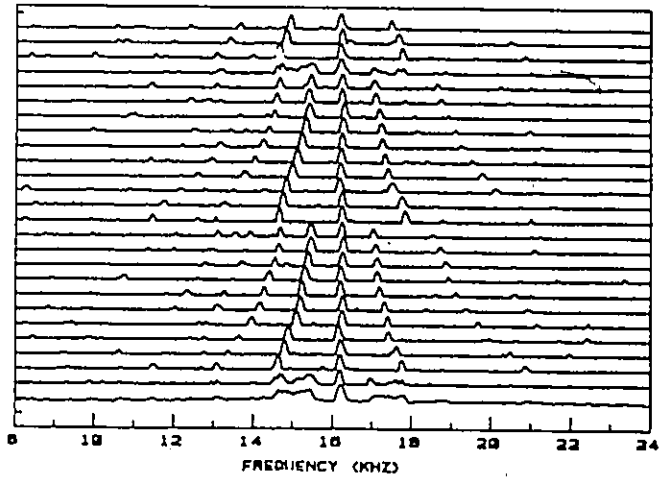
Fig. 2.3   Sequence of 25 consecutive Pointer ELT periodograms.
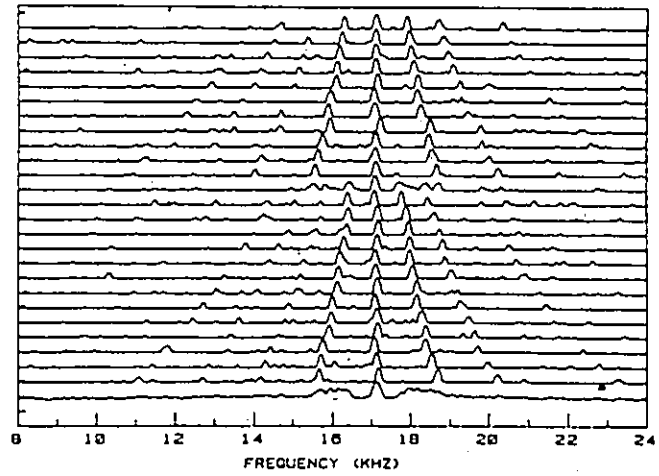
Fig. 2.4   Sequence of 25 consecutive Garrett ELT periodograms.
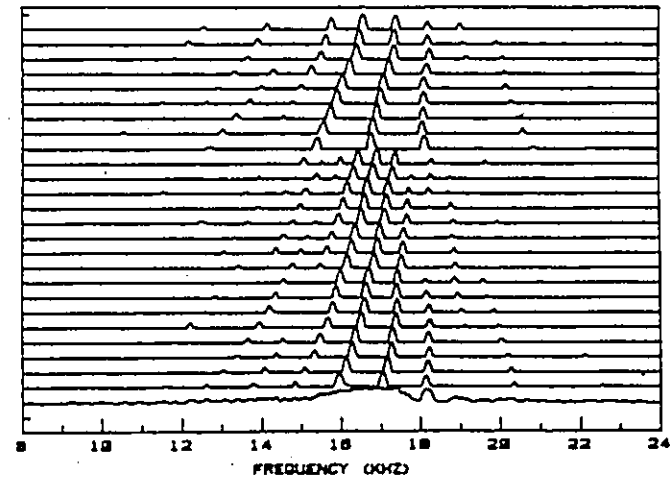
Fig. 2.5   Sequence of 25 consecutive Narco ELT periodograms.

TABLE 2.2

		Measured		Calculated	
ELT Type	pulse number in the sweep	pulse width T in ms	dT/dt	pulse width T in ms	dT/dt
Pointer	First	0.65	2.5×10^{-3}	0.65	2.46×10^{-3}
	Median	0.95	3.3×10^{-3}	0.935	3.23×10^{-3}
	Last	1.3	4.1×10^{-3}	1.3	4.13×10^{-3}
Garrett	First	0.66	2.1×10^{-3}	0.66	2.27×10^{-3}
	Median	0.96	3.2×10^{-3}	0.948	3×10^{-3}
	Last	1.32	3.6×10^{-3}	1.32	3.8×10^{-3}
Narco	First	0.75	2.8×10^{-3}	0.75	2.6×10^{-3}
	Median	1.06	3.5×10^{-3}	1.05	3.32×10^{-3}
	Last	1.42	4.3×10^{-3}	1.42	4.36×10^{-3}

where

- a(t)   = amplitude modulation of the signal

- w(t)   = window length of data

- ω(t)   = angular frequency of the carrier

- θ(t)   = phase angle of the carrier

Equation (2.8) can be rewritten in terms of the complex envelope by

$$s(t) = \text{Re}\{a(t)\,w(t)\,\exp[j(\omega(t){\cdot}t + \theta(t))]\} \qquad (2.9)$$

Since a(t) and w(t) are always real, we have

$$s(t) = a(t){\cdot}w(t){\cdot}\text{Re}\{\exp[j(\omega(t){\cdot}t + \theta(t))]\} \qquad (2.10)$$

Let us assume

$$x(t) = a(t){\cdot}w(t) \qquad (2.11)$$

and

$$y(t) = \text{Re}\{\exp[j(\omega(t){\cdot}t + \theta(t))]\} \qquad (2.12)$$

Then, we have

$$s(t) = x(t){\cdot}y(t) \qquad (2.13)$$

where

- x(t)   = amplitude term of the signal

- y(t)   = phase and frequency term of the signal

Taking the Fourier transform yields

$$F(f) = X(f) \otimes Y(f) \qquad (2.14)$$

where X(f) is the Fourier transform of the amplitude term, Y(f) is the Fourier transform of the frequency term and $\otimes$ denotes convolution.

Consider the structure of X(f). From a practical standpoint, this calculation can best be performed by combining the window function with the modulation since the window simply shapes the amplitude response. Thus,

$$X(f) = F\{a(t) \cdot w(t)\} \qquad (2.15)$$

where $\quad F = $ Fourier transform operator

For $Y(f)$, the problem is slightly more complex.

$$Y(f) = F\{y(t)\}$$

$$= F\{\text{Re}\,[e^{j\omega(t) \cdot t} \cdot e^{j\theta(t)}]\}$$

$$= F\{\text{Re}\,[e^{j\omega(t) \cdot t}] \cdot \text{Re}[\,e^{j\theta(t)}] - \text{Im}[e^{j\omega(t) \cdot t}] \cdot \text{Im}[\,e^{j\theta(t)}]\}$$

or

$$Y(f) = B(f) \otimes C(f) - D(f) \otimes E(f) \qquad (2.16)$$

where

$$B(f) = F\{\text{Re}[e^{j\omega(t) \cdot t}]\}$$

$$C(f) = F\{\text{Re}[e^{j\theta(t)}]\}$$

$$D(f) = F\{\text{Im}[e^{j\omega(t) \cdot t}]\} \qquad (2.17)$$

$$E(f) = F\{\text{Im}[e^{j\theta(t)}]\}$$

We now investigate the spectra produced by certain practical selections of $x(t)$ and $y(t)$.

2.4 Ideal and Non-Ideal Coherent ELT Signals

There are many different modulation characteristics which can be chosen. Several different cases are now considered in detail, assuming the carrier frequency is constant

2.4.1 Ideal Coherent ELT Signal

In this case, consider

$$a(t) = A\,m(t) \qquad (2.18)$$

where

$\quad A \qquad = $ the amplitude of the signal

$\quad m(t) \qquad = $ the modulating signal

$$w(t) \quad = 1, \qquad 0 \leq t \leq T_D$$

$$= 0, \qquad \text{otherwise}$$

$$\omega(t) \quad = 2\pi f_c$$

$$f_c \quad = \text{constant carrier frequency}$$

$$\theta(t) \quad = \theta_0$$

$$\theta_0 \quad = \text{constant phase shift.}$$

The Amplitude Term

First, the amplitude term is simply

$$x(t) = A\, m(t)\, w(t) \tag{2.19}$$

Consider the modulating signal m(t) to be a rectangular pulse train, as shown in Fig. 2.1. For one pulse, we have

$$X(f) = AdT\, \text{sinc}(fdT) \tag{2.20}$$

where

$$d \quad = \text{duty cycle}$$

$$T \quad = \text{pulse period}$$

$$\text{sinc}(fdT) \quad = \sin(\pi\, fdT)/(\pi\, fdT)$$

Assume the modulating signal m(t) consists of a set of N_p pulse-null pairs (Fig. 2.1) in the window length T_D. For a real ELT signal, the pulses are shifted in time. Thus, to find the Fourier transform of this signal, the time shifting property of the Fourier transform is used. This property states that for a time shift t_0 [13],

$$g(t - t_0) \rightleftharpoons e^{-j2\pi f t_0}\, G(f) \tag{2.21}$$

Thus, the Fourier transform of the amplitude term for the ith pulse is given by

$$X_i(f) = Ad\, T_i\, \text{sinc}(fd\, T_i)\, e^{-j2\pi f t_i} \tag{2.22}$$

where

T_i = the duration of the ith pulse-null pair

t_i = time shift from the first pulse to the ith pulse.

Then, the Fourier transform of the amplitude term for N_p pulses is given by

$$X(f) = \sum_{i=1}^{N_p} [AdT_i \, \text{sinc}(fdT_i) e^{-j2\pi ft_i}] \qquad (2.23)$$

The Frequency Term

Now, we examine the Fourier transform of the frequency term $y(t)$. In this case, the parameters $B(f)$, $C(f)$, $D(f)$ and $E(f)$ are given by (from Eq. (2.17))

$$B(f) = \frac{1}{2}[\delta(f-f_c) + \delta(f+f_c)]$$

$$C(f) = \cos\theta_0 \cdot \delta(f)$$

$$D(f) = \frac{1}{2j}[\delta(f-f_c) - \delta(f+f_c)] \qquad (2.24).$$

$$E(f) = \sin\theta_0 \cdot \delta(f)$$

Substituting from Eqs. (2.24) into Eq. (2.16) gives

$$Y_C(f) = \frac{1}{2}\left\{\cos\theta_0[\delta(f-f_c) + \delta(f+f_c)] \right. \qquad (2.25)$$
$$\left. + j\sin\theta_0[\delta(f-f_c) - \delta(f+f_c)]\right\}$$

Neglecting the negative frequency term (i.e. $(f + f_c)$), we have

$$Y_{CP}(f) = \frac{1}{2} \cdot \delta(f-f_c) e^{j\theta_0} \qquad (2.26)$$

Substituting from Eqs. (2.23) and (2.26) into Eq. (2.14) yields the Fourier transform for N_p pulses given by

$$F_C(f) = \sum_{i=1}^{N_p} \frac{AdT_i}{2} \, \text{sinc}[(f-f_c)d\,T_i] e^{-j2\pi(f-f_c)t_i} \cdot e^{j\theta_0} \qquad (2.27)$$

Now, we examine two cases which represent constant T_i and linearly increasing T_i.

Case 1 <u>Constant Duration T</u>

Let us assume the duration of all pulse-null pairs is T. Then,

$$T_i = T \quad \text{for all } i = 1, 2, ..., N_p \qquad \circ \tag{2.28}$$

There are N_p pulse-null pairs in the window length, T_D, therefore

$$T = \frac{T_D}{N_p} \quad . \tag{2.29}$$

Substituting from Eq. (2.28) into Eq. (2.27) yields

$$F_{C1}(f) = \frac{AdT}{2} e^{j\theta_0} \text{sinc}[(f-f_c)d T] \sum_{i=1}^{N_p} e^{-j2\pi(f-f_c)t_i} \tag{2.30}$$

In general, t_i for the first N_p pulses is given by (Fig. 2.6).

$$t_i = (i-1)T , \quad i = 1, 2, ..., N_p \tag{2.31}$$

Substituting from Eq. (2.31) into Eq. (2.30) yields

$$F_{C1}(f) = \frac{AdT}{2} e^{j\theta_0} \text{sinc}[(f-f_c)d T] \sum_{i=1}^{N_p} e^{-j2\pi(f-f_c)(i-1)T} \tag{2.32}$$

Now, we simplify Eq. (2.32) since the summation term can be reduced to

$$\sum_{i=1}^{N_p} e^{-j2\pi(f-f_c)(i-1)T} = \frac{1 - e^{-j2\pi(f-f_c)N_pT}}{1 - e^{-j2\pi(f-f_c)T}} \tag{2.33}$$

Thus, Eq. (2.32) is given by

$$F_{C1}(f) = \frac{AdT}{2} e^{j\theta_0} \text{sinc}[(f-f_c)d T] \frac{1 - e^{-j2\pi(f-f_c)N_pT}}{1 - e^{-j2\pi(f-f_c)T}}$$

Computing the spectrum as the squared magnitude of $F_{C1}(f)$, we get

$$S_{C1}(f) = \left[\frac{AdT}{2}\right]^2 \text{sinc}^2\left[(f-f_c)dT\right] \left\{\frac{\sin[\pi(f-f_c)N_pT]}{\sin[\pi(f-f_c)T]}\right\}^2 \tag{2.34}$$

Equation (2.34) gives the spectrum for N_p pulses with equal duration T. From this expression, it is seen that the spectrum $S_{C1}(f)$ consists of three terms described as i) the amplitude $[AdT/2]^2$ which is chosen to be equal to unity in this analysis; ii) the $(\text{sinc}^2[(f-f_c)dT])$ term which has a peak at $f = f_c$, this peak being the main carrier peak; and
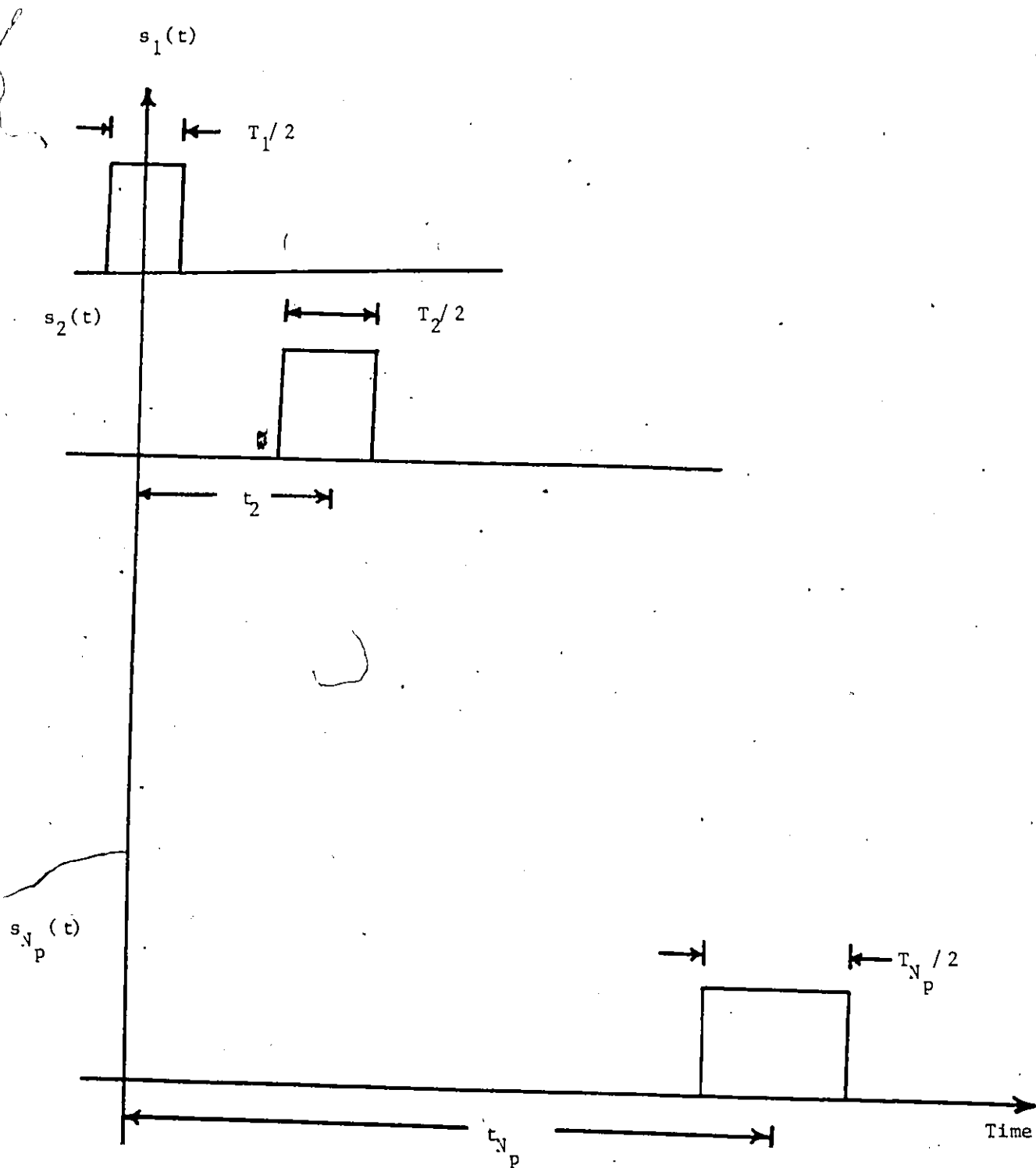
Fig. 2.6   Decomposition of the ELT signal into components.

iii) the ratio of two sine functions, $\{(\sin[\pi(f - f_c)N_pT]/(\sin[\pi(f-f_c)T])\}^2$, which gives a multi-peak pattern with the peaks being located at $f = f_c \pm (K/T)$, $K = 1, 2, 3, ...$

Figures 2.7 to 2.9 illustrate the spectra for different numbers of pulses N_p in the window length $T_D = 10$ ms. The ELT signal is examined here with carrier frequency $f_c = 15$ kHz and in the case of N_p equal 5, 10 and 15. From these results, we conclude that i) the main peak at $f = f_c$ is due to the carrier frequency; ii) the peaks at other frequencies are due to the sidebands; and iii) as the number of pulses N_p increases, the main carrier peak at $f = f_c$ remains stationary while the sideband peaks move away from f_c. Also, the number of sideband peaks decreases as the number of pulses N_p increases. (Note for all the spectrum plots the x-axis is in Hz and y-axis is in dB).

Case 2 Linearly Varying Duration T

As we considered before, the modulating signal m(t) is a rectangular pulse train consisting of N_p pulses in the window length T_D. Consider the case where the pulse duration T_i is increasing linearly with the pulse number N_p. Thus, we have

$$T_i = T + (i-1)\Delta T , \quad i = 1, 2, ..., N_p \tag{2.35}$$

where ΔT is constant

The expression for t_i is given by

$$t_1 = 0$$

$$t_i = \sum_{k=1}^{i-1} T_k , \qquad i = 2, 3, \cdots, N_p \tag{2.36}$$

Substituting from Eq. (2.35) into Eq. (2.36) yields

$$t_i = \sum_{k=1}^{i-1} T + (k-1)\Delta T$$

$$= (i-1)T_{EQ} + \frac{(i-1)(i-2)}{2}\Delta T , \quad i = 1, 2, ..., N_p \tag{2.37}$$
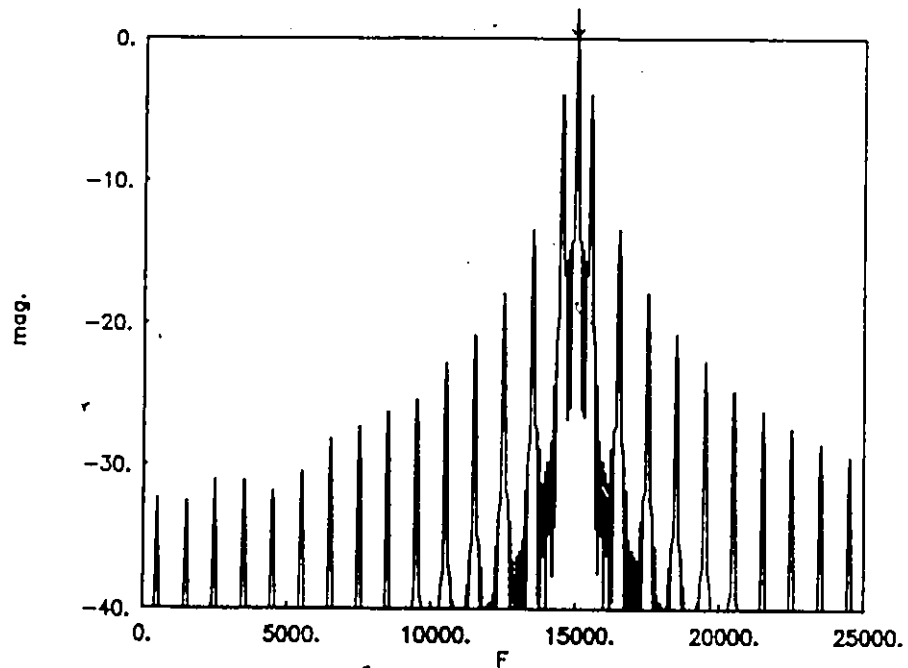
Fig. 2.7   Plot of $S_{C1}(f)$ with $N_p = 5$ pulses.
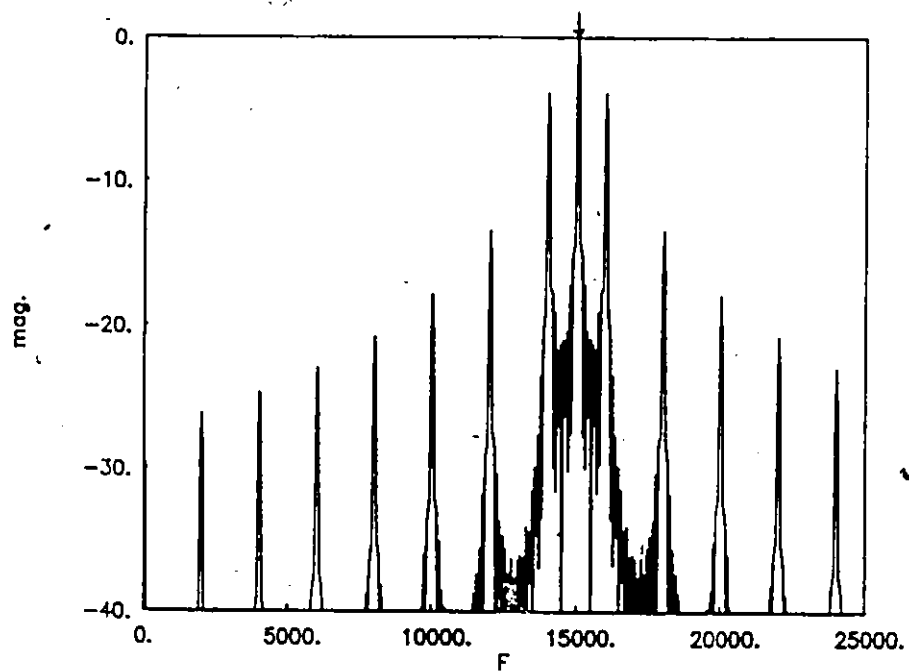
Fig. 2.8   Plot of $S_{C1}(f)$ with $N_p = 10$ pulses.
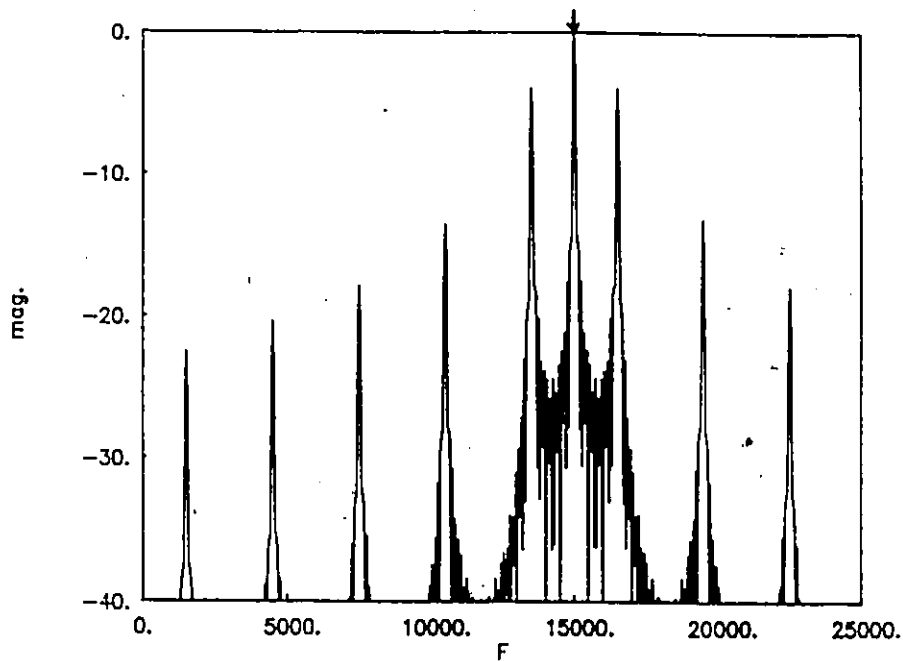
Fig. 2.9   Plot of $S_{C1}(f)$ with $N_p = 15$ pulses.
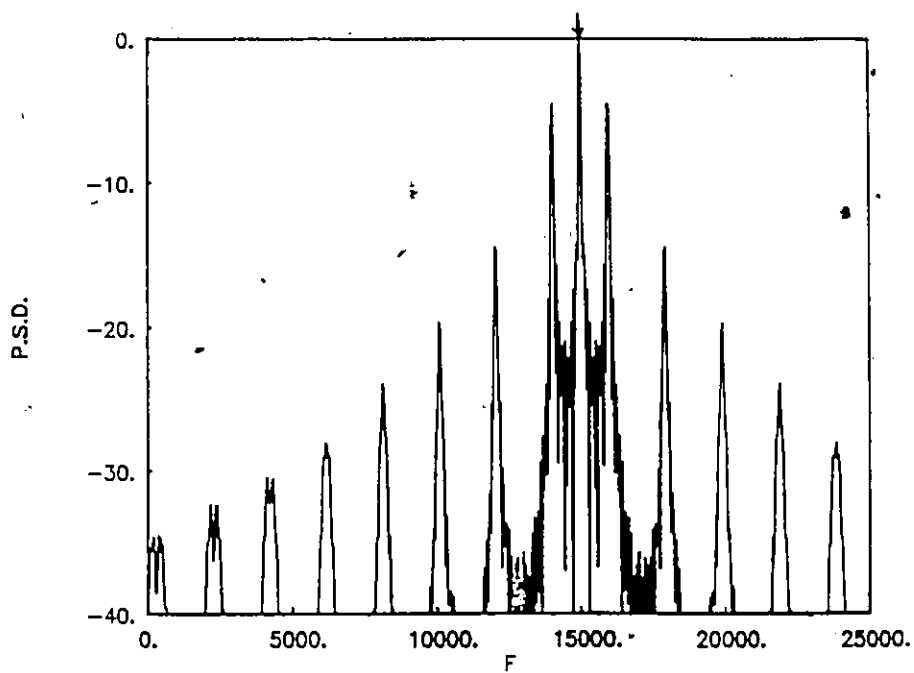
Fig. 2.10   Plot of $S_{C2}(f)$ with $N_p = 10$ pulses and $\Delta T = 5\ \mu s$.

where $T_{EQ} = T + (d/2)\,\Delta T$. Substituting from Eqs. (2.35) and (2.37) into Eq. (2.27), yields

$$F_{C2}(f) = \frac{Ad}{2} \sum_{i=1}^{N_p} [T + (i-1)\,\Delta T] \cdot \operatorname{sinc}[d(f-f_c)(T + (i-1)\,\Delta T)]$$

$$\cdot \exp\left[-j\,2\pi\,(f-f_c)\left((i-1)T_{EQ} + \frac{(i-1)(i-2)}{2}\,\Delta T\right)\right] e^{j\theta_0} \tag{2.38}$$

Equation (2.38) gives the Fourier transform for N_p pulses in the case of the duration for each pulse increasing linearly with respect to the pulse number (N_p). From this expression, we can calculate the spectrum $S_{C2}(f)$ from the squared magnitude of $F_{C2}(f)$.

This expression consists of three terms described as: i) the amplitude; ii) the sinc function term which gives a peak at $f = f_c$, this peak being the carrier peak component; and iii) the exponential term which gives a multi-peak pattern. This exponential term is reduced as ΔT increases, which consequently reduces the level of the sideband peaks.

Figures 2.10 to 2.13 give the spectra for the ELT signal with 10 pulses in the window length with carrier frequency 15 kHz and $\Delta T = 5\,\mu s$, $= 10\,\mu s$, $= 25\,\mu s$ and $= 50\,\mu s$. respectively. From these figures, it is clear that as ΔT increases, the main carrier peak at $f = f_c$ remains stationary while the levels of the first upper and lower sidebands around the carrier peak are reduced. This can be used as a possible identifier for the ELT signal. We further note that the remaining sidebands no longer produce sharp interfering peaks, especially with larger values of ΔT.

2.4.2   Non-Ideal Coherent ELT Signal

For this case, consider each pulse has an additional shift $\Delta\theta_i$, $i = 2, 3, ..., N_p$. The additional phase shift $\Delta\theta_1$ belongs to the first pulse equal to zero. In this case, the amplitude term remains the same as the previous two cases, while the frequency term changes. We

Fig. 2.11   Plot of $S_{C2}(f)$ with $N_p = 10$ pulses and $\Delta T = 10$ µs.

Fig. 2.12   Plot of $S_{C2}(f)$ with $N_p = 10$ pulses and $\Delta T = 25$ µs.
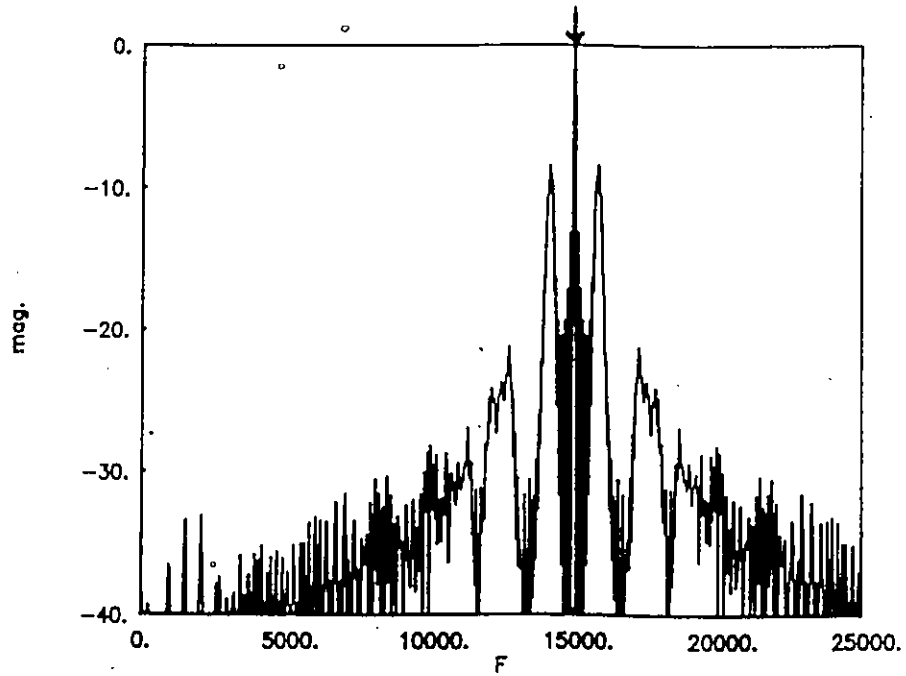
Fig. 2.13 · Plot of $S_{C2}(f)$ with $N_p = 10$ pulses and $\Delta T = 50$ µs.
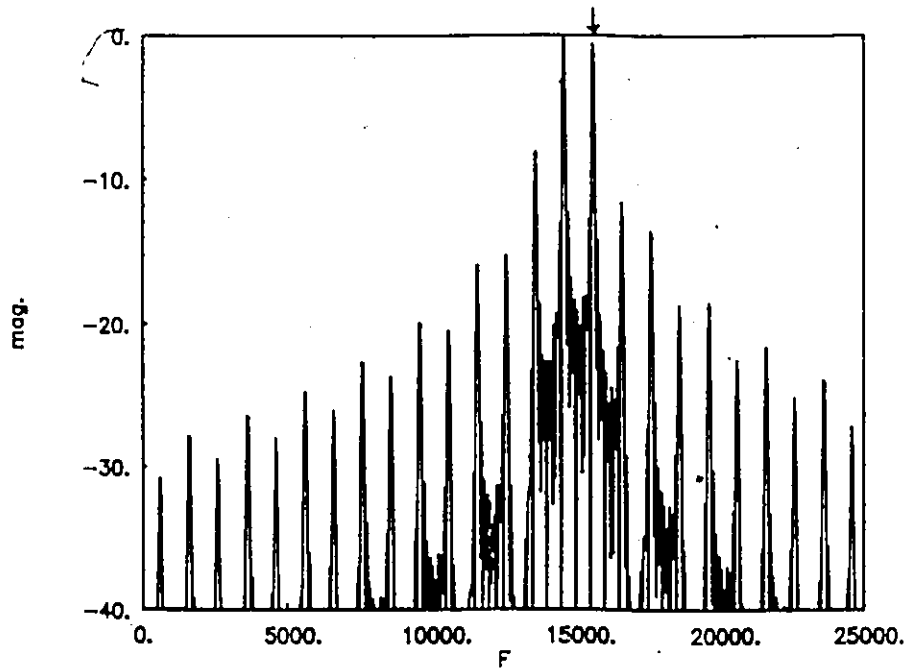
Fig. 2.14 · Plot of $S_{N1}(f)$ with $N_p = 10$ pulses and $f_s = 600$ Hz.

consider here the modulating signal, as before, as a rectangular pulse with N_p pulses in the window length T_D. Thus,

$$\omega(t) = 2\pi f_c$$

$$\theta(t) = \theta_0 + \Delta\theta_i, \quad i = 2, 3, 4, ..., N_p \qquad (2.39)$$

where

$$\Delta\theta_1 = 0$$

Now, Eq. (2.9) can be represented as

$$s(t) = \sum_{i=1}^{N_p} s_i(t)$$

where

$$s_i(t) = A \cdot \mathrm{Re}\left\{\exp\left[j(2\pi f_c t + \theta_0 + \Delta\theta_i)\right]\right\}, \quad t_i - \frac{dT_i}{2} < t < t_i + \frac{dT_i}{2} \qquad (2.40)$$

$$= 0 \qquad \qquad , \text{ otherwise}$$

The Fourier transform of the amplitude term $(X(f))$ is given by Eq. (2.23). However, the frequency term is represented by

$$y(t) = \mathrm{Re}\{\exp[j(2\pi f_c t + \theta_0 + \Delta\theta_i)]\}, \quad i = 1, 2, .., N_p \qquad (2.41)$$

The phase shift at the beginning of the second pulse when no frequency pulling is present is given by

$$\theta_2 = 2\pi f_c \left[\frac{dT_1}{2} + (1-d)T_1\right] \qquad (2.42)$$

When frequency pulling occurs, the phase shift at the beginning of the second pulse is

$$\theta_{2p} = 2\pi f_c \frac{dT_1}{2} + 2\pi(f_c + f_p)(1-d)T_1 \qquad (2.43)$$

where f_p is the change in frequency due to frequency pulling.

Thus, the additional phase shift due to frequency pulling is

$$\Delta\theta = \theta_{2p} - \theta_2 \qquad (2.44)$$

$$= 2\pi f_p (1-d)T_1$$

Let $f_s = f_p(1-d)$. Then,

$$\Delta\theta = 2\pi f_s T_1$$

Thus, at the beginning of the ith pulse, the total additional phase shift is

$$\Delta\theta_i = \sum_{k=1}^{i-1} 2\pi f_s T_k \qquad i = 2, 3, \cdots, N_p \tag{2.45}$$

where f_s = the frequency shift.

In order to calculate the Fourier transform of the frequency term, first we will define the parameters $B(f)$, $C(f)$, $D(f)$ and $E(f)$, using Eq. (2.17). Thus

$$B(f) = \frac{1}{2} \{\delta(f-f_c) + \delta(f+f_c)\}$$

$$C(f) = \cos(\theta_0 + \Delta\theta_i) \cdot \delta(f)$$

$$D(f) = \frac{1}{2j} \{\delta(f-f_c) - \delta(f+f_c)\}$$

$$E(f) = \sin(\theta_0 + \Delta\theta_i) \cdot \delta(f) \tag{2.46}$$

Substituting from Eq. (2.46) into Eq. (2.16) yields

$$Y_N(f) = \frac{1}{2} \left\{ [\delta(f-f_c) + \delta(f+f_c)] \cos(\theta_0 + \Delta\theta_i) \right.$$
$$\left. + j[\delta(f-f_c) - \delta(f+f_c)] \sin(\theta_0 + \Delta\theta_i) \right\} \tag{2.47}$$

Simplifying Eq. (2.47) by neglecting the negative frequency term (i.e. $(f + f_c)$), we have

$$Y_{NP}(f) = \frac{1}{2} [\delta(f-f_c)] \cdot \exp[j(\theta_0 + \Delta\theta_i)] \tag{2.48}$$

Convolving $X(f)$ given by Eq. (2.23) with $Y_{NP}(f)$ given by Eq. (2.48) yields

$$F_N(f) = \sum_{i=1}^{N_p} \frac{Ad\,T_i}{2} \, \text{sinc}[(f-f_c)dT_i] e^{j(\theta_0 + \Delta\theta_i)} e^{-j2\pi(f-f_c)t_i} \tag{2.49}$$

Case 1 <u>Constant Duration T</u>

In this case, we consider that all N_p pulses in the window of length T_D have equal duration T. Thus, we have

$$\Delta\theta_i = \sum_{k=1}^{i-1} 2\pi f_s T_k , \qquad i = 2, 3, \cdots, N_p$$

$$= 2\pi f_s (i-1) T , \qquad i = 1, 2, 3, \cdots, N_p \qquad (2.50)$$

Substituting from Eqs. (2.28), (2.31) and (2.50) into Eq. (2.49), we get

$$F_{N1}(f) = \frac{AdT}{2} e^{j\theta_0} \text{sinc}\left[(f-f_c)dT\right] \sum_{i=1}^{N_p} e^{-j2\pi\left[(f-f_c-f_s)(i-1)T\right]} \qquad (2.51)$$

Simplifying Eq. (2.51) as illustrated previously in Eq. (2.32) yields

$$F_{N1}(f) = \frac{AdT}{2} e^{j\theta_0} \text{sinc}\left[(f-f_c)dT\right] \frac{1 - e^{-j2\pi(f-f_c-f_s)N_p T}}{1 - e^{-j2\pi(f-f_c-f_s)T}}$$

Computing the spectrum gives

$$S_{N1}(f) = \left| \frac{AdT}{2} \right|^2 \text{sinc}^2\left[(f-f_c)dT\right] \left| \frac{\sin[\pi(f-f_c-f_s)N_p T]}{\sin[\pi(f-f_c-f_s)T]} \right|^2 \qquad (2.52)$$

From Eq. (2.52), we note that the spectrum is the product of three terms as in Case 1 for ideal coherent ELT signals. The first term is the amplitude, the second term is the sinc function which produces a peak a $f = f_c$, and the third term is the ratio of two sine functions. This third term has a frequency shift f_s which shifts the multi-peak pattern.

Figures 2.14 to 2.16 illustrate the spectrum for the ELT signal with carrier frequency equal to 15 kHz. The total number of pulses contained in the window (T_D = 10 ms) is 10 with all pulses having equal duration. These figures depict the results for three different values of frequency shift f_s, i.e. for f_s equal to 600 Hz, 1200 Hz and 1800 Hz respectively. The main consideration is the fact that the first nulls of the sinc function and peaks of the sine relation can overlap together. From these figures we note that the carrier component peak moves to the right as indicated by the arrow.
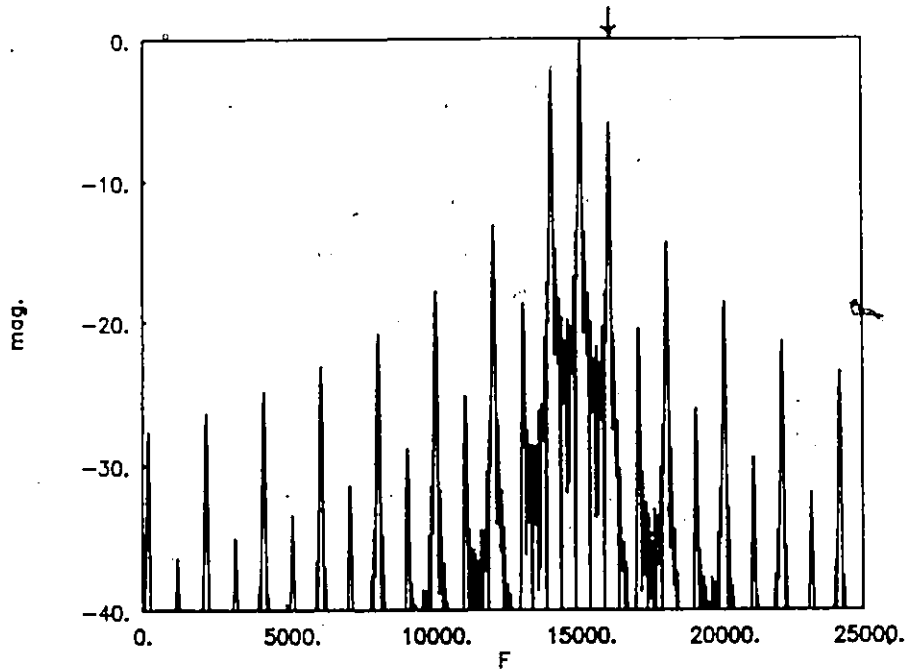
Fig. 2.15   Plot of $S_{N1}(f)$ with $N_p = 10$ pulses and $f_s = 1200$ Hz.
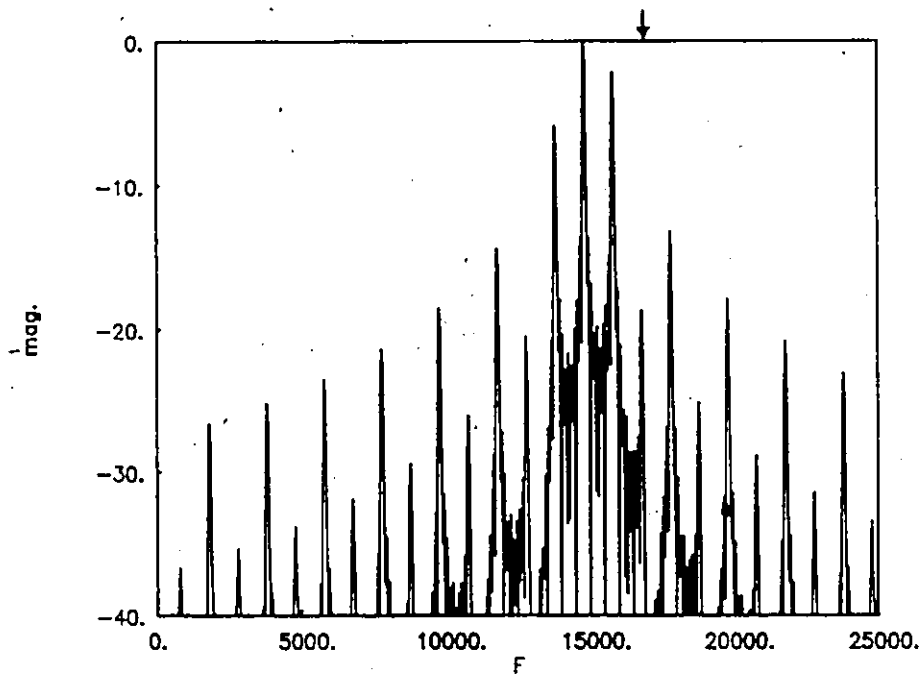
Fig. 2.16   Plot of $S_{N1}(f)$ with $N_p = 10$ pulses and $f_s = 1800$ Hz.

Case 2 <u>Linearly Varying Duration T</u>

In this case, we consider the duration for each pulse in the window increases linearly with respect to the pulse number (N_p). Making use of Eq. (2.35) and substituting in Eq. (2.45), we get $\Delta\theta_1 = 0$ and:

$$\Delta\theta_i = \sum_{k=1}^{i-1} 2\pi f_s T_k, \quad i = 2, 3, \cdots, N_p.$$

$$= 2\pi f_s \left[(i-1) T_{EQ} + \frac{(i-1)(i-2)}{2} \Delta T \right], \quad i = 1, 2, 3 \cdots N_p. \tag{2.53}$$

Substituting from Eqs. (2.35), (2.37) and (2.53) into Eq. (2.49) yields

$$F_{N2}(f) = \frac{Ad}{2} e^{j\theta_0} \sum_{i=1}^{N_p} [T + (i-1)\Delta T] \cdot \text{sinc} [d(f-f_c)(T + (i-1)\Delta T)]$$

$$\cdot \exp\left\{ -j2\pi (f-f_c-f_s) \left[(i-1) T_{EQ} + \frac{(i-1)(i-2)}{2} \Delta T \right] \right\} \tag{2.54}$$

Equation (2.54) gives the Fourier transform representation for ELT signal when the pulse duration period increases linearly with respect to the pulse number N_p in the window length T_D.

Comparing Eqs. (2.54) and (2.38), we note that these two equations are the same except the exponential term in Eq. (2.54) has a frequency shift f_s. This frequency shift f_s shifts the multi-peak pattern.

The spectrum $S_{N2}(f)$ can be calculated by performing the squared magnitude of $F_{N2}(f)$. Figures 2.17 to 2.20 illustrate the spectrum for the ELT signal with carrier frequency $f_c = 15$ kHz and 10 pulses in the window length T_D. The frequency shift f_s is equal 600 Hz. These figures depict the spectrum for different values of ΔT, i.e. for $\Delta T = 5$ μs., 10 μs., 25 μs., and 50 μs., respectively. From these results, it is seen that as ΔT increases, the level of the sideband peaks are reduced which consequently improves the detection of the ELT signal.
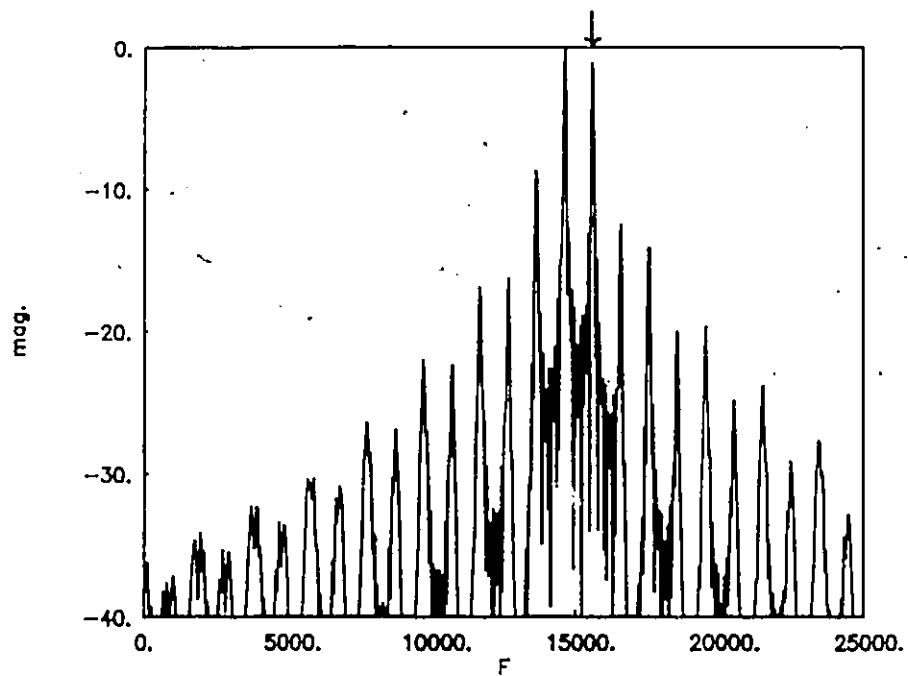
Fig. 2.17   Plot of $S_{N2}(f)$ with $N_p = 10$ pulses, $f_s = 600$ Hz and $\Delta T = 5$ µs.
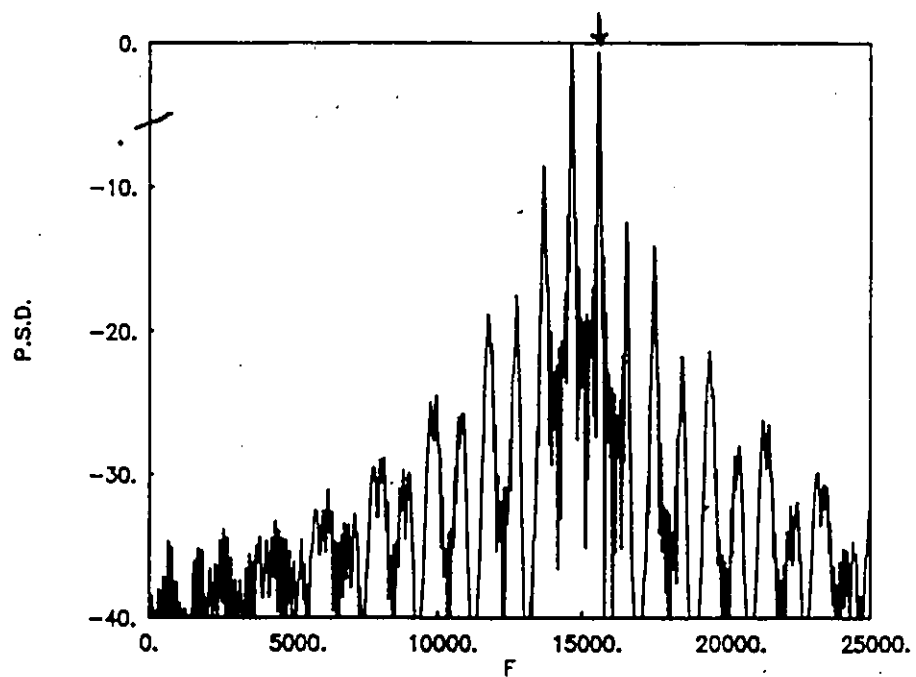
Fig. 2.18   Plot of $S_{N2}(f)$ with $N_p = 10$ pulses, $f_s = 600$ Hz and $\Delta T = 10$ µs.
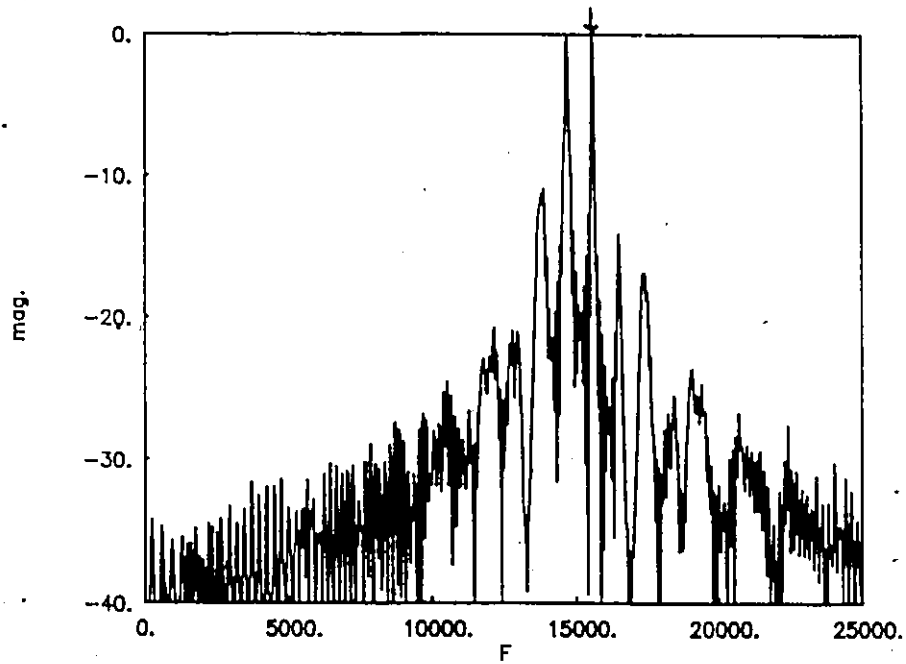
Fig. 2.19   Plot of $S_{N2}(f)$ with $N_p = 10$ pulses, $f_s = 600$ Hz and $\Delta T = 25$ μs.
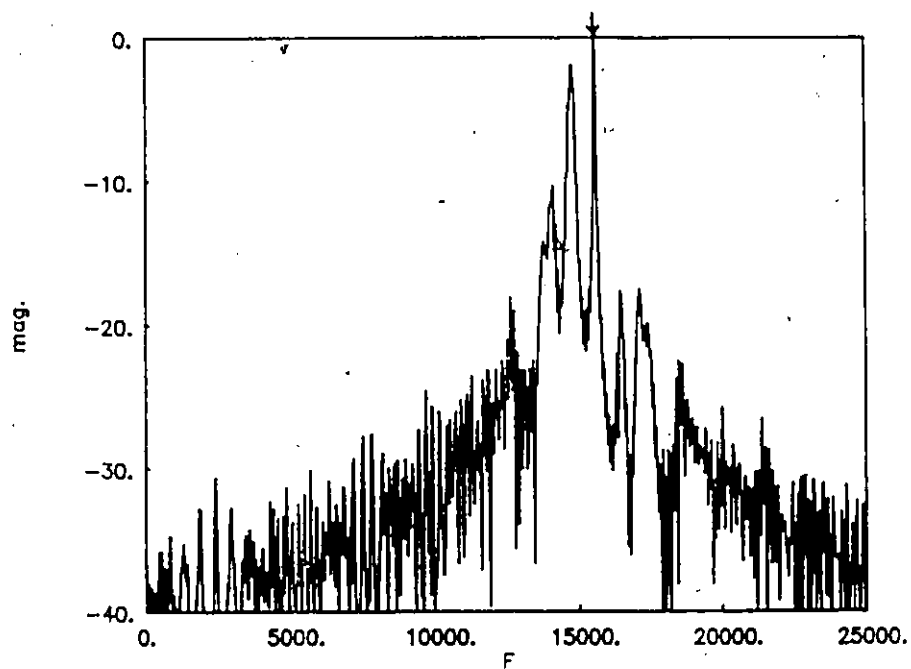
Fig. 2.20   Plot of $S_{N2}(f)$ with $N_p = 10$ pulses, $f_s = 600$ Hz and $\Delta T = 50$ μs.

2.5 Non-Coherent ELT Signals

2.5.1 Random Phase ELT Signal

In this case, we consider that there is no phase coherence between the pulses. Thus, we have

$$\omega(t) = 2\pi f_c$$

$$\theta(t) = \theta_i, \quad i = 1, 2, ..., N_p$$

where θ_i is considered to be uniformly distributed random variable between 0 and 2π.

Making use of these specifications and substituting in Eq. (2.9), we have

$$s(t) = \sum_{i=1}^{N_p} s_i(t)$$

where

$$s_i(t) = A \cdot Re \left\{ exp \left[j(2\pi f_c t + \theta_i) \right] \right\} \quad , \quad t_i - \frac{dT_i}{2} \leq t \leq t_i + \frac{dT_i}{2} \tag{2.55}$$

$$= 0 \quad , \quad \text{otherwise}$$

Since the amplitude term x(t) is exactly the same as for the coherent ELT signal, then the Fourier transform X(f) is given by Eq. (2.23).

Now, the frequency term is represented by

$$y(t) = Re\{exp[j(2\pi f_c t + \theta_i)]\}, \quad i = 1, 2, ..., N_p \tag{2.56}$$

In order to determine Y(f), we will calculate the parameters B(f), C(f), D(f) and E(f) using Eq. (2.17). These parameters are given by

$$B(f) = \frac{1}{2} [\delta(f - f_c) + \delta(f + f_c)]$$

$$C(f) = \cos(\theta_i) \cdot \delta(f)$$

$$D(f) = \frac{1}{2j} [\delta(f - f_c) - \delta(f + f_c)]$$

$$E(f) = \sin(\theta_i) \cdot \delta(f) \tag{2.57}$$

Substituting from Eq. (2.57) into Eq. (2.16) and simplifying the obtained equation, as in Eq. (2.25), we get

$$Y_{RP}(f) = \frac{1}{2} \cdot \delta(f-f_c)e^{j\theta_i} \qquad , i=1,2,...,N_p \qquad (2.58)$$

Convolving X(f) given by Eq. (2.23) with $Y_{RP}(f)$ given by Eq. (2.58) yields

$$F_R(f) = \sum_{i=1}^{N_p} \frac{AdT_i}{2} \, sinc\,[(f-f_c)d\,T_i]e^{-j[2\pi(f-f_c)t_i-\theta_i]} \qquad (2.59)$$

If all pulses having equal duration T, then Eq. (2.59) becomes

$$F_R(f) = \frac{AdT}{2} \, sinc\,[(f-f_c)d\,T] \sum_{i=1}^{N_p} e^{-j[2\pi(f-f_c)t_i-\theta_i]} \qquad (2.60)$$

$$S_R(f) = |F_R(f)|^2 \qquad (2.61)$$

Fig. 2.21 illustrates the spectrum for a random phase ELT signal with carrier frequency 15 kHz. From this figure it is seen that there is no peak in the spectrum at the carrier frequency. Thus the detection of the random phase ELT signal is difficult if not impossible.

Since θ_i is a random variable, we can evaluate the averaged spectrum as.

$$S_{av}(f) = E\left\{F_R(f) \cdot F_R^*(f)\right\}$$

$$= \left|\frac{AdT}{2}\right|^2 \, sinc^2\,[(f-f_c)dT]$$

$$\cdot E\left\{\sum_{i=1}^{N_p} e^{-j(2\pi(f-f_c)t_i-\theta_i)} \cdot \sum_{k=1}^{N_p} e^{+j(2\pi(f-f_c)t_k-\theta_k)}\right\} \qquad (2.62)$$

Since the expectation of the sum of all products for $i \neq k$ is equal to zero, then Eq. (2.62) becomes

$$S_{av}(f) = \left|\frac{AdT}{2}\right|^2 \cdot N_p \cdot sinc^2\,[(f-f_c)dT] \qquad (2.63)$$
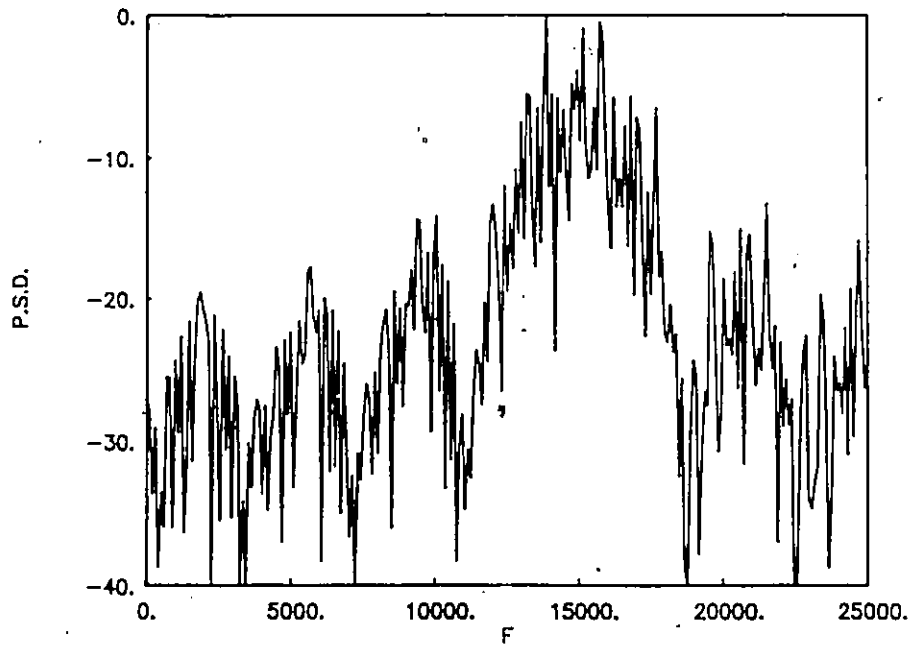
Fig. 2.21   Plot of $S_R(f)$.
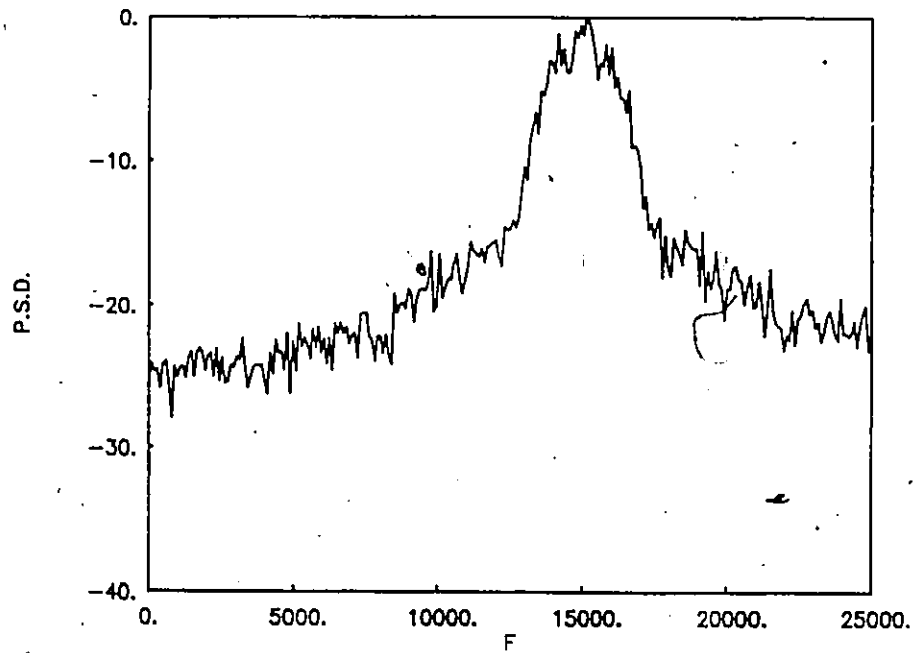
Fig. 2.22   Plot of $S_{av}(f)$.

Equation (2.63) provides the averaged spectrum for a non-coherent signal. It is seen that it has a shape which is $\text{sinc}^2[(f-f_c)dT]$. This averaged spectrum is far broader than the previous spectra. Thus, the carrier frequency estimation for non-coherent ELT signals cannot easily be performed by using Fourier transform.

Figure 2.22 depicts the averaged spectrum for a non-coherent signal using Eq. (2.63). From this figure, it is clear that the spectrum produces a broader peak as compared to the previous spectrum. The carrier frequency is not easily measured. Further, there is little point in considering the spectrum for linearly varying duration T.

2.5.2   Varying Carrier Frequency ELT Signal

In this case, the modulating signal m(t) is described as in the previous cases. It is a rectangular pulse and consists of N_p pulses in the window with length T_D. In this case, each pulse in the sweep is modulated by a different carrier frequency. Furthermore, the amplitude term is the same as all previous cases. Thus, in this case, we have

$$\omega(t) = 2\pi f_{ci}, \quad i = 1, 2, ..., N_p$$

$$\theta(t) = \theta_0$$

Then Eq. (2.9) becomes

$$s(t) = \sum_{i=1}^{N_p} s_i(t)$$

where

$$s_i(t) = A \cdot \text{Re}\left\{\exp[j(2\pi f_{ci} t + \theta_0)]\right\} \quad , \quad t_i - \frac{dT_i}{2} \leq t \leq t_i + \frac{dT_i}{2}$$

$$= 0 \quad , \quad \text{otherwise}$$

(2.64)

The structure of the amplitude term is the same as Ideal Coherent; therefore the Fourier transform X(f) is represented by Eq. (2.23).

The frequency term representation is given by

$$y(t) = \text{Re}\{\exp[j(2\pi f_{ci} t + \theta_0)]\}, \quad i = 1, 2, ..., N_p \tag{2.65}$$

In order to calculate the Fourier transform $Y(f)$, first we calculate the parameters $B(f)$, $C(f)$, $D(f)$ and $E(f)$ using Eq. (2.17). Then we have

$$B(f) = \frac{1}{2} [\delta(f - f_{ci}) + \delta(f + f_{ci})]$$

$$C(f) = \cos(\theta_0) \cdot \delta(f)$$

$$D(f) = \frac{1}{2j} [\delta(f - f_{ci}) - \delta(f + f_{ci})]$$

$$E(f) = \sin(\theta_0) \cdot \delta(f) \tag{2.66}$$

Substituting from Eq. (2.66) into Eq. (2.16), we get

$$Y_F(f) = \frac{1}{2} \left\{ [\delta(f - f_{ci}) + \delta(f + f_{ci})] \cos\theta_0 + j\sin\theta_0 \ [\delta(f - f_{ci}) + \delta(f + f_{ci})] \right\} \tag{2.67}$$

Neglecting the negative frequency term, i.e. $(f + f_c)$, we have

$$Y_{FP}(f) = \frac{1}{2} \cdot \delta(f - f_{ci}) \cdot e^{j\theta_0} \quad , i = 1, 2, ..., N_p \tag{2.68}$$

Convolving the amplitude $X(f)$ given by Eq. (2.23) with the frequency $Y_{FP}(f)$ given by Eq. (2.68) yields

$$F_F(f) = \sum_{i=1}^{N_p} \frac{AdT_i}{2} \text{sinc}[(f - f_{ci})d\, T_i] e^{-j2\pi(f - f_{ci})t_i} e^{j\theta_0} \tag{2.69}$$

Case 1 Constant Duration T

In this case, we consider all N_p pulses in the window length as having equal duration T. Thus, using Eqs. (2.28) and (2.31) and substituting in Eq. (2.69) yields the Fourier transform of N_p pulses given by

$$F_{F1}(f) = \frac{AdT}{2} e^{j\theta_0} \sum_{i=1}^{N_p} \text{sinc}[(f - f_{ci})d\,T] e^{-j2\pi(f - f_{ci})(i-1)T} \tag{2.70}$$

Consider the carrier frequency for each pulse increases linearly with the pulse number N_p and represented by

$$f_{ci} = f_c + (i-1)\Delta F, \quad i = 1, 2, ..., N_p \tag{2.71}$$

where

$f_c =$ constant carrier frequency

$\Delta F =$ increase in the frequency per pulse.

Substituting from Eq. (2.71) into Eq. (2.70) yields

$$F_{F1}(f) = \frac{AdT}{2} e^{j\theta_0} \sum_{i=1}^{N_p} \text{sinc}\left[(f - f_c - (i-1)\Delta F)dT\right]$$

$$\cdot \exp\left\{-j2\pi(f - f_c - (i-1)\Delta F)(i-1)T\right\} \tag{2.72}$$

The spectrum $S_{F1}(f)$ can be calculated by performing the squared magnitude of $F_{F1}(f)$ given by Eq. (2.72).

A pulse-wave modulated ELT signal with carrier frequency $f_c = 15$ kHz and 10 pulses in the window length $T_D = 10$ ms. is examined here. Figures 2.23 to 2.26 illustrate the spectra for the case where the carrier frequency varies by 15, 30, 75 and 150 Hz per pulse respectively. From these figures we note that as ΔF increases the detection of the carrier peak component becomes extremely difficult if not impossible.

Case 2 Linearly Varying Duration T

Now we study the signal spectra produced by an ELT signal when each pulse-null duration increases linearly with the pulse number (N_p). In this case, making use of Eqs. (2.35), (2.37) and substituting in Eq. (2.69) yields the Fourier transform representation of N_p pulses given by
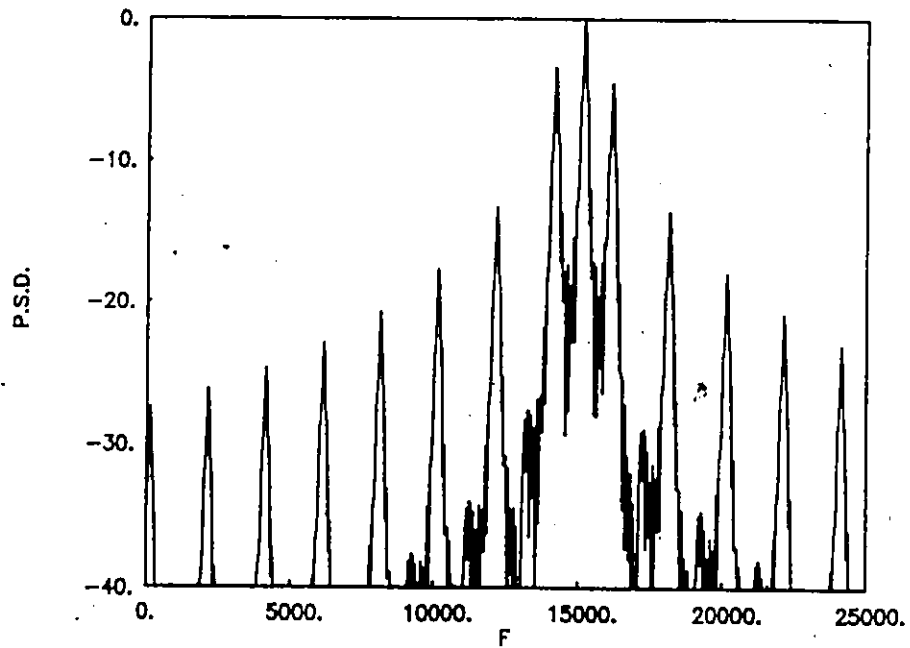
Fig. 2.23   Plot of $S_{F1}(f)$ with $N_p = 10$ pulses and $\Delta F = 15$ Hz.
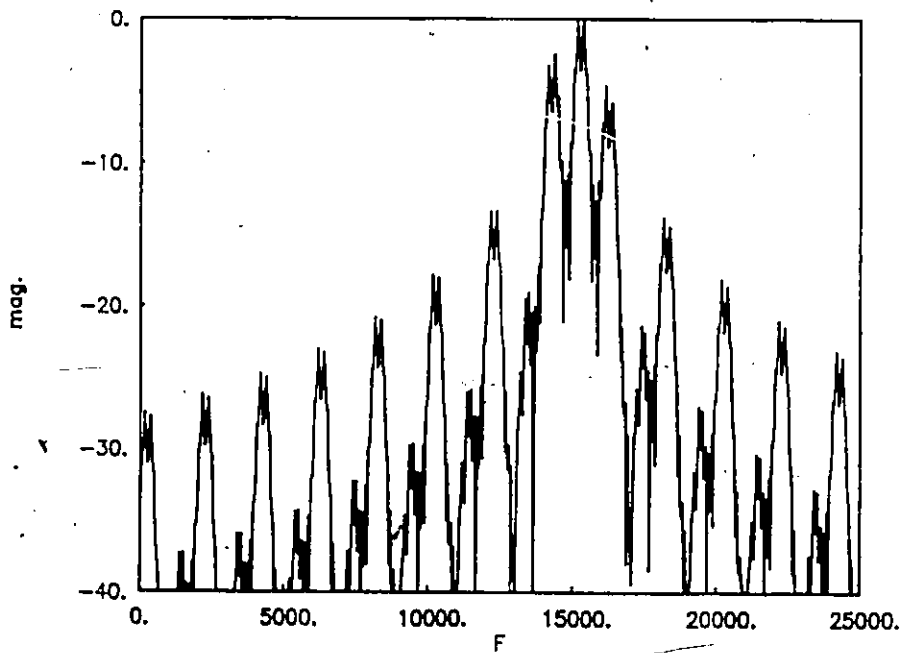
Fig. 2.24   Plot of $S_{F1}(f)$ with $N_p = 10$ pulses and $\Delta F = 30$ Hz.

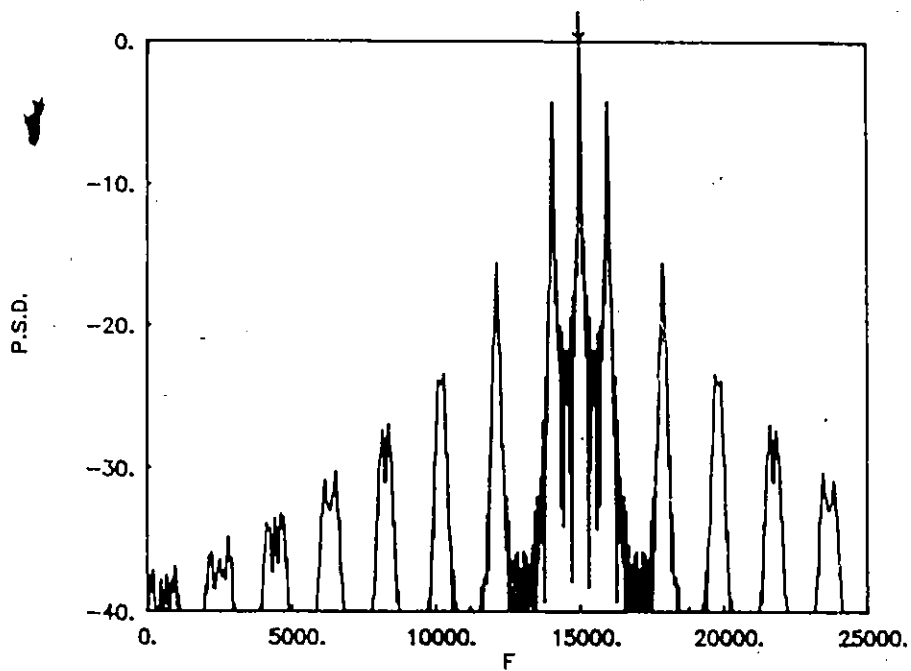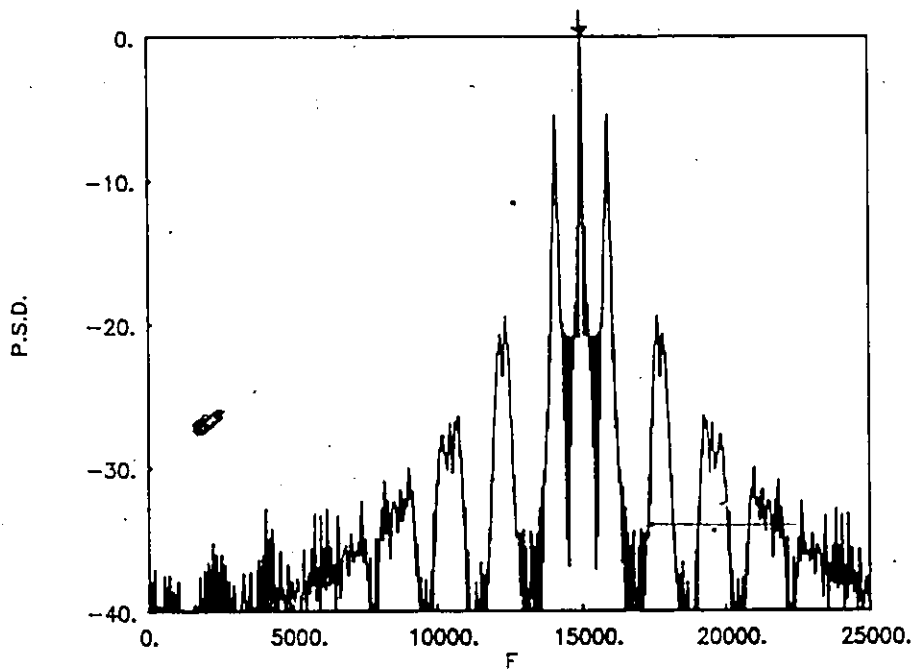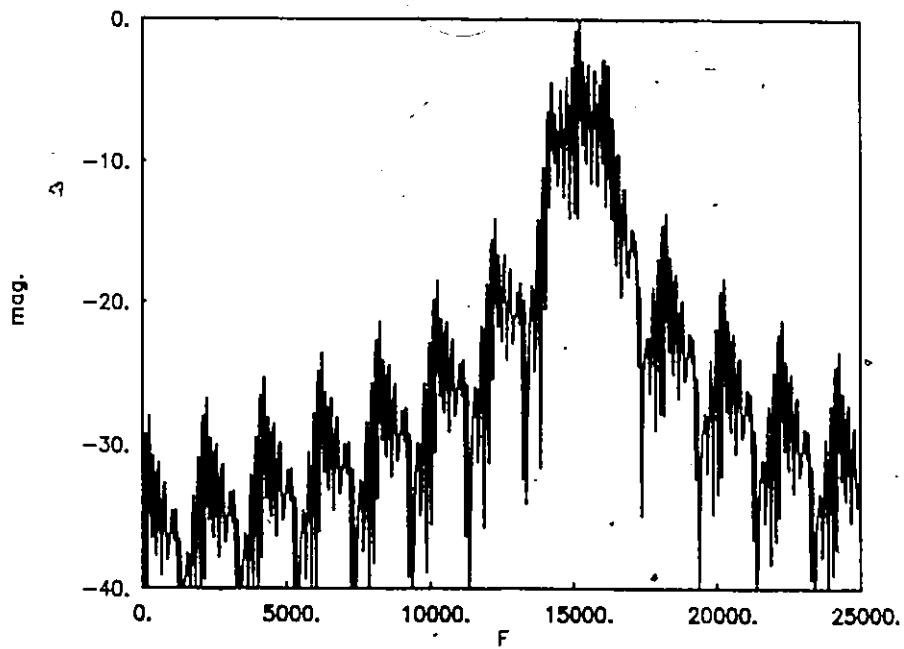Fig. 2.25   Plot of $S_{F1}(f)$ with $N_p = 10$ pulses and $\Delta F = 75$ Hz.
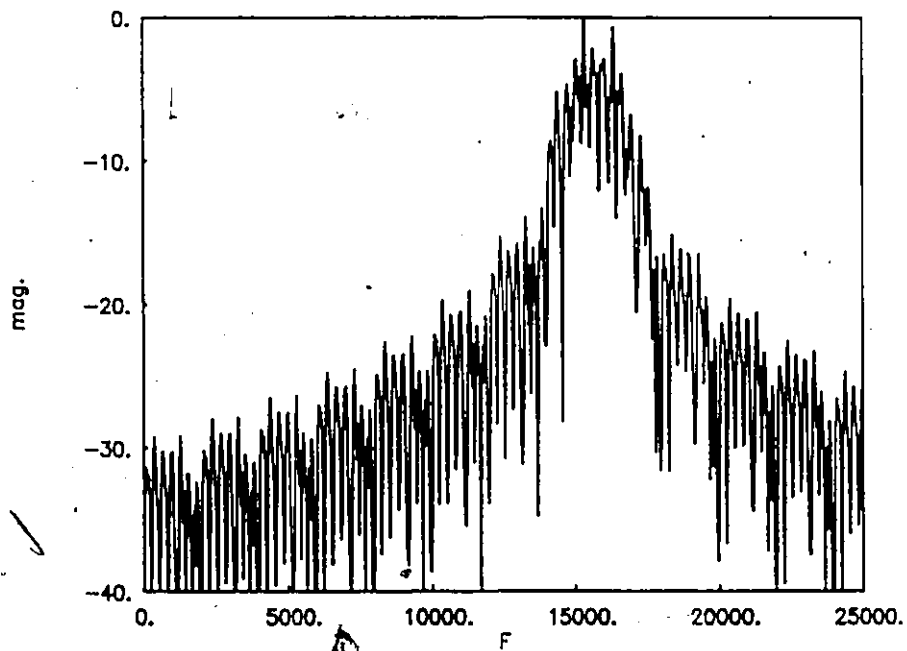
Fig. 2.26   Plot of $S_{F1}(f)$ with $N_p = 10$ pulses and $\Delta F = 150$ Hz.

$$F_{F2}(f) = \frac{Ad}{2} e^{j\theta_0} \sum_{i=1}^{N_p} [T + (i-1)\Delta T] \cdot \text{sinc}[d(f-f_{ci})(T + (i-1)\Delta T)]$$

$$\cdot \exp\left\{-j2\pi(f-f_{ci})\left[(i-1)T_{EQ} + \frac{(i-1)(i-2)}{2}\Delta T\right]\right\} \tag{2.73}$$

The carrier frequency f_{ci}, $(i = 1, 2, ..., N_p)$ is given by Eq. (2.71). Then, substituting from Eq. (2.71) into Eq. (2.73), we get

$$F_{F2}(f) = \frac{Ad}{2} e^{j\theta_0} \sum_{i=1}^{N_p} [T + (i-1)\Delta T] \cdot \text{sinc}[d(f-f_c - (i-1)\Delta F)(T + (i-1)\Delta T)]$$

$$\cdot \exp\left\{-j2\pi(f-f_c - (i-1)\Delta F)\left[(i-1)T_{EQ} + \frac{(i-1)(i-2)}{2}\Delta T\right]\right\} \tag{2.74}$$

The spectrum $S_{F2}(f)$ is given by

$$S_{F2}(f) = \left| F_{F2}(f) \right|^2$$

Figures 2.27 to 2.29 illustrate the spectrum obtained by performing the squared magnitude of Eq. (2.74). In these figures, we choose $\Delta T = 100$ µs and ΔF equal to 15 Hz, 30 Hz and 75 Hz. From these figures it is seen that for $\Delta F = 15$ Hz the spectrum is good due to the reduction of the level of the sidebands. Increasing ΔF to 30 Hz and 75 Hz makes the detection of the carrier component difficult.

2.5.3 Varying Amplitude ELT Signal

In this case, the amplitude $a(t)$ for each pulse in the sweep is not constant, i.e. each pulse in the window length T_D is modulated by different amplitude. Then, in this case, we have

$$a(t) = A_i m(t), \quad i = 1, 2, ...$$
$$\omega(t) = 2\pi f_c \tag{2.75}$$
$$\theta(t) = \theta_0$$

From Eqs. (2.75) and (2.9), it is seen that $s(t)$ can be represented as
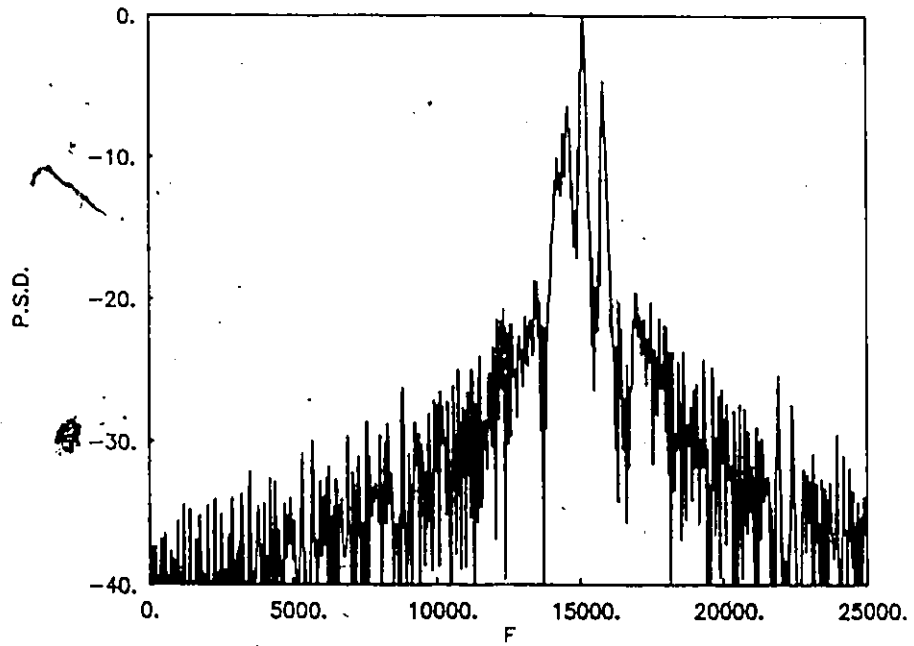
Fig. 2.27   Plot of $S_{F2}(f)$ with $N_p = 10$ pulses, $\Delta T = 100\,\mu s$ and $\Delta F = 15\,Hz$.
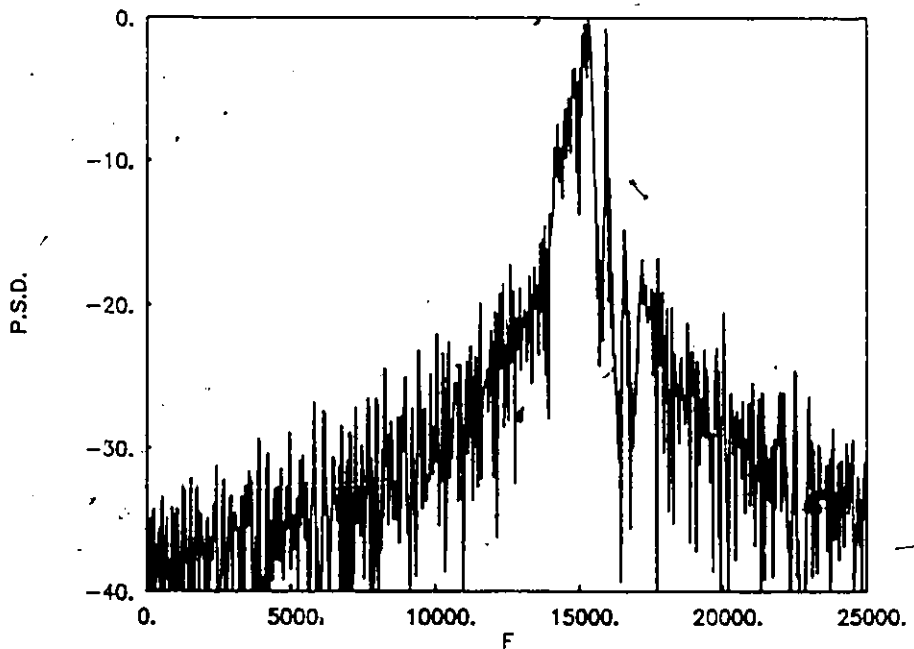
Fig. 2.28   Plot of $S_{F2}(f)$ with $N_p = 10$ pulses, $\Delta T = 100\,\mu s$ and $\Delta F = 30\,Hz$
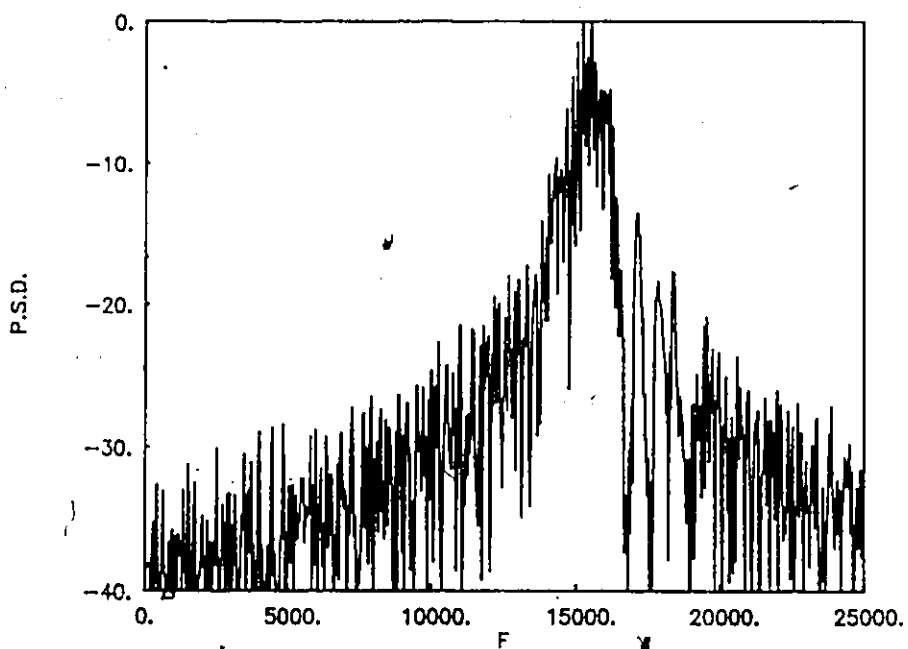
Fig. 2.29   Plot of $S_{F2}(f)$ with $N_p = 10$ pulses, $\Delta T = 100\,\mu s$ and $\Delta F = 75\,Hz$
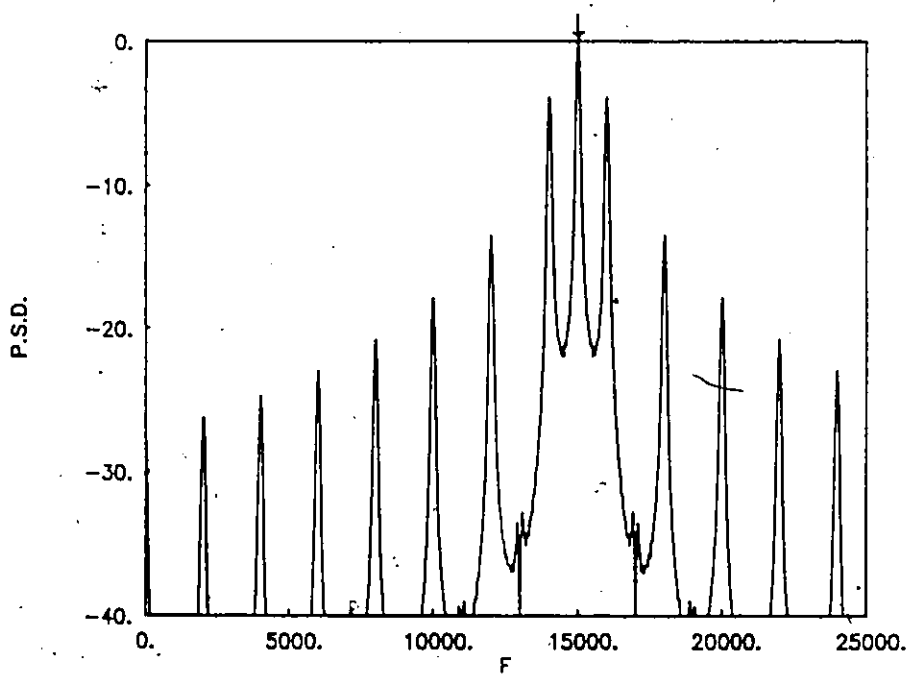
Fig. 2.30   Plot of $S_{A1}(f)$ with $N_p = 10$ pulses and $\Delta A = 0.1\,A$.

$$s(t) = \sum_{i=1}^{N_p} s_i(t)$$

where

$$s_i(t) = A_i \, \mathrm{Re} \left\{ \exp\left[j(2\pi f_c t + \theta_0) \right] \right\} \qquad , \quad t_i - \frac{dT_i}{2} \le t \le t_i + \frac{dT_i}{2}$$

$$= 0 \qquad\qquad\qquad\qquad , \quad \text{otherwise}$$

(2.76)

In this case, the Fourier transform of the amplitude term x(t) is given by

$$X(f) = \sum_{i=1}^{N_p} A_i \, dT_i \, \mathrm{sinc}\,(fd\,T_i) \, e^{-j2\pi ft_i} \qquad\qquad (2.77)$$

The frequency term for this case is similar to $Y_{CP}(f)$. Then convolving X(f) given by Eq. (2.77) with $Y_{CP}(f)$ given by Eq. (2.26) yields

$$F_A(f) = \sum_{i=1}^{N_p} \frac{A_i dT_i}{2} \, \mathrm{sinc}\,[(f-f_c)d\,T_i] \, e^{-j2\pi(f-f_c)t_i} \, e^{j\theta_0} \qquad\qquad (2.78)$$

Case 1 Constant Duration T

Here, we consider that all N_p pulses in window T_D have equal duration T. Thus, the Fourier transform representation for N_p pulses is given by

$$F_{A1}(f) = \frac{dT}{2} \, e^{j\theta_0} \mathrm{sinc}\,[(f-f_c)d\,T] \sum_{i=1}^{N_p} A_i \, e^{-j2\pi(f-f_c)(i-1)T} \qquad\qquad (2.79)$$

Let us consider the amplitude for each pulse increasing linearly with respect to the pulse number N_p, i.e.

$$A_i = A + (i-1)\Delta A, \quad i = 1, 2, \ldots, N_p \qquad\qquad (2.80)$$

where

$A =$ amplitude of the first pulse in the sweep

$\Delta A =$ increases in the amplitude per pulse.

Substituting from Eq. (2.80) into Eq. (2.79) yields

$$F_{A1}(f) = \frac{AdT}{2} e^{j\theta_0} \text{sinc}[(f-f_c)dT] \sum_{i=1}^{N_p} e^{-j2\pi(f-f_c)(i-1)T}$$

(2.81)

$$+ \frac{\Delta A dT}{2} e^{j\theta_0} \text{sinc}[(f-f_c)dT] \sum_{i=1}^{N_p} (i-1) e^{-j2\pi(f-f_c)(i-1)T}$$

The summation in the second term can be simplified by noting [14]

$$I = \sum_{i=1}^{N_p} (i-1) e^{-j2\pi(f-f_c)(i-1)T}$$

$$= \sum_{K=0}^{N_p-1} K Z^K$$

(2.82)

$$= \frac{Z - N_p Z^{N_p} + (N_p-1)Z^{N_p+1}}{(1-Z)^2}$$

where

$$Z = e^{-j2\pi(f-f_c)T} \quad \text{and} \quad K = i - 1$$

Equation (2.81) can be written in this form

$$F_{A1}(f) = \frac{dT}{2} e^{j\theta_0} \text{sinc}[(f-f_c)dT] \left\{ A \frac{1-Z^{N_p}}{1-Z} + \Delta A \frac{Z - N_p Z^{N_p} + (N_p-1)Z^{N_p+1}}{(1-Z)^2} \right\}$$

(2.83)

Equation (2.83) gives the Fourier transform of N_p pulses with equal duration T. The spectrum $S_{A1}(f)$ can be calculated by performing the squared magnitude of $F_{A1}(f)$. $F_{A1}(f)$ consists of two main terms described as: i) the first term is the sinc function term, which has a peak at $f = f_c$. This is called the carrier component peak; ii) the second term consists of two parts ; the first part is due to the amplitude A, while the second part is due to the increases in the amplitude by the amount ΔA. Both of these term gives a multi-peak pattern.

The spectra in the case of $\Delta A = 0$ is exactly the same as Fig. 2.8. (We choose the same number of pulses N_p in the window length T_D, i.e. $N_p = 10$). Choosing ΔA equal 10% of

the actual amplitude 'A gives the spectra depicted in Fig. 2.30. From this figure, it is clear that the carrier peak is stationary while the background side peaks are reduced and become smoother as compared to the spectrum given in Fig. 2.8.

Case 2 <u>Linearly Varying Duration T</u>

In this case, we consider that each pulse duration in the window increases linearly with respect to the pulse number (N_p). Thus, substituting from Eqs. (2.35) and (2.37) into Eq. (2.78), we have

$$F_{A2}(f) = \sum_{i=1}^{N_p} \frac{A_i d}{2} [T + (i-1)\Delta T] \cdot sinc[d(f-f_c)(T + (i-1)\Delta T)]$$

$$\cdot \exp\left\{-j2\pi(f-f_c)\left[(i-1)T_{EQ} + \frac{(i-1)(i-2)}{2}\Delta T\right]\right\} e^{j\theta_0} \tag{2.84}$$

Consider A_i to be represented by Eq. (2.80). By substituting from this equation into Eq. (2.84), we have

$$F_{A2}(f) = \sum_{i=1}^{N_p} \frac{d}{2} [A + (i-1)\Delta A] \cdot [T + (i-1)\Delta T] \cdot sinc[d(f-f_c)(T + (i-1)\Delta T)]$$

$$\cdot \exp\left\{-j2\pi(f-f_c)\left[(i-1)T_{EQ} + \frac{(i-1)(i-2)}{2}\Delta T\right]\right\} e^{j\theta_0} \tag{2.85}$$

Equation (2.85) represents the Fourier transform of N_p pulses for the case where the pulse duration and amplitude increases linearly with respect to the pulse number N_p. As discussed in Case 2 for Ideal Coherent ELT signal, we note that by increasing ΔT, the level of the sideband peaks around the carrier are reduced while the carrier peak component remains stationary. Furthermore, the effect of varying amplitude smooths the multi peak spectrum as illustrated before.

Figure 2.31 illustrates the obtained spectrum $S_{A2}(f)$ using Eq. (2.85) for $\Delta T = 100 \mu s$ and $\Delta A = 10\%$ of the actual value of the amplitude A. From this figure, we note
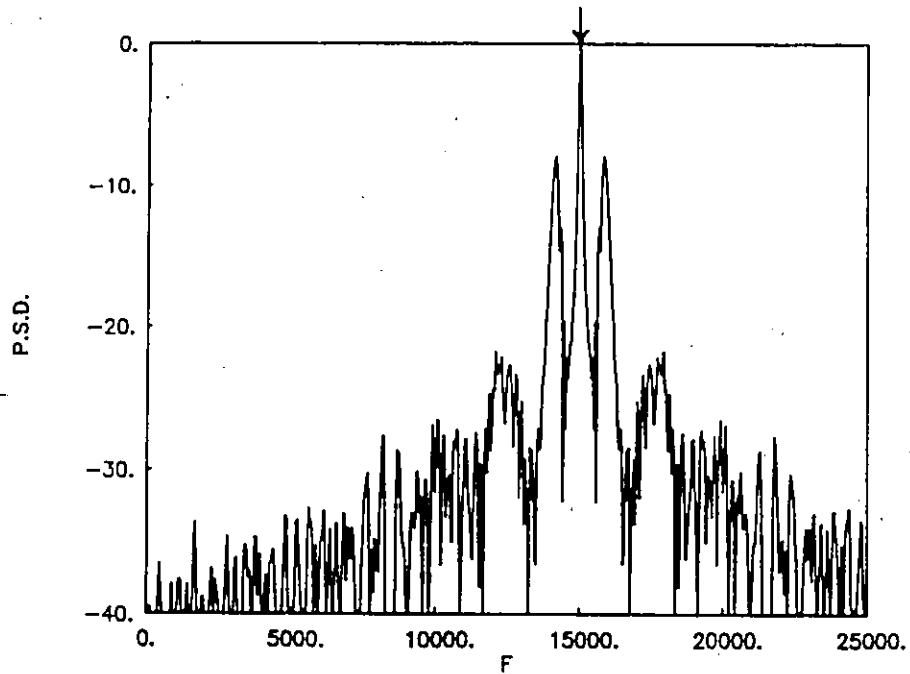
Fig. 2.31   Plot of $S_{A2}(f)$ with $N_p = 10$ pulses, $\Delta T = 100 \,\mu s$ and $\Delta A = 0.1$ A.
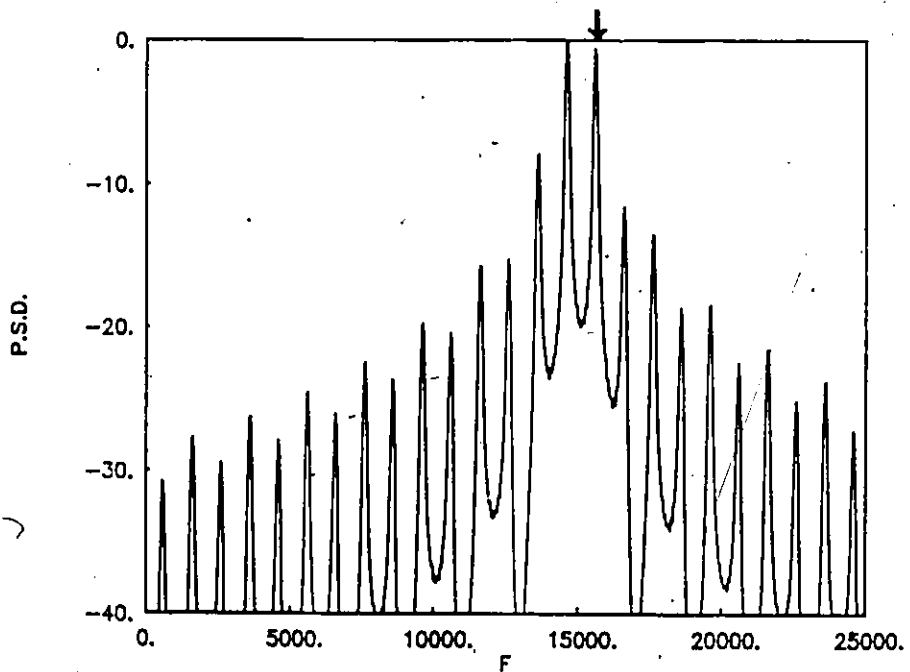
Fig. 2.32   Plot of $S_{AN1}(f)$ with $N_p = 10$ pulses, $f_s = 600$ Hz and $\Delta A = 0.1$ A.

that the sidebands are reduced and the two major sidebands around the carrier become smoother, while the carrier peak component remains stationary and very sharp.

2.5.4 Varying Amplitude With Added Phase Shift

For this case, we consider each pulse to have an additional phase shift $\Delta\theta_i$, $i = 2, 3, 4, ..., N_p$, as represented by Eq. (2.45). This section studies the signal spectra produced by the ELT signal when each pulse has an additional phase shift $\Delta\theta_i$ and modulated with different amplitude A_i, $i = 1, 2, ..., N_p$. Thus, in this case, we have

$$s_i(t) = A_i \operatorname{Re}\left\{\exp[j(2\pi f_c t + \theta_0 + \Delta\theta_i)]\right\}, \quad t_i - \frac{dT_i}{2} \le t \le t_i + \frac{dT_i}{2} \tag{2.86}$$

$$= 0 \qquad\qquad\qquad , \quad \text{otherwise}$$

The Fourier transform of N_p pulses is given by

$$F_{AN}(f) = \sum_{i=1}^{N_p} \frac{A_i d T_i}{2} \operatorname{sinc}[(f-f_c)d T_i] e^{-j2\pi(f-f_c)t_i} \cdot e^{j(\theta_0 + \Delta\theta_i)} \tag{2.87}$$

Case 1 Constant Duration T

In this case, we have $T_i = T$ for all values of i. Thus,

$$\Delta\theta_i = \sum_{k=1}^{i-1} 2\pi f_s T_k, \qquad i = 2, 3, ..., N_p$$

$$= 2\pi f_s (i-1)T, \qquad i = 1, 2, ..., N_p \tag{2.88}$$

Thus, Eq. (2.87) becomes

$$F_{AN1}(f) = \frac{dT}{2} e^{j\theta_0} \operatorname{sinc}[(f-f_c)dT] \sum_{i=1}^{N_p} A_i e^{-j2\pi[(f-f_c-f_s)(i-1)T]} \tag{2.89}$$

Let us consider A_i, as given by Eq. (2.80). Then, substituting from Eq. (2.80) into Eq. (2.89) yields

$$F_{AN1}(f) = \frac{dT}{2} e^{j\theta_0} \mathrm{sinc}\left[(f-f_c)\,dT\right] \cdot \left\{ A \sum_{i=1}^{N_p} e^{-j2\pi(f-f_c-f_s)(i-1)T} \right.$$

$$\left. + \quad \Delta A \sum_{i=1}^{N_p} (i-1)\, e^{-j2\pi(f-f_c-f_s)(i-1)T} \right\} \tag{2.90}$$

The second summation simplifies to [14]

$$\sum_{i=1}^{N_p} (i-1)\, e^{-j2\pi(f-f_c-f_s)(i-1)T} = \frac{Z - N_p Z^{N_p} + (N_p-1)Z^{N_p+1}}{(1-Z)^2} \tag{2.91}$$

where

$$Z = e^{-j2\pi(f-f_c-f_s)T}$$

Thus using Eq. (2.91), Eq. (2.90) becomes

$$F_{AN1}(f) = \frac{dT}{2} e^{j\theta_0} \mathrm{sinc}\left[(f-f_c)\,dT\right] \cdot \left\{ A \frac{1-Z^{N_p}}{1-Z} + \Delta A \frac{Z - N_p Z^{N_p} + (N_p-1)Z^{N_p+1}}{(1-Z)^2} \right\} \tag{2.92}$$

The power spectral density $S_{AN1}(f)$ can be calculated by performing the squared magnitude of $F_{AN1}(f)$ represented by Eq. (2.92).

Figure 2.32 illustrates the spectrum for the ELT signal with carrier frequency equal to 15 kHz and shifting frequency $f_s = 600\,Hz$. We choose ΔA equal 10% of the actual value of amplitude A. From this figure, we note that the sidebands are reduced and become smoother as compared to the spectrum depicted in Fig. 2.14.

Case 2 Linearly Varying Duration T

In this case, we have T_i as given by Eq. (2.35) and $\Delta\theta_i$ as represented by Eq. (2.53).

$$T_i = T + (i-1)\Delta T, \quad i = 1, 2, ..., N_p$$

Substituting from Eqs. (2.35), (2.37) and (2.53) into Eq. (2.87) yields

$$F_{AN2}(f) = \sum_{i=1}^{N_p} \frac{A_i d}{2} [T + (i-1)\Delta T] \operatorname{sinc}[(f-f_c)d(T + (i-1)\Delta T)]$$

$$\cdot \exp\left\{-j2\pi(f-f_c-f_s)\left[(i-1)T_{EQ} + \frac{(i-1)(i-2)}{2}\Delta T\right]\right\} e^{j\theta_0} \tag{2.93}$$

Substituting from Eq. (2.80) into Eq. (2.93), we have

$$F_{AN2}(f) = \sum_{i=1}^{N_p} \frac{d}{2} [A + (i-1)\Delta A][T + (i-1)\Delta T] \operatorname{sinc}[d(f-f_c)(T + (i-1)\Delta T)]$$

$$\cdot \exp\left\{-j2\pi(f-f_c-f_s)\left[(i-1)T_{EQ} + \frac{(i-1)(i-2)}{2}\Delta T\right]\right\} e^{j\theta_0} \tag{2.94}$$

Equation (2.94) represents the Fourier transform of N_p pulses. The pulse duration and amplitude increase linearly with respect to the pulse number N_p.

Figure 2.33 depicts the power spectral density $S_{AN2}(f)$ obtained by square magnitude of $F_{AN2}(f)$ given by Eq. (2.94). From this figure, it is clear that the sidebands are reduced. Furthermore, the carrier peak component remains stationary and very sharp.

2.5.5 Varying Amplitude and Carrier Frequency

In this case, each pulse in the sweep is modulated by a different carrier frequency and also by a different amplitude. Thus, we have

$$s(t) = \sum_{i=1}^{N_p} s_i(t)$$

where

$$s_i(t) = A_i \operatorname{Re}\left\{e^{j(2\pi f_{ci}t + \theta_0)}\right\}, \quad t_i - \frac{dT_i}{2} \le t \le t_i + \frac{dT_i}{2}$$

$$= 0 \quad , \quad \text{otherwise} \tag{2.95}$$

We see that the Fourier transform representation of N_p pulses is given by
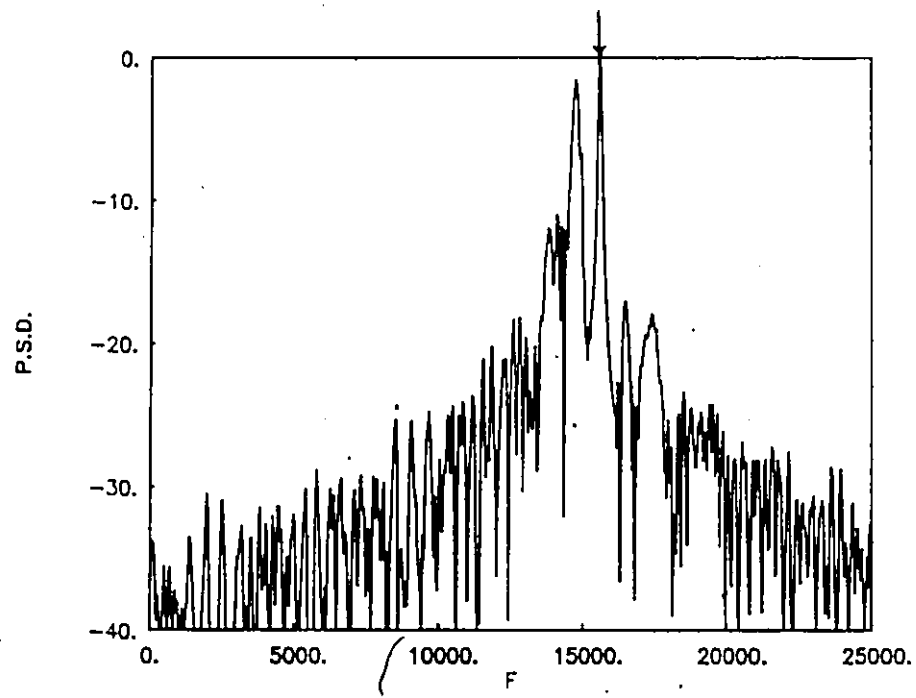
Fig. 2.33   Plot of $S_{AN2}(f)$ with $N_p = 10$ pulses, $f_s = 600$ Hz, $\Delta T = 100$ µs and $\Delta A = 0.1$ A.

$$F_{AF}(f) = \sum_{i=1}^{N_p} \frac{A_i d\,T_i}{2} \operatorname{sinc}[(f-f_{ci})\,d\,T_i] e^{-j2\pi(f-f_{ci})t_i} e^{j\theta_0} \tag{2.96}$$

Case 1 <u>Constant Duration T</u>

For this case, we have

$$T_i = T, \qquad i = 1, 2, ..., N_p \tag{2.97}$$

and

$$t_i = (i-1)T, \quad i = 1, 2, ..., N_p$$

Now, the carrier frequency increases linearly with respect to the pulse number N_p.

Thus,

$$f_{ci} = f_c + (i-1)\Delta F \tag{2.98}$$

If we consider that the amplitude A_i increases linearly with respect to the pulse

number N_p as given by Eq. (2.80).

Thus, substituting from Eqs. (2.80), (2.97) and (2.98) into Eq. (2.96) yields

$$F_{AF1}(f) = \sum_{i=1}^{N_p} \frac{dT}{2} [A + (i-1)\Delta A] \cdot \operatorname{sinc}[((f-f_c - (i-1)\Delta F)dT]$$

$$\cdot \exp\left\{-j2\pi\left[(f-f_c - (i-1)\Delta F)(i-1)T\right]\right\} e^{j\theta_0} \tag{2.99}$$

The spectrum $S_{AF1}(f)$ is given by

$$S_{AF1}(f) = \left| F_{AF1}(f) \right|^2$$

Case 2 <u>Linearly Varying Duration T</u>

In this case, we consider

$$T_i = T + (i-1)\Delta T, \qquad i = 1, 2, ..., N_p$$

$$t_i = (i-1)T_{EQ} + \frac{(i-1)(i-2)}{2}\Delta T, \qquad i = 1, 2, ..., N_p \tag{2.100}$$

Substituting from Eqs. (2.80), (2.98) and (2.100) into Eq. (2.96), we have

$$F_{AF2}(f) = \sum_{i=1}^{N_p} \frac{d}{2} \left[A + (i-1)\Delta A \right] \cdot \left[T + (i-1)\Delta T \right]$$

$$\cdot \quad sinc\left[(f-f_c - (i-1)\Delta F)\, d\,(T + (i-1)\Delta T) \right]$$

$$\cdot \quad exp\left\{ -j2\pi\,(f-f_c - (i-1)\Delta F)\left[(i-1)T_{EQ} + \frac{(i-1)(i-2)}{2}\Delta T \right] \right\} e^{j\theta_0} \qquad (2.101)$$

By performing the squared magnitude of $F_{AF2}(f)$ given by Eq. (2.101), we get the power spectral density $S_{AF2}(f)$.

2.5.6   General Model for ELT Signals

In this case, we consider each pulse in the sweep is modulated by a different amplitude, different carrier frequency and has additional phase shift $\Delta\theta_i$. Thus we have

$$s(t) = \sum_{i=1}^{N_p} s_i(t) \qquad (2.102)$$

where

$$s_i(t) = A_i R_e\left\{ e^{j(2\pi f_{ci}t + \theta_0 + \Delta\theta_i)} \right\}, \quad t_i - \frac{dT_i}{2} \le t \le t_i + \frac{dT_i}{2}$$

$$= 0 \qquad\qquad , \quad o.w$$

As discussed before we see that the Fourier transform representation of N pulses is given by

$$F_G(f) = \sum_{i=1}^{N_p} \frac{A_i d\,T_i}{2} sinc[(f-f_{ci})\,dT_i]e^{-j[2\pi(f-f_{ci})t_i - \theta_0 - \Delta\theta_i]} \qquad (2.103)$$

Case 1 <u>Constant Duration T</u>

For this case substituting from Eqs. (2.28), (2.31), (2.50), (2.71) and (2.80) into Eq. (2.103) yields

$$F_{G1}(f) = \frac{dT}{2} e^{j\theta_0} \sum_{i=1}^{N_p} [A + (i-1)\Delta A] \cdot sinc[(f - f_c - (i-1)\Delta F)dT] \tag{2.104}$$

$$\cdot \exp\{-j2\pi[(f - f_c - (i-1)\Delta F - f_s)(i-1)T]\}$$

The spectrum $S_{G1}(f)$ is given by

$$S_{G1}(f) = \left| F_{G1}(f) \right|^2$$

Case 2 <u>Linear Varying Duration T</u>

In this case substituting from Eqns. (2.35), (2.37), (2.53), (2.71), and (2.80) into Eq. (2.103) yields

$$F_{G2}(f) = \sum_{i=1}^{N_p} \frac{d}{2} [A + (i-1)\Delta A] \cdot [T + (i-1)\Delta T]$$

$$\cdot \quad sinc[(f - f_c - (i-1)\Delta F)d(T + (i-1)\Delta T)]$$

$$\cdot \quad \exp\{-j2\pi[(f - f_c - (i-1)\Delta F - f_s)][(i-1)T_{EQ} + \frac{(i-1)(i-2)}{2}\Delta T]\} \tag{2.105}$$

$$e^{j\theta_0}$$

The spectrum $S_{G2}(f)$ is obtained by performing the square magnitude of $F_{G2}(f)$ given by Eq. (2.105).

2.6   Proposed Models

We have demonstrated that many unusual spectra are produced by the different imperfections in the ELT signal parameters with the simple pulse modulation. Now, we propose two signal designs which still provide the desired modulation for manual detection of signals, but in addition offer spectral properties more suited to automatic detection in a crowded frequency band.

2.6.1   Model No. 1

The most popular type of ELT signal is the pulse-wave amplitude modulated signal, because of the simplicity with which it can be generated. This type of ELT signal produces a host of sidebands in addition to the carrier component.

In this section we study the averaged spectrum for an ideal coherent pulse-modulated ELT signal. Figure 2.34 illustrates the general block diagram for generating this model of signal and Fig. 2.35 depicts the averaged spectrum of a pulse-wave modulated ELT signal with carrier frequency equal to 15 kHz. This spectrum is the optimum that can exist for this type of ELT signal. From this figure we note that: 1) a sharp distinct peak occurs at the carrier frequency, this peak being the carrier component; 2) the 1st upper and lower sidebands are symmetric in amplitude around the carrier component, and 3) there is an undesirable background due to the higher order sidebands. These sidebands create false peaks in the presence of noise and can mask the carrier component of the ELT signal.

Now, we describe two proposed models with nearly ideal spectral properties. These models produce spectra which reduce the background considerably leaving essentially only the carrier peak and the first upper and lower sidebands.

2.6.2   1st Proposed Model

For this proposed model rather than using pulse amplitude modulation we use sinusoidal modulation. Figure 2.36 illustrates the block diagram used for generating this model. For the case of sinusoidal modulation, the ELT signal can be represented mathematically in the form

$$s(t) = A[1 + m(t)] \cos[2\pi f_c t + \theta_\theta] \qquad (2.106)$$

where $m(t)$ = the modulating signal can be written as

$$m(t) = \mu \cos(\omega_m t) \qquad (2.107)$$

Switch

Crystal Oscillator

filter

tuned power amplifier

sweep pulse generator

antenna
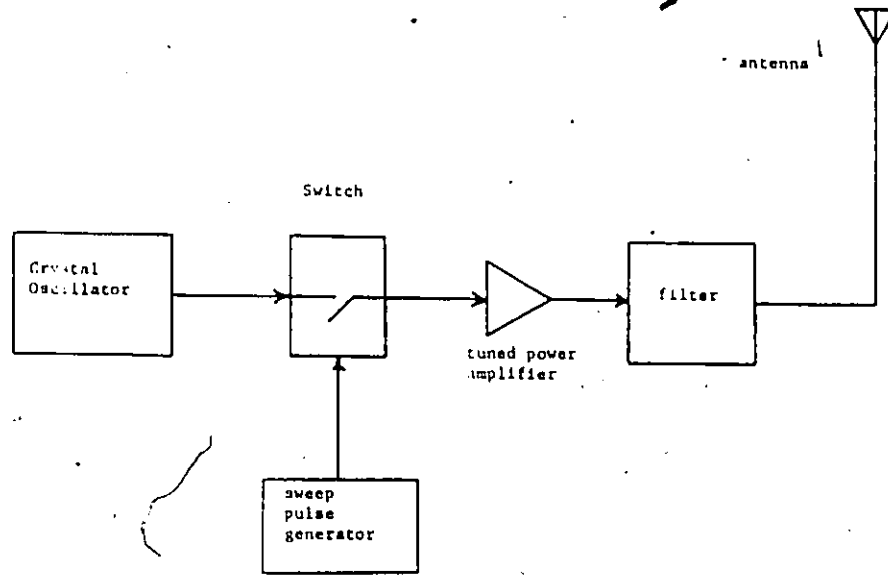
Fig. 2.34   Block diagram for generating Model No.1 of ELT signals.
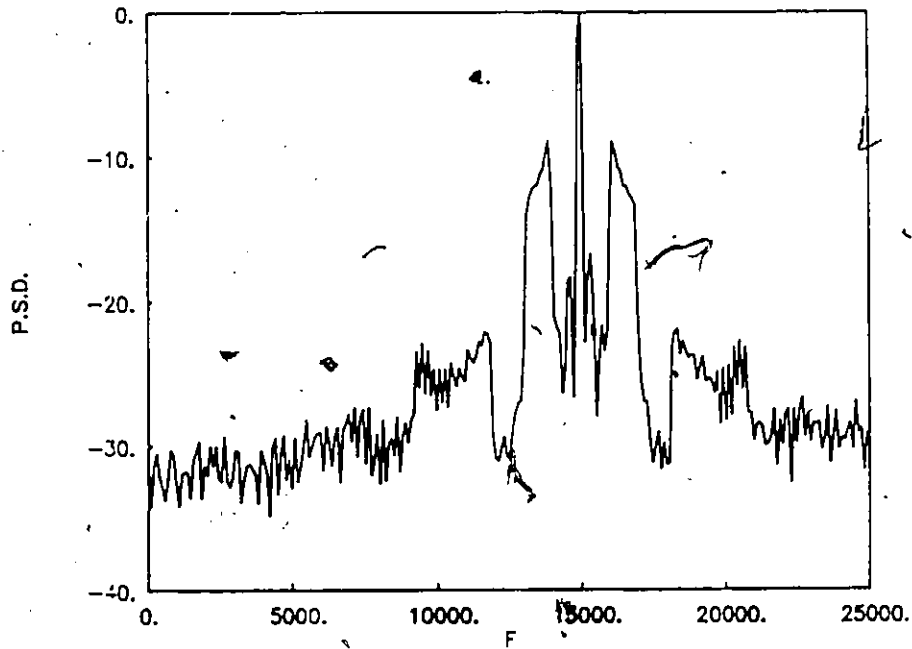
Fig. 2.35   The averaged spectrum for the ELT signal obtained using Model No.1.
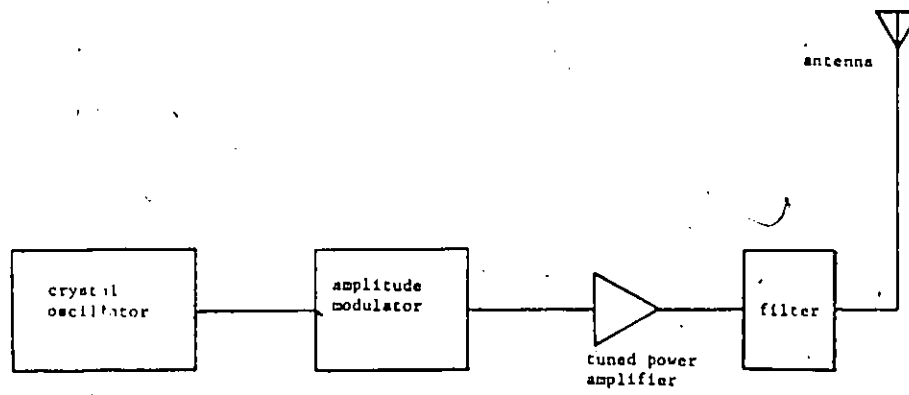
Fig. 2.36   Block diagram for the 1st proposed model.
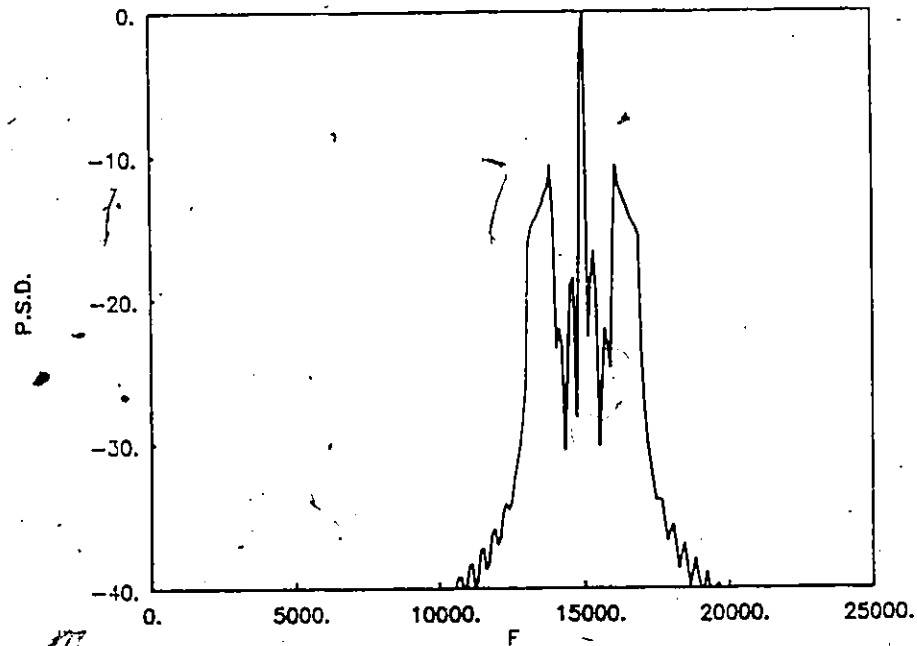
Fig. 2.37   The averaged spectrum for the ELT signal obtained using the 1st proposed model.

where

$\mu =$ modulation factor

$\omega_m = 2\pi f_m$

where

$f_m =$ constant modulating signal frequency

Thus

$$s(t) = A\{1 + \mu \cos(2\pi f_m t)\} \cdot \text{Re} \left\{ e^{j(2\pi f_c t + \theta_0)} \right\} \qquad (2.108)$$

Figure 2.37 depicts the averaged spectrum of sinusoidal modulated ELT signal with carrier frequency equal to 15 kHz. From this figure it is seen that: 1) A sharp peak occurs at the carrier frequency, this peak being the carrier component peak; 2) the 1st upper and lower sidebands around the carrier peak, are symmetric in amplitude; and 3) the higher order upper and lower sidebands are reduced due to the absence of nulls between pulses of the signal.

2.6.3   2nd Proposed Model

For this model, a pulse-amplitude modulated ELT signal is used. This type of signal is more popular because of the simplicity with which it can be generated, namely, modulating a carrier with a string of pulses and passing the ELT signal through a bandpass filter with bandwidth equal to 6 kHz. Since the carrier frequency of the ELT signal is 121.5 MHz, the design of this bandpass filter with center frequency of 121.5 MHz and a bandwidth of 6 kHz which is difficult due to the high quality factor $\{(121.5 \times 10^6)/(6 \times 10^3) = 20250\}$.

Thus, the idea is to design a new ELT signal with carrier frequency in the range of 3 MHz to 5 MHz and feed this signal through the bandpass filter with bandwidth equal to 6 kHz which can be implemented easily in practice. After the ELT signal is mixed to a carrier

frequency equal to 121.5 MHz. Figure 2.38 gives the general block diagram for this second proposed model.

Figure 2.39 illustrates the averaged spectrum for pulse-wave modulated ELT signal·using the second proposed model. This signal has a carrier frequency of 15 kHz. Comparing this spectrum with that depicted in Fig. 2.35 obtained using Model No. 1, we note that the background sidebands are rejected. Figure 2.40 depicts the comparison between all spectra obtained using Model No. 1, 1st proposed model, and 2nd proposed model. From these results it is seen that the 1st and 2nd proposed models produce spectra with nearly ideal spectral properties.
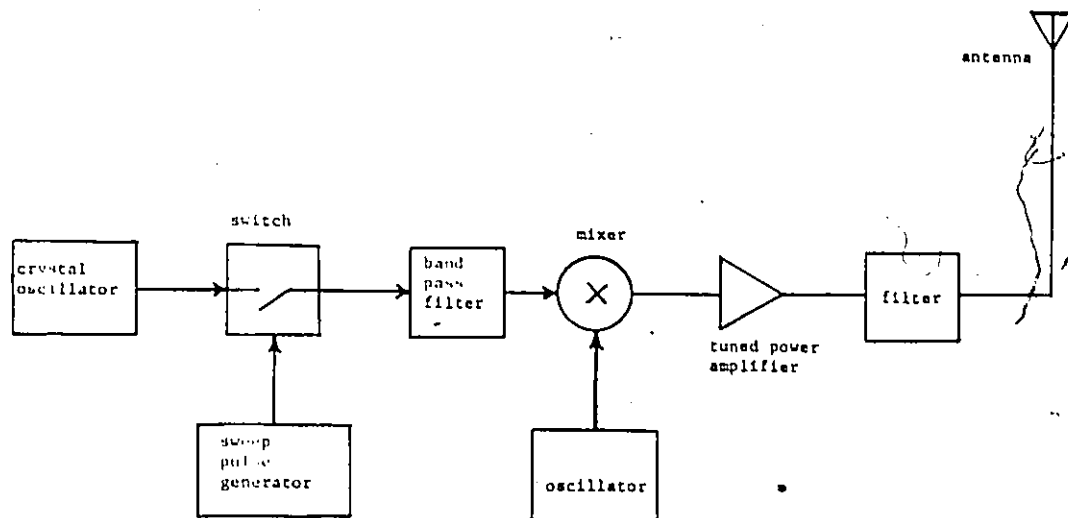
Fig. 2.38　　· Block diagram for the 2nd proposed model.
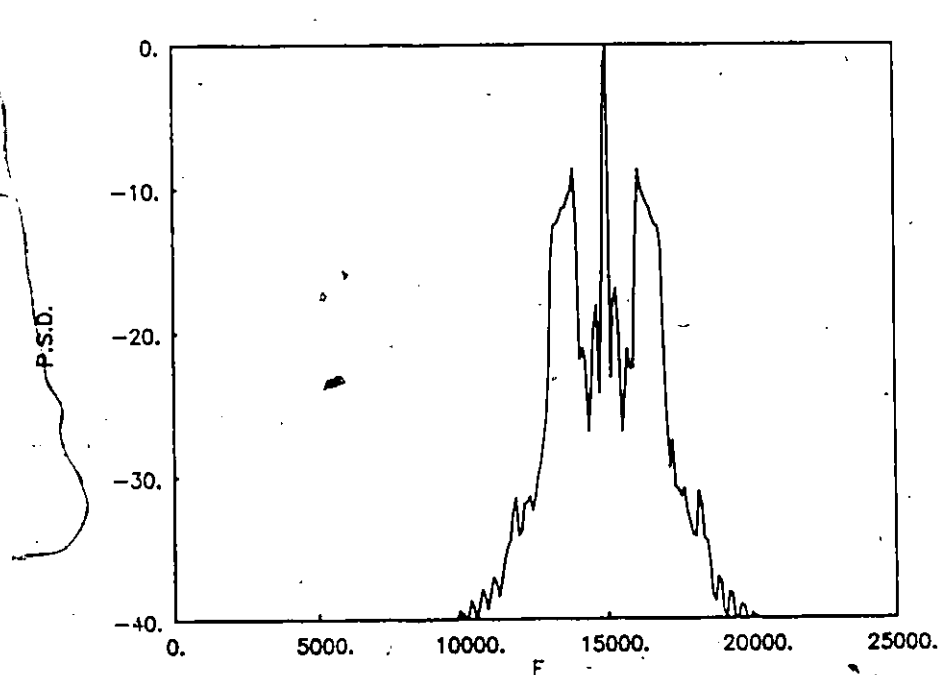
Fig. 2.39　　The averaged spectrum for the ELT signal obtained using the 2nd proposed model.
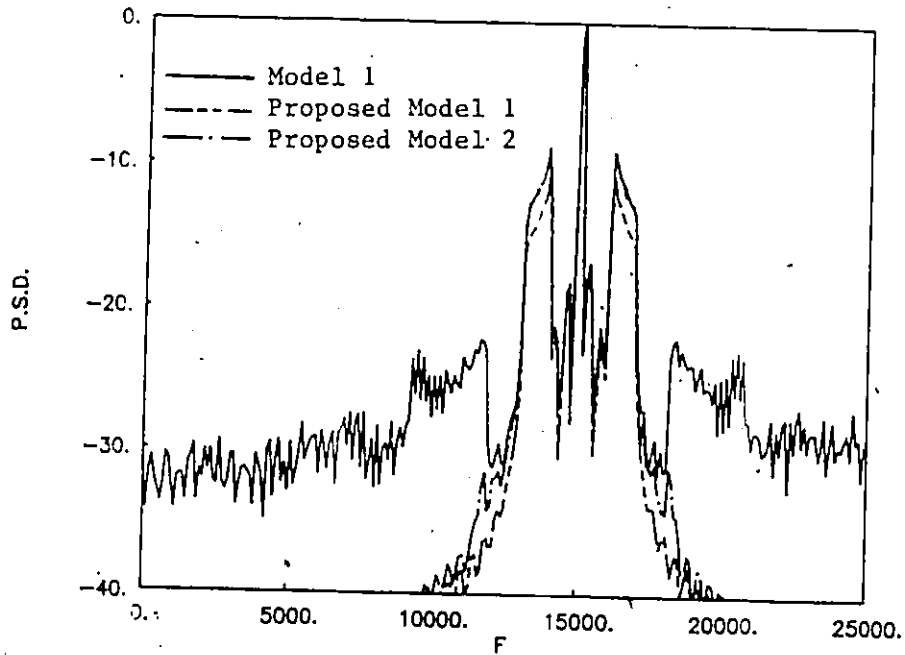
Fig. 2.40 Comparison between the averaged spectrum for the ELT signal obtained from all models.

2.7   Summary

The probability of locating the downed aircraft is closely related to the quality of the ELT signal itself. Thus the main consideration is the characteristics of the spectrum of the ELT signal. In this chapter different models for ELT signals have been developed. Furthermore, the spectral properties for these models have been discussed. The first model is the ideal coherent model ELT signal. This model produces a highly idealized spectrum which is not found to exist in practice. Consequently, non-ideal ELT signal models have been developed and analysed. These models include:

1)   phase imperfection

2)   carrier frequency imperfection

3)   amplitude imperfection

4)   combinations of 1), 2), and 3).

From the above analysis we note that: poor design strategy in the modulation or even small imperfections in the signal can lead to disastrous results. For instance, if the oscillator has constant carrier frequency but is switched on and off in order to generate the signal, then a random phase shift on each pulse of the signal is produced and no peak in the spectrum at the carrier frequency is obtained. If the carrier frequency is constant but each pulse in the signal has a small phase shift, then an interaction between the phase shift and the modulation can occur which produces a null in the spectrum at the carrier frequency. This null can exist for an appreciable part of the sweep and greatly reduces the probability of detection.

Finally, new models for ELT signals are proposed which provide signals with greatly improved spectral characteristics.

CHAPTER 3

A BASEBAND PROCESSOR

FOR SARSAT SIGNALS

3.1   Introduction

In this chapter we review briefly the thoery of the signal processing methods used for spectral estimation. These methods can be classified as linear and non-linear. Linear spectral estimation methods include the matched filtering, the periodogram and the averaged periodogram. The non-linear spectral estimation methods include the maximum entropy method (MEM) and the averaged MEM. The advantages and disadvantages of these methods as applied for SARSAT signals are presented. A new baseband processor for processing the distress ELT signals is developed. We also study in this chapter the problem of minimum detectable signal. A comparison is made between the periodogram and matched filtering techniques. A minimum detectable level of the carrier-to-noise density ratio (CNDR) has been theoretically developed. These theoretical results are verified by using computer simulation.

3.2.   Signal Processing Methods

The main element in the earth station is a digital signal processor whose function is to detect and measure the carrier frequency of the ELT signals relayed by satellite. Digital signal processing techniques are used for this application because of the very unusual performance requirements imposed by the system.

In order to have an accurate estimation of the crash site, it is important to measure the Doppler shift information contained in the ELT carrier frequency. This measurement is strongly dependent on the effectiveness of the signal processing methods.

3.2.1   Spectral Density Estimation Techniques

In this-section, two different types of spectral density estimation procedures have been used for estimating the power spectral densities for the ELT signals: first, the linear spectral estimation methods. These methods including, the matched filter [15], the periodogram (FFT) [16,17,18] and the averaged periodogram. The second type is the non-linear spectral estimation. These methods are the maximum entropy method (MEM) [19-25], and the averaged MEM [26].

3.2.2   Linear Spectral Estimation

This section gives a brief review of the linear spectral estimation methods. The advantages and disadvantages of each method as applied for SARSAT signals are also presented.

3.2.2.1   Matched Filtering

It is well known that the matched filter receiver provides the highest signal-to-noise ratio at its output of all receivers. It is also possible to use the matched filters for spectral estimation [15]

In order to explain this form of detection, we provide an example requiring the formulation of a matched filter.

Consider the situation where we have a transmitted signal $s_i(t)$ $\{i = 0,1...,N_F - 1\}$ corresponding to a message M_i $(i = 0,1,...N_F - 1)$ which occurs with probability $p[m_i]$. Let the signal $s_i(t)$ be defined by:

$$s_i(t) = \begin{cases} A\cos(2\pi f_i t), & 0 \le t \le T \\ 0, & \text{otherwise} \end{cases} \tag{3.1}$$

It can be shown [15] that the optimum receiver is realized in the form of Fig. 3.1, where $s_i(T-t)$ is a filter whose impulse response is a delayed, time reversed version of the signal $s_i(t)$. The filters $s_i(T-t)$ are said to be matched to the original signal $s_i(t)$, i.e. the impulse response of the optimum system is the mirror image of the desired message signal $s_i(t)$, delayed by an interval T.

If the received signal is given by:

$$y_R(t) = s(t) + n(t) \tag{3.2}$$

Then the input to the decision box is:

$$\int_{-\infty}^{\infty} y_R(t)\, s_i(t)\, dt + C_i \tag{3.3}$$

where the term C_i is independent of time but dependent on the variance of noise process ($N_0/2$), the a-priori probabilities $p[m_i]$ and the energy of the ith signal E_i, Thus,

$$C_i = \frac{1}{2}\left[N_0\, \ell n\, p[m_i] - E_i\right] \tag{3.4}$$

The 'Select Largest Of' chooses the largest output from the N_F matched filters and identifies this as message M_i, which is the estimate of the received message.

The advantage of using this method is that, matched filterig is the optimum form of receiver realization.

The disadvantage of this method is that each type of ELT signal would require a receiver with the set of filters $s_i(T-t)$ matched to that signal at frequencies f_i. Considering the
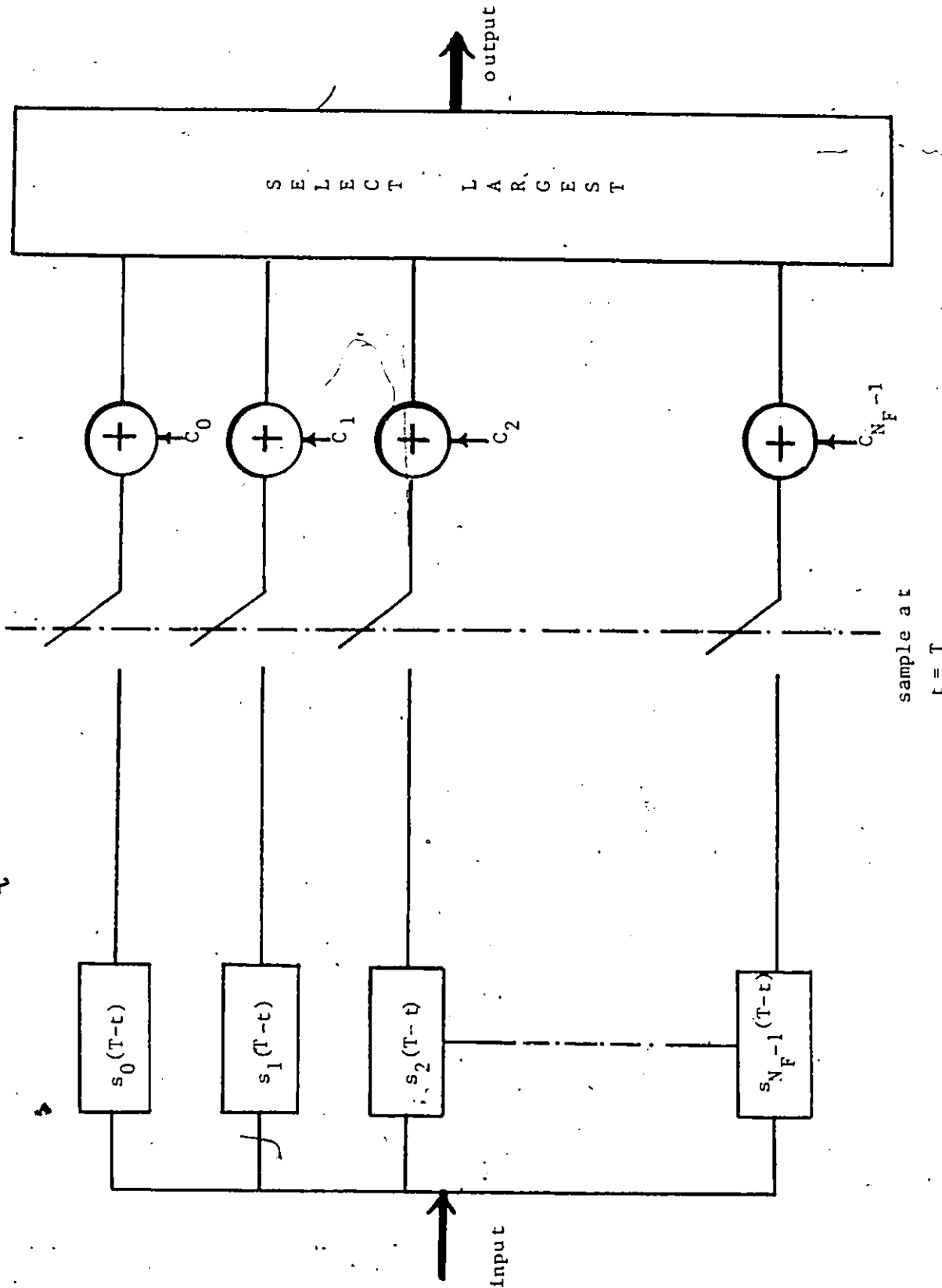
Fig. 3.1   An optimum receiver with N_F matched filters.

variety of ELT's in use at present, with each type transmitting a different kind of signal, the required receiver structure would be very complex and expensive.

In order to calculate the number of matched filters required in this case, consider that each matched filter covers a bandwidth B_F. Thus, the total number of filters required is simply

$$N_F = \frac{B}{B_F} \tag{3.5}$$

where

$\quad B \;=\;$ total bandwidth of the signal spectrum

$\quad N_F \;=\;$ number of matched filters.

3.2.2.2 Periodogram (FFT)

The fast Fourier transform (FFT) is a computational tool which facilitates signal analysis such as power spectrum analysis by means of digital computer. It is a method for efficiently computing the discrete Fourier transform of a series of data samples [16,17,18].

The discrete Fourier transform (DFT) of a given finite length sequence $\{u(n)\}$, where $0 \leq n \leq N-1$ is given by

$$U(k) = \sum_{n=0}^{N-1} u(n)\, e^{-j\frac{2\pi nk}{N}}, \quad k=0,1,...,N-1 \tag{3.6}$$

To solve this equation, N^2 complex multiplications and $N(N-1)$ complex additions are necessary to perform the required matrix computation. For reasonably large values of N, direct evaluation of an N-point DFT requires a large amount of computation. The FFT owes its success to the fact that the algorithm reduces the number of multiplications and additions required in the computation of Eq. (3.6). For $N = 2^m$, where m is an interger, the FFT

algorithm is simply a procedure for factoring an $N \times N$ matrix into m matrices (each $N \times N$) such that each of the factored matrices has the special property of minimizing the number of complex multiplications and additions. The FFT requires $(N/2)\log_2 N$ complex multiplications and Nm complex additions, whereas in comparison with the number of operations required for the calculation of the DFT coefficients with straightforward procedures, it is seen that the FFT algorithm reduces the total number of computations. If we assume that the computing time is proportional to the number of multiplications, then the approximate ratio of direct method to FFT computing time is given by

$$\frac{N^2}{\frac{N}{2} \log_2 N} = \frac{2N^2}{Nm} = \frac{2N}{m} \tag{3.7}$$

For $N = 1024 = 2^{10}$ samples, the computational reduction is more than 200 to 1.

The advantage of the FFT is that the spectral density can be calculated by performing the squared magnitude of the FFT of a given time sequence. This technique is usually referred to as the periodogram.

Since the Fourier transform of the real finite-length sequence $u(n)$, $0 \leq n \leq N-1$, is

$$U(f) = \sum_{n=0}^{N-1} u(n) e^{-j2\pi fn} \tag{3.8}$$

The spectrum estimate $I_N(f)$, which is defined by

$$I_N(f) = \frac{1}{N} \left| U(f) \right|^2 \tag{3.9}$$

is called the periodogram.

The advantages of the periodogram technique are that[26]:

1)   it is computatonally efficient when the FFT algorithm is employed;

2)   the power spectral density (PSD) estimate is directly proportional to the power for

         sinusoid processes; and

3)   the method gives good performance for ideal coherent ELT signals (within 2.6 to 4.8 dB of that provided by matched filtering as will be shown later).

The disadvantages include:

1)   degraded performance when the ELT signal is non-ideal. For poor quality signals, such as the non-coherent ELT signal, no estimate of carrier frequency is obtained;

2)   the performance is affected by the Doppler frequency shift due to satellite motion. Whereas a phase lock loop can actually adjust for a change of frequency, the FFT smears the energy over adjacent frequency bins which reduces signal-to-noise ratio;

3)   windowing the data is required in order to avoid the sidelobe problem. Of course, this broadens the carrier peak resulting in reduced resolution;

4)   the resolution is limited to about the reciprocal of the window length; and

5)   the variance of the estimate does not decrease with increasing window length.

3.2.2.3   Averaged Periodogram

The first estimator to be used is the periodogram. The variance of the spectral estimation using the periodogram method does not decrease as the length of the data increases. High variance of spectral estimate leads to an unsmoothed spectrum.

One method used for reducing the variance of the power spectrum estimate is known as segmental averaging, which is called the Bartlett method. In this method, the data record is divided into a number of blocks covering different time intervals, and then calculates the periodogram of individual segments of the data record. These periodograms are then averaged [17].

Bartlett's Procedure

The approach used for reducing the variance of the power spectrum estimates involves sectioning the record, taking the periodograms of these sections, and averaging these periodograms. In this approach, a data sequence u(n), n = 0,1,2,...,N–1, is divided into K segments each with P points covering consecutive time intervals. Thus

$$N = KP$$

To form the segments, we let $u_1(n)$, n = 0,1,..., P−1 be the first segment. Then

$$u_1(n) = u(n), \qquad n = 0,1,...,P-1$$

similarly

$$u_2(n) = u(n + P), \qquad n = 0,1,...,P-1$$

and the Kth segment is given by

$$u_K(n) = u(n + (K-1)P), \qquad n = 0,1,...,P-1 \qquad (3.10)$$

In general,

$$u_i(n) = u(n + (i-1)P), \qquad n = 0,1,...,P-1 \qquad (3.11)$$
$$i = 1,2,...,K$$

We suppose we have K such segments, $u_1(n)$, $u_2(n)$, $u_3(n)$, ..., $u_K(n)$, and then calculate the K periodograms.

$$I_{P_i}(f) = \frac{1}{P} \left| \sum_{n=0}^{P-1} u_i(n) e^{-j2\pi fn} \right|^2, \quad i=1,2,...,K \qquad (3.12)$$

The spectral estimate is the average of these periodograms, i.e.

$$B_{xx}(f) = \frac{1}{K} \sum_{i=1}^{K} I_{P_i}(f) \qquad (3.13)$$

Therefore,

$$\mathrm{Var}[B_{xx}(f)] = \frac{1}{K} \cdot \mathrm{Var}[I_{P_i}(f)] \qquad (3.14)$$

From Eq. (3.14), it is clear that, if we average over K segments, we can obtain a reduction of the variance by the factor K, and as K increases, the variance approaches zero. For a fixed record length, as the number of periodograms, K, increases, the variance decreases but the number of sample points, P, decreases; therefore, the spectrum resolution decreases. Thus, there is a tradeoff between spectrum resolution and the variance of the estimate in the Bartlett procedure.

The advantages of averaging the periodograms are [26]:

1) the variance due to sidebands and noise are reduced which give a smooth spectrum estimate;

2) the main carrier peak is sharp and stationary while the sidebands become broad which can be used to identify ELT signals; and

3) good performance is obtained for ideal coherent ELT signals.

The disadvantages include:

1) poor performance for non-coherent ELT signals;

2) sidebands are integrated to produce wide bands of interference for other signals;

3) averaging tends to further broaden the carrier peaks which in turn reduces resolution and

4) averaging blocks of spectra provides only small improvements in signal-to-noise ratio. Nevertheless the averaged periodogram is an important spectral estimator for SARSAT signals.

3.2.3   Non-linear Spectral Estimation

3.2.3.1   Maximum Entropy Method

Some of the problems encountered with the periodogram can be resolved by employing the maximum entropy method (MEM) of spectral estimation. For example, the resolution of MEM is not restricted by window length (as is the case for the periodogram), and carrier frequency estimates can be obtained for non-coherent signals. The MEM has the useful property that when employed to estimate the power at one frequency, it adjusts itself to be least disturbed by power at other frequencies.

We provide a short discussion of a simple procedure for MEM spectral estimation of a set of complex-valued weakly stationary time series $\{u_n\}$ of zero mean, where $n = 1, 2, ..., N$, with equal sample spacing Δt.

The MEM power spectrum $S(f)$ of the given time series is estimated by using the formula [19,25].

$$S(f) = \frac{P(M)}{2B \left[1 + \sum_{m=1}^{M} a(M, m) \exp(-j2\pi m f \Delta t)\right]^2} \tag{3.15}$$

where

B   = the bandwidth of the signal.

Δt = the sampling time.

       = 1/2B for Nyquist rate sampling.

M   = the order of prediction error filter.

P(M)   = ouput power of a prediction error filter of order M.

a(M,m) = prediction error filter coefficients (m = 1, 2, ..., M)

The prediction error filter coefficients, as proposed by Burg, are estimated recursively using Levinson recursion [20]. In this case the problem is equivalent to one of determining the prediction error filter coefficients, which are related to the prediction filter coefficients, and minimizing the total prediction-error power, P(M). The output power P(M) and the corresponding values of filter coefficients a (M,m) are determined by solving this equation [20-25].

$$\sum_{k=0}^{M} a(M,k) R_u(m-k) = \begin{cases} P(M), & m=0 \\ 0, & m=1,2,\ldots,M \end{cases} \tag{3.16}$$

where $R_u(\cdot)$ is the autocorrelation function for the stationary process $\{u(n)\}$. Since the autocorrelation matrix is Toeplitz, the Levinson algorithm applies. The parameter $a(M,k)$ is the kth coefficient for the prediction error filter of order M. The values of these coeffiecients can be determined by employing the Levinson's recursion formula

$$a(M,k) = a(M-1,k) + a(M,M) \cdot a^*(M-1, M-k)$$

$$, k=0,1,2,\ldots,M. \tag{3.17}$$

The parameter $a(M,k)$ has the following properties:

$$a(M,k) = \begin{cases} 1, & k=0 \\ 0, & k>M \end{cases} \tag{3.18}$$

From eq. (3.17) and eq. (3.18) it is clear that, we have obtained the coefficients of prediction error filter of order M from an $(M-1)^{st}$ order filter in such way as to minimize the total prediction-error power. Assume we have obtained the coefficients of a prediction error filter of order $M-1$ and the corresponding prediction error power $P(M-1)$. In order to calculate the parameters for the next higher filter order (that is order M), the output power P(M) is expressed as the average power resulting from forward and backward prediction error power, given by [23].

$$P(M) = \frac{1}{2}\left[P_f(M) + P_b(M)\right]$$

(3.19)

$$= \frac{1}{2(N-M)} \sum_{n=M+1}^{N} \left[\left|f_M(n)\right|^2 + \left|b_M(n)\right|^2\right]$$

where N is the total number of data points and $f_M(n)$ and $b_M(n)$ are the forward and backward prediction-errors respectively, given by

$$f_M(n) = u(n) + \sum_{k=1}^{M} a(M,k)\,u(n-k)$$

and

$$b_M(n) = u(n-M) + \sum_{k=1}^{M} a^*(M,k)\,u(n-M+k)$$

(3.20)

and

$$n = M+1, M+2, \ldots, N$$

Introducing the recursions, derived using Eq. (3.17) and Eq. (3.20), we have

$$f_M(n) = f_{M-1}(n) + a(M,M)\cdot b_{M-1}(n-1)$$

$$b_M(n) = b_{M-1}(n-1) + a^*(M,M)\cdot f_{M-1}(n)$$

(3.21)

substituting from Eq. (3.21) into Eq. (3.19) yields

$$P_M = \frac{1}{2(N-M)} \sum_{n=M+1}^{N} \left\{\left[f_{M-1}(n) + a(M,M)\cdot b_{M-1}(n-1)\right]^2\right.$$

$$\left. + \left[b_{M-1}(n-1) + a^*(M,M)\cdot f_{M-1}(n)\right]^2\right\}$$

(3.22)

From equation (3.22) the unknown coefficient a(M,M), can be determined using the minimization criterion,

$$\frac{\partial P(M)}{\partial a(M,M)} = 0$$

(3.23)

This yields the optimum value of a (M, M) for which P(M) is minimum given by.

$$a(M,M) = \frac{-2 \sum_{n=M+1}^{N} f_{M-1}(n) \cdot b_{M-1}^{\bullet}(n-1)}{\sum_{n=M+1}^{N} \left\{ \left| f_{M-1}(n) \right|^2 + \left| b_{M-1}(n-1) \right|^2 \right\}} \qquad (3.24)$$

Solving Eqns. (3.17), (3.22) and (3.24) give the ouput power P(M) which is given by a simple expression as

$$P(\tilde{M}) = P(M-1) \left\{ 1 - \left| a(M, M) \right|^2 \right\} \qquad (3.25)$$

Thus, making use of Eqns. (3.17), (3.24) and (3.25), we have now calculated all the quantities necessary for evaluating the maximum entropy power spectral estimate given by Eq. (3.15). To see specifically how these results are used in actual computation we start with the prediction-error filter of zero-order (M = 0). For this value of M, we know that a(0) is equal to unity. Also we first estimate

$$P(0) = R_u(0) = \frac{1}{N} \sum_{n=1}^{N} \left| x(n) \right|^2 \qquad (3.26)$$

We increment the filter order by one, i.e. put M = 1, and reapply the above equations. Continue in repeating these procedures until the computation is terminated when we reach the prescribed order, M, for the prediction error filter. Having computed the complete set of prediction - error filter coefficients {a(M, k)}, k = 0, 1, . . . ,M, we next compute the maximum-entropy estimate of the power spectrum by using the formula of Eq. (3.15).

The main advantages of using the MEM for processing the ELT signal are that [26]:

1)   it does not require the use of a window function;

2)   the resolution of MEM is usually superior to that obtained by using conventional linear method;

3)   the MEM spectrum is smooth without averaging;

4)   good performance is obtained with low order MEM estimates when detecting the non-coherent ELT signal;

5)   near zero frequency the MEM spectral estimates are very accurate for all ELT signals; and

6)   MEM spectral estimates can be averaged to improve performance when noise is present.

The disadvantages include:

1)   high order MEM calculations are very time consuming for general purpose computers;

2)   low order MEM estimates may have a bias near minimum frequency and maximum frequency.

3.2.3.2   Averaged MEM

Averaging MEM spectral estimates improves the detection of a carrier peak in noise and reduces the undesired sideband peaks as in the case of the averaged periodogram. Although a theoretical justification for averaging the MEM estimates is not available, simulation results support the usefulness of the method.

3.3   Baseband System

Spectral analysis of the ELT signal is the central problem. An ELT is a low-powered emergency radio transmitter radiating about 100 mW with a pulse-amplitude-modulated signal having a carrier frequency of either 121.5 MHz or optionally 243 MHz. This ELT signal has total sweep between 0.25 s and 0.5 s, as illustrated in Fig. 3.2, and the signal
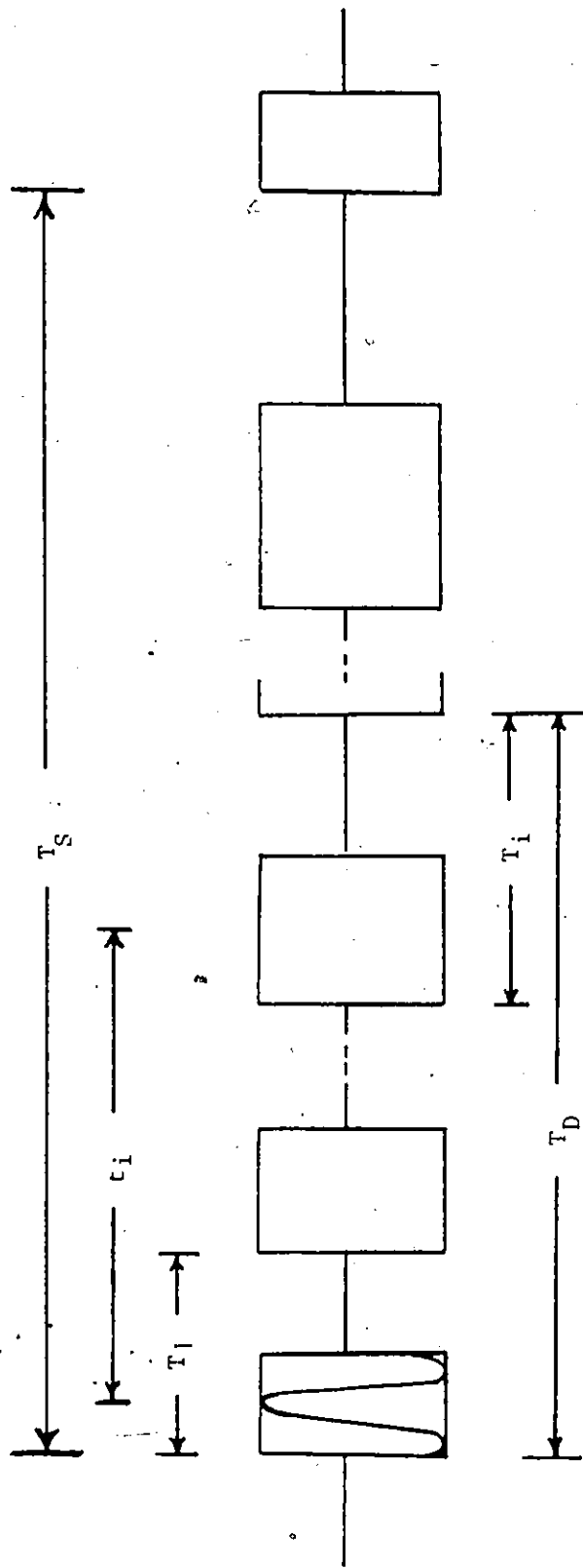
Fig. 3.2   Typical ELT signal.

repeats continuously. The pulse-shaped modulation can be classified either as coherent ELT signal, i.e. the phase from pulse to pulse is continuous as depicted in Fig. 3.3, or non-coherent ELT signal, where the phase from pulse-to-pulse is no longer related as shown in Fig. 3.4. (In both cases, the pulse modulated signals produce a carrier peak and host of sidebands generating potential interference).

To date, the ELT signals have been processed using the averaged periodogram in a bandpass processor implementation in which the signal is mixed to the frequency range from 0 to 25000 Hz [9,10,12,27,28]. In this chapter, we examine the processing of the ELT signals using the complex baseband equivalent of the signal. Baseband processing has certain advantages over bandpass processing including [26,29,30]:

1)   a portion of the spectrum can be analyzed at reduced sampling rate using only mixers and low-pass filters;

2)   detailed signal analysis can be performed for identification;

3)   rate reduction filtering can be implemented which leads to increased signal-to-noise ratio (SNR); and

4)   tracking of a signal is possible by adjusting the mixing frequency. Both, the linear periodogram method (FFT) and, the non-linear maximum entropy method (MEM) are evaluated.

3.3.1   Baseband ELT Signals

Figure 3.5 illustrates the overall block diagram of a complex baseband processor [26,29]. The ELT signal (Fig. 3.2) can be represented by a sinusoidal carrier wave that is

Time in ms.
COHERENT ELT SIGNAL
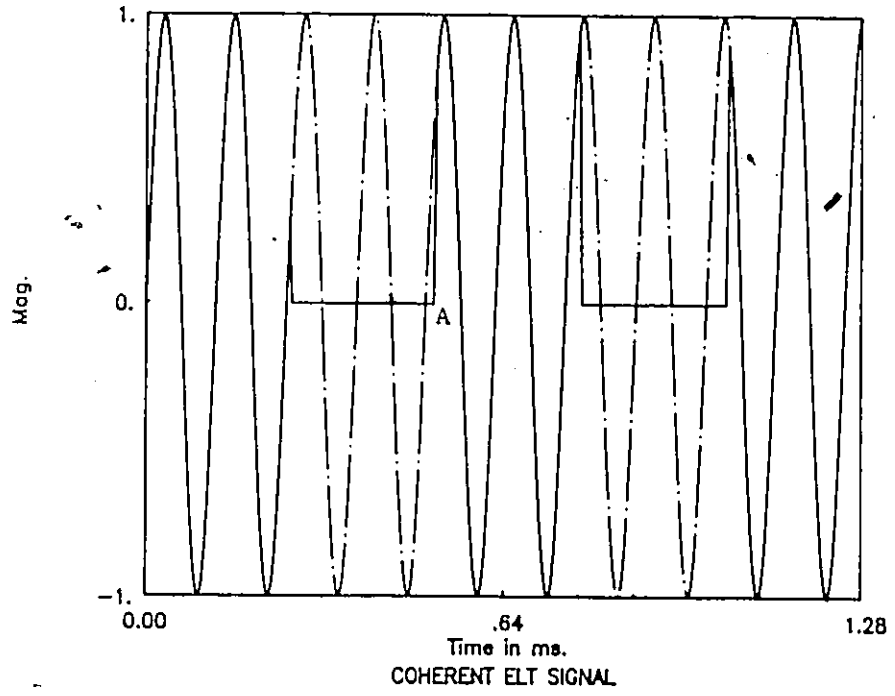
Fig. 3.3   Coherent ELT signal. Note phase continuity at point A.

Time in ms.
NON-COHERENT ELT SIGNAL
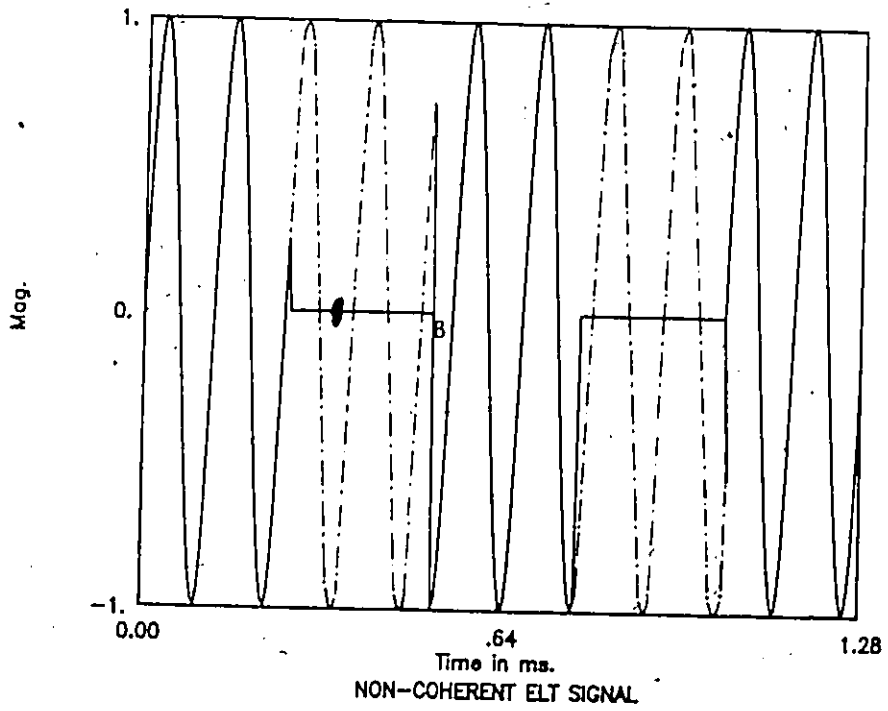
Fig. 3.4   Non-coherent ELT signal. Note phase discontinuity at point B.
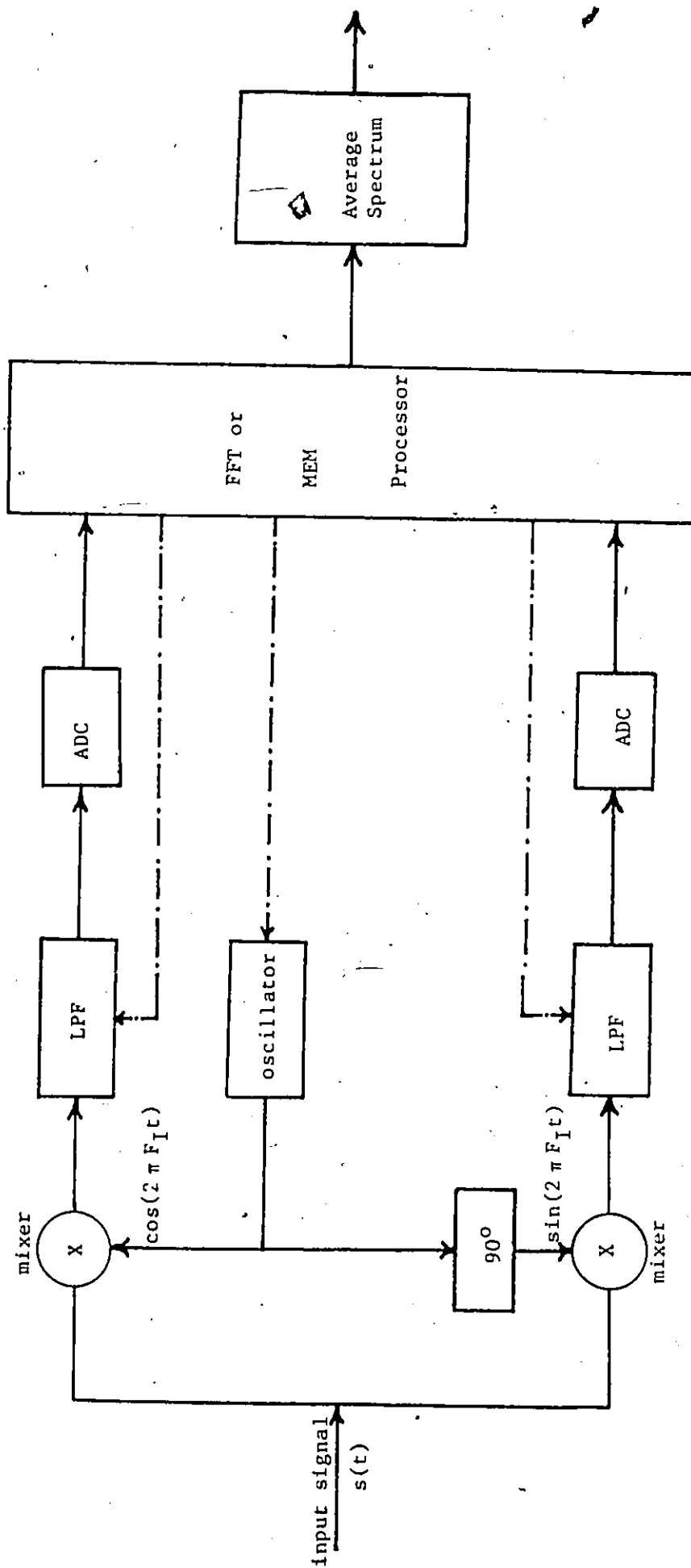
Fig. 3.5   Overall block diagram of complex baseband processor.

amplitude-modulated by a pulse train which has an increasing pulse period. The mathematical representation of this signal is given by

$$s(t) = A\, m(t) \cos\left[2\pi f_c t + \theta(t)\right]$$

(3.27)

where

A = carrier signal amplitude.

$m(t)$ = modulating signal.

f_c = carrier signal frequency.

$\theta(t)$ = phase angle.

We assume the nominal carrier frequency to be 121.5 MHz. Processing at the optional frequency is identical. Due to the tolerance in the value for the carrier frequency of the ELT units and the Doppler frequency shift, it is expected that the range of processing must cover approximately 25 KHz centered at 121.5 MHz. For the baseband processor, this translates to the range from –12.5 KHz to + 12.5 KHz.

The complex baseband equivalent of the signal is generated by first multiplying the signal by $\cos(2\pi F_I t)$ and $\sin(2\pi F_I t)$ (where $F_I = 121.5$ MHz is the mixing frequency) [26]. Then the signals are filtered using low-pass filters having cut-off frequency equal to B_c. Thus, we have

$$s_I(t) = \frac{A}{2}\, m(t) \cos\left[2\pi (f_c - F_I) t + \theta(t)\right]$$

(3.28)

$$s_Q(t) = \frac{A}{2}\, m(t) \sin\left[2\pi (f_c - F_I) t + \theta(t)\right]$$

(3.29)

where the frequency $f_c - F_I$ is called the 'mixed carrier frequency' F_{MIX}.

These inphase-channel and quadrature-channel components are applied to the spectral estimation processor. Normally, the entire band from –12.5 KHz to + 12.5 KHz is

analyzed. However, any particular part of the band can be isolated for detailed analysis by adjusting the oscillator frequency to any desired frequency and selecting the bandwidth of the low-pass filters (Switched-capacitor type filters would be suitable for this application). This is particularly useful since long record lengths at reduced sampling rates can be processed without changing the length of the FFT or MEM.

In addition, more sophisticated processing strategies can be easily implemented such as using one processor operating on the full bandwidth to provide initial identification of possible ELT or EPIRB signals. A second processor could then be used at reduced sampling to provide isolation and more detailed analysis of these possible signals.

3.4   Processing ELT Signals With No Noise

We now consider the processing of ELT signals using the baseband periodogram, the baseband averaged periodogram, the baseband MEM and the baseband averaged MEM techniques with 512 complex points at a sampling rate of 25,000 inphase and quadrature samples per second in each case. Both coherent and non-coherent ELT signals have been processed for many combinations of carrier frequency and duty cycle [30]. We now present the results for one typical combination with mixed carrier frequency $F_{MIX} = -5$ kHz, duty cycle $d = 0.36$ and baseband low pass filter cutoff frequency $B_c = 12.5$ kHz [26].

3.4.1   Processing Results Using the Periodogram

Coherent ELT Signal

Figure 3.6 illustrates the spectral density result for the coherent ELT signal. From the results given in this figure, several prominent peaks are observable, including the main
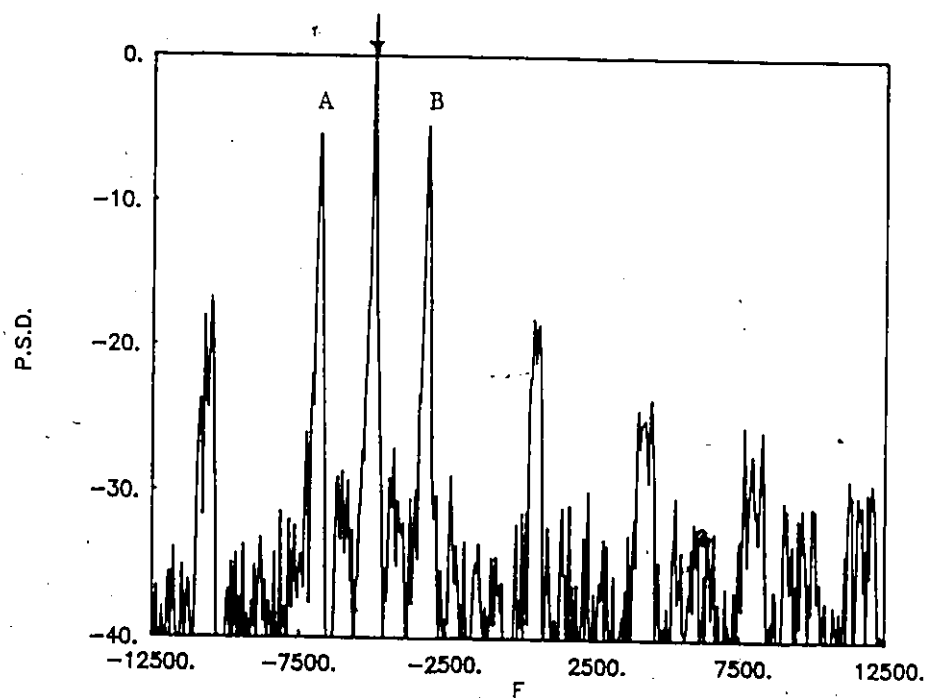
Fig. 3.6   Periodogram spectrum for coherent ELT signal.
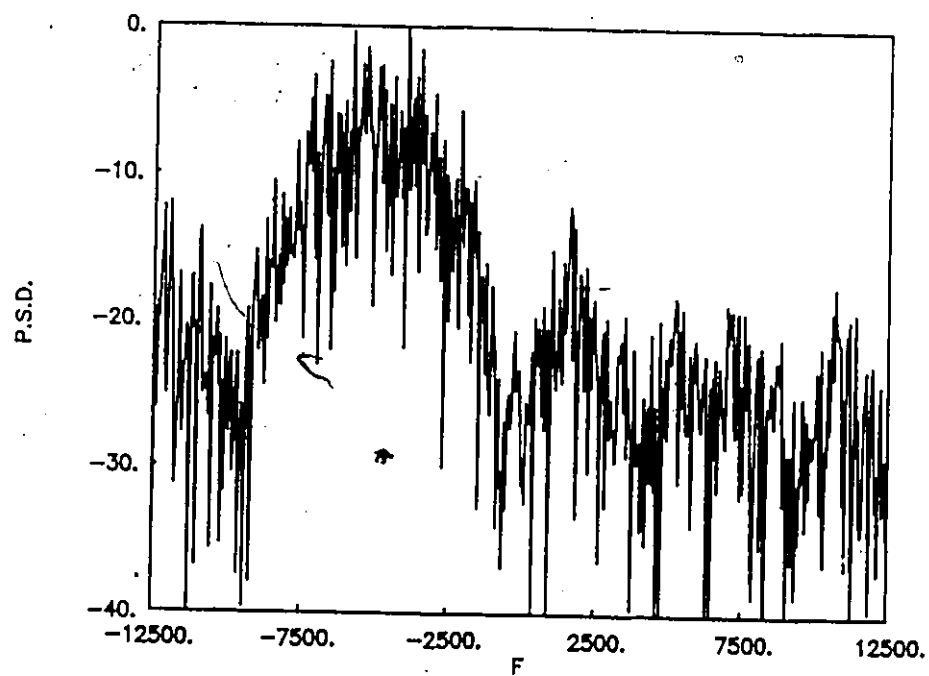
Fig. 3.7   Periodogram spectrum for non-coherent ELT signal.

carrier peak and two major sidebands (about 5 dB down) around the main carrier peak (labelled A and B). It is seen that the main carrier peak occurs at $F_{MIX} = -5$ kHz as expected. Although the sidebands are likely to increase the possibility of false alarms in detecting multiple signals, they can be useful in identifying a particular ELT signal.

Non-coherent ELT Signal

The spectral estimation performance for the non-coherent pulse modulated ELT signal using the baseband processor is shown in Fig. 3.7. The random phase characteristic causes "smearing" of the sharp spectral peaks of Fig. 3.6 which leads to a broad, ill-defined carrier spectral peak. Thus, measurement of the carrier frequency is difficult if not impossible.

3.4.2 Processing Results Using the Averaged Periodogram

Coherent ELT Signal

Figure 3.8 shows the averaged periodogram spectra for the coherent pulse modulated ELT signal. These results show that a sharp peak occurs at $F_{MIX} = -5$ kHz. The averaged sideband structure appears at about 13 dB below the level of the carrier peak component. Furthermore, the width of the sidebands are broad, in this case, about 1000 Hz. Thus, we conclude that 1) the carrier peak is well defined, and 2) the sidebands are prominent but produce interference with respect to other signals.

Comparing the spectrum obtained using the baseband periodogram technique (Fig. 3.6) with that using the averaged periodogram (Fig. 3.8) we note that:

1)   the main carrier peak is very sharp and occurs in the same location for both spectra;
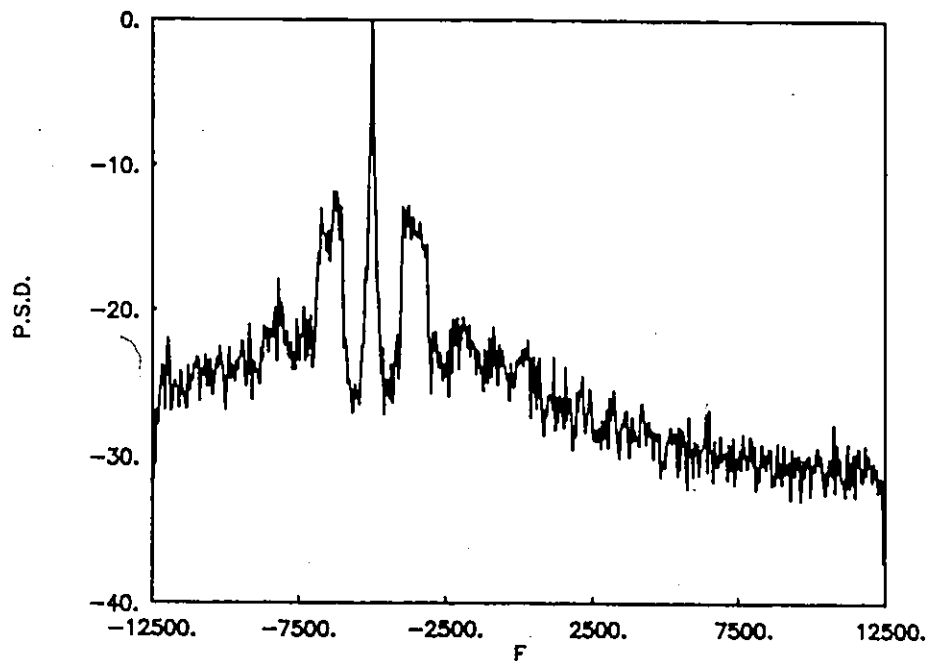
Fig. 3.8   Averaged periodogram spectrum for coherent ELT signal,
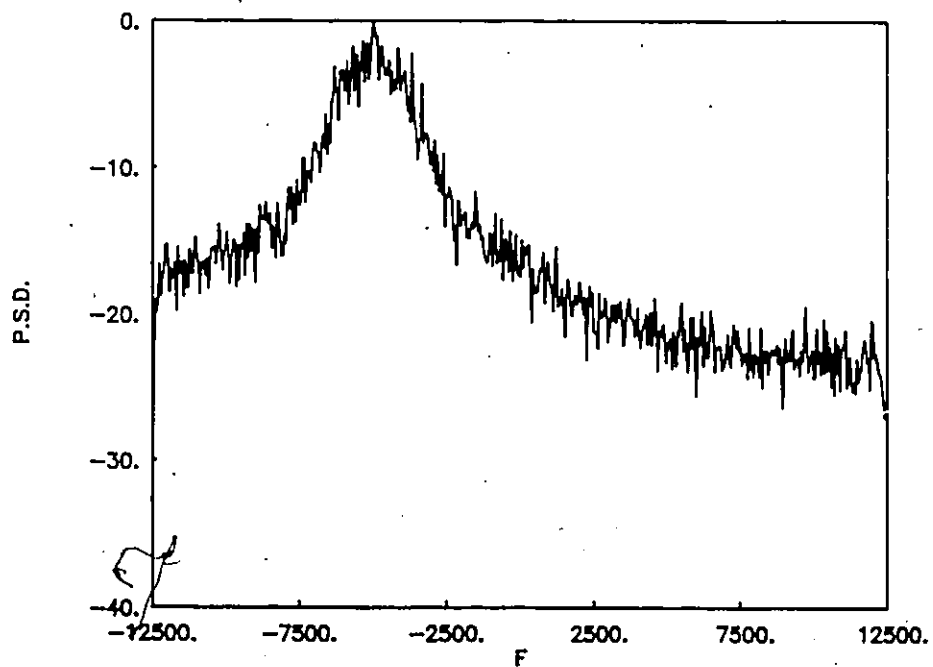
Fig. 3.9   Averaged periodogram spectrum for non-coherent ELT signal.

2)   by using the averaged periodogram technique, the levels of the two major

sidebands are reduced by 8 dB as compared to Fig. 3.6. and;

3)   the width of these sidebands becomes broad as illustrated in Fig. 3.8.

Non-coherent ELT Signal

The averaged periodogram spectra for the non-coherent pulse modulated ELT signal is given in Fig. 3.9. From this figure it is seen that the baseband averaged periodogram produces a spectrum which is far broader than the previous spectra for the coherent ELT signal. The carrier peak is not well defined. This makes the detection of the carrier frequency of the ELT signal difficult.

Comparing the spectra given in Fig. 3.7 and 3.9 it is seen that the spectra produced have broad ill-defined carrier peaks of width between about 3 and 5 kHz. Averaging does smooth the spectrum but no information of carrier frequency is obtained.

3.4.3   Processing Results Using the Maximum Entropy Method

Using the same coherent pulse modulated ELT signal as before, we now study the MEM spectral estimation performance and compared with the result obtained from the periodogram technique. The ELT signal is processed using the baseband processing algorithm with $F_{MIX} = -5$ kHz. The MEM filter order used for this analysis is 15 which is arbitrarily chosen and the MEM spectral result is given in Fig. 3.10. The choice of MEM order is investigated more fully when noise is added. With noise, it is seen that the filter order must be increased to give good performance.

From this figure, it is clear that, the prominent peaks previously detected are still present, these peaks including the main peak of carrier and two major sidebands around the
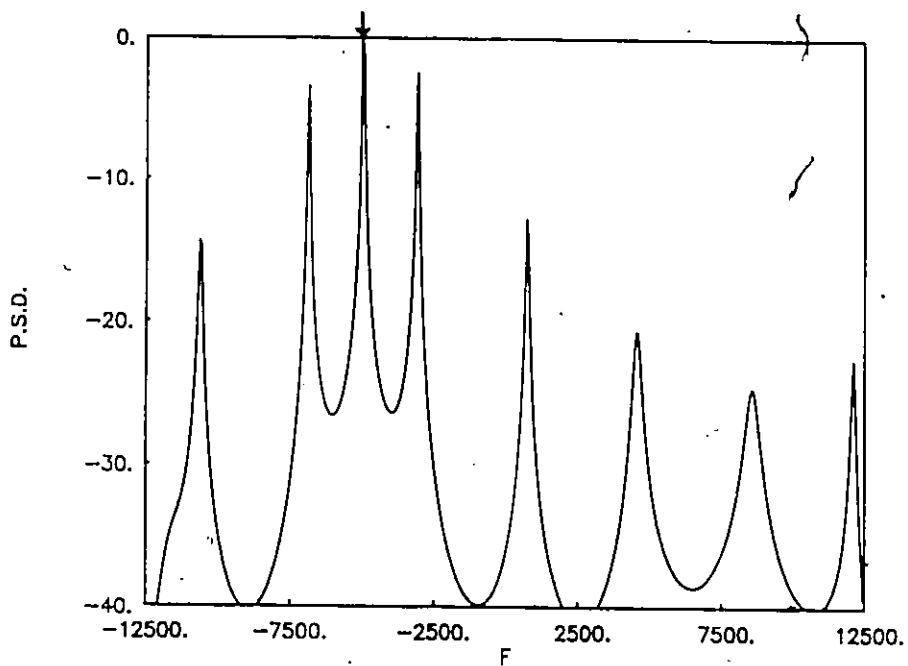
Fig. 3.10   MEM = 15 spectra for coherent ELT signal.
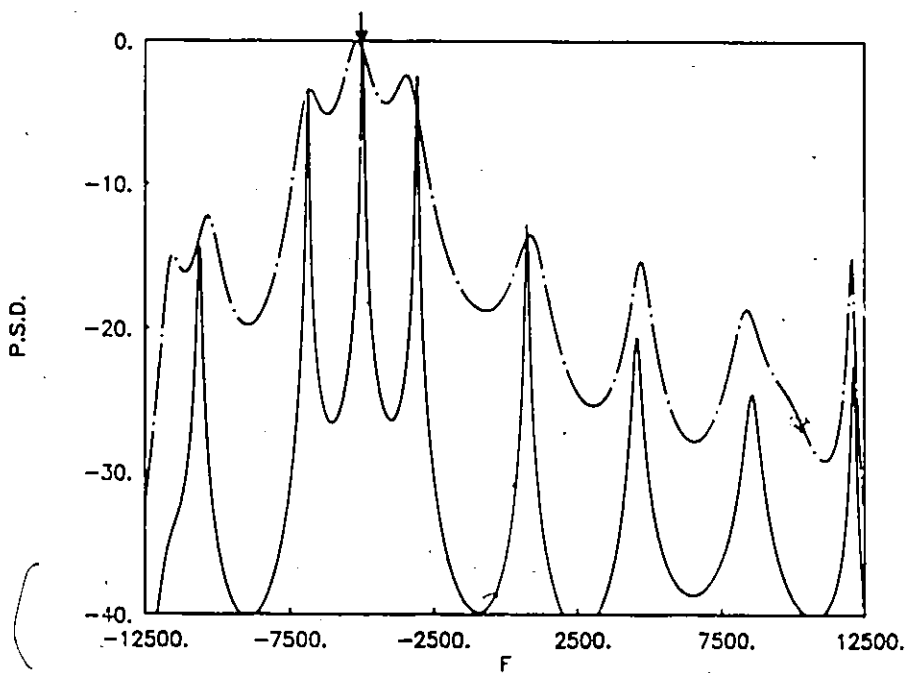
Fig. 3.11   MEM = 15 spectra for coherent and non-coherent ELT signals.

carrier component. Also it is observed that, the main carrier peak occurs at $F_{MIX} = -5$ KHz, as expected.

.Comparing the periodogram and MEM results for the same pulse modulated ELT signal, we find that the number of peaks for both FFT and MEM techniques are the same at the -10 dB threshold level, namely, 3 peaks. At lower threshold levels, the width of the peaks for the MEM spectrum tends to be less than for the FFT spectrum.

Non-coherent ELT Signal

Using the non-coherent ELT signal, we see the effect of introducing a random phase to the signal. Both continuous phase and random phase signals are processed using the baseband MEM technique with MEM = 15. The MEM spectra result is given in Fig. 3.11. From this figure it is clear that the resolution is reduced as a result of introducing a random phase. Figure 3.12 illustrates the comparison between the MEM = 3 and MEM = 40 for the, same random phase pulse modulated ELT signal. It is seen that the lower MEM filter order is preferred to combat the pulse-modulated random phase ELT signal.

One possible strategy for processing non-coherent ELT signals is to first isolate the signal by mixing to low frequency and low pass filtering. Then process the signal, using a low order MEM estimator.

3.4.4 Processing Results Using the Averaged MEM

Figure 3.13 shows the result using the averaged MEM = 15 estimator for the coherent pulse-modulated ELT signal. We see that the detection of the carrier peak component is excellent and the sideband structure is at least 10 dB below the level of the carrier component peak.

Comparing this plot with that of Fig. 3.10, we conclude:
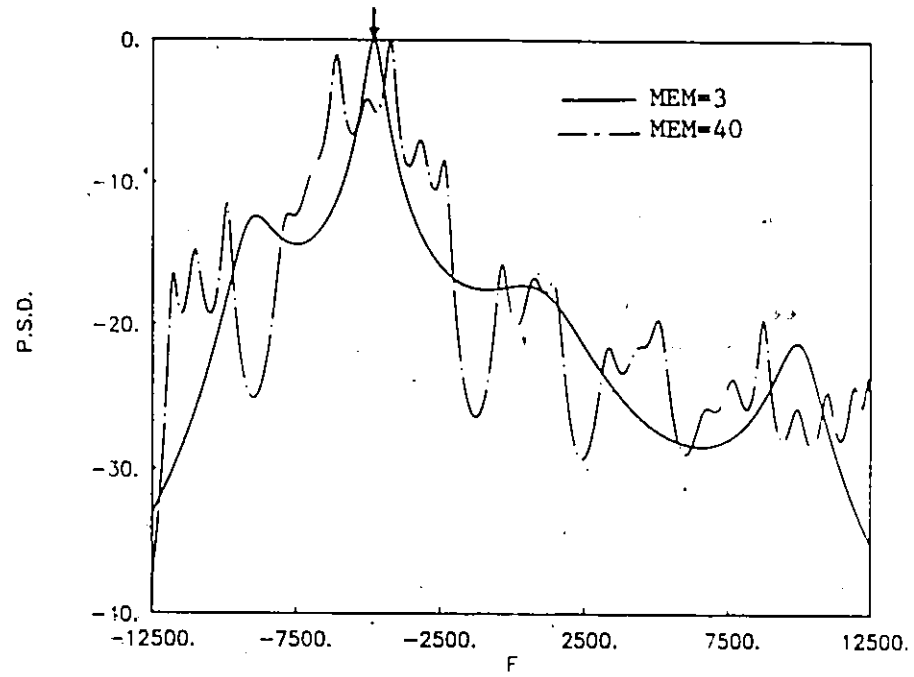
- Fig. 3.12   MEM = 3 and MEM = 40 spectra for non-coherent ELT signal.
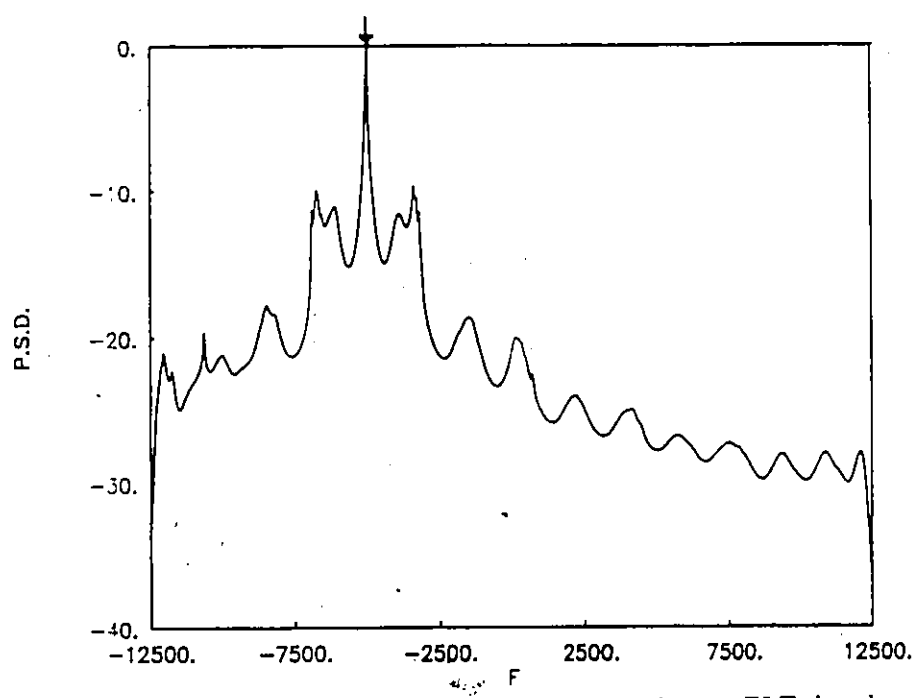
Fig. 3.13   Averaged MEM = 15 spectra for coherent ELT signal.

1) the carrier component is very sharp and stationary for both spectra,

2) the levels of the two major sidebands around the carrier peak are reduced by about

7 dB by using averaging; and

3) the remaining sidebands are reduced to approximately –20 dB or less.

3.5 Processing ELT Signals With Noise

In this section, our discussion centres on the spectral performances of the periodogram and MEM signal processors when applied to single ELT signals in the presence of noise.

3.5.1 Comparison of Periodogram With Matched Filter

Assume the received signal at the earth station consists of the sum of an ELT signal and receiver noise, given by

$$y_R(t) = s(t) + n(t) \qquad (3.30)$$

where

$s(t) =$ input ELT signal

$n(t) =$ additive white Gaussian noise (AWGN)

To represent the noise $n(t)$, we use the Gaussian random variable with zero mean and noise density N_0 as a good approximation in this analysis.

A comparison of the performance of the periodogram to a matched filter can be deduced by comparing the spectra of a coherent ELT signal with that of unmodulated carrier, with each signal having the same energy and duration.

First, we assume a duration T_D of carrier $s_u(t)$, which consists of a sinusoidal wave of amplitude A_1 and frequency f_c with energy $E_1 = \frac{1}{2} A_1^2 T_D$ represented by:

$$s_u(t) = A_1 \cos(2\pi f_c t) \quad , \qquad 0 \le t \le T_D \tag{3.31}$$

The Fourier transform of this signal is given by

$$F_U(f) = \frac{A_1 T_D}{2} \operatorname{sinc}[(f - f_c) T_D] \tag{3.32}$$

Thus, the spectrum is given by

$$S_U(f) = \left(\frac{A_1 T_D}{2}\right)^2 \operatorname{sinc}^2[(f - f_c) T_D] \tag{3.33}$$

Next, we compute the spectrum of a coherent ELT signal of duration T_D and amplitude A_2, as shown in Fig. 3.2. This can be represented by a set of N_p pulse-null pairs in time domain given by

$$s_m(t) = \sum_{i=1}^{N_p} s_i(t) \tag{3.34}$$

where

$$s_i(t) = A_2 \cos(2\pi f_c t + \theta_i) \quad , \quad t_i - \frac{dT_i}{2} \le t \le t_i + \frac{dT_i}{2} \tag{3.35}$$

$$= 0 \quad , \quad \text{otherwise}$$

where d is the duty cycle, θ_i is the phase shift of the ith pulse, t_i is the time from the center of the first pulse to the center of the ith pulse and T_i is the duration of the ith pulse-null pair (see Fig. 3.2).

The energy of this signal is given by

$$E_2 = \frac{1}{2} A_2^2 d T_D \tag{3.36}$$

The Fourier transform of N_p pulses of signal using linearity and shifting property is given by

$$F_M(f) = \sum_{i=1}^{N_p} \frac{A_2 d T_i}{2} \operatorname{sinc}[(f - f_c) d T_i] \cdot e^{-j(2\pi f t_i - \theta_i)} \tag{3.37}$$

The exponential term must be exactly unity when $f = f_c$. Hence

$$\theta_i = 2\pi f_c t_i \tag{3.38}$$

Thus Eq. (3.37) becomes

$$F_M(f) = \sum_{i=1}^{N_p} \frac{A_2 d\, T_i}{2} \operatorname{sinc}[(f-f_c)\, d\, T_i] \cdot e^{-j2\pi(f-f_c)t_i} \tag{3.39}$$

Since the sweep varies slowly with time, assume a set of N_p pulses with $T_i = T$. For these first N_p pulses, t_i is given by

$$t_i = \frac{(i-1)}{N_p}\, T_D \tag{3.40}$$

where

$$T_D = N_p T$$

Hence, the Fourier Transform of the N_p pulses is represented by

$$F_M(f) = \sum_{i=1}^{N_p} \frac{A_2 d\, T}{2} \operatorname{sinc}[(f-f_c)\, d\, T]\, e^{-j\, 2\pi(f-f_c)(i-1)T} \tag{3.41}$$

The summation can be simplified by noting

$$\sum_{i=1}^{N_p} e^{-j\, 2\pi(f-f_c)(i-1)T} = \frac{1 - e^{-j\, 2\pi(f-f_c)N_p T}}{1 - e^{-j\, 2\pi(f-f_c)T}} \tag{3.42}$$

Computing the spectrum, we get

$$S_M(f) = \left(\frac{A_2 d\, T}{2} \right)^2 \operatorname{sinc}^2[(f-f_c)\, d\, T] \left[\frac{\sin[\pi(f-f_c)N_p T]}{\sin[\pi(f-f_c)T]} \right]^2 \tag{3.43}$$

$$= \left(\frac{A_2 d N_p\, T}{2} \right)^2 \operatorname{sinc}^2[(f-f_c)\, d\, T] \left[\frac{\operatorname{sinc}[(f-f_c)N_p T]}{\operatorname{sinc}[(f-f_c)T]} \right]^2 \tag{3.44}$$

Comparing $S_U(f)$ with $S_M(f)$ at $f = f_c$, we have

$$S_U(f_c) = \left(\frac{A_1 T_D}{2} \right)^2 \qquad (3.45)$$

$$S_M(f_c) = \left(\frac{A_2 d T_D}{2} \right)^2 \qquad (3.46)$$

Since the energy of both signals are equal, i.e., $E_1 = E_2$, we find $A_1{}^2 = A_2{}^2 d$

Therefore,

$$\frac{S_M(f_c)}{S_U(f_c)} = d \qquad (3.47)$$

Hence, for the coherent ELT signal the FFT produces a peak which is d times that of a matched filter. Since d ranges from 0.33 to 0.55, this loss is of the order of 2.6 to 4.8 dB.

3.5.2 Minimum Detectable Level of CNDR

Since we have related the spectral peak of the ELT signal to that of a pulse of carrier, we can now deduce the minimum detectable carrier-to-noise density ratio (CNDR) by following the procedure for detection of radar pulses [31,32]. First, we note that the periodogram has the frequency response of $\text{sinc}^2[(f - f_c)T_D]$, which is identical in shape to the spectrum of the pulse of carrier given in Eq. (3.33). Thus, we see that the periodogram provides a matched filter implementation for the pulse of carrier.

The maximum signal-to-noise ratio at the output of a receiver using the matched filter is given by [33]

$$SNR_{MAX} = \frac{2E}{N_0} \qquad (3.48)$$

where E is the energy of the signal and N_0 is the noise spectral density. For the pulse of carrier, we have $E_1 = \frac{1}{2}A_1{}^2 T_D$, and consequently,

$$SNR_{MAX} = \frac{A_1^2}{N_0} T_D \tag{3.49}$$

Now, define $(\frac{1}{2}A_1^2/N_0)$ to be the CNDR required for detection of the pulse of carrier,

then,

$$CNDR_C = \frac{SNR_{MAX}}{2\,T_D} \tag{3.50}$$

For detection of the ELT signal, the level must be increased by a factor of 1/d,

yielding

$$CNDR_E = \frac{SNR_{MAX}}{2\,dT_D} \tag{3.51}$$

The detection of a weak signal is limited by noise energy that occupies the same portion of the frequency spectrum as does the signal energy. Detection is based on establishing a threshold level at the output of the receiver. If the receiver output exceeds the threshold, a signal is assumed to be present.

Normally, the spectra of contiguous windows of data are averaged to reduce the variance of the spectral estimate. Assuming a total length of 1 s of data and 512 complex point periodograms, each of duration 20 ms (25000 samples per second), there are 50 independent windows of data. Using standard curves [32, p. 2-21], we find that for probability of detection of 0.95 and 50 integrated pulses, the SNR varies from 0 to 2.5 dB for a false alarm probability ranging from 10^{-4} to 10^{-12}. For d = 0.36, SNR = 2.5 dB and T_D = 20 ms, we find that the minimum detectable value of CNDR is approximately 21 dB-Hz. For the integrator-based matched filter with SNR_N = 10 dB, d = 0.36 and T_D = 1s, the CNDR level is 14 dB-Hz [34] which agrees well with the present derivation since integrating 50 spectra leads to a loss of $(50)^{1/2}$ or 8.4 dB, as compared to the matched filter.

3.5.3 Simulation Using Periodogram

Coherent ELT Signal

The effect of varying the CNDR on pulse-modulated, coherent ELT signal is now studied, using a pulse-modulated ELT signal with mixed carrier frequency $F_{MIX} = 100\,Hz$ and duty cycle equal 0.36.

Figures 3.14 to 3.16 show the performance of the periodogram for this ELT signal as the CNDR is reduced from 40 dB-Hz to 30 dB-Hz in 5 dB-Hz steps. From these results, it is clear that above 30 dB-Hz, the results are acceptable, below 30 dB-Hz, signal detection becomes more difficult.

To improve the signal detection using the periodogram, for the same pulse-modulated ELT signal with CNDR = 30 dB-Hz, we increase the number of data points from 512 to 1024 complex points. Figure 3.17 depicts the periodogram spectral results. Comparing Fig. 3.16 with Fig. 3.17 shows the increase in CNDR due to increase in the data length. In addition, the resolution is also doubled.

The spectrum can also be enhanced by averaging 50 contiguous blocks of the 512-complex point periodogram, as shown in Figs. 3.18, 3.19 and 3.20 for CNDR values of 30 dB-Hz, 25 dB-Hz and 20 dB-Hz, respectively. We see that the signal peak is prominent at 25 dB-Hz but tentative at 20 dB-Hz, indicating that the 21 dB-Hz theoretical estimate is reasonably accurate.

Non-coherent ELT Signal

Figures 3.21 and 3.22 show the periodogram spectral estimate performance results as the CNDR is decreased from 45 dB-Hz to 40 dB-Hz for non-coherent pulse- modulated ELT signal with the mixed carrier frequency of 100 Hz. From these figures, it is seen that the
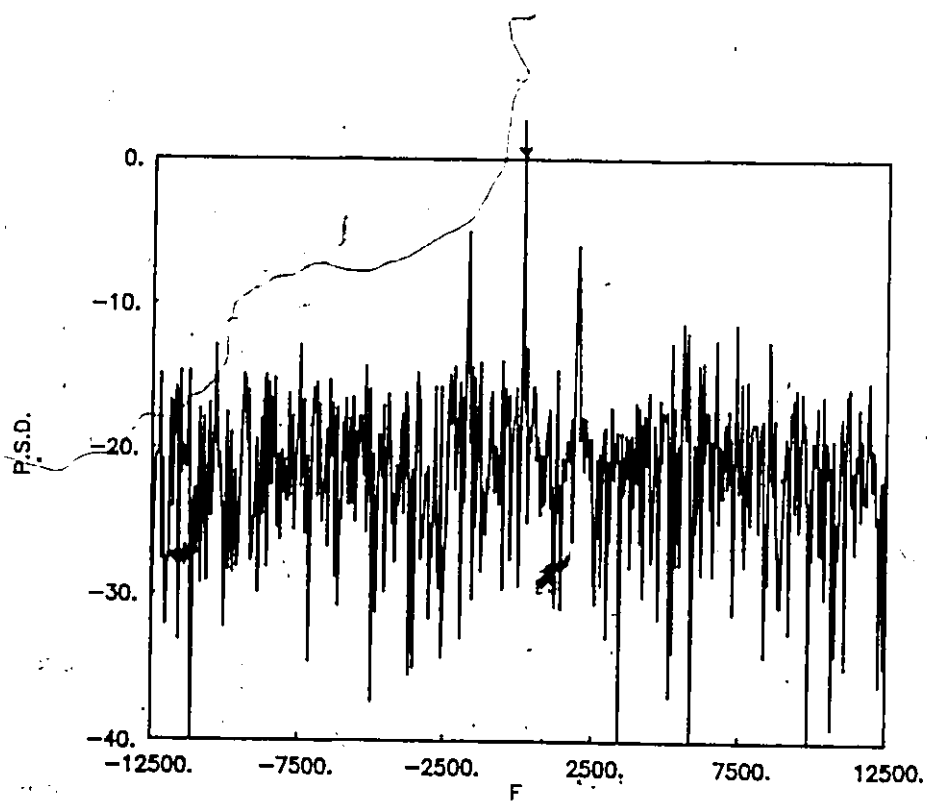
Fig. 3.14   Periodogram spectrum for coherent ELT signal with CNDR = 40 dB-Hz.
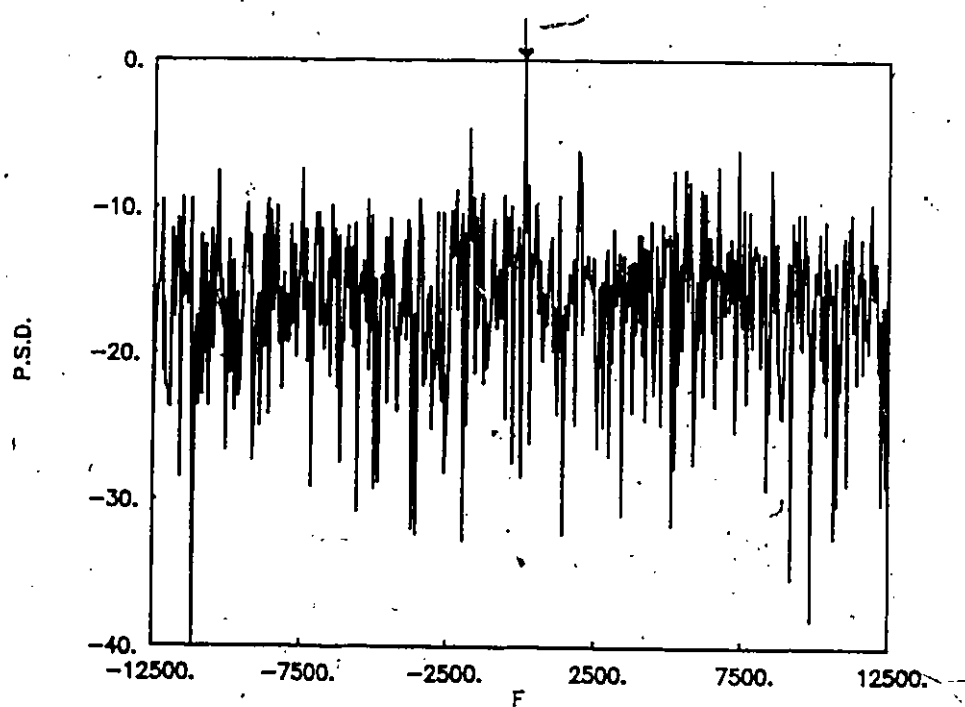
Fig. 3.15   Periodogram spectrum for coherent ELT signal with CNDR = 35 dB-Hz.
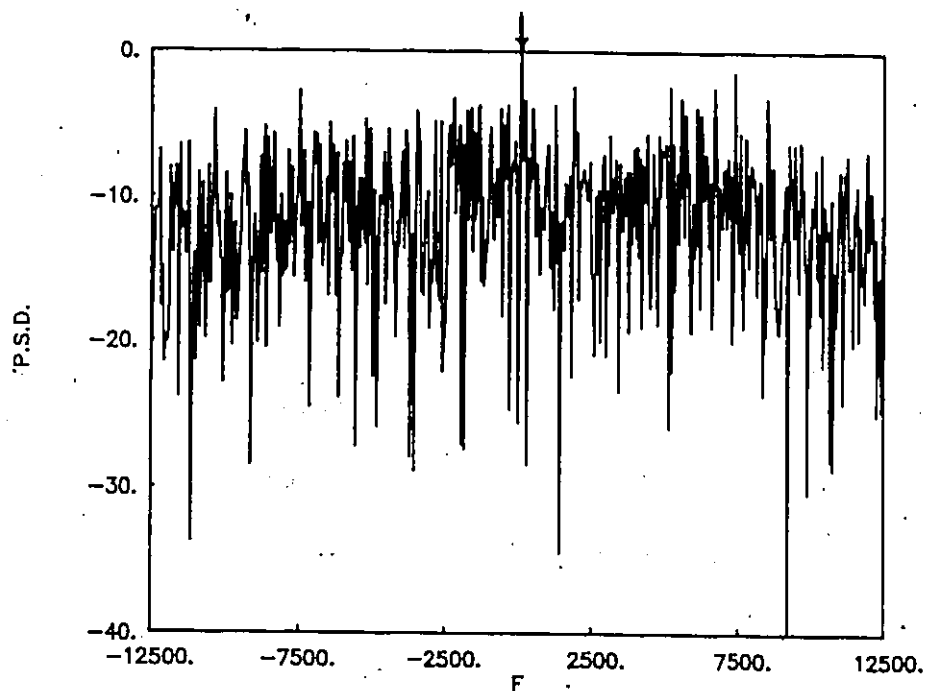
Fig. 3.16   Periodogram spectrum for coherent ELT signal with CNDR = 30 dB-Hz.
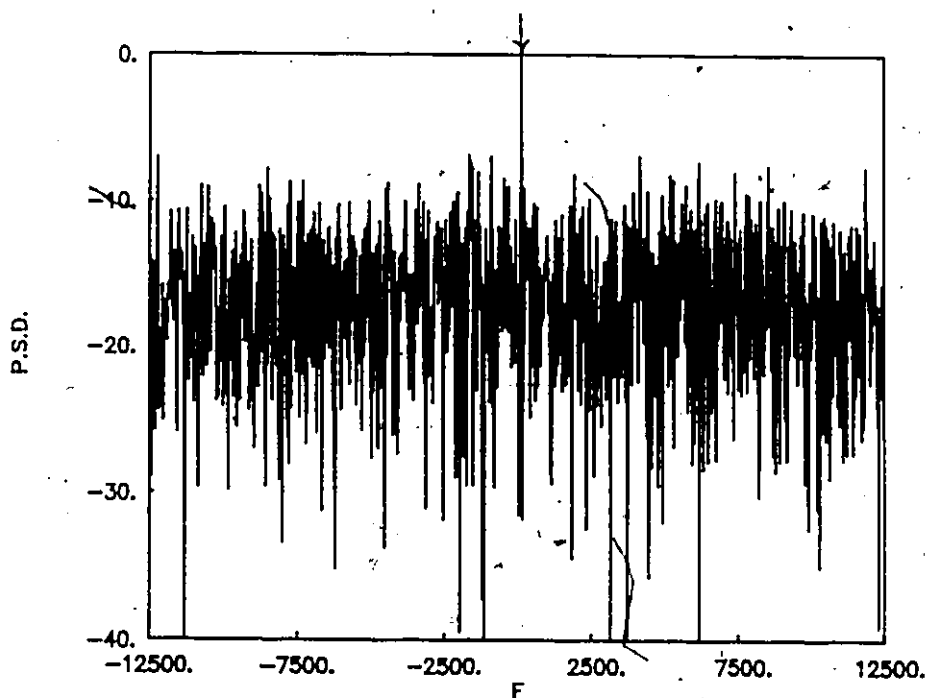
Fig. 3.17   1024-complex point periodogram spectrum for coherent ELT signal with CNDR = 30 dB-Hz.
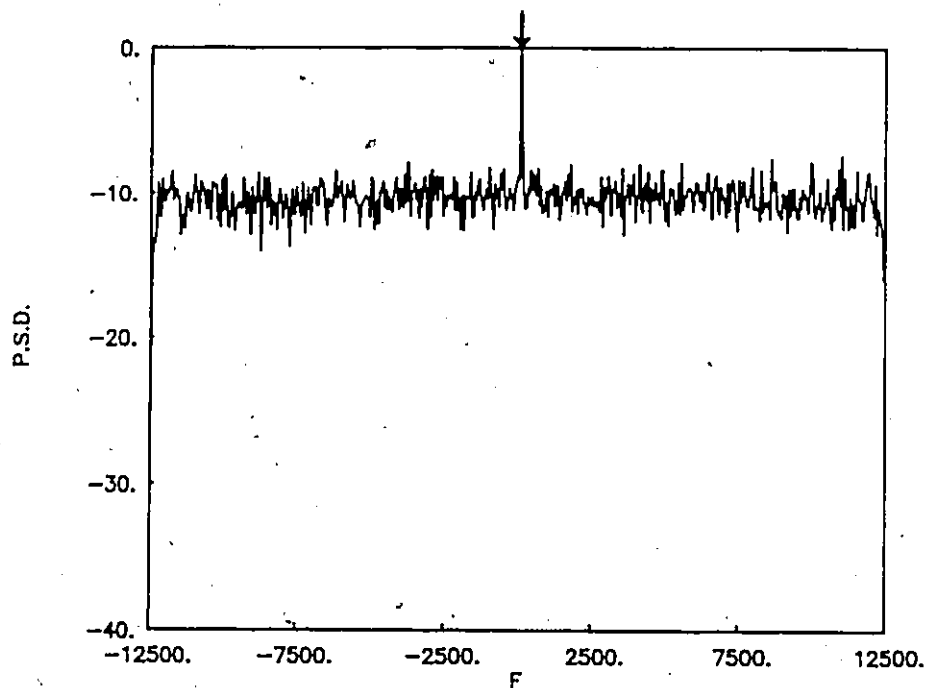
Fig. 3.18   Averaged periodogram spectrum for coherent ELT signal with CNDR = 30 dB-Hz.
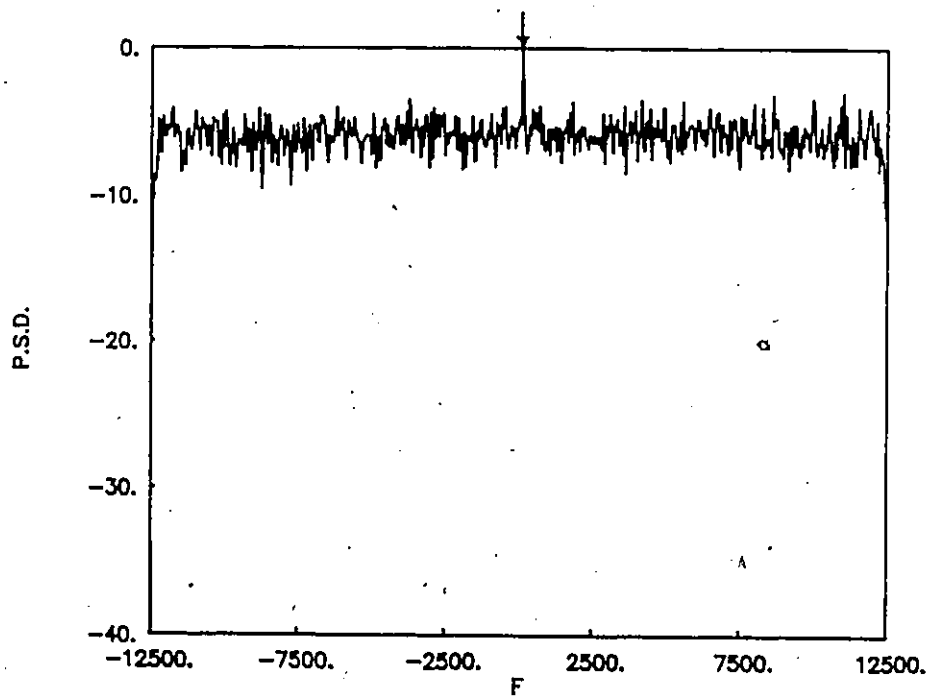
Fig. 3.19   Averaged periodogram spectrum for coherent ELT signal with CNDR = 25 dB-Hz.
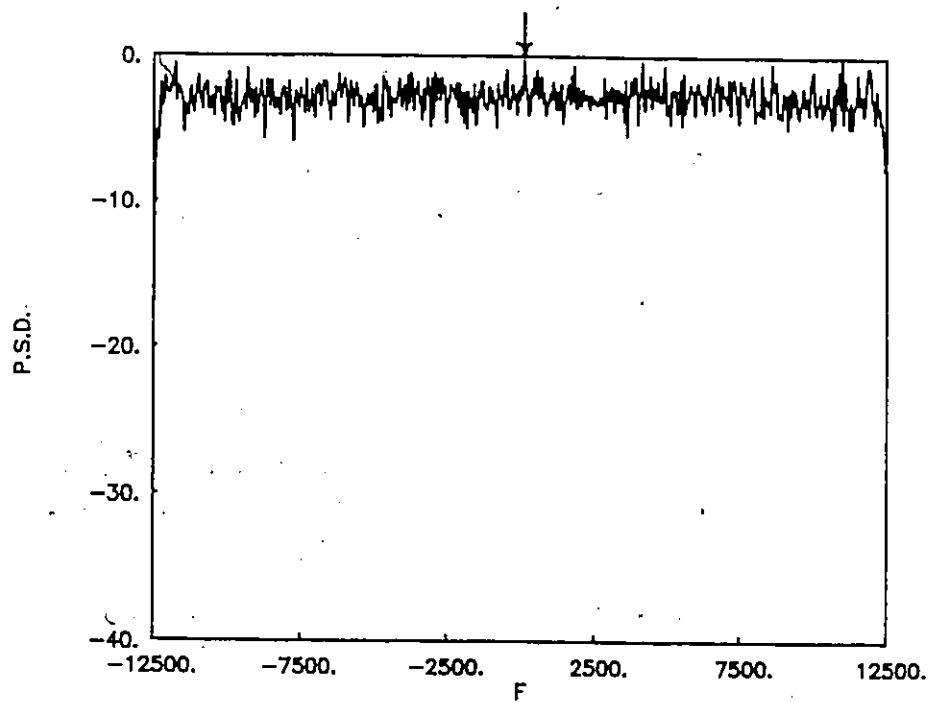
Fig. 3.20 Averaged periodogram spectrum for coherent ELT signal with CNDR = 20 dB-Hz.
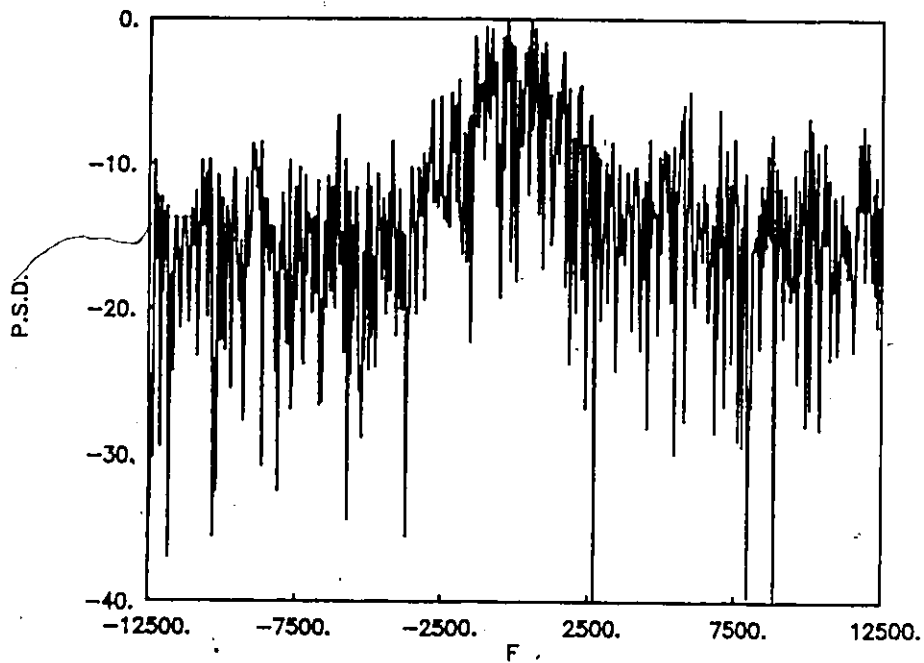
Fig. 3.21   Periodogram spectrum for non-coherent ELT signal with
             CNDR = 45 dB-Hz.
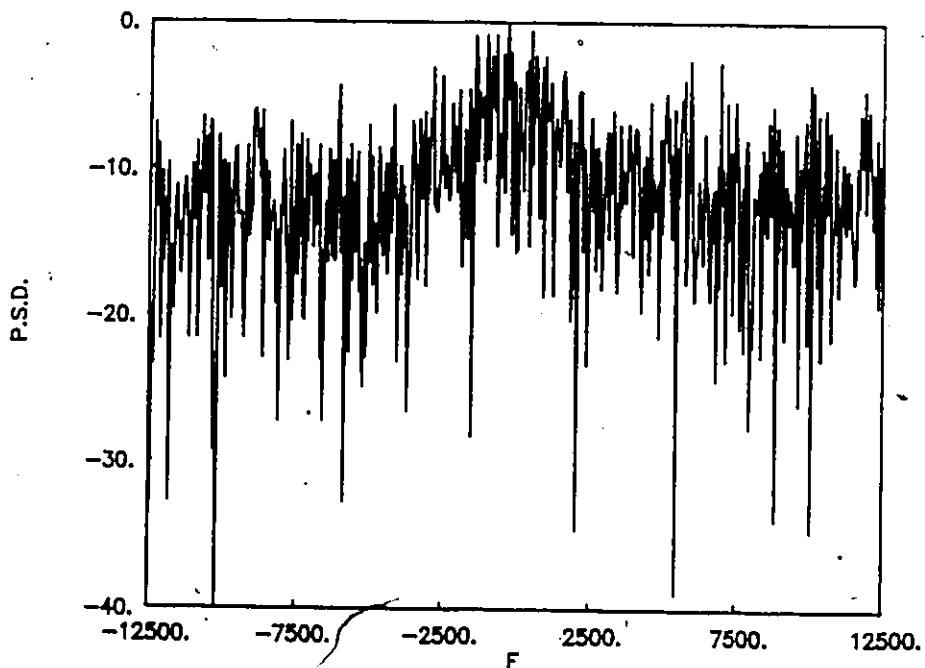
Fig. 3.22   Periodogram spectrum for non-coherent ELT signal with
             CNDR = 40 dB-Hz.

periodogram produces multiple peaks near the carrier frequency, which makes the detection of this ELT signal very difficult. Averaging provides little improvement unfortunately.

3.5.4   Simulation Using MEM

Here we study the MEM performance for the pulse-modulated ELT signal with mixed carrier frequency $= 100\,Hz$ in the presence of different CNDR levels ranging from 45 dB-Hz to 35 dB-Hz in 5 dB-Hz steps.

Coherent ELT Signal

First, a coherent pulse-modulated ELT signal is processed using MEM of order 25 and the different values of CNDR. Figures 3.23 to 3.25 show the MEM performance of this ELT signal. From these results it is clear that reducing the CNDR to 35 dB-Hz causes severe degradation in signal detection, which makes the signal detection impossible.

To improve the detection of the ELT signal, we further increase the MEM filter order and apply a signal with CNDR level of 30 dB-Hz. Figure 3.26 illustrates the improvement with MEM order equal to 100. From this figure, we note that the topmost peak which is the carrier component peak is located at 98 Hz. This is equivalent to frequency error of 2 Hz. In addition, it is seen that the performance of MEM = 100 and the periodogram (Fig. 3.16) are essentially equal. Beyond MEM = 100, the improvement is marginal.

MEM averaging provides considerable improvement in the spectrum. Figure 3.27 illustrates the average of 50 contiguous estimates at CNDR = 30 dB-Hz using MEM filter order 100. From these results, it is clear that the level of the undesirable sidepeaks is reduced which consequently improves the detection of the carrier component peak of the ELT signal.
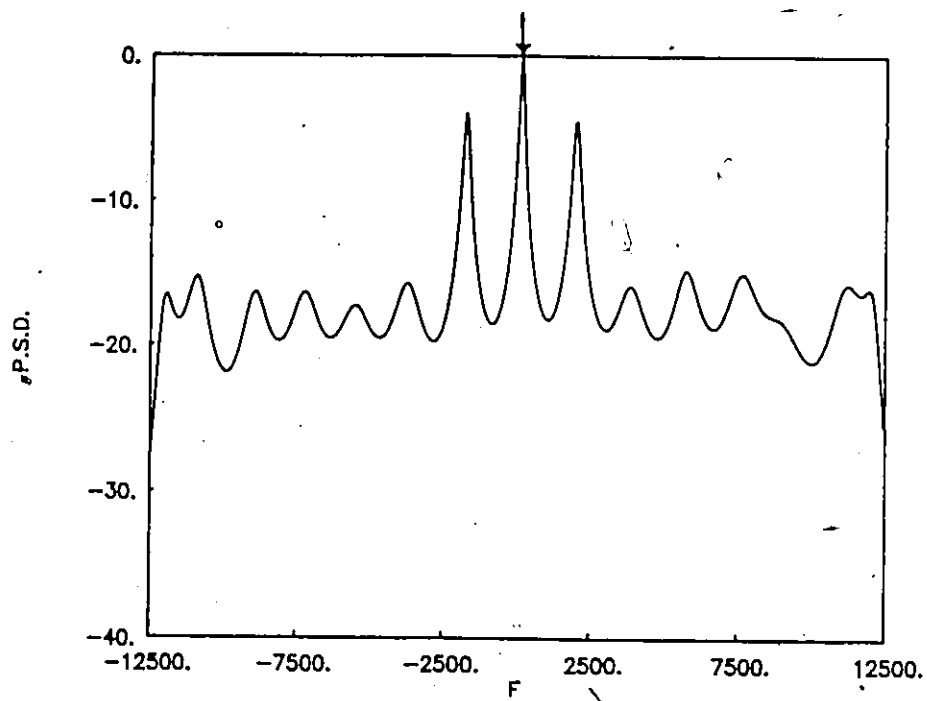
Fig. 3.23   MEM = 25 spectrum for coherent ELT signal with CNDR = 45 dB-Hz.
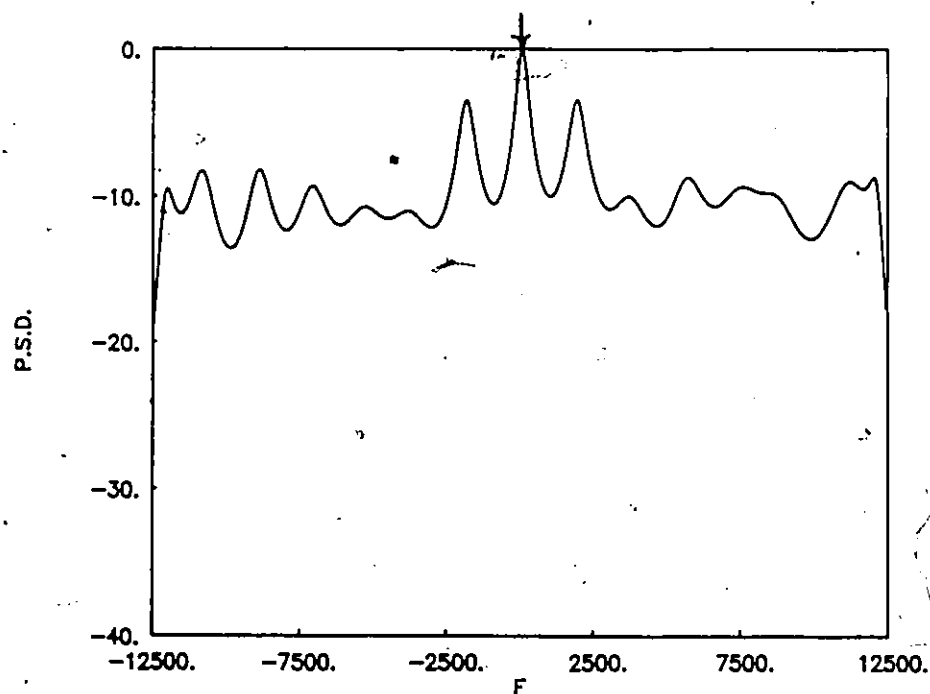
Fig. 3.24   MEM = 25 spectrum for coherent ELT signal with CNDR = 40 dB-Hz.
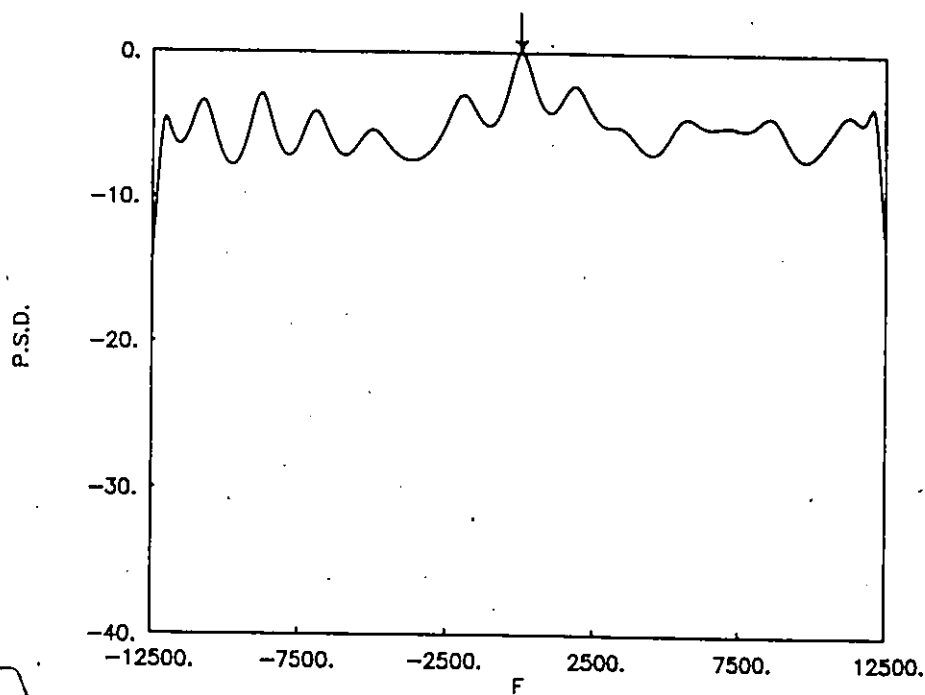
Fig. 3.25   MEM = 25 spectrum for coherent ELT signal with CNDR = 35 dB-Hz.
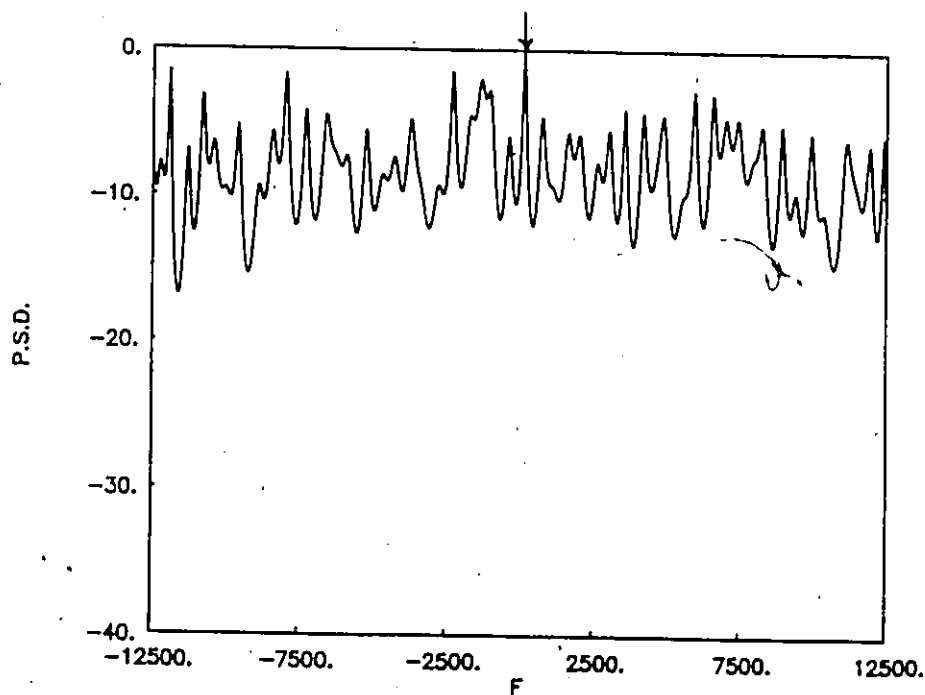
Fig. 3.26   MEM = 100 spectrum for coherent ELT signal with CNDR = 30 dB-Hz.
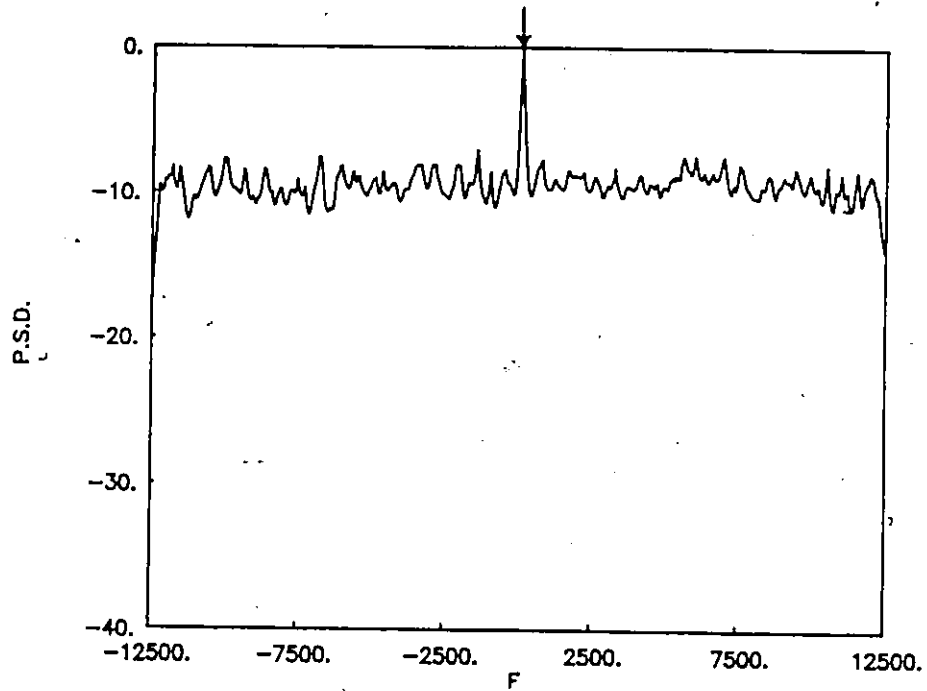
Fig. 3.27   Averaged MEM = 100 spectrum for coherent ELT signal with
              CNDR = 30 dB-Hz.
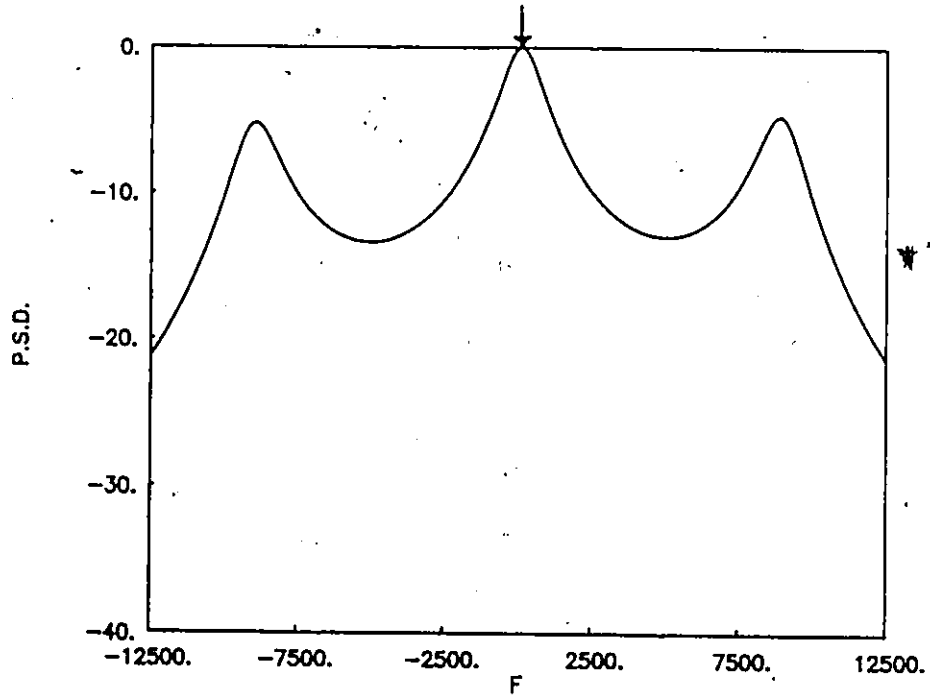
Fig. 3.28   MEM = 3 spectrum for non-coherent ELT signal with CNDR = 45 dB-Hz.

Non-coherent ELT Signal

Figures 3.28 illustrates the MEM spectral estimate for the non-coherent ELT signal using MEM order equal 3 and CNDR = 45 dB - Hz. We find that the estimated carrier frequency is affected by the level of CNDR and that the measurement is difficult for all values less than 40 dB-Hz.

3.6   Summary

A new baseband processor for ELT signals has been described and tested using computer generated coherent and non-coherent ELT signals. A theoretical bound for minimum detectable CNDR has also been evaluted.

Linear spectral estimation methods including the periodogram and averaged periodogram and non-linear spectral estimation methods including the MEM and averaged MEM are employed to process a single computer-generated ELT signal. Detection of coherent pulse-modulated ELT signal using these methods is relatively straight forward and all these methods gives excellent results in the absence of noise. But for the non-coherent pulse-modulated ELT signal, the performance is not good using the linear spectral estimation method. The presence of high-level sidebands in the periodogram method makes it less desirable in certain cases. The random phase ELT signal, which suffers from the multiple-peaks problem in the FFT spectra, possesses limited detection capability with MEM. The advantage of using the MEM spectral analysis for these random phase pulse modulated ELT signals is that it can suppress the sidebands of the signal at a low order of prediction error filter.

For the random phase type of ELT signal, we conclude that the lower order MEM is preferred over the higher order to combat the signal.

A comparison is made between the periodogram and matched filtering method. This comparison indicates that the periodogram gives good performance for coherent ELT signal within 2.6 to 4.8 dB of that provided by matched filtering.

A theortical bound for minimum detectable carrier to noise density ratio (CNDR) has been evaluated.

The linear and non-linear spectral estimation methods are employed to process a single ELT signal in the presence of noise at different values of CNDR levels.

Concerning the periodogram spectral estimatoin results, it is clear that the effect of noise produces multiple peaks near the carrier component peak of the ELT signal at low values of CNDR, which makes the signal detection difficult.

Detection of the carrier compenent peak is improved by increasing the number of data points or using the averaged periodogram. The variance due to sidebands and noise are reduced which give a smooth spectrum estimate using the averaged periodogram method. But for random phase ELT signal, the detection becomes more difficult if is not impossible in the presence of noise because this type of ELT signal suffers from multiple peaks problem in the FFT spectra.

At lower values of CNDR level, the error in the frequency estimate is reduced with higher MEM filter orders for coherent pulse-modulated ELT signals. MEM averaging improves the detection of this ELT signal at lower values of CNDR level.

CHAPTER 4

RATE REDUCTION FILTERING

TECHNIQUE AND APPLICATIONS

4.1   Introduction

The capability of each processor to detect the ELT signals, in the presence of noise, is an important characteristic of its performance. In this chapter we will see how to enhance the signal-to-noise ratio (SNR) of the ELT signal and consequently improve the signal detection. Two different methods have been used for sampling-rate reduction. The first method is referred to as decimation in time and the second technique is called rate-reduction filtering. Both of these methods improve the frequency resolution. However, rate reduction filtering method provides other advantages including a reduction in the frequency error and improvement in the SNR, which consequently improves the detection of the carrier component peak of the ELT signal. The application of using these two methods with the periodogram is presented and the comparison between these two methods is also discussed.

In addition, the application of rate reduction filtering when using MEM is given in this chapter. An algorithm called "ELT Tracking Algorithm" is then proposed. We have shown that by employing this method we can estimate the ELT signal mixed carrier frequency, which makes the detection of this ELT signal simple.

4.2   Decimation in Time

The process of sampling rate reduction by deleting samples from the data is often called decimation. The sampling rate is reduced by certain decimation steps d, i.e. by factors of 2 until a desired power of 2 sampling rate reduction is achieved [35,36].

First, let us define the process of decimation in time which involves a sampling rate reduction. We start out with an input signal, $\{u_n\}$, which was derived from an analog signal u(t) by sampling it every Δt seconds, that is, a sampling frequency F_{sa} equal $1/\Delta t$ as shown in Fig. 4.1

Suppose that an analog signal u(t) is sampled every Δt seconds as shown in Fig. 4.1. At the output of the sampler, we obtain a digital signal $\{u_n\}$ where

$$u_n = u(n\Delta t) \tag{4.1}$$

The digital spectrum of $\{u_n\}$, U(f) is periodic and consists of the spectrum of the analog signal u(t) repeated infinitely around $\pm kF_{sa}$ multiples of the sampling frequency (k = 1,2,3, . . .).

The process of decimating a signal u(n) by an integer ratio d is depicted in Fig. 4.2. This figure illustrates the block diagram of a general integer ratio d decimator.

Let us consider an example of such a sequence $\{u_n\}$ which has been derived by sampling at original sampling rate F_{sa}. We wish to reduce the sampling rate to F_{sa}/d, that is, decimate with ratio of d. Obviously, it only makes sense to reduce the sampling rate if the information content of the signal that we wish to preserve is bandlimited to less than $F_{sa}/2d$, ie. half the desired sampling rate, since any spectral components above this frequency will be aliased into frequencies below $F_{sa}/2d$.

As illustrated in Fig. 4.2, the received signal is first passed through a digital lowpass filter giving the signal $y_R(n\Delta t)$. The sampling rate reduction is then achieved by
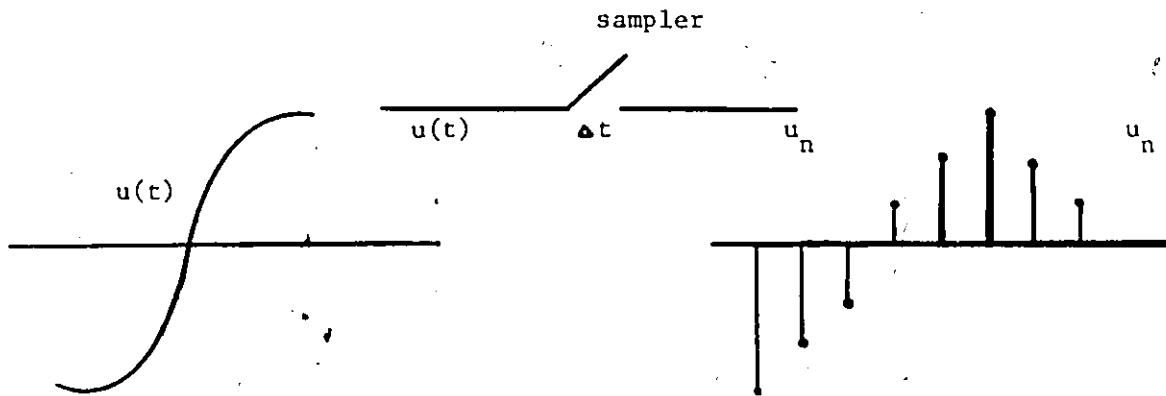
Fig. 4.1   Sampling of an analog signal to obtain a digital signal.
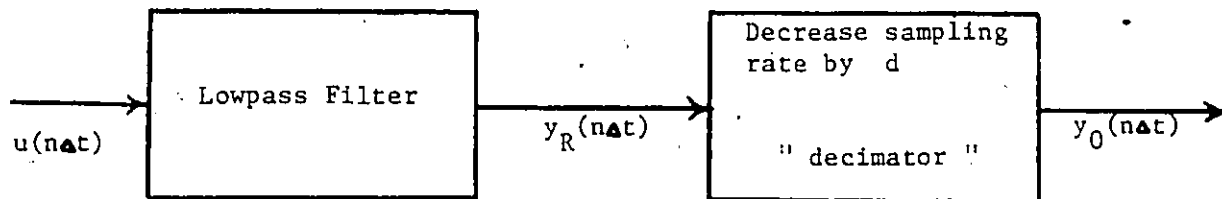
Fig. 4.2   The block diagram of a d times decimator.

passing the output of the lowpass filter through the decimator which simply keeps every dth point, i.e. by forming a new sequence $y_0(n\Delta t)$ by extracting every dth sample of $y_R(n\Delta t)$.

4.2.1   Decimation in Time Procedure

We represent the decimation steps by d, where d is given by

$$d = 2^r \qquad , r = 0, 1, 2, \ldots . \qquad (4.2)$$

Then for $r = 0$, $d = 1$, corresponds to no decimation, while for $r = 1$, $d = 2$, represents decimation by 2 and so on. If the sampling rate of the sequence is F_{sa}, then the final rate is then F_{sa}/d.

Let us represent the received signal at the output of the lowpass filter mathematically in discrete form as

$$y_R(q\Delta t) = s(q\Delta t) + n(q\Delta t) \qquad q = 1, 2, \ldots, N \qquad (4.3)$$

where

s(q\Delta t) = input ELT signal,

n(q\Delta t) = additive noise.

The expression for the index used to calculate the decimation procedure in general is given by

$$m_d = (q-1)d + 1 \qquad , q = 1, 2, \ldots, N$$
$$, d = 1, 2, 4, 8, \ldots \qquad (4.4)$$

Thus, we can represent the signal in terms of decimation steps as

$$y_0(q\Delta t) = y_R(m_d \cdot \Delta t) \qquad (4.5)$$

Substituting from Eq. (4.3) into Eq. (4.5) yields

$$y_0(q\Delta t) = s(m_d \Delta t) + n(m_d \Delta t) \qquad q = 1, 2, \ldots, N \qquad (4.6)$$

Substituting from Eq. (4.4) into Eq. (4.6) we have

$$y_0(q\Delta t) = s\left\{[(q-1)d+1]\Delta t\right\} + n'\left\{[(q-1)d+1]\Delta t\right\}$$

$$q = 1,2,\dots,N$$ (4.7)

$$d = 1,2,4,8,\dots$$

From Eq. (4.7) we note that as the decimation steps d increases, large amounts of data are discarded. This consequently affects the signal-to-noise ratio.

4.2.2 Processing Results using the Periodogram with Decimation in Time

In this section we study the periodogram spectra of one ELT signal, in the presence of additive noise, processed using decimation in time technique represented by Eq. (4.7).

A pulse-modulated ELT signal is processed using the baseband processing technique with mixed carrier frequency 100 Hz and CNDR 30 dB-Hz. This signal is tested using 512 complex points for the periodogram technique with decimation steps d equal 1, 2, 4 and 8 and the results are presented in Figs. 4.3 to 4.6.

Figure 4.3 gives the periodogram result in the case of no decimation (i.e. d = 1). From this figure it can be seen that it is difficult to detect the carrier component peak due to multiple peaks near this carrier component peak. Increasing the decimation steps d to 2, 4, and to 8 provides no improvement, however, in detecting the signal as is seen in Figs. 4.4, 4.5 and 4.6 respectively.

4.3 Rate Reduction Filtering Technique

An important advantage of using the baseband processing technique is the ease in implementing rate reduction filtering of the sequence. We will show in this section that rate reduction filtering results in an improvement in both the signal-to-noise ratio and the
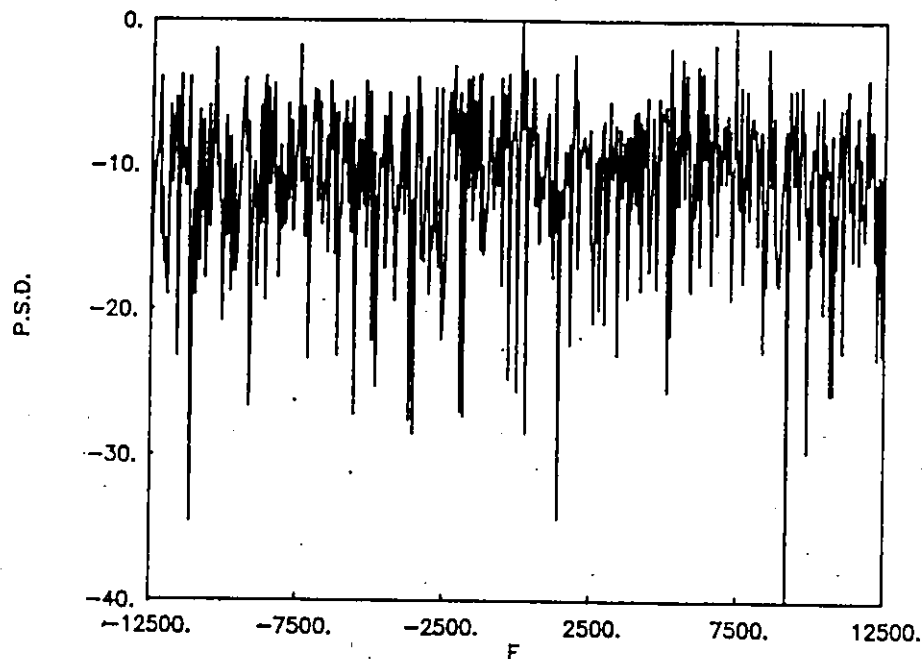
Fig. 4.3   Periodogram spectrum for coherent ELT signal with CNDR = 30 dB-Hz. No decimation in time.
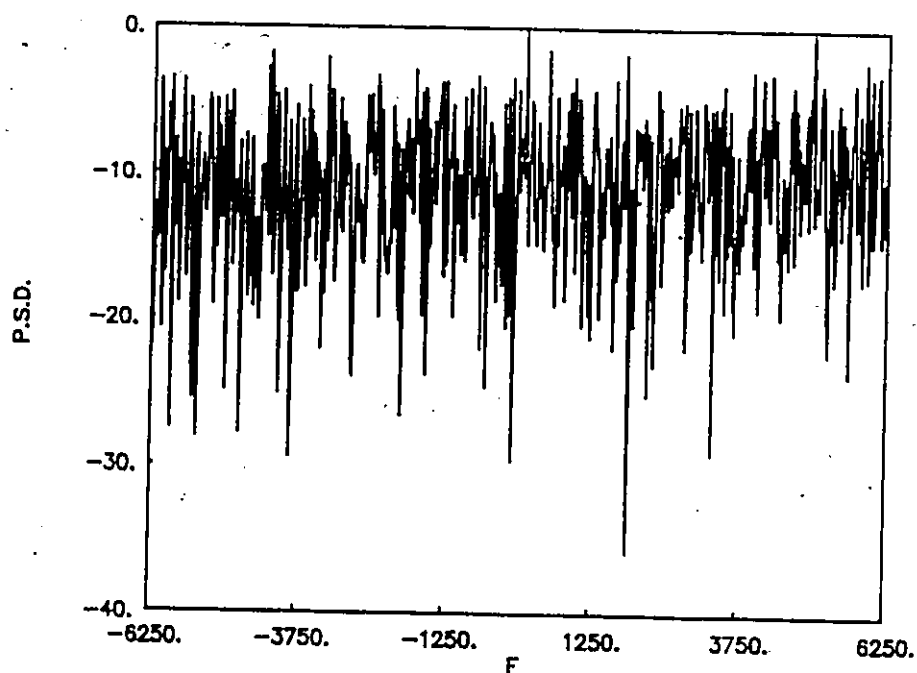
Fig. 4.4   Periodogram spectrum for coherent ELT signal with CNDR = 30 dB-Hz. Decimation in time = 2.
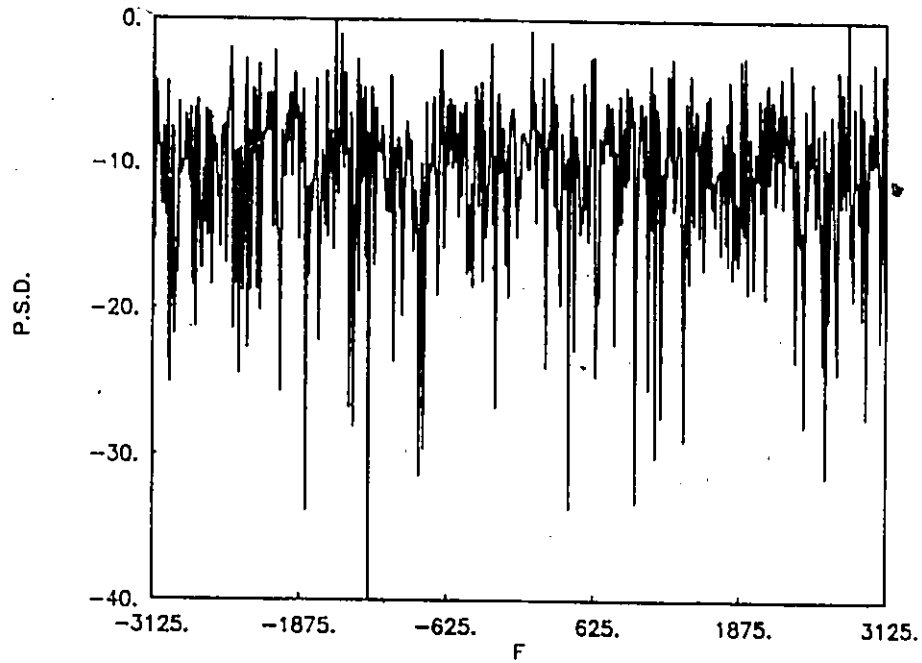
Fig. 4.5   Periodogram spectrum for coherent ELT signal with
                  CNDR = 30 dB-Hz. Decimation in time = 4.
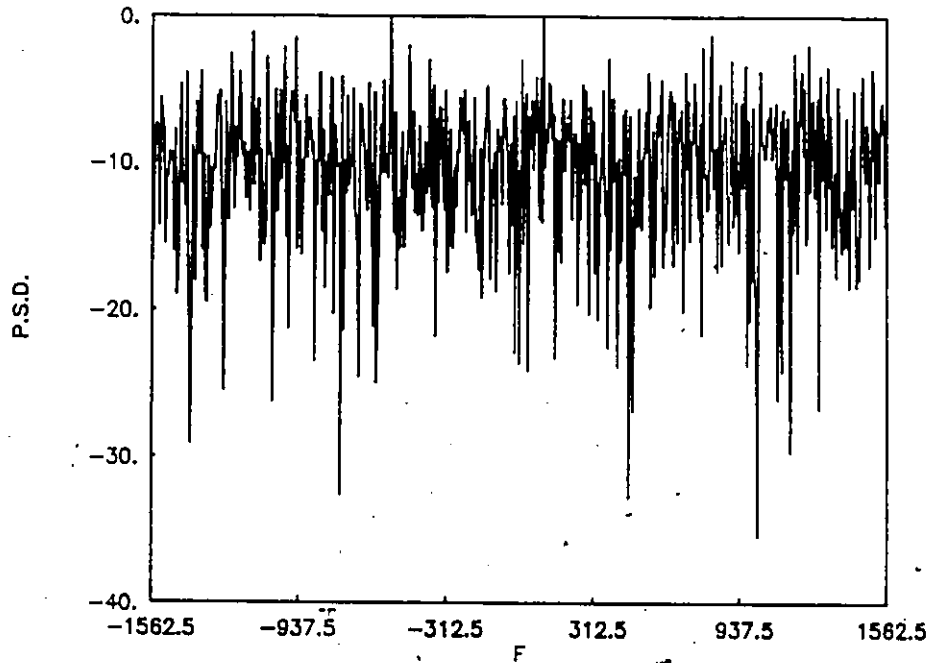
Fig. 4.6   Periodogram spectrum for coherent ELT signal with
                  CNDR = 30 dB-Hz. Decimation in time = 8.

frequency resolution. Furthermore, one could use a common FFT computing machine for rate reduction filtering since the number of points for the FFT computation do not change with this technique [26].

Let us represent the received ELT signal, in a discrete form as

$$y_R(q\,\Delta t) = s(q\,\Delta t) + n(q\,\Delta t) \qquad (4.8)$$

where

$$t = q\,\Delta t, \quad q = 1,2,3,...,N$$

and

$$N = \text{total number of points in the data.}$$

4.3.1   Rate Reduction Filtering Procedure

The concept of rate reduction filtering is based on taking the average over contiguous samples i.e.; for rate reduction by two, we take the average over two points; for rate reduction by four, we take the average over four points; and for rate reduction by ℓ, we take the average over ℓ points. This procedure can be explained mathematically as [26]:

We represent the rate reduction (averaging) steps by ℓ, which is given by

$$\ell = 2^r \quad , \quad r = 0, 1, 2, 3, ... \qquad (4.9)$$

Thus, $\ell = 1$ corresponds to no averaging, while $\ell = 2$ represents averaging by 2 and so on.

The signal can be represented mathematically as given in Eq. (4.8), and the expression for the index used to calculate the rate reduction filtering procedure in general is given by

$$m_\ell = (q-1)\ell + 1 \quad , \quad q = 1, 2, 3, ..., N$$

$$\ell = 1, 2, 4, ..., L \qquad (4.10)$$

We can represent the signal in terms of averaging steps as

$$y_o(q\Delta t) = \frac{1}{\ell} \sum_{m_\ell = (q-1)\ell+1}^{q\ell} y_R(m_\ell\Delta t), \qquad \begin{array}{l} q = 1,2,3,..., N \\ \ell = 1, 2, 4,..., L \end{array} \qquad (4.11)$$

Substituting from Eq. (4.8) into Eq. (4.11), we get:

$$y_o(q\Delta t) = \frac{1}{\ell} \sum_{m_\ell = (q-1)\ell+1}^{q\ell} \left[s(m_\ell\Delta t) + n(m_\ell\Delta t) \right], \qquad \begin{array}{l} q = 1,2,..., N \\ \ell = 1, 2, 4, ..., L \end{array} \qquad (4.12)$$

The effect of averaging reduces the effect of noise and improves the carrier-to-noise density ratio (CNDR). The average takes place over a certain number of averaging steps, i.e. averaging by two, by four and by ℓ, as described before. Thus, the general form of CNDR using this technique with averaging steps ℓ, can be expressed

$$CNDR_\ell = \ell \cdot CNDR$$

$$= 2^r \; CNDR \; , \quad r = 0, 1, 2, ... \qquad (4.13)$$

Applying the decibel notation yields

$$(CNDR_\ell)_{dB-Hz} = (CNDR)_{dB-Hz} + (3\ r)_{dB-Hz} \quad , r = 0, 1, 2, ... \; . \qquad (4.14)$$

where

$CNDR)_{dB-Hz}$ = carrier-to-noise density ratio in dB-Hz in the case of no rate reduction, i.e. in the case of $r = 0$.

Comparing the power level of CNDR in the case of no rate reduction , and these cases; rate reduction by two, by four, ..., and by ℓ, it is clear that the CNDR is improved by 3 dB-Hz in the case of averaging by two, and by 6 dB-Hz in the case of averaging by four, and consequently by 3r dB-Hz in the case of averaging by ℓ.

4.3.2 Rate Reduction Filtering Using Periodogram Technique

We now examine the periodogram spectra of one ELT signal, in the presence of additive noise, processed using the rate reduction filtering technique. The signal is processed using the baseband technique with cut-off frequency of the low-pass filter $B_c = 12.5$ kHz,

mixed carrier frequency $F_{MIX} = 100$ Hz and carrier-to-noise density ratio (CNDR) level equal 30 dB-Hz. We choose 512 complex points for the FFT technique with averaging steps, ℓ, equal to 1, 2, 4 and 8.

Figures 4.7 to 4.10 show the periodogram spectral estimation results for the four values of ℓ. From these results, it is seen that in Figure 4.7 in the case of no averaging, it is difficult to detect the carrier peak of the signal due to multiple peaks near the carrier frequency of the signal. Figure 4.8 illustrates the results in the case of averaging by 2. In this figure, the level of the side peaks is reduced by 3 dB. Figure 4.9 gives the results in the case of $\ell = 4$. Also, the level of the side peaks is reduced by a further 3 dB which improves the detection of the carrier component. In this figure, at the –8 dB threshold level, only one peak is detected, which is the carrier component peak. Figure 4.10 depicts the results in the case of $\ell = 8$. In this figure, it is clear that the level of the side peaks is reduced, and only one peak is detected above the threshold level of –11 dB, this peak being the carrier peak component. From the above analysis, we note that the periodogram technique with rate reduction filtering with $\ell = 8$ gives an excellent improvement in the signal-to-noise ratio and the frequency resolution.

4.3.3   Comparison of Decimation in Time and Rate Reduction Filtering

In this section we compare the results using decimation in time and rate reduction filtering techniques obtained from the periodogram method. Figure 4.6 depicts the result using decimation in time with decimation step (d) equal to 8 and Fig. 4.10 illustrates the result using rate reduction filtering method with averaging step (ℓ) equal to 8. We note that:

1.   For the result shown in Fig. 4.6, it is difficult to detect the carrier component peak of the ELT signal since large amounts of the data are discarded.
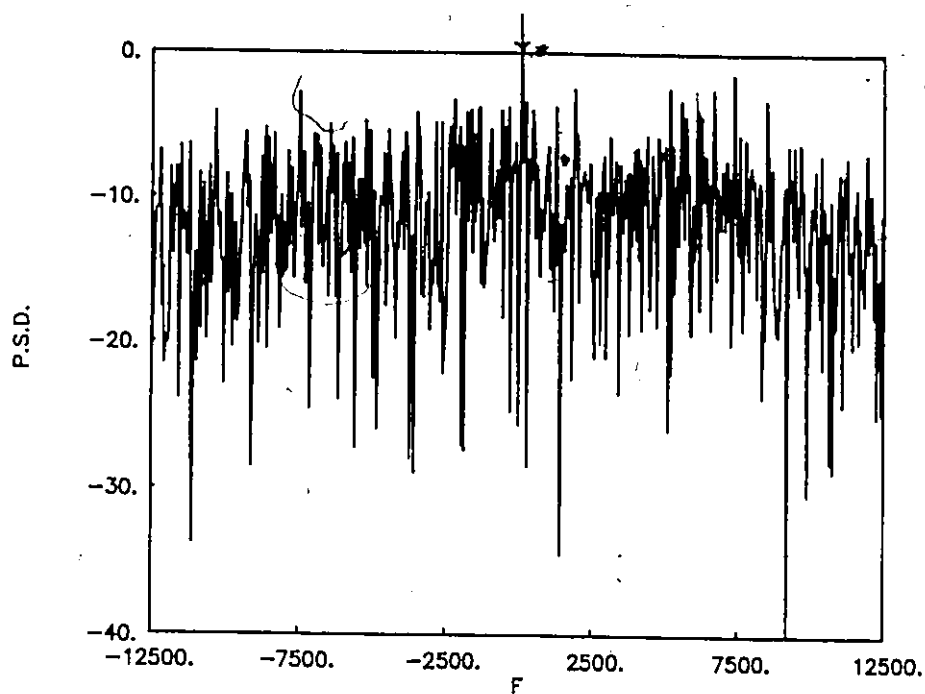
Fig. 4.7   Periodogram spectrum for coherent ELT signal with
CNDR = 30 dB-Hz. No rate reduction.

Fig. 4.8   Periodogram spectrum for coherent ELT signal with
CNDR = 30 dB-Hz. Rate reduction = 2.

Fig. 4.9.   Periodogram spectrum for coherent ELT signal with
CNDR = 30 dB-Hz. Rate reduction = 4.

Fig. 4.10   Periodogram spectrum for coherent ELT signal with
CNDR = 30 dB-Hz. Rate reduction = 8.

2.   For the rate reduction filtering method result given in Fig. 4.10, the one peak can be detected easily above −11 dB threshold level. This peak being the carrier component peak.

Thus, from the above analysis and computer simulation results we conclude that rate reduction filtering method improves the frequency resolution and the signal-to-noise ratio which consequently improves the detection of the carrier component peak of the ELT signal.

4.4   Baseband Processing Strategies

In the real signal environment, the data set to be processed has a frequency bandwidth of 25000 Hz and a time continuance ranging from a few seconds up to approximately 900 s. The main restriction in processing this data is the capability of the spectrum analyser be it either the periodogram or the MEM processor. Thus, let us examine three different processing strategies [26].

4.4.1   Strategies

Case 1

The first strategy assumes the data to be divided into K continguous blocks with the number of samples in each block P equal to the length of the spectral processor; e.g. 1024 points for the 1K FFT. Then, the spectral estimator processes the data and the K blocks are averaged, as previously discussed in Chapter 3.

The advantage of averaging the K blocks lies in the fact that the variance of the estimate is reduced by the factor K. However, for a single estimate the ratio of standard deviation to mean is $\{[2(2-\pi/2)]/\pi\}^{1/2} = 0.522$ since the output of the periodogram is Rayleigh

distributed. If the square of the mean is taken to be 1 (0 dB), then most of the peaks of the spectral estimate will be within approximately 1.522 (3.7 dB above) the 0 dB reference. If this variance is to be reduced to, say 1 dB, then approximately 18 periodograms must be averaged.

Let us now calculate the time requirement, the SNR, the resolution and the reduction in variance using this method. For K blocks of P points, the time required is proportional to the number of mutiplications which is approximately

$$T_1 = T_M \, K \, P \log_2 (P) \tag{4.15}$$

where T_M is time for one multiplication.

The signal-to-noise ratio at $f = f_c$ is [31]

$$SNR = \left(\frac{A_2^2 \, d \, T_D}{N_0} \right) K^{1/2} = SNR_N \, K^{1/2} \tag{4.16}$$

where SNR_N is the normalized signal-to-noise ratio. The reduction in the variance of the estimate is given by K, and the resolution is approximately $1/T_D$.

Case 2

The second strategy assumes the data to be divided into Q separate frequency bands using bandpass filters (perhaps switched-capacitor filters), as shown in Fig. 4.11, with each band then separately being mixed to baseband. Since the bandwidth of each band is now B/Q, the sampling rate can be reduced by a factor of Q using rate reduction filtering described earlier. Then, the spectral estimator processes each of these separate bands averaging K/Q blocks for each band.

For this case, the number of multiplications is

$$T_2 = T_M \, Q \, K/Q \, P \log_2 (P) = T_M \, K \, P \log_2 (P) \tag{4.17}$$

However, the signal-to-noise ratio is now
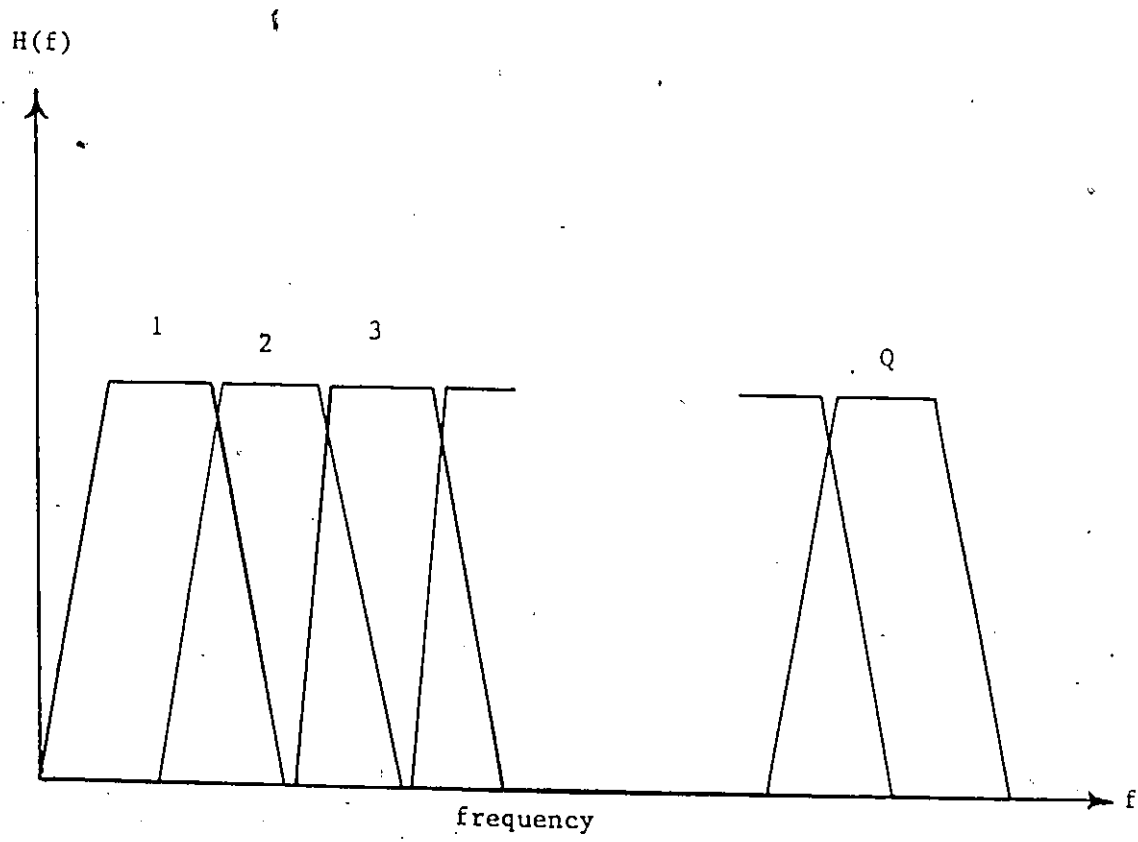
Fig. 4.11   Bandpass filtering using a contiguous bank of filters.

$$SNR = \left(\frac{A_2^2 d\, Q\, T_D}{N_O} \right) \left(\frac{K}{Q} \right)^{1/2} = SNR_N (KQ)^{1/2} \qquad (4.18)$$

and the resolution is about $1/QT_D$. The reduction in variance is now $[K/Q]$.

Case 3

The third strategy assumes the use of a one-shot processor in which all $N = K\,P$ samples are processed in one operation. In this case, the time requirement is simply

$$T_3 = T_M\, K\, P \log_2 (K\, P)$$

$$= T_M\, K\, P\, [\log_2 (K) + \log_2 (P)] \qquad (4.19)$$

The signal-to-noise ratio is given by

$$SNR = \left(\frac{A_2^2 d\, K\, T_D}{N_O} \right) = SNR_N\, K \qquad (4.20)$$

The resolution in this case is approximately $1/KT_D$. Finally, since there is no averaging, there is no reduction in variance which is the main drawback of this strategy.

4.4.2 . Comparison of Strategies

It is recognized that in Case 1 and Case 2, some time must be allotted for computing the averages. Normally, this amount of time is small compared to the computation of the periodograms and is ignored here. As well, some added hardware would be required in order to implement Case 2 but this addition is relatively small compared to the overall system. Table 4.1 provides a sample comparison of the strategies for the processing of 1 s of data assuming a sampling rate of 51200 samples per second (B = 25000 Hz), with K = 50, P = 1024 and Q = 8. From these results, we see that Case 2 has better performance in SNR and

resolution than Case 1 and greater reduction in variance than Case 3. Thus, the technique of dividing the signal into bands and processing using rate reduction filtering is now examined.

Table 4.1

Case	Normalized Computation Time T_i/T_M	SNR/SNR$_N$ in dB	Resolution Hz	Reduction in Variance
1	512000	8.5	± 49	50
2	512000	13.0	± 6.1	6.25
3	801000	17.0	± 1	1

4.5   Rate Reduction Filtering Using MEM

We now apply the MEM to the output of the rate reduction filter. The same pulse-modulated ELT signal with mixed carrier frequency equal 100 Hz and CNDR level equal 30 dB-Hz is processed using the baseband system. In order to detect this ELT signal without using rate reduction filtering we use higher MEM filter order (i.e. MEM = 100) as discussed before in Chapter 3. By using MEM with this technique, the MEM filter order can be reduced considerably. Figures 4.12 to 4.15 illustrates the MEM = 50 spectra of this pulse-modulated ELT signal with averaging steps ℓ equal 1, 2, 4 and 8. In Fig. 4.12, there are many false peaks located across the frequency band. These false peaks mask the signal and make detection difficult. In Fig. 4.13, the MEM spectra is given using ℓ equals 2, and the carrier component occurs at 85 Hz which is equivalent to a frequency error equal 15 Hz. Increasing ℓ to 4, the MEM spectral estimation is depicted in Fig. 4.14. In this figure, the main peak of
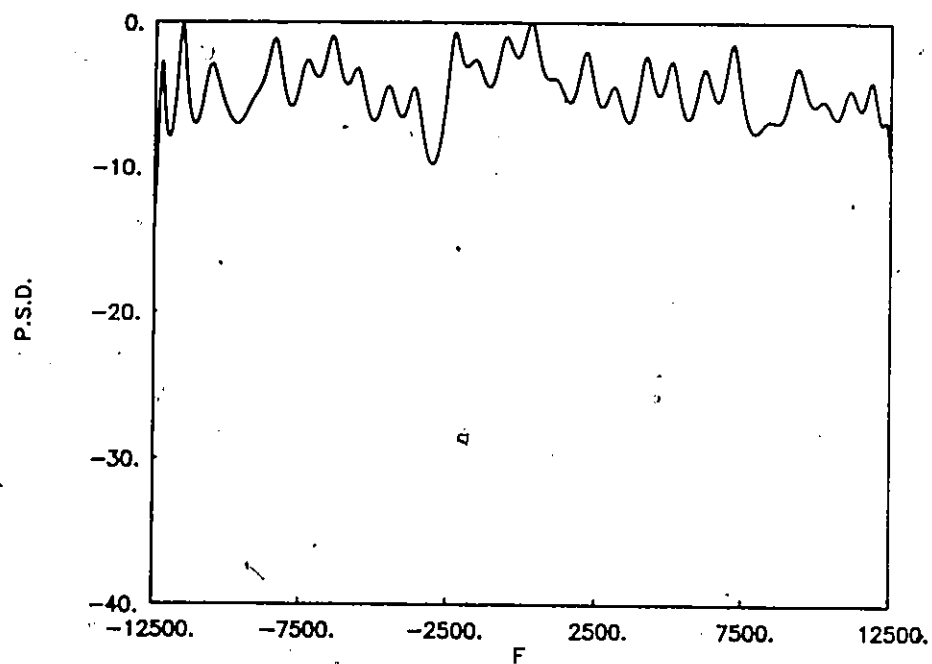
Fig. 4.12   MEM = 50 spectrum for coherent ELT signal with CNDR = 30 dB-Hz.
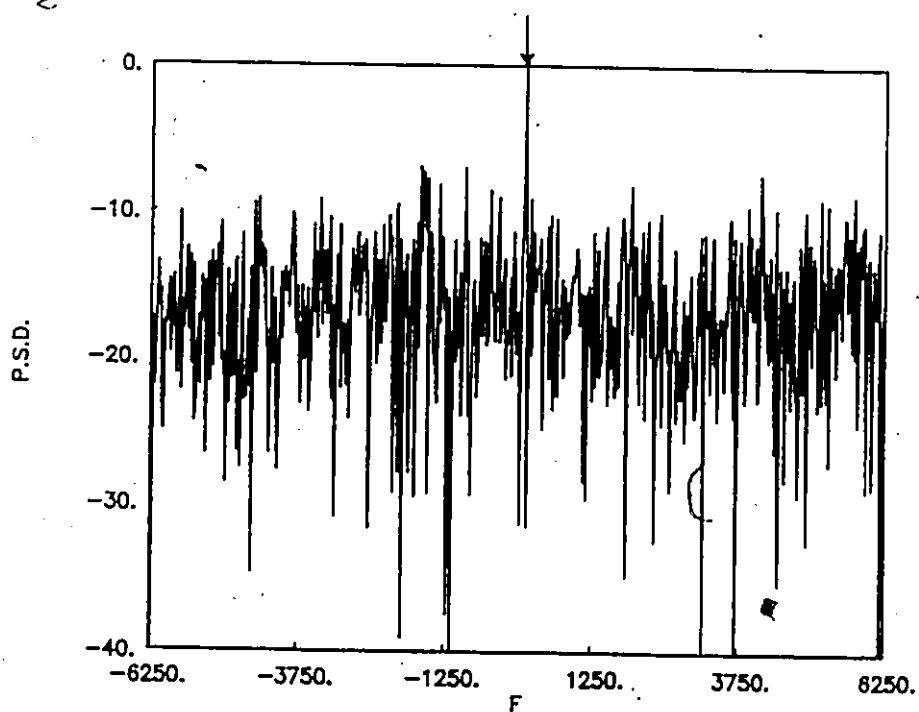   No rate reduction.
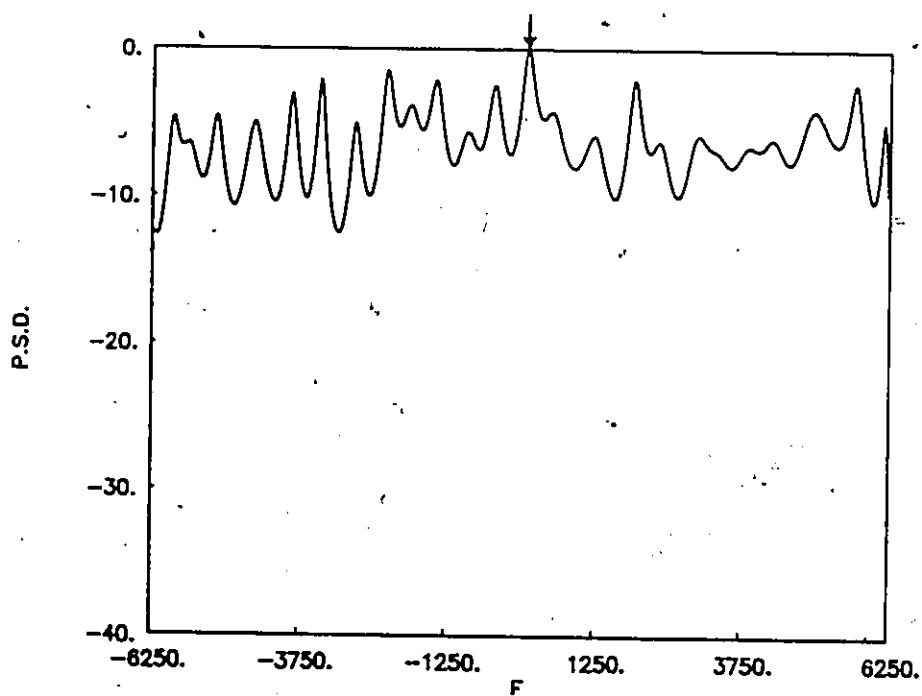
Fig. 4.13   MEM = 50 spectrum for coherent ELT signal with
                   CNDR = 30 dB-Hz. Rate reduction = 2.
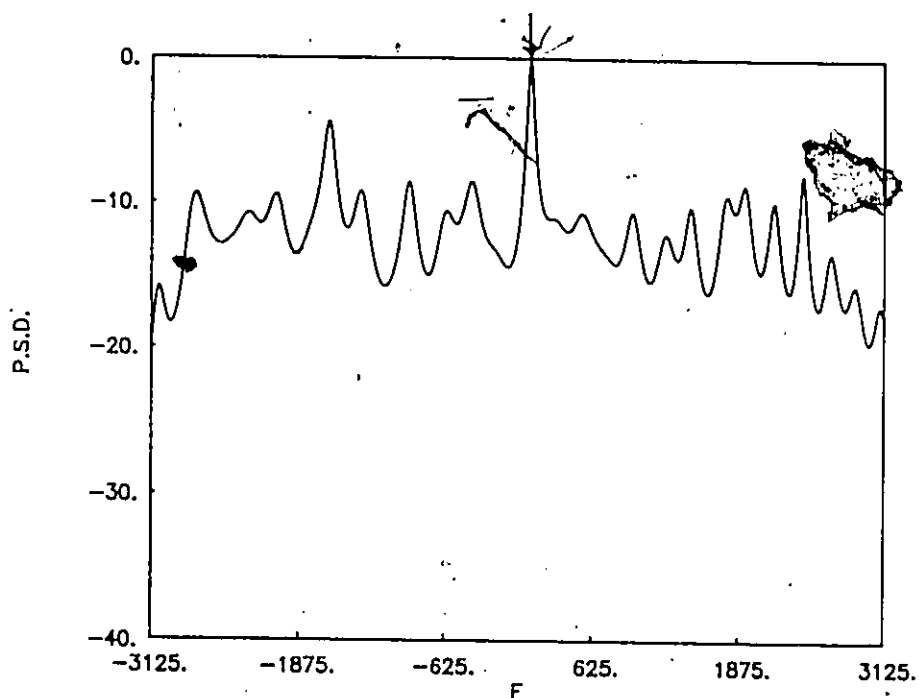
Fig. 4.14   MEM = 50 spectrum for coherent ELT signal with
CNDR = 30 dB-Hz. Rate reduction = 4.
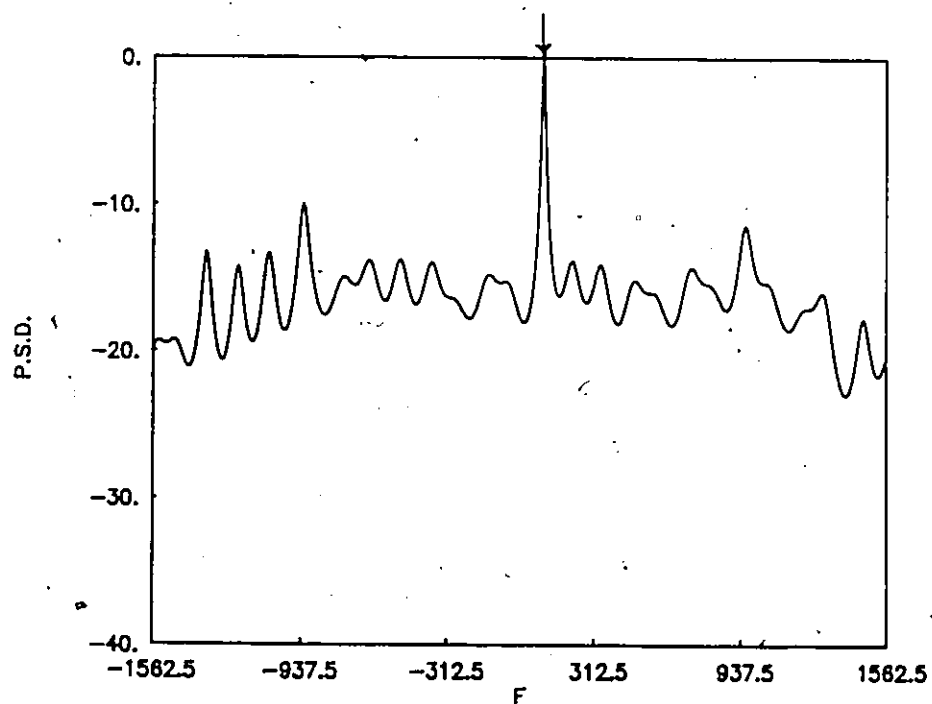
Fig. 4.15   MEM = 50 spectrum for coherent ELT signal with
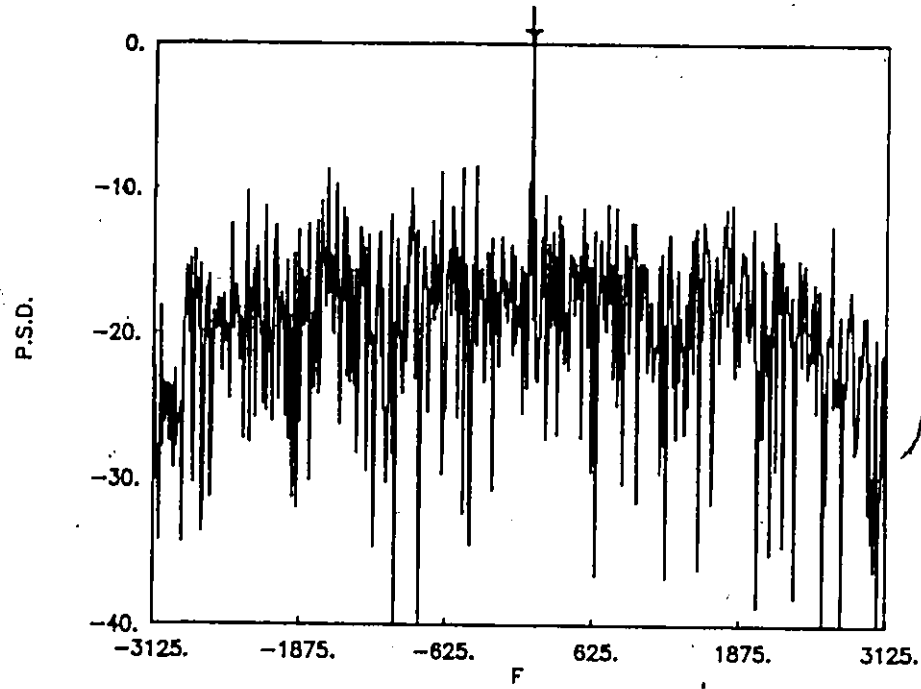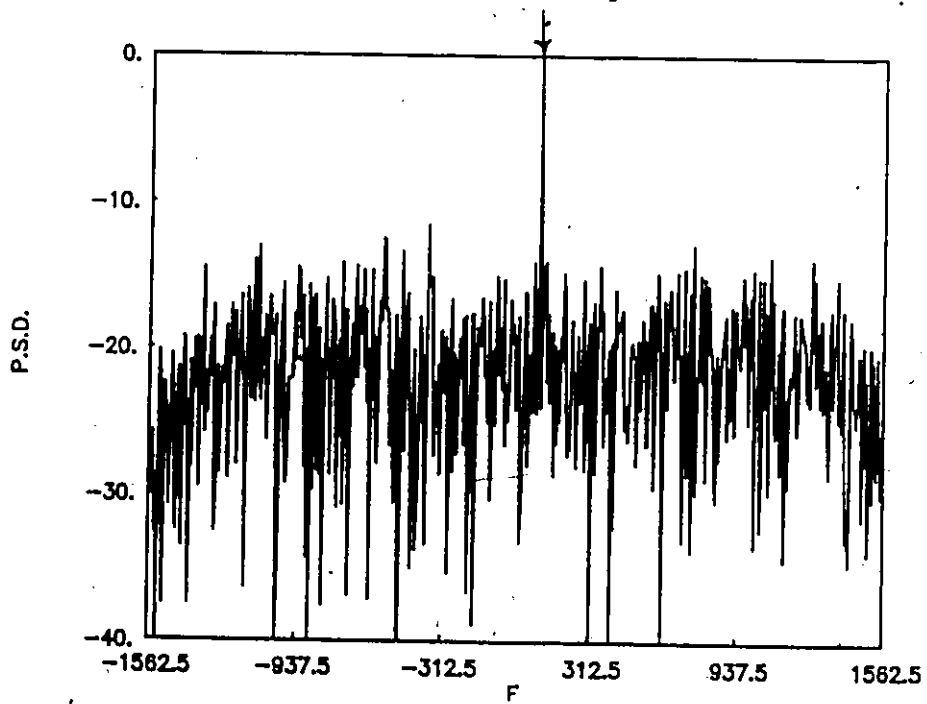CNDR = 30 dB-Hz. Rate reduction = 8.

carrier is located at 92 Hz which is equivalent to frequency error of 8 Hz. As ℓ increases to 8, the MEM spectral estimation is given in Fig. 4.15. The carrier peak component is located at 98 Hz which corresponds to a frequency error equal to 2 Hz. From the above analysis it is clear that the frequency error is reduced as the averaging steps ℓ increase. Thus, we note that the combination of linear filtering and non-linear spectral estimation improves the performance considerably.

Comparing the results obtained using MEM = 100 without using rate reduction filtering with those using MEM = 50 using this technique with $\ell = 8$ (Fig. 3.26 and Fig. 4.15), we observe that the frequency error is the same for both cases, but the new method reduces the MEM filter order which consequently reduces the computation time, since high MEM filter orders are very consuming of computer time. Thus, by using the MEM technique with rate reduction filtering, the signal at low CNDR levels can be resolved using lower MEM filter order and excellent results are obtained with very small frequency error.

4.6 Emergency Locator Transmitter (ELT) Signal Tracking

This section describes a proposed method called "ELT Signal Tracking". By using this method we can track the ELT signal and estimate its mixed carrier frequency which eases the detection of the ELT signal. The idea of this method is based on processing the ELT signal using the MEM with rate reduction filtering technique.

First, we will discuss the frequency error as a function of CNDR level for the ELT signal processed using the MEM with low MEM filter order. The frequency error is reduced by processing the ELT signal at the same CNDR level using the baseband MEM with rate reduction filtering technique and the same MEM filter order. Furthermore, by using this method the frequency resolution is improved.

4.6.1   Noise and Frequency Error

This section is concerned with the study of the variation of frequency error through the whole frequency band for different values of CNDR. In addition, we investigate the effect of reducing the CNDR level on the frequency error using low MEM filter order.

We consider the values of CNDR ranging from 84 dB-Hz to 44 dB-Hz in 20 dB-Hz steps. The pulse modulated ELT signal is processed using the baseband MEM processing technique with MEM filter order equal to 3.

Three different mixed carrier frequencies are examined here using 512 complex points at a sampling rate of 25,000 inphase and quadrature samples per second. These frequencies are chosen equal to -11000 Hz, 11000 Hz and 200 Hz respectively.

In order to study the variation of the frequency error through the frequency band, these frequencies are selected such that two of them lie at the edges of the frequency band and the third is located near the center of the band. We define frequency error as the difference between the true mixed carrier frequency and the estimated mixed carrier frequency.

First, the ELT signal with mixed carrier frequency equal to -11 kHz is examined here using the baseband MEM processing technique. Table 4.2 summarizes the variation of the frequency error as the CNDR level reduces from 84 dB-Hz to 44 dB-Hz. Figure 4.16 shows the MEM $= 3$ spectra of this ELT signal for three different values of CNDR level. From these results it is clear that, the frequency error increases as the CNDR level decreases. This causes severe degradation in signal performance.
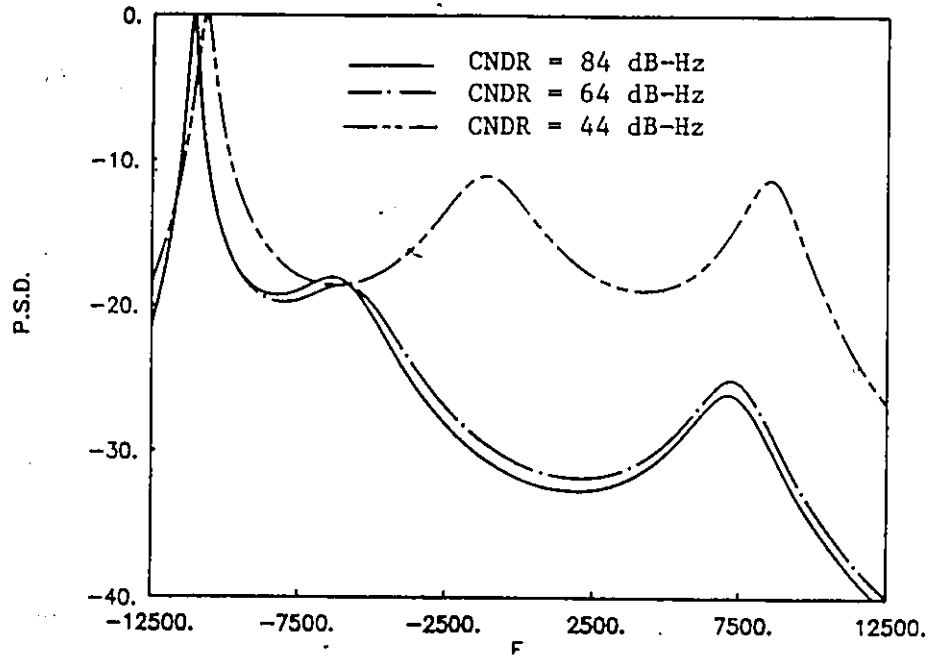
Fig. 4.16 .   MEM = 3 spectrum for coherent ELT signal with mixed carrier frequency = -11 kHz.
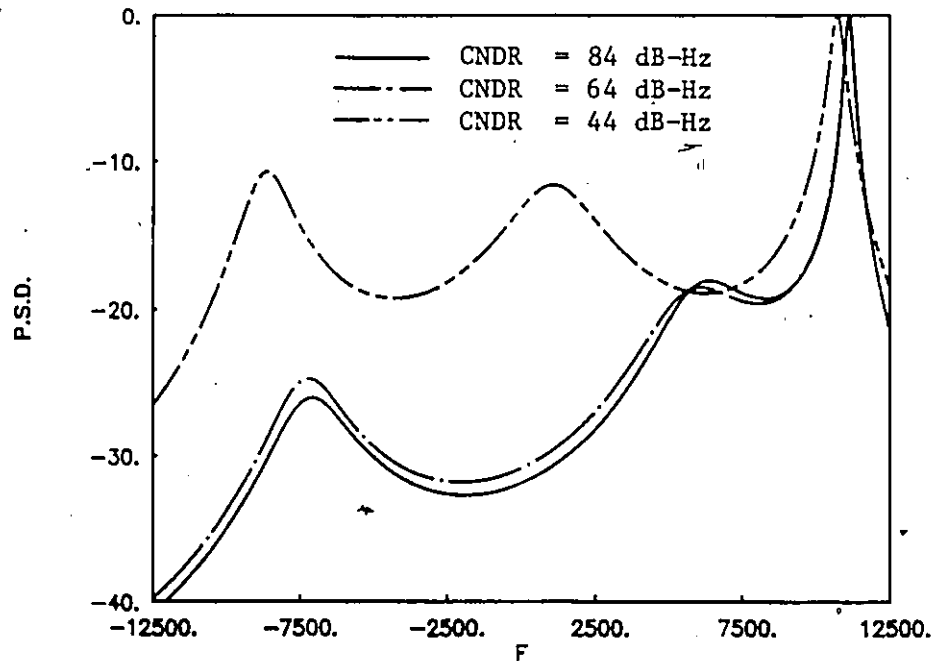
Fig. 4.17   MEM = 3 spectrum for coherent ELT signal with mixed carrier frequency = 11 kHz.

TABLE 4.2

MEM Filter Order = 3

Mixed carrier Frequency Hz	CNDR dB-Hz	estimated peak Location Hz	frequency error Hz
− 11000	84	− 11132.8	133
− 11000	64	− 11132.8	133
− 11000	44	− 10742.2	258

The second mixed carrier frequency examined here equals 11000 Hz. Table 4.3 summarizes the frequency error for the various CNDR level. Figure 4.17 depicts the MEM spectrum results for this ELT signal with three different values of CNDR level. From these results, again it is seen that reducing the CNDR level to 44 dB-Hz increases the frequency error which consequently affects the signal detection.

TABLE 4.3

MEM Filter Order = 3

Mixed carrier Frequency Hz	CNDR dB-Hz	estimated peak Location Hz	frequency error Hz
11000	84	11132.8	133
11000	64	11132.8	133
11000	44	10742.2	258

Table 4.4 gives the variation of the frequency error with different CNDR levels for the ELT signal, this time, with mixed carrier frequency 200 Hz. Figure 4.18 depicts the MEM spectra for this ELT signal with three different values of CNDR level. Again, we note that reducing the CNDR level to 44 dB-Hz increases the frequency error and causes severe degradation in signal detection performance using low MEM filter order.

TABLE 4.4

MEM Filter Order = 3

Mixed carrier Frequency Hz	CNDR dB-Hz	estimated peak Location Hz	frequency error Hz
200	84	147	53
200	64	147	53
200	44	0	200
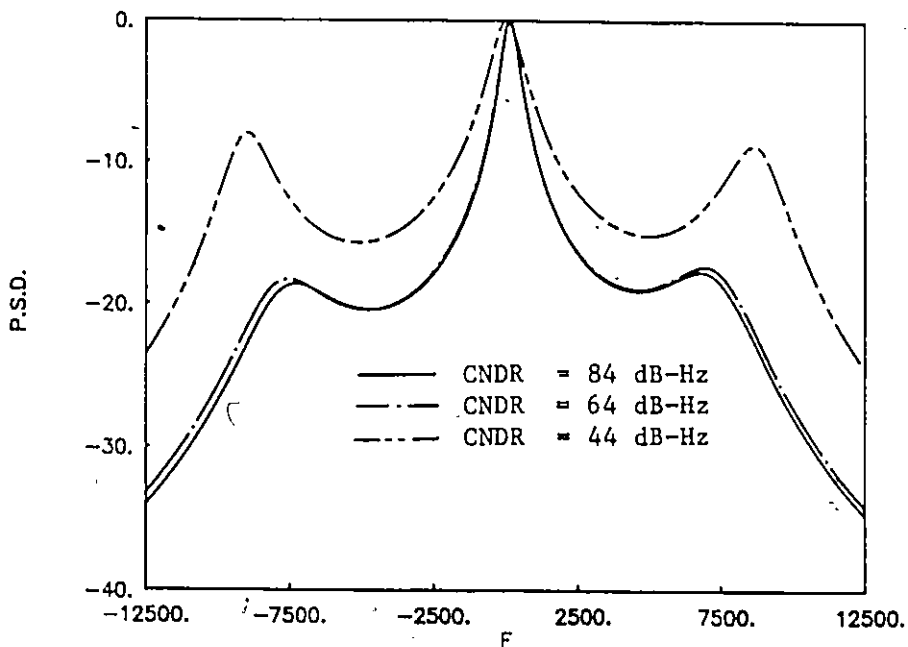
Fig. 4.18   MEM = 3 spectra for coherent ELT signal with mixed carrier frequency = 200 Hz.
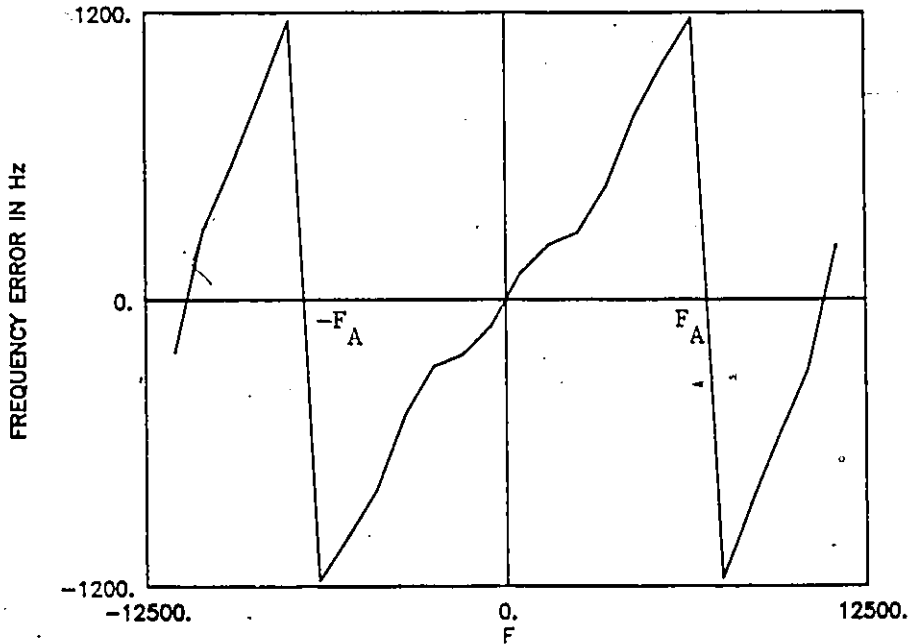
Fig. 4.19   Frequency error performance for coherent ELT signal.

Thus, from the above we conclude that, at high CNDR level, e.g. 84 dB-Hz, the frequency error is reduced. This frequency error increases as the CNDR level decreases to 44 dB-Hz.

Error Curve

This section discusses the frequency error performance curve (error curve) of a pulse wave modulated ELT signal with CNDR level equal 44 dB-Hz processed using the baseband MEM processing technique with MEM filter order 3. Figure 4.19 illustrates the frequency error curve for this pulse-modulated ELT signal. From the simulation results shown in this figure, and earlier analysis, we observe that:

1. When $f_c - R_I = 0$, the frequency error is approximately zero.

2. The error curve is an odd function around the origin.

3. As an approximation, a straight line curve can be drawn between frequencies $-F_A$ and F_A, with slope $K_c = 0.18$. This will be used later to demonstrate the tracking feature.

4. The frequency error depends on the mixed carrier frequency of the ELT signal. The frequency error increases as the mixed carrier frequency of the ELT signal moves away from the center band frequency, i.e. near the edges of the frequency band.

4.6.2   Reducing the Effect of Noise

The capability of each processor to detect the ELT signals in the presence of noise is an important characteristic of its performance. In order to reduce the frequency error and improve the detection of the ELT at low CNDR level using low MEM filter order, we process

the ELT signal using the baseband MEM with rate reduction filtering. By using this method, improved resolution is obtained and increased signal-to-noise ratio is achieved.

In this section we study the frequency error versus the CNDR level of the ELT signal, processed using the baseband MEM with rate reduction filtering technique. A pulse-modulated ELT signal with mixed carrier frequency equal to 200 Hz is processed using this method with MEM filter order 3 and averaging steps equal to 8. This ELT signal is examined at three different values of CNDR level. The CNDR level is reduced from 84 dB-Hz down to 44 dB-Hz in steps of 20 dB-Hz.

Table 4.5 summarizes the frequency error as a function of the CNDR levels for this ELT signal, using the MEM with rate reduction filtering technique. Figure 4.20 illustrates the baseband MEM spectra for this ELT signal at these three different values of CNDR level. These results indicate that, processing the ELT signal using this technique with averaging steps equal to 8 reduces the frequency error. In addition, a sharp peak is obtained with excellent frequency resolution at high CNDR level, e.g. 84 or 64 dB-Hz, this peak being the carrier component of the ELT signal.

Comparing the frequency error results summarized in Table 4.4, Table 4.5, Fig. 4.18 and Fig. 4.20, we conclude the following:

1.   Processing the ELT signal using the baseband MEM with rate reduction filtering technique and with averaging steps equal to 8 reduces the frequency error.

2.   The ELT signal at low CNDR level can be resolved using low MEM filter order by using this technique.

3.   This method improves the sharpness in the carrier component peak as shown in Fig. 4.20 and the detection of the ELT signal.
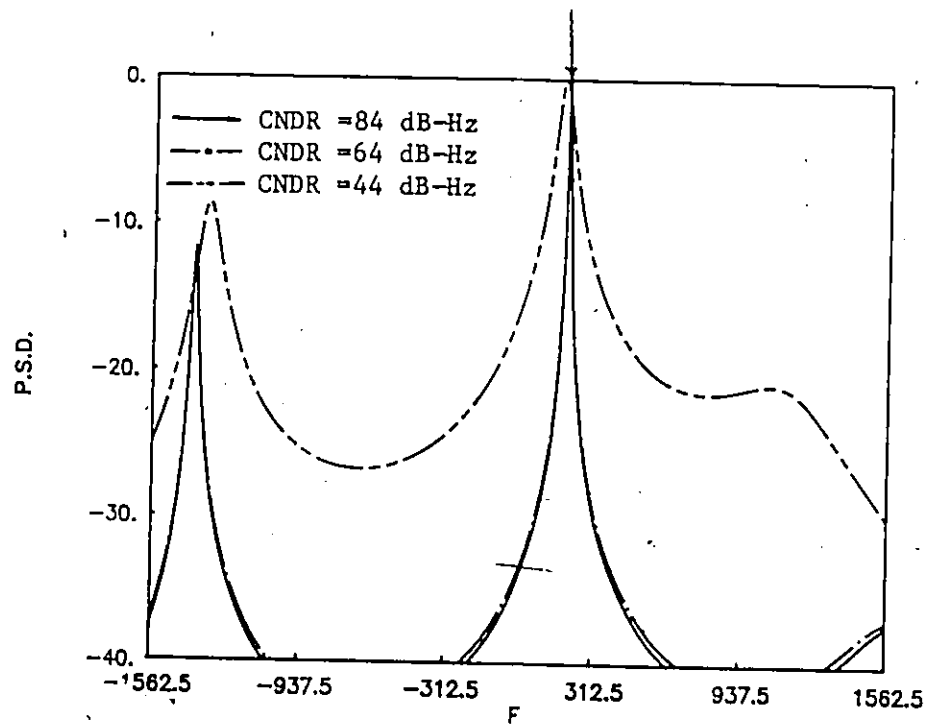
Fig. 4.20   MEM = 3 spectrum for coherent ELT signal with mixed carrier frequency = 200 Hz . Rate reduction = 8.

TABLE 4.5

MEM Filter Order = 3

Rate Reduction (averaging) steps = 8

Mixed carrier Frequency Hz	CNDR dB-Hz	estimated peak Location Hz	frequency error Hz
200	84	196	4
200	64	196	4
200	44	177	23

4.7 Evaluation of the Location of the Carrier Component Peak

In this section, we evaluate and estimate location of the carrier component peak using an iterative approach. Consider a pulse-modulated ELT signal with constant carrier frequency $f_c = f_{co}$ processed using the baseband processing technique with mixing frequency F_I. The carrier component peak then occurs at mixed carrier frequency F_c given by,

$$F_c = f_{co} - F_I \tag{4.21}$$

The carrier component peak is estimated using MEM filter order 3 and located at measured frequency f_m which is given by

$$f_m = F_c - f_e \tag{4.22}$$

where

F_c = mixed carrier frequency

f_e = frequency error

Then, the frequency error f_e is represented by

$$f_e = F_c - f_m \qquad (4.23)$$

From Fig. 4.19, it is seen that the frequency error is approximately zero at $F_c = 0$. Thus, using an iterative approach, we mix the signal in such a way to produce a carrier peak close to zero frequency. In order to demonstrate convergence, we assume the straight-line approximation.

1st Iteration

After the first measurement, the carrier component peak is located at estimated frequency f_{m1}. The mixed carrier frequency and the frequency error corresponding to this case are F_{c1} and f_{e1}, respectively.

Thus, Eq. (4.22) corresponding to this case becomes

$$f_{m1} = F_{c1} - f_{e1} \qquad (4.24)$$

and the mixed carrier frequency F_{c1} is given by

$$F_{c1} = f_{co} - F_{I1} \qquad (4.25)$$

where ·

F_{I1} = the mixing frequency used for the first measurement.

We note that, the frequency error varies linearly as a function of the mixed carrier frequency as shown in Fig. 4.19.

Then,

$$f_{e1} = K_c F_{c1} \qquad (4.26)$$

where

K_c = constant

substituting from Eq. (4.26) into Eq. (4.24), yields

$$f_{m1} = (1 - K_c) F_{c1} \qquad (4.27)$$

2nd Iteration

Now, the ELT signal is mixed using new mixing frequency F_{I2} given by,

$$F_{I2} = F_{I1} + f_{m1} \qquad (4.28)$$

where

F_{I1} = mixing frequency for the first measurement

After the second measurement, the carrier component peak has mixed carrier frequency F_{c2}, and located at estimated frequency f_{m2} with frequency error f_{e2}.

Then,

$$f_{m2} = F_{c2} - f_{e2} \qquad (4.29)$$

Using linearity as considered earlier, we have

$$f_{e2} = K_c F_{c2}$$

Then, using this equation, Eq. (4.29) becomes

$$f_{m2} = (1 - K_c) F_{c2} \qquad (4.30)$$

3rd Iteration

For the 3rd iteration, the ELT signal is mixed using mixing frequency F_{I3} represented by

$$F_{I3} = F_{I2} + f_{m2} \qquad (4.31)$$

After this measurement, we have

The mixed carrier frequency of the ELT signal = F_{c3}.

The carrier component peak is located at   = f_{m3}

The corresponding frequency error   = f_{e3}

Thus, for this case we have

$$f_{m3} = F_{c3} - f_{e3} \qquad (4.32)$$

and

$$f_{e3} = K_c \, F_{c3}$$

yielding

$$f_{m3} = (1 - K_c) \, F_{c3} \qquad (4.33)$$

ith Iteration

Similarly, using the same procedure, we have

$$f_{mi} = (1 - K_c) \, F_{ci} \qquad (4.34)$$

where

f_{mi} = the estimated location of the carrier component peak after ith measurement.

F_{ci} = mixed carrier frequency of the carrier component peak at this iteration.

Now, we will formulate Eq. (4.34) in terms of the mixing frequency.

For the first measurement, we consider the mixing frequency is given by

$$F_{I1} = F_{I0} + f_{m0}$$

where $\quad f_{m0} = 0$

For the second measurement, the ELT signal is mixed with new mixing frequency

F_{I2} given by

$$F_{I2} = F_{I1} + f_{m1}$$

For the 3rd measurement, the mixing frequency is given by

$$F_{I3} = F_{I2} + f_{m2}$$

or

$$F_{I3} = F_{I0} + f_{m0} + f_{m1} + f_{m2}$$

Similarly, for the ith measurement, the mixing frequency is represented by

$$F_{Ii} = F_{I(i-1)} + f_{m(i-1)}$$
$$= F_{I0} + f_{m0} + f_{m1} + f_{m2} + \ldots f_{m(i-1)}$$

Thus, in general, the mixing frequency is given by

$$F_{In} = F_{I0} + \sum_{i=0}^{n-1} f_{mi} \qquad , n = 1,2,...$$ (4.35)

At the nth iteration, the carrier component peak has mixed carrier frequency given by

$$F_{cn} = f_{c0} - F_{In}$$ (4.36)

This carrier component peak is located at measured frequency f_{mn} which is represented by (using Eq. (4.34))

$$f_{mn} = (1 - K_c) F_{cn}$$ (4.37)

substituting Eq. (4.35) and Eq. (4.36) into Eq. (4.37) yields

$$f_{mn} = (1 - K_c) \left\{ f_{co} - F_{I0} - \sum_{i=0}^{n-1} f_{mi} \right\} \qquad , n = 1,2,...$$ (4.38)

since $F_{c1} = f_{c0} - F_{I1}$ from (4.25), and using Eq. (4.35) we have

$$f_{mn} = (1 - K_c) \left\{ F_{c1} - \sum_{i=0}^{n-1} f_{mi} \right\} \qquad , n = 1,2,...$$ (4.39)

Expanding Eq. (4.39), yields

$$f_{m1} = (1 - K_c) F_{c1}$$

$$f_{m2} = (1 - K_c) \{F_{c1} - f_{m1}\}$$

$$= K_c (1 - K_c) F_{c1}$$

$$f_{m3} = (1 - K_c)\{F_{c1} - f_{m1} - f_{m2}\}$$

$$= K_c^2 (1 - K_c) F_{c1}$$

similarly,

$$f_{mn} = (1 - K_c) \left\{ F_{c1} - f_{m1} - f_{m2} .... - f_{m(n-1)} \right\}$$ (4.40)

$$= K_c^{n-1} (1 - K_c) F_{c1}$$

Since K_c is less than 1 ($K_c = 0.18$), we have with a modest value of n (4 or 5)

$$f_{mn} \rightarrow 0$$ (4.41)

Thus, from Eq. (4.39), we have the true mixed carrier frequency given by

$$F_{c1} = \sum_{i=0}^{n-1} f_{mi} \qquad , n = 1,2,3,...$$

(4.42)

Now, we describe an ELT Tracking Algorithm using this iterative approach.

4.8   ELT Tracking Algorithm

One of the most important advantages of using the baseband processing technique is the ease in implementing the ELT tracking technique. In this section we describe a new algorithm called ELT tracking algorithm. The algorithm is summarized in the following steps.

Step 1

Process the ELT signal using the baseband MEM technique using rate reduction technique with averaging steps equal to 8. This signal is processed using low MEM filter order (e.g. order = 3) with mixing frequency equal to F_{I1} and the location of the carrier component peak, is denoted by f_{m1}.

Step 2

Mix this ELT signal with new mixing frequency, F_{I2} equal to $F_{I1} + f_{m1}$, and process it again using the baseband MEM with rate reduction filtering with averaging steps equal 8. Measure the location of the carrier component peak, i.e. f_{m2}.

Step 3

Repeat step no. 2 using new mixing frequency F_{I3} equal $F_{I2} + f_{m2}$, and estimate the location of the carrier component peak, i.e., f_{m3}.

<u>Step 4</u>

Continue repeating the above procedure until the carrier component occurs at approximately 0 Hz. Then, the carrier frequency of this ELT signal equals the new mixing frequency, i.e. $f_{c0} = F_{I1} + f_{m1} + f_{m2} + \ldots + f_{m(n-1)}$

4.8.1   Results

In this section, we study the processing results of the ELT signal using "ELT Tracking Algorithm" described above. A pulse-wave modulated ELT signal with mixed carrier frequency 200 Hz and at CNDR level equal 44 dB-Hz is examined here using the procedure described with MEM filter order 3 and 512 complex points.

Table 4.6 summarizes the results obtained using this procedure. Figure 4.21 illustrates the MEM spectra for this ELT signal using the ELT Tracking Algorithm steps. From these results it is seen that the mixed carrier frequency of this ELT signal equals 201 which is in error by only 1 Hz.
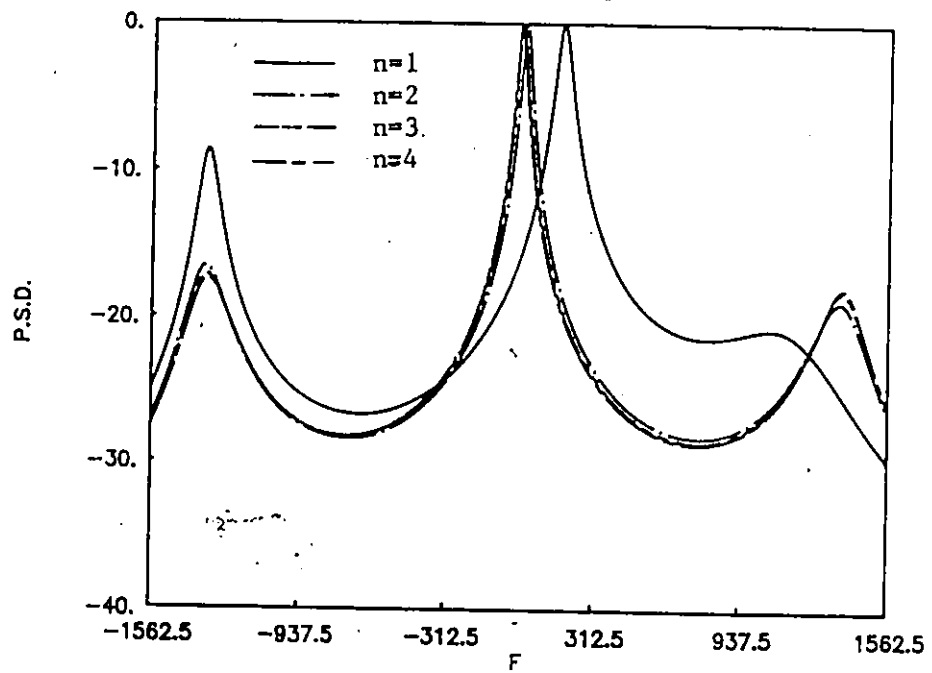
Fig. 4.21   MEM = 3 spectrum for coherent ELT signal using tracking algorithm.

Table 4.6

ELT Specification

Mixed carrier frequency = F_{c1} = 200 Hz

CNDR   = 44 dB-Hz

Rate Reduction (averaging) steps = 8

MEM filter order   = 3

Step Number	Mixed Carrier frequency Hz F_{ci}	Estimated Peak location Hz f_{mi}	Frequency error Hz f_{ei}
step 1	200	177	23
step 2.	23	18	5
step 3	5	6	−1
step 4	−1	0	−1

4.9   Summary

In this chapter we have examined the advantages of using the baseband processing technique. A theoretical analysis of two different techniques used for sampling rate reduction have been described; namely, 1) decimation in time, and 2) rate reduction filtering. A comparison between these two methods has also been given. This comparison indicates that rate reduction filtering method provides certain advantages over decimation in time. The application of using this method with the periodogram and MEM are described in detail.

In this chapter we have also discussed the frequency error across the frequency band. In all cases described, we conclude the following:

1. Reducing the CNDR level increases the frequency error and causes severe degradation in signal detection using the MEM with low filter order.

2. The frequency error across the frequency band is dependent on the mixed carrier frequency of the ELT signal.

3. The frequency error is small if the mixed carrier frequency of the ELT signal lies near the mid-band range.

4. The frequency error is large if the mixed carrier frequency of the signal lies at the edges of the band range.

Processing an ELT signal at constant CNDR level with the MEM and increasing the order of the rate reduction filtering reduces the frequency error, increases the signal to noise ratio and produces a sharp peak at the carrier frequency of the ELT signal. This consequently improves the detection of the carrier component peak of the ELT signal.

In this chapter we have also described a new method called "ELT tracking". By using this method we can easily track the ELT signal and estimate its mixed carrier frequency which simplifies the detection of the carrier component peak.

CHAPTER 5

BASEBAND PROCESSING FOR THE MULTIPLE

ELT SARSAT ENVIRONMENT

5.1   Introduction

In earlier chapters we assumed only one ELT signal. However, in most practical situations, the received signal comprises more than one ELT signal due to false alarms which may mask the signal from a platform in distress. In addition the ELT signal is a pulse-amplitude modulated signal which produces a host of sidebands in addition to the carrier component. With multiple sidebands, it is obvious that the signal band is extremely congested. In particular it is possible for one or more very powerful ELT signals to have strong sidebands which sweep through the bandwidth of a weak ELT signal.

In this chapter we address the problem of processing multiple ELT signals using the baseband processor. First, we discuss the computer simulation results for multiple ELT signals with equal power levels using linear and non-linear spectral estimation methods. Then, we consider the results for multiple ELT signals with different power levels and examine the effects of rate reduction filtering. Finally, we will investigate the detection of a weak ELT signal using this technique.

5.2   Baseband Processing of Multiple ELT Signals

For the received signal comprising more than one ELT signal with different carrier frequencies and different amplitudes, the mathematical representation is given by [37,38]

$$s(t) = \sum_{i=1}^{N_s} A_i \, m_i(t) \cos[2\pi f_{ci} t + \theta_i(t)] \tag{5.1}$$

where

A_i = carrier amplitude of the ith signal, $i = 1,2,.....,N_s$

$m_i(t)$ = modulating signal of the ith signal.

f_{ci} = carrier frequency of the ith signal.

N_s = number of ELT signals contained in the received signal.

$\theta_i(t)$ = phase angle of the ith signal.

The complex baseband equivalent of the signal is generated by the inphase component and quadrature component of the input signal. These components are generated in the usual way by multiplying the signal by $\cos(2\pi F_I t)$ and $\sin(2\pi F_I t)$, where F_I is the intermediate mixing frequency and filtering the results using low-pass filter having cut-off frequency equal to B_c.

Thus we have

$$s_I(t) = \sum_{i=1}^{N_s} \frac{A_i}{2} m_i(t) \cos[2\pi (f_{ci} - F_I) t + \theta_i(t)] \tag{5.2}$$

$$s_Q(t) = \sum_{i=1}^{N_s} \frac{A_i}{2} m_i(t) \sin[2\pi (f_{ci} - F_I) t + \theta_i(t)] \tag{5.3}$$

where $(f_{ci} - F_I)$ is the mixed carrier frequency of the ith ELT signal.

5.3   Processing of Multiple ELT Signals With Equal Strength

In this section, we discuss the processing of multiple ELT signals using the baseband periodogram (FFT), the averaged periodogram, the baseband MEM and the averaged MEM methods. The analysis which is given here is for three and ten ELT signals. The former represents the case of a small number of signals in a pass while the latter provides results for a crowded spectrum. The carrier frequencies of these signals are selected randomly. The process assumes the use of 512 complex points at a sampling rate of 25000

inphase and quadrature samples per second. The cut off frequency of the baseband low pass filter (B_c) is 12.5 kHz. We consider pulse modulation ELT signals with continuous phase and no noise. In this case all ELT signals contained in the received signal have the same amplitude, i.e. $A_i = A, i = 1,2,....N_s$. Thus, the inphase and quadrature components become

$$s_I(t) = \sum_{i=1}^{N_s} \frac{A}{2} \, m(t) \cos[2\pi(f_{ci} - F_I)t + \theta_i(t)] \qquad (5.4)$$

$$s_Q(t) = \sum_{i=1}^{N_s} \frac{A}{2} \, m(t) \sin[2\pi(f_{ci} - F_I)t + \theta_i(t)] \qquad (5.5)$$

The spectral estimation performance degrades as a result of increasing the number of ELT signals. The detection of multiple ELT signals using the baseband periodogram is difficult and restricted in some cases because the FFT spectrum suffers from numerous peaks. In order to avoid this problem we use the baseband averaged periodogram or the averaged MEM techniques for detecting multiple ELT signals. One of difficulties of the MEM technique is choosing an approprate filter order for processing all the received ELT signals which gives good spectral estimation performance. The filter order which gives the best performance varies from one case to another, for multiple ELT signals. A strategy for choosing the proper filter order is given in this section.

5.3.1   Processing Results Using the Periodogram

A problem affecting the spectral estimation using the periodogram analysis in processing ELT signals is sideband problem. We expect that in processing multiple signals, the sideband interference will increase.

5.3.1.1   Three ELT Signals

Three pulse-modulated ELT signals having mixed carrier frequencies -10 kHz, 100 Hz and 5 kHz are processed and Fig. 5.1 illustrates the periodogram spectrum. From this figure it is seen that the three topmost peaks are detected easily. These peaks are the carrier components and described as one peak for each transmitted ELT signal. Furthermore, two major sidebands (about 5 dB down) around each carrier component for every ELT signal are observed. From these results, we note that it is easy to identify and detect all transmitted ELT signals since the carrier component peak for every signal is well defined.

5.3.1.2   Ten ELT signals

For ten ELT signals with mixed carrier frequencies (-5 kHz, -4 kHz, -2.9 kHz, -2 kHz, -700 Hz, 100 Hz, 1.1 kHz, 2.3 kHz, 3.6 kHz and 5.5 kHz), the result is given in Fig. 5.2. From this result, it is clear that at the -10 dB threshold level there are more than 10 peaks. Some of these peaks are the carrier components of the ten ELT signals and occur at the proper frequencies as expected but there are undesirable peaks which may create false alarms. At the -5 dB threshold level, the 10 peaks correspond to the carrier components. However, the FFT spectrum for ten pulse-modulated ELT signals is crowded which makes the detection of these ten ELT signals difficult.

5.3.2   Spectral Estimation using the Averaged Periodogram

Our aim is to improve the detection of multiple ELT signals using the averaged periodogram technique. This section examines the spectral estimation performance using this method with $K = 50$ segments with $P = 512$ complex samples for each block.
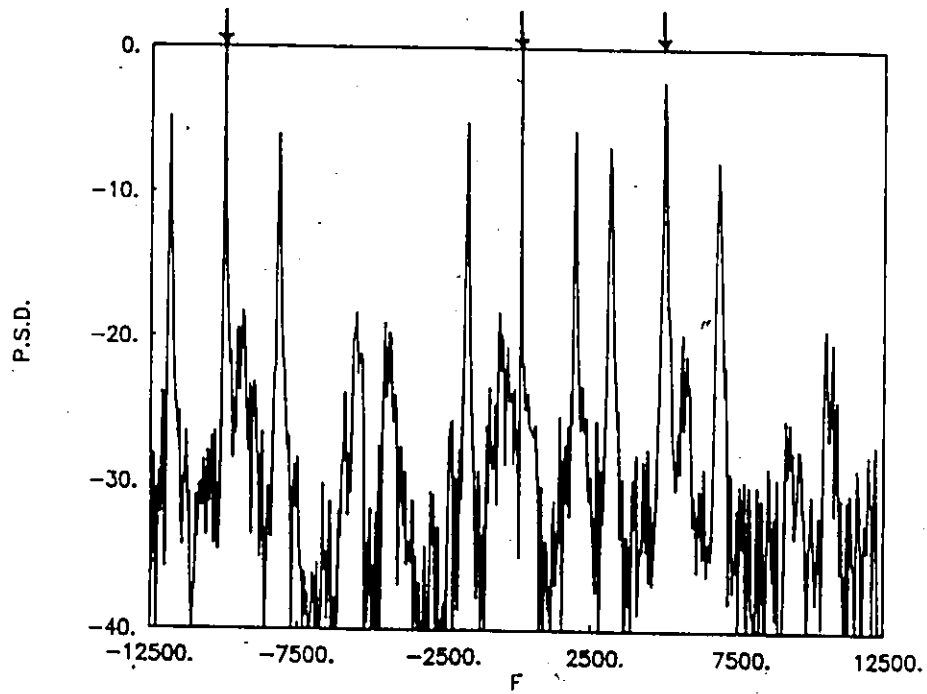
Fig. 5.1   Periodogram spectrum for three ELT signals.
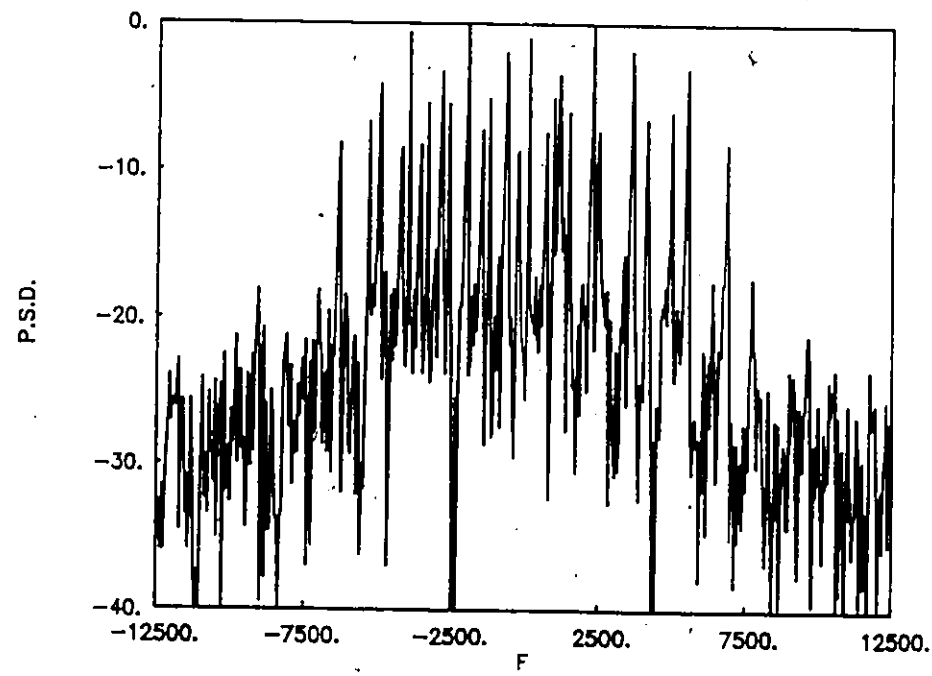
Fig. 5.2   Periodogram spectrum for ten ELT signals.

5.3.2.1   Three ELT Signals

The spectral estimation result using the averaged periodogram method for the three pulse-modulated ELT signals is given in Fig.5.3. From this figure it is clear that, above the - 10 dB threshold level, the three topmost peaks are detected easily. These peaks are the carrier component which is described as one carrier peak for each transmitted ELT signal. Furthermore, around every carrier component, two broad sideband peaks (13 dB down) are detected easily. It can also been seen that the averaged periodogram performs well and the results in improved performance for the three ELT signals due to the reduction of the level of the sidebands.

Comparing these results using the baseband periodogram (Fig.5.1) with those using the averaged periodogram (Fig.5.3) we note that:

1.   For both spectra, the carrier component peak for each transmitted ELT signal is very sharp and stationary. However, it is seen from Fig. 5.3 that the levels of the carrier component peaks of these ELT signals vary by about 1 dB indicating that the processor is not truly linear.

2.   By using the averaged periodogram the levels of the two major sidebands are reduced by 10 dB as compared to Fig.5.1.

3.   The width of these two major sidebands around the carrier component for every ELT signal becomes broad as depicted in Fig. 5.3. This provides an identifier for the carrier component for each signal, which consequently improves the detection of the ELT signal.

5.3.2.2   Ten ELT signals

Figure 5.4 illustrates the averaged periodogram spectrum result for the ten ELT signals. From this figure, it is clear that at the -10 dB threshold level, ten peaks are detected
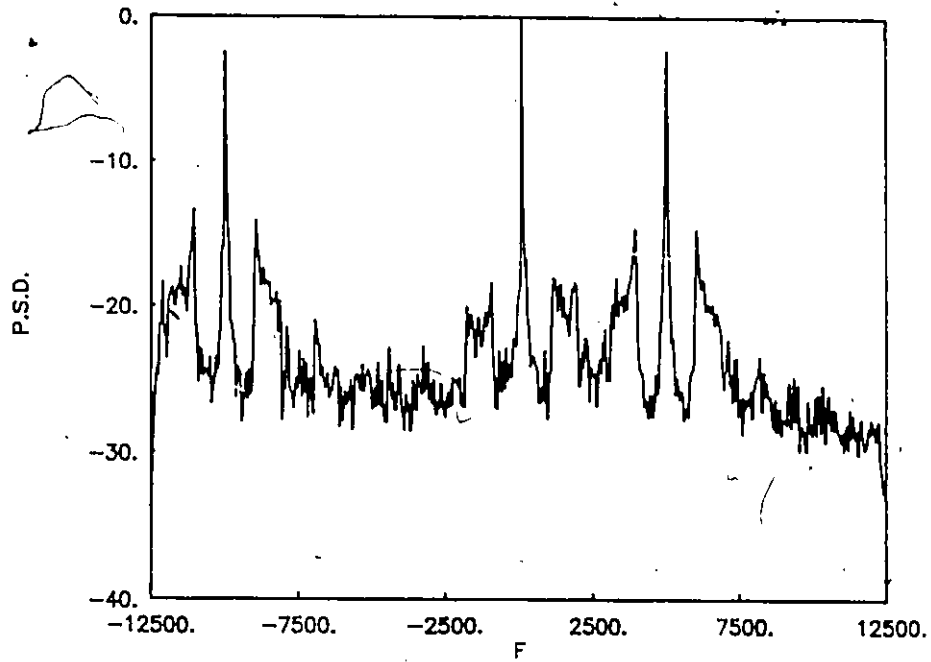
Fig. 5.3   Averaged periodogram spectrum for three ELT signals.
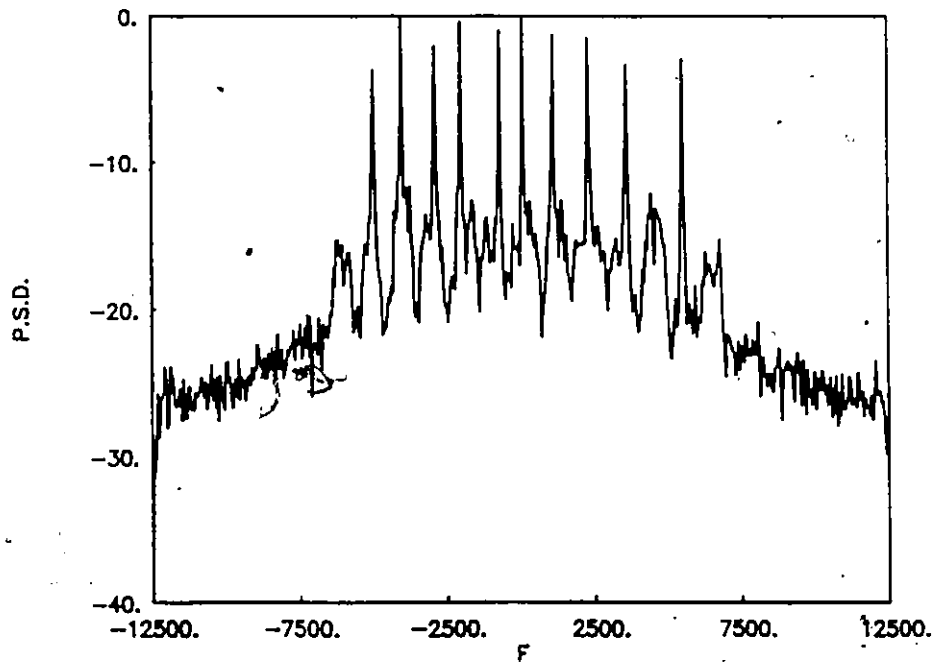
Fig. 5.4   Averaged periodogram spectrum for ten ELT signals.

easily with these peaks being the carrier component peaks. Further, we can identify and detect each received ELT signal because the spectral estimation performance is uncluttered. The carrier frequency component peaks are very sharp and the level of undesirable sidebands are reduced. The levels of the carrier component peaks of these ten ELT signals vary by about 3 dB.

Thus, from the above analysis of these results we note that the averaged periodogram technique performs well in the case of multiple ELT signals (three and ten cases) with equal power levels. By using this method, the levels of undesirable sidebands are reduced relative to the level of the carrier component peaks which consequently improves the detection of the present ELT signals.

5.3.3   Processing Results Using the MEM

In this section, the baseband MEM is used for detecting multiple ELT signals with equal strength. The main difficulty in using the MEM approach is in choosing the prediction error filter order. For a single ELT signal, a lower MEM filter order gives good results. For multiple ELT signals, the filter order can be deduced by noting that the optimum value of MEM filter order lies in the range from 0.05 N to 0.2 N, where N is the number of data points. Here, we study the spectral estimation characteristics for the same three and ten pulse modulated ELT signal cases processed using the baseband MEM with 512 complex points and cut off frequency of the lowpass filter equal 12.5 kHz.

5.3.3.1   Three ELT Signals

First, we solve the problem of evaluating a reasonable MEM spectrum and determine an optimum filter order of the MEM. For these three ELT signals (with mixed carrier frequencies -10 kHz, 100Hz and 5 kHz), filter orders 2, 20, 30 and 50 are tested using

the MEM analysis. The results are illustrated in Fig.5.5 to Fig.5.8 respectively. From these results, we conclude that as the filter order increases, the number of peaks also increases. For low MEM filter order (MEM = 2), the MEM spectrum is not good because the spectrum which is shown in Fig.5.5 generates two broad peaks and from this we might conclude that the received emergency ELT signal is due to two ELT signals. In addition, it is seen from this figure that the frequency error is very large due to the broad peak. However, as the MEM filter order is increased the number of peaks also increases and the performance improves considerably and the spectrum becomes clearer as illustrated for MEM order 20. Figure 5.6 depicts the MEM spectrum computed using this MEM filter order for these three pulse modulated ELT signals. The three carrier component peaks are separately located at -9961 Hz, 195 Hz and 4980 Hz respectively which are equivalent to frequency errors of -39 Hz, -95 Hz and 20 Hz respectively.

Now, we estimate the Root Mean Square (RMS) error obtained using different MEM filter orders. The RMS error is defined by

$$RMS = \sqrt{\varepsilon_1^2 + \varepsilon_2^2 + ... + \varepsilon_i^2}, \quad i = 1, 2, ..., N_s \tag{5.6}$$

where

ε_i = the frequency error for ith ELT signal.

Then, for the case of three ELT signals, the RMS error is given by

$$RMS = \sqrt{\varepsilon_1^2 + \varepsilon_2^2 + \varepsilon_3^3} \tag{5.7}$$

For MEM filter order 20, the RMS error is

$$RMS = \sqrt{(-39)^2 + (-95)^2 + (20)^2} = 104.6 \text{ Hz}$$

Figure 5.7 gives the MEM spectra of these three ELT signals using MEM filter order 30. The three carrier component peaks are located at -10009 Hz, 49 Hz and 4980 Hz, respectively which are equivalent to frequency errors of 9 Hz, 51 Hz and 20 Hz respectively, for these three ELT signals.

Fig. 5.5   MEM = 2 spectrum for three ELT signals.

Fig. 5.6   MEM = 20 spectrum for three ELT signals.
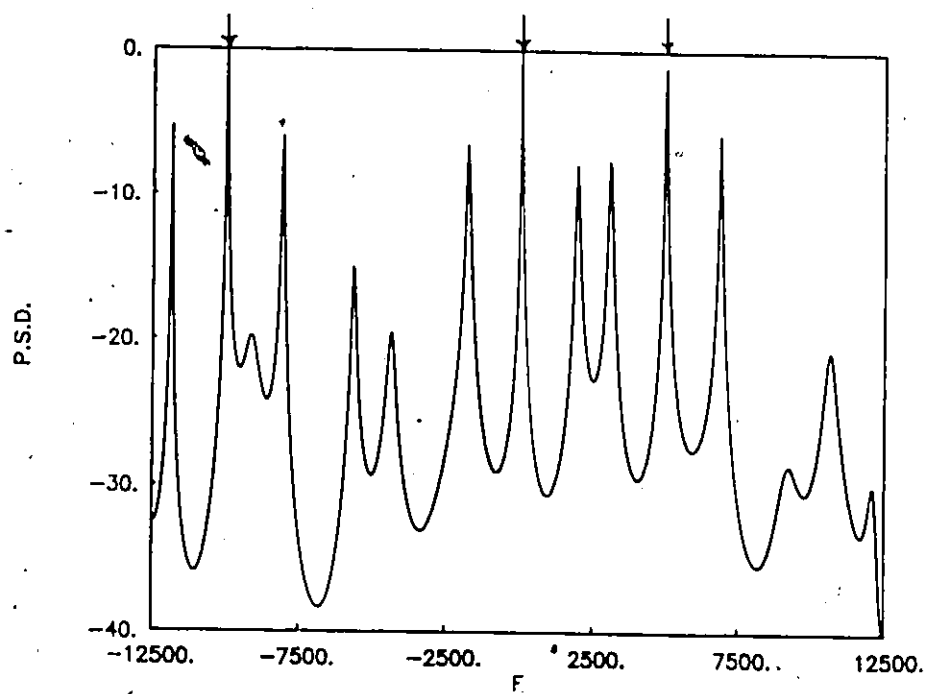
Fig. 5.7   MEM = 30 spectrum for three ELT signals.
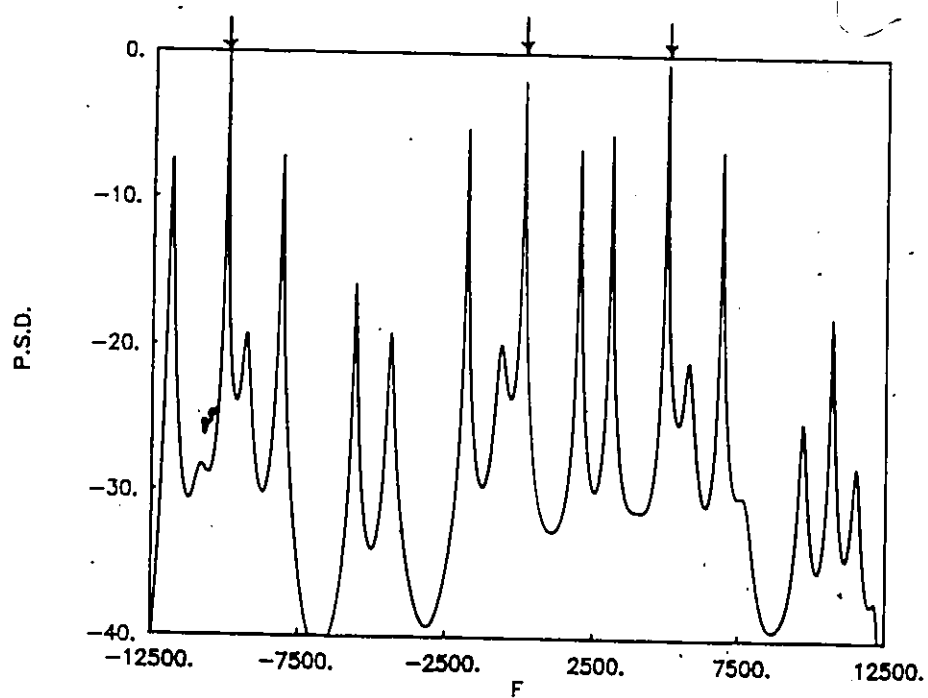
Fig. 5.8.   MEM = 50 spectrum for three ELT signals.

For MEM filter order 30, the RMS error is given by

$$RMS = \sqrt{(9)^2 + (51)^2 + (20)^2} = 55.5 \text{ Hz}$$

Increasing the MEM filter order to 50 gives the MEM spectra shown in Fig.5.8. From this figure, we observe that the three carrier component peaks are separately located at -10009 Hz, 98 Hz, and 5004 Hz, corresponding to frequency errors of 9 Hz, 2 Hz and -4 Hz respectively.

Then for MEM filter order equal 50, the RMS frequency error is given by

$$RMS = \sqrt{(9)^2 + (2)^2 + (-4)^2} = 10 \text{ Hz}$$

Comparing the RMS frequency errors obtained using MEM filter order equal 20, 30 and 50, we conclude that increasing the MEM filter order by 10 reduces the RMS frequency error by 2 and improves the sharpness of the carrier component peaks of the ELT signals. Thus, MEM filter order 50 offer good frequency resolution for the analysis of three ELT signals with small RMS frequency errors.

5.3.3.2   Ten ELT Signals

Ten pulse modulated ELT signals with mixed carrier frequencies of -5 kHz, -4 kHz, -2.9 kHz, -2 kHz, -700 Hz, 100 Hz, 1.1 kHz, 2.3 kHz, 3.6 kHz and 5.5 kHz are now examined using the baseband MEM. The MEM filter orders used for this analysis are increased from order 3 to order 100. The MEM spectral results are given in Figs.5.9 to 5.12. For low MEM filter orders, i.e. order 3 and order 20, the MEM spectral estimates are as expected not good; that is, no clear indication is given of how many ELT signals are present as illustrated in Figs.5.9 and 5.10 respectively. For MEM filter orders of 50 and 100, it is seen that at the -10 dB threshold level, the number of peaks exceeds 10. Some of these peaks are located at the correct frequencies but there are other undesirable peaks, which may increase the number of false alarms.
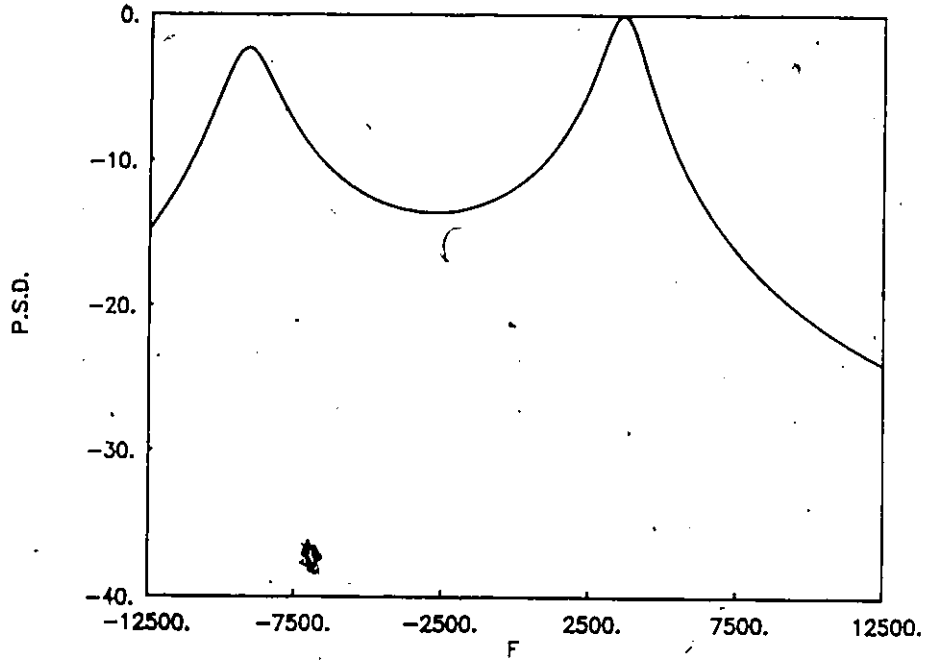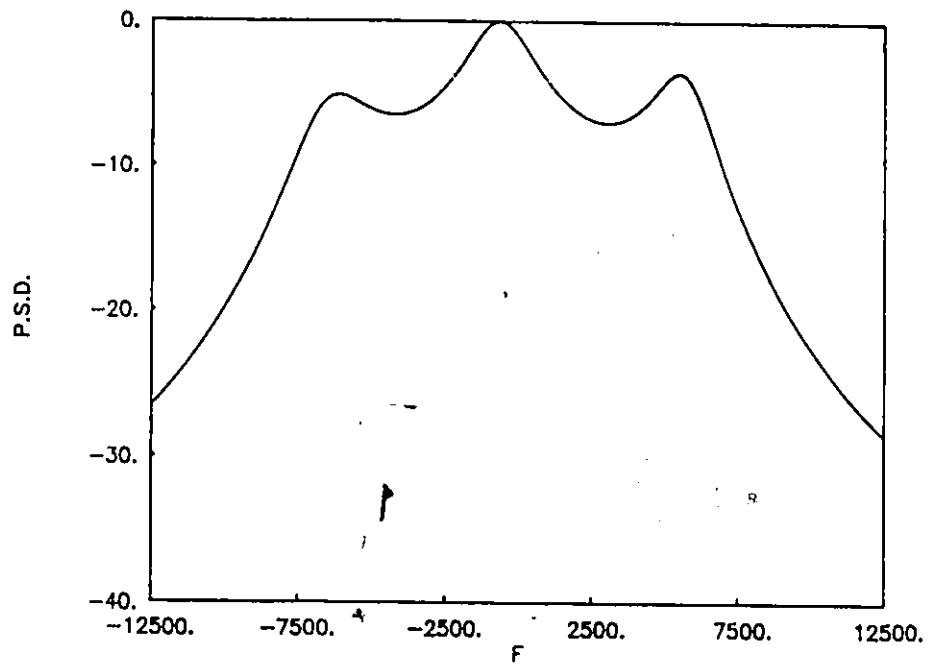
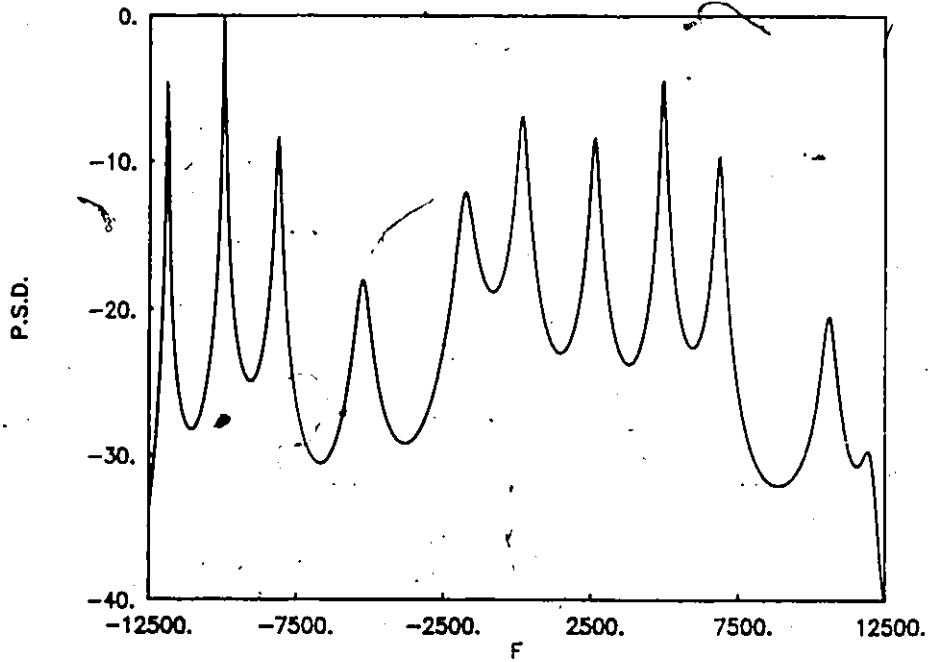Fig. 5.9   MEM = 3 spectrum for ten ELT signals.
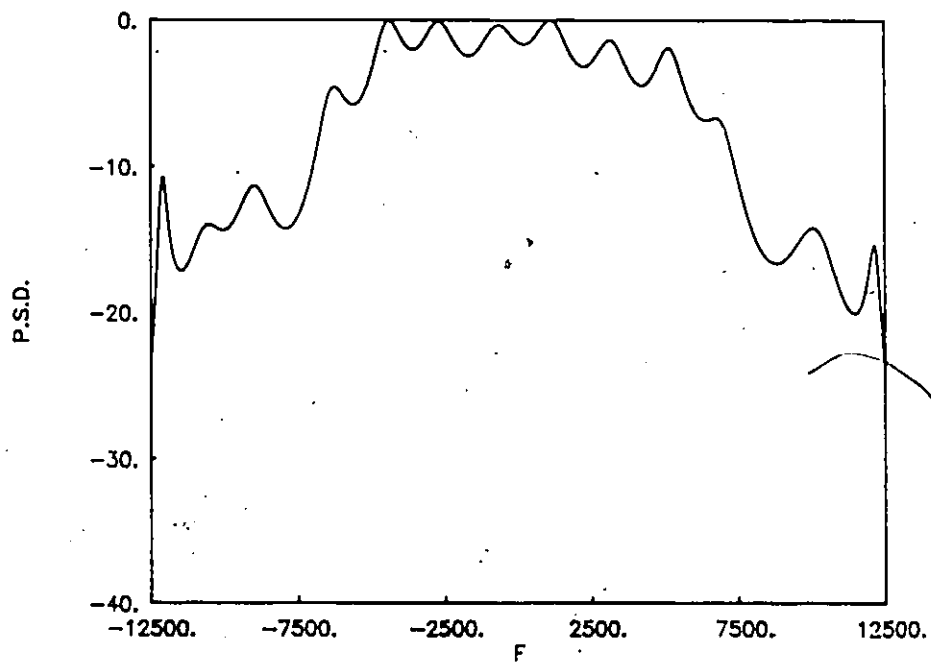
Fig. 5.10   MEM = 20 spectrum for ten ELT signals.
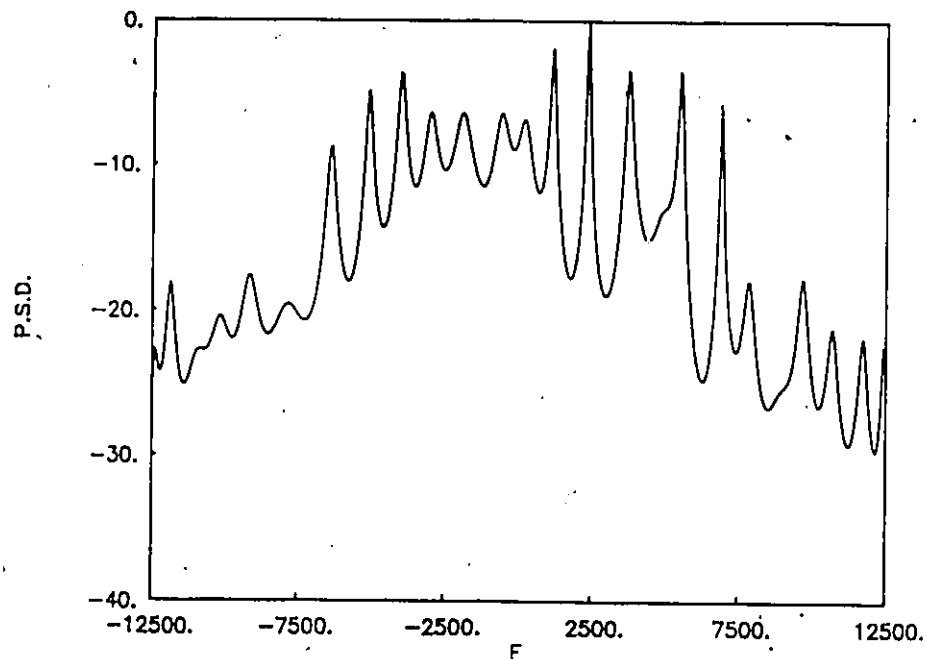
Fig. 5.11   MEM = 50 spectrum for ten ELT signals.
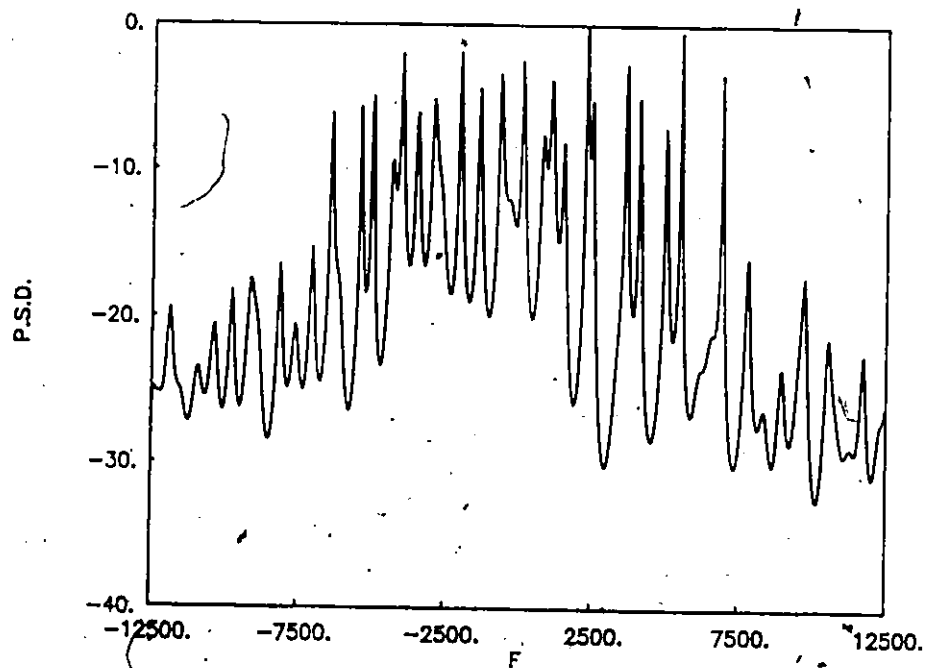

Fig. 5.12   MEM = 100 spectrum for ten ELT signals.

Figure 5.11 illustrates the MEM spectra for these 10 ELT signals using MEM filter order 50. The carrier peaks are located at -5.078 kHz, -4.003 kHz, -2.978 kHz, -2.001 kHz, -683 Hz, 146 Hz, 1.123 kHz, 2.343 kHz, 3.662 kHz and 5.517 kHz which are equivalent to frequency error values of 78 Hz, 3 Hz, 78 Hz, 1 Hz, -17 Hz, -46 Hz, -23 Hz, -43 Hz, -62 Hz and -17 Hz respectively. This corresponds to an RMS error, from eq.(5.6), of

$$RMS = \sqrt{(78)^2 + (3)^2 + (78)^2 + (1)^2 + (-17)^2 + (-46)^2}$$

$$\overline{+(-23)^2 + (-43)^2 + (-62)^2 + (-17)^2}$$

$$= 145.2 \, Hz$$

Increasing the MEM filter order to 100 gives the MEM spectra for the 10 pulse modulated ELT signals shown in Fig. 5.12. The carrier peaks located at -4.981 kHz, -4.003 kHz, -2.929 kHz, -2.001 kHz, -684 Hz, 97 Hz, 1.075 kHz, 2.295 kHz, 3.613 kHz and 5.517 kHz respectively. These values correspond to frequency errors of -19 Hz, 3 Hz, 29 Hz, 1 Hz, -16 Hz, 3 Hz, 25 Hz, 5 Hz, -13 Hz and -17 Hz respectively. Thus, the RMS error for MEM filter order 100 is equivalent to

$$RMS = \sqrt{(-19)^2 + (3)^2 + (29)^2 + (1)^2 + (-16)^2 + (3)^2}$$

$$\overline{+(25)^2 + (5)^2 + (-13)^2 + (-17)^2}$$

$$= 50.8 \, Hz$$

Comparing the RMS frequency errors obtained using MEM filter order 50 with those using filter order 100, we conclude that increasing MEM filter order to 100 reduces the RMS frequency errors to one third the RMS value obtained using MEM filter order 50.

5.3.4   Processing Results Using the Averaged MEM

MEM averaging is used to reduce the effect of undesirable sidebands on the spectral estimation. Here, we study the spectral estimation characteristics for multiple ELT signals with equal power levels using the baseband averaged MEM.

5.3.4.1   Three ELT Signals

The same three pulse modulated ELT signals are examined here using the averaged MEM with MEM filter order equal 50. Fig.5.13 illustrates the averaged MEM spectrum for these signals. From these results, it is seen that the averaged MEM reduces the level of the undesirable sidebands and the three carrier components peaks can be detected easily above the - 10 dB threshold level. This makes the detection of the carrier component peak for each transmitted ELT signal easy.

Comparing these results obtained using the baseband MEM (Fig.5.3) with those using the averaged MEM (Fig.5.13) with MEM filter order 50, we note that :

1.   For these two spectra, the carrier component peak for each signal is stationary and very sharp. The levels of these carrier peaks vary by about 1 dB.

2.   The averaged MEM reduces the level of the two major sideband peaks around the carrier component by 7 dB as compared to, Fig.5.8.

3.   The width of these two major sidebands become broad as illustrated in Fig.5.13.

5.3.4.2   Ten ELT Signals

In the case of ten pulse modulated ELT signals, the multiple peaks near the carrier frequencies make the detection difficult. Using the averaged MEM with MEM filter order 100, we obtain the result of Fig.5.14. From this figure, we observe that the level of undesirable sidebands is reduced, which improves the detection of the carrier component peaks. Furthermore, we note that, the ten carrier peaks can be detected easily above the -7 dB threshold level, and the levels of these ten peaks change by about 3 dB.

Thus, from the above analysis for three and ten ELT signals, we note that the averaged MEM provides good detection properties for the multiple ELT signals. This is due to
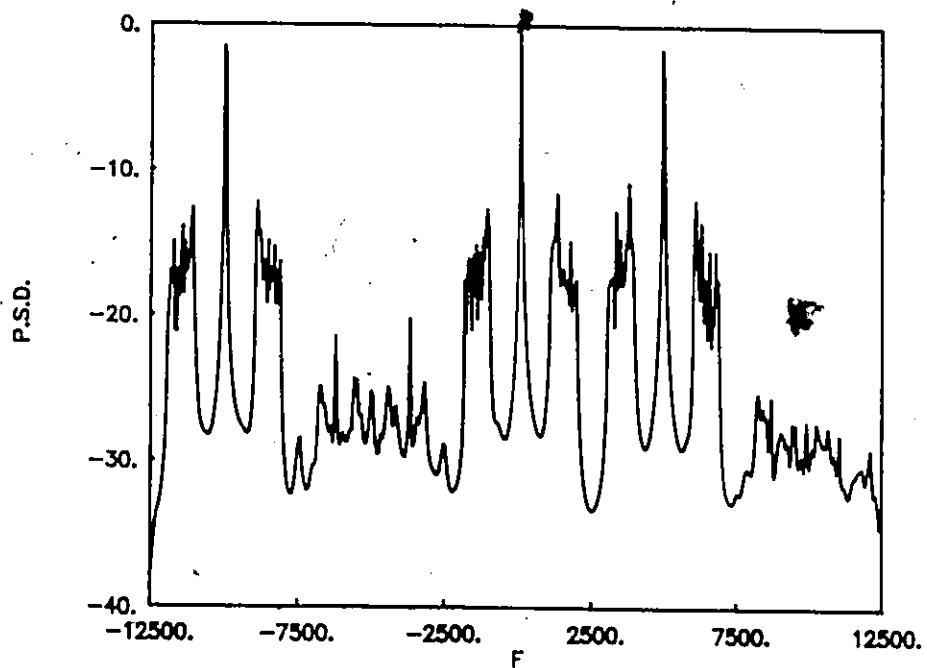
Fig. 5.13   Averaged MEM = 50 spectrum for three ELT signals.
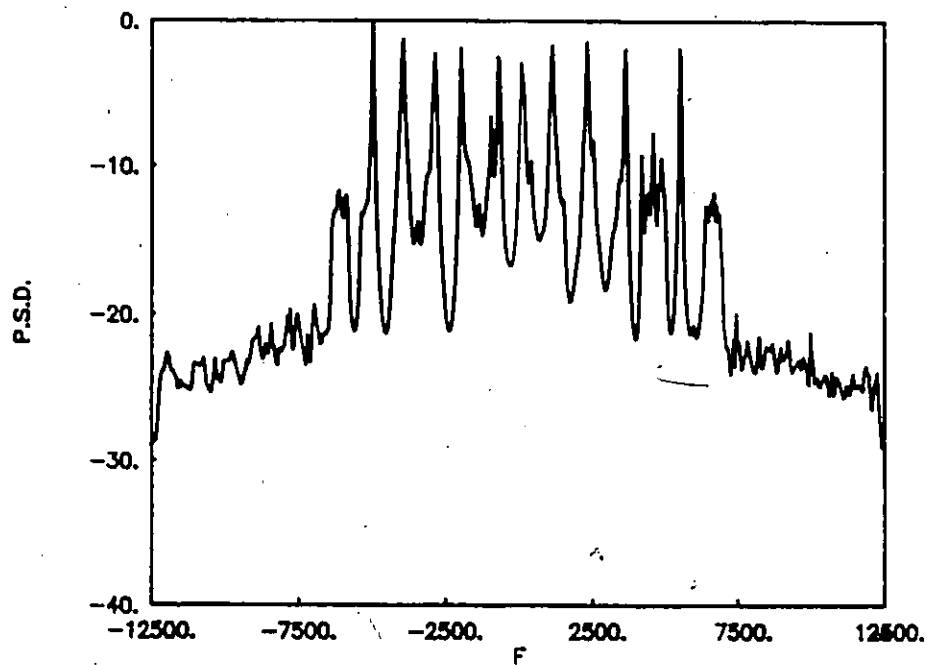
Fig. 5.14   Averaged MEM = 100 spectrum for ten ELT signals.

the reduction of the level of the undesirable sidebands relative to the level of the carrier component peaks.

5.4   Processing of Multiple ELT Signals with different strengths

In this section, we discuss the processing of multiple ELT signals with different strengths, i.e. the signal power levels are not equal. The analysis which is given here is again for three and ten ELT signals.

The ELT signals contained in the received signal have different amplitudes. Eq.(5.1) can be written in the form

$$s(t) = \sum_{i=1}^{N_s} s_i(t) \tag{5.8}$$

Now, P_1 is the average power corresponding to $s_1(t)$, P_2 the average power corresponding to $s_2(t)$,......, and P_k the average power corresponding to $s_k(t)$. Since the average power $P_k \propto A_k$, we get

$$\frac{P_k}{P_1} = \left(\frac{A_k}{A_1}\right)^2 \tag{5.9}$$

Applying the decible (dB) notation for both sides of Eq.(5.9) yields

$$10 \log\left(\frac{P_k}{P_1}\right) = 20 \log\left(\frac{A_k}{A_1}\right) \tag{5.10}$$

Let us suppose the normalized amplitude of $s_1(t)$, i.e. A_1 equals unity. This means that the normalized power corresponding to $s_1(t)$ is referenced to 0 dB and used as a reference level for comparison with the normalized power level of other ELT signals. For example, if the received signal contains two ELT signals, i.e. $s_1(t)$ and $s_k(t)$, then these signals have normalized average power P_1 and P_k, respectively. If the power level P_1 of $s_1(t)$ is referenced at 0 dB, then the power level P_k of $s_k(t)$ can be reduced by amounts of, say, 5 dB, 10 dB, 15 dB and 20 dB with respect to the power level P_1. We summarize the above results in Table 5.1.

TABLE 5.1

$10 \log (P_k/P_1)$ dB	A_1	A_k
−5	1	0.56234
−10	1	0.31622
−15	1	0.17782
−20	1	0.1

5.4.1 Processing Results Using the periodogram Method

The detection of multiple ELT signals using the baseband periodogram technique is difficult and restricted in some cases because the FFT spectrum suffers from numerous peaks (sidebands problem). This section examines the spectral estimation performance of the three and ten ELT signal cases with different power levels.

5.4.1.1 Three ELT Signals

A received signal containing three pulse modulated ELT signals ($s_1(t)$, $s_2(t)$, and $s_3(t)$) with mixed carrier frequencies -10 kHz, 100 Hz and 5 kHz respectively are considered. We arbitrarily choose $P_3 = P_1$ and vary P_2 in level from -5 dB to -20 dB in 5 dB steps.

The power spectral densities for the four cases are given in Figs.5.15 to 5.18. Figure 5.15 illustrates the FFT spectra when the average power P_2 of $s_2(t)$ is reduced by 5 dB as compared to P_1 of $s_1(t)$. From this figure it is clear that at the -10 dB threshold level, there are nine peaks for the three ELT signals with three peaks for each signal, which comprise the carrier peak component and two major sidebands around this carrier component. Reducing

Fig. 5.15   Periodogram spectrum for three ELT signals with P2/P1 = −5 dB.

Fig. 5.16   Periodogram spectrum for three ELT signals with P2/P1 = −10 dB.

Fig. 5.17   Periodogram spectrum for three ELT signals with P2/P1 = − 15 dB

Fig. 5.18   Periodogram spectrum for three ELT signals with P2/P1 = − 20 dB.

the power level P_2 of $s_2(t)$ by 10 dB as compared to the power level P_1 gives the FFT spectra depicted in Fig.5.16. From this figure it is seen that, at the -10 dB threshold level seven peaks for the three ELT signals are detected, six of the seven peaks are related to $s_1(t)$ and $s_3(t)$, and the remaining peak is the carrier component peak for $s_2(t)$. Reducing the power level P_2 of $s_2(t)$ by amounts of 15 dB and 20 dB as compared to the power level P_1 of $s_1(t)$ gives the periodogram spectral estimation results shown in Figs.5.17 and 5.18 respectively. From these results, we observe that, at the -10 dB threshold level, only six peaks are detected. these peaks belonging to $s_1(t)$ and $s_3(t)$. The weak ELT signal $s_2(t)$ has disappeared with other undesirable sidebands which makes the detection of this weak ELT signal difficult.

All the periodogram spectral estimation results illustrated in the above figures indicate that the ratio between the power levels of the strong and weak ELT signals (P_1/P_2) in dB at the input is equal to the ratio of the power spectrum $\{S_1(f_{c1} - F_I)/S_2(f_{c2} - F_I)\}$ at the output of the processor where $S_1(f_{c1} - F_I)$ is the spectrum peak at the mixed carrier frequency $(f_{c1} - F_I)$ of $s_1(t)$ and $S_2(f_{c2} - F_I)$ is the spectrum peak at the mixed carrier frequency $(f_{c2} - F_I)$ of ELT signal $s_2(t)$. This is due to the linearity of the spectral estimation method.

Thus, we conclude that, for three pulse modulated ELT signals $s_1(t)$, $s_2(t)$, and $s_3(t)$, with $P_1 = P_3$ we can identify all three ELT signals when the power level of the third signal is within 10 dB. If the difference in the power levels is more than 10 dB, i.e. 15 dB or 20 dB or more, detection of the weak ELT signal becomes difficult.

5.4.1.2   Ten ELT Signals

Ten pulse modulated ELT signals $s_1(t)$, $s_2(t)$, $s_3(t)$,.......,$s_{10}(t)$ with mixed carrier frequencies -5 kHz, -4 kHz, -2.9 kHz, -2 kHz, -700 Hz, 100 Hz, 1.1 kHz, 2.3 kHz, 3.6 kHz and 5.5 kHz are examined here using the baseband periodogram technique. The average powers for all ELT signals are the same except $s_6(t)$ with mixed carrier frequency 100 Hz, which is

varied in level from -5 dB to -20 dB in 5 dB steps. The periodogram spectra for all four cases are plotted in Figures 5.19 through 5.22 respectively. From these figures, we note that at the -10 dB threshold level , there are more than 10 peaks which makes the detection of these ELT signals difficult. The carrier component peak of the weak ELT signal $s_6(t)$ in embedded with the other undesirable sidebands which makes the detection of this weak ELT signal difficult. It is seen that, the power level of the spectrum of the weak ELT signal at the output of the processor varies linearly with its power level at the input (before processing) using the periodogram, as expected.

5.4.2 Processing Results Using the Averaged Periodogram

This section is devoted to study the spectral estimation performance using the baseband averaged periodogram for multiple ELT signals with different power levels. The sidebands of the powerful ELT signals overlap with the weak ELT signal making the detection of this signal difficult. The averaged periodogram reduces the level of the sidebands relative to the level of the weak ELT signal which consequently improves the detection of this weak signal.

As discussed earlier, the data record is divided into a number of blocks K covering different time intervals, and each block contains P complex points. In this section we choose $K = 50$ and $P = 512$ complex points as before.

5.4.2.1 Three ELT Signals

The three pulse modulated ELT signals are examined here using the baseband averaged periodogram. The spectral estimation results are plotted in Figures 5.23 through 5.26 for all four cases which the power level P_2 of $s_2(t)$ is reduced by amounts 5 dB, 10 dB, 15 dB, and 20 dB while the power levels of the signals $s_1(t)$ and $s_3(t)$ are kept equal. From these

Fig. 5.19   Periodogram spectrum for ten ELT signals with P6/P1 = −5 dB.

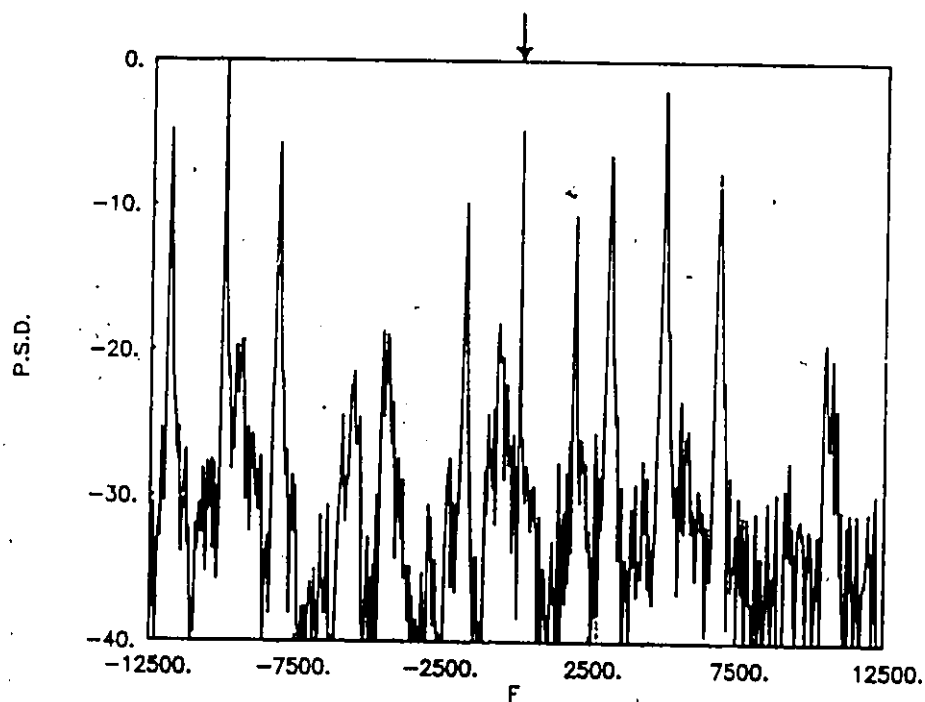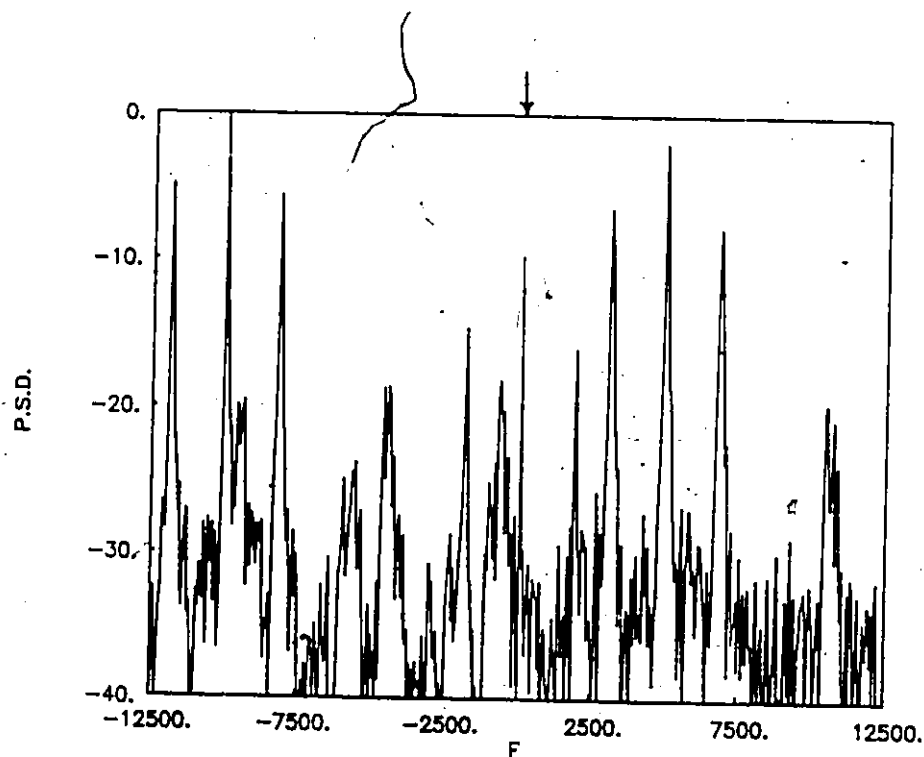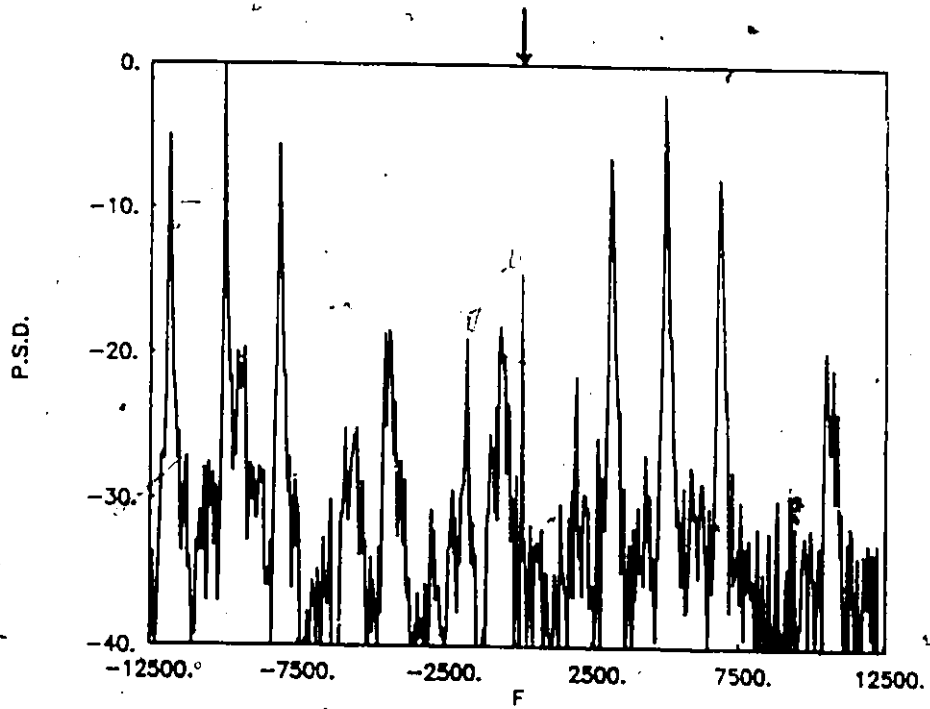Fig. 5.20   Periodogram spectrum for ten ELT signals with P6/P1 = −10 dB.

Fig. 5.21   Periodogram spectrum for ten ELT signals with P6/P1 = −15 dB.
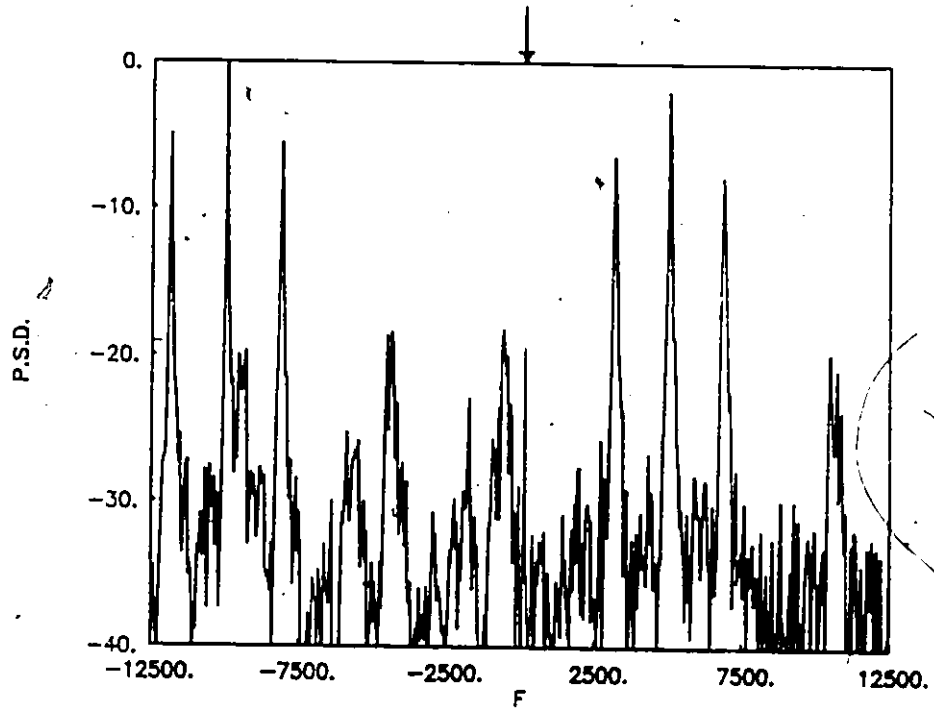

Fig. 5.22   Periodogram spectrum for ten ELT signals with P6/P1 = −20 dB.

Fig. 5.23   Averaged periodogram spectrum for three ELT signals with
P2/P1 = − 5 dB.

Fig. 5.24   Averaged periodogram spectrum for three ELT signals with
P2/P1 = − 10 dB.

Fig. 5.25   Averaged periodogram spectrum for three ELT signals with P2/P1 = −15 dB.
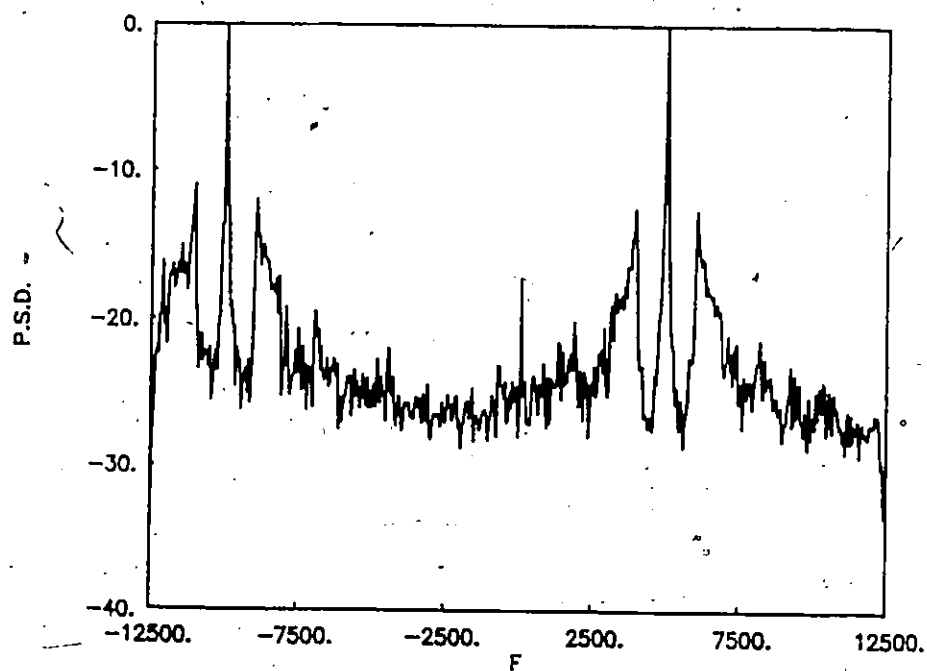
Fig. 5.26   Averaged periodogram spectrum for three ELT signals with P2/P1 = −20 dB.

results illustrated in Figures 5.23, 5.24 and 5.25, it is seen that the levels of the sidebands are reduced by about 7 dB as compared to single-shot FFT shown in Fig.5.1. This makes the level of the carrier component peak of the weak ELT signal comparable to the level of the carrier component peaks of the powerful ELT signals which consequently makes the detection of the weak ELT signal easy. Reducing the power level P_2 by 20 dB gives the spectral estimation result illustrated in Figure 5.26. From this figure it is clear that the width of the sidebands becomes broadened as compared to the width of the carrier peak of the weak ELT signal which is very sharp. By using an adaptive threshold, we can identify and detect the weak ELT signal $s_2(t)$ however. Thus, we conclude that:

1.   The baseband averaged periodogram improves the detection of the weak ELT signal since it gives good spectral estimation characteristics as compared to the results obtained using the single-shot periodogram for the case of three ELT signals.

2.   The power level for the spectrum of the weak ELT signal using this linear spectral estimation method varies linearly as compared to the power level for this ELT signal at the input before processing.

5.4.2.2   Ten ELT Signals

Ten pulse modulated ELT signals with the same mixed carrier frequencies as before are used to test the capability of the averaged periodogram technique. The power level P_6 of signal $s_6(t)$ with mixed carrier frequency 100 Hz is varied in level from -5 dB to -20 dB in 5 dB steps while all other ELT signals have equal power level. The spectral estimation results are given in Figures 5.27 through 5.30 for all four cases respectively. The results illustrated in Figures 5.27 and 5.28 for the first two cases with P_6 at -5 dB and -10 dB, respectively indicate that at the -10 dB threshold level, ten peaks are detected. These peaks
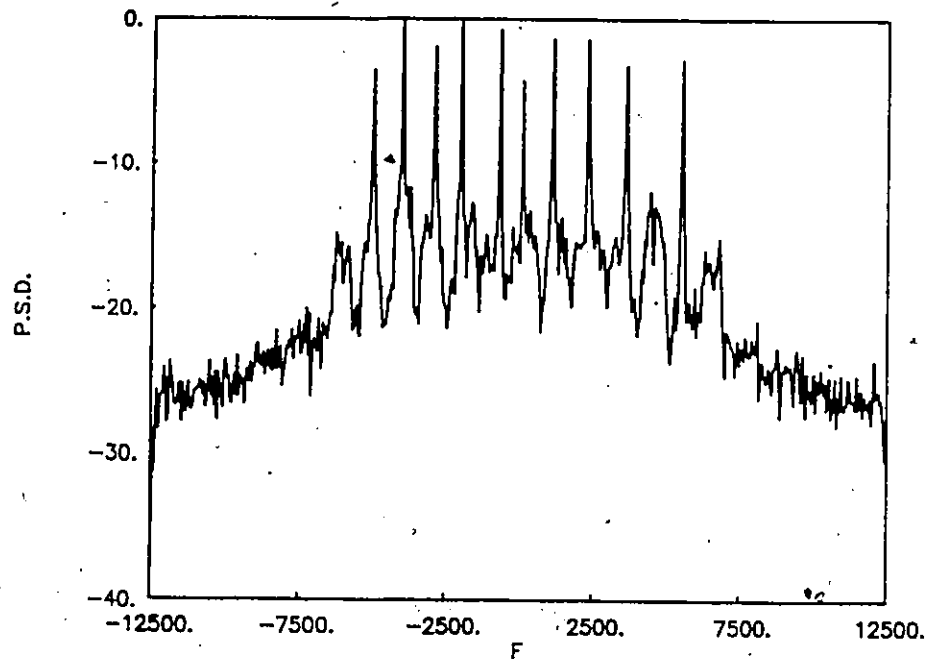
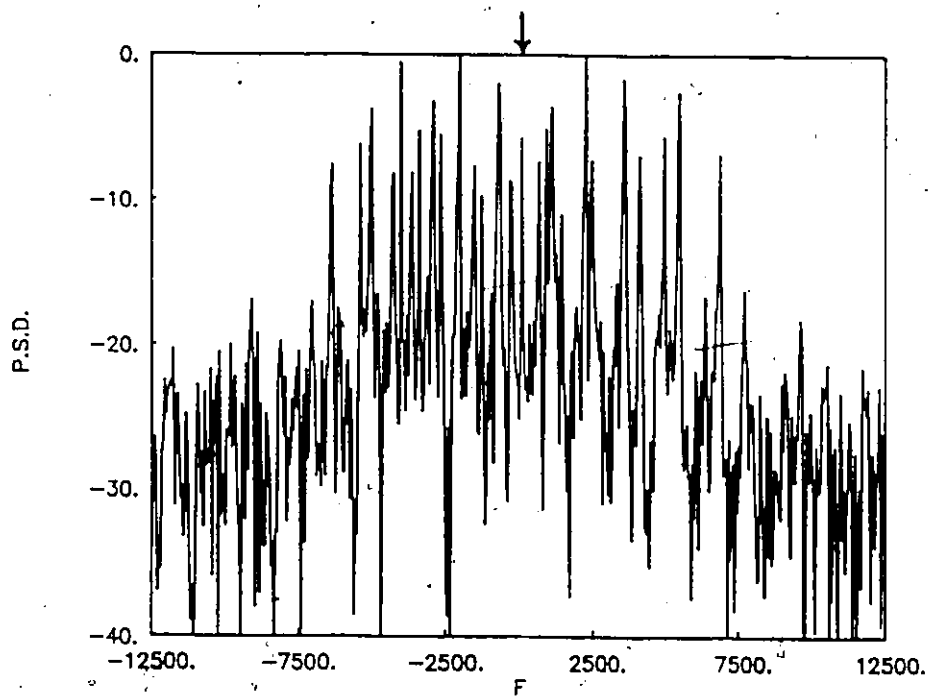Fig. 5.27   Averaged periodogram spectrum for ten ELT signals with
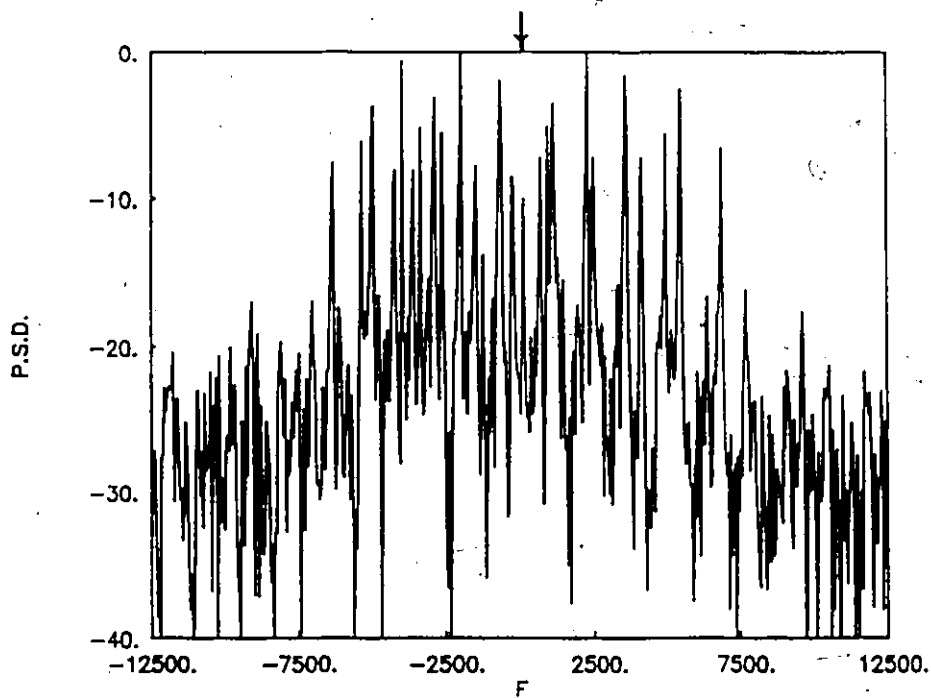   P6/P1 = −5 dB.
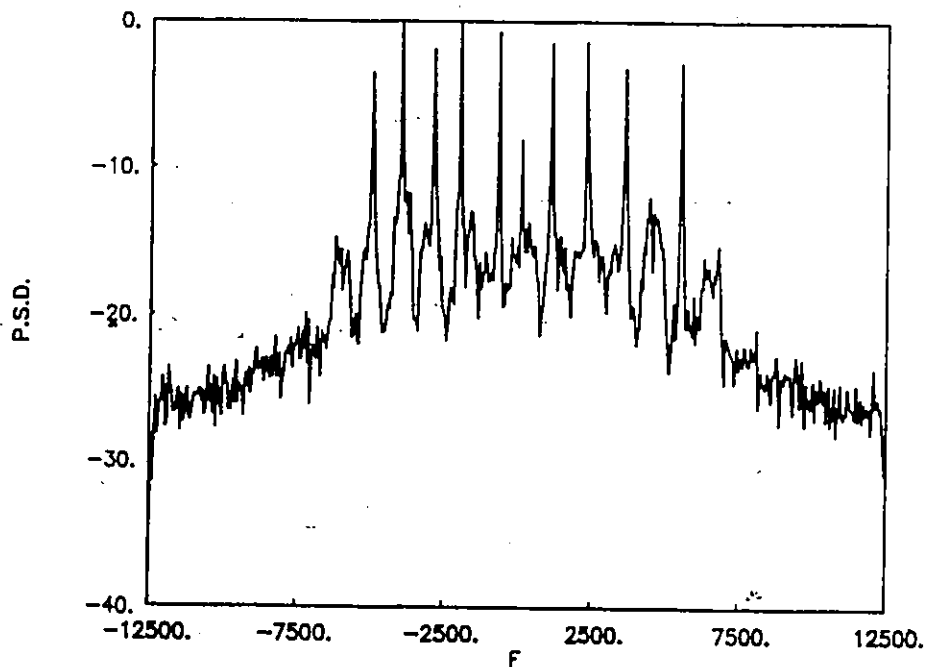
Fig. 5.28   Averaged periodogram spectrum for ten ELT signals with
             P6/P1 = −10 dB.
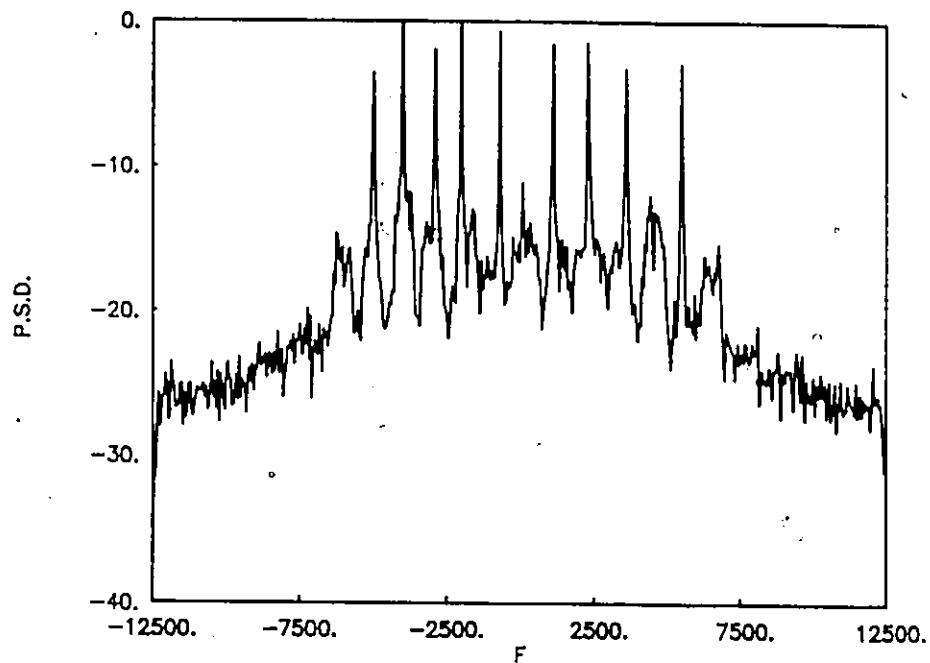
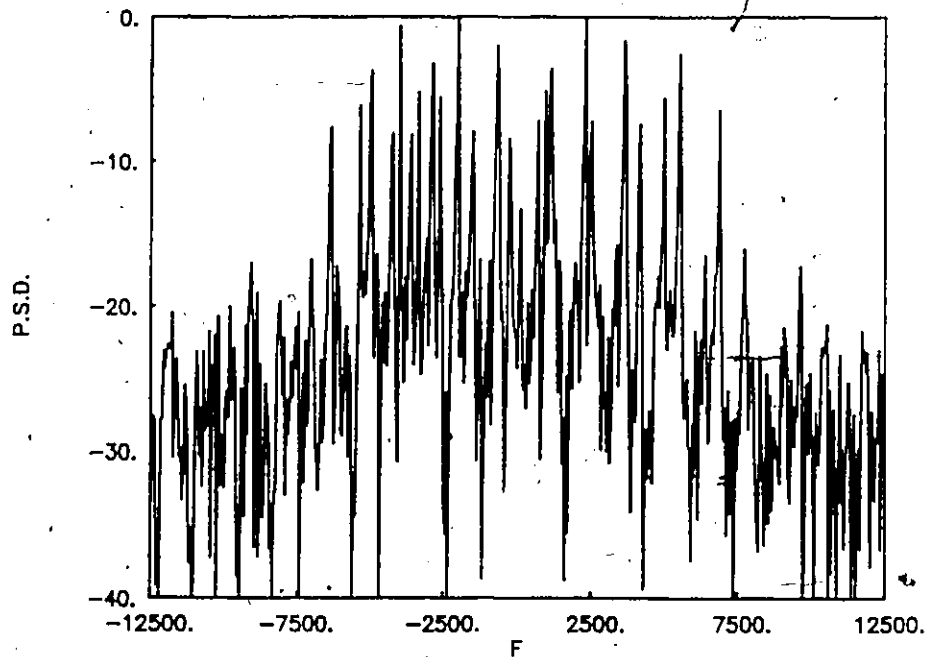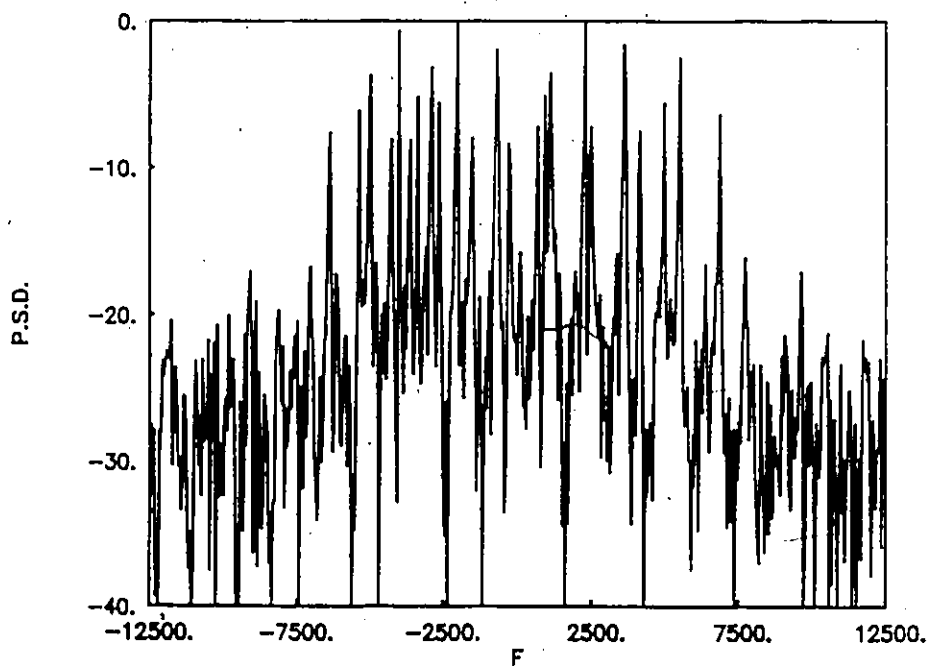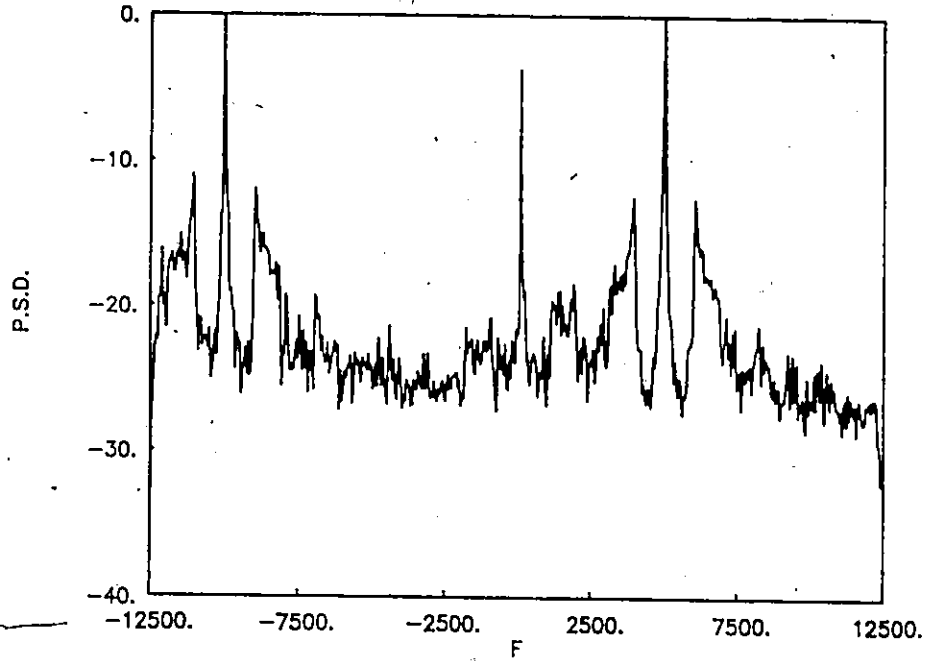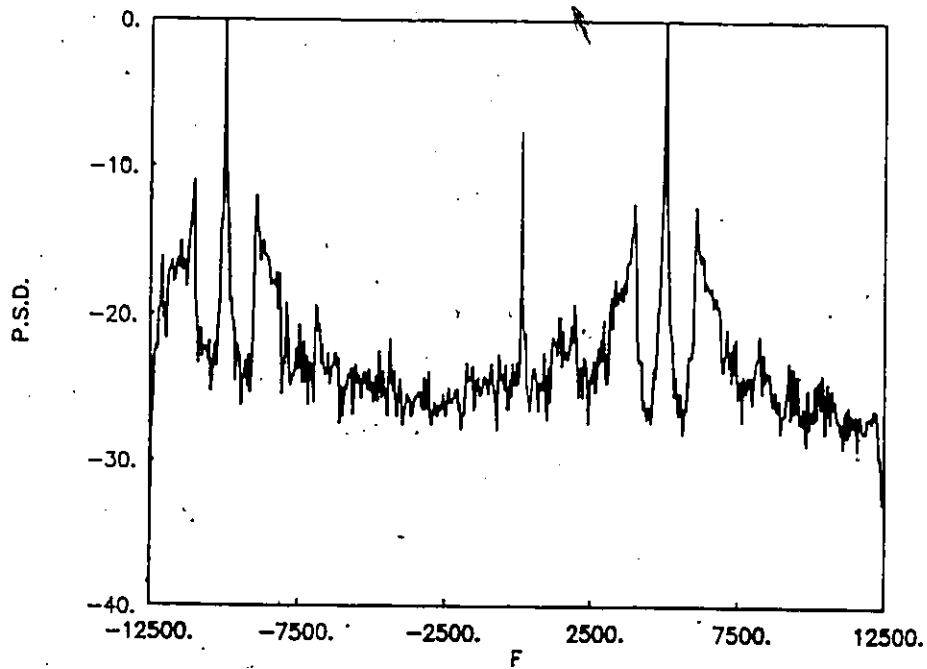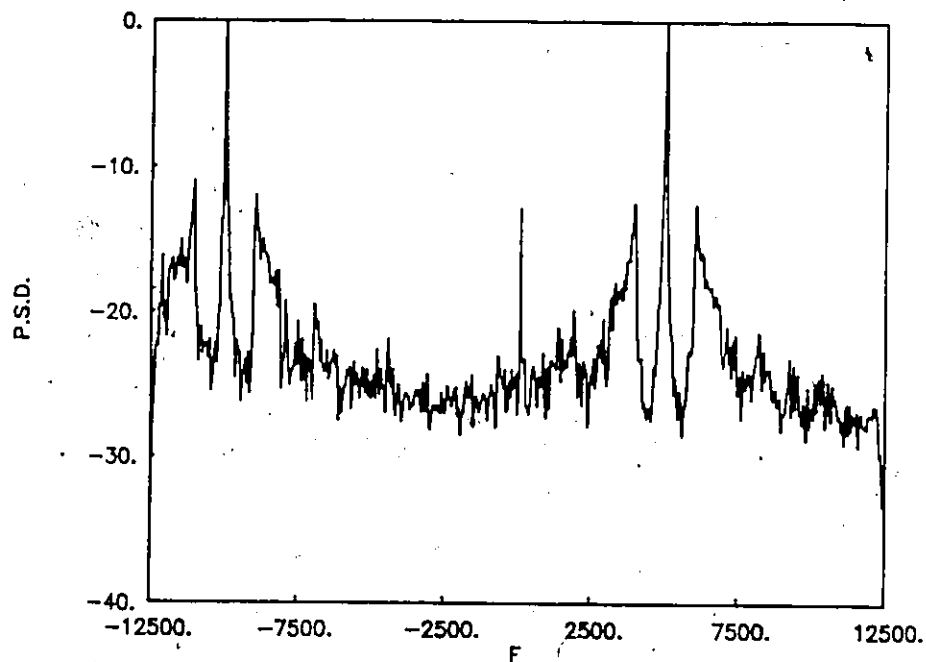Fig. 5.29   Averaged periodogram spectrum for ten ELT signals with
P6/P1 = −15 dB.
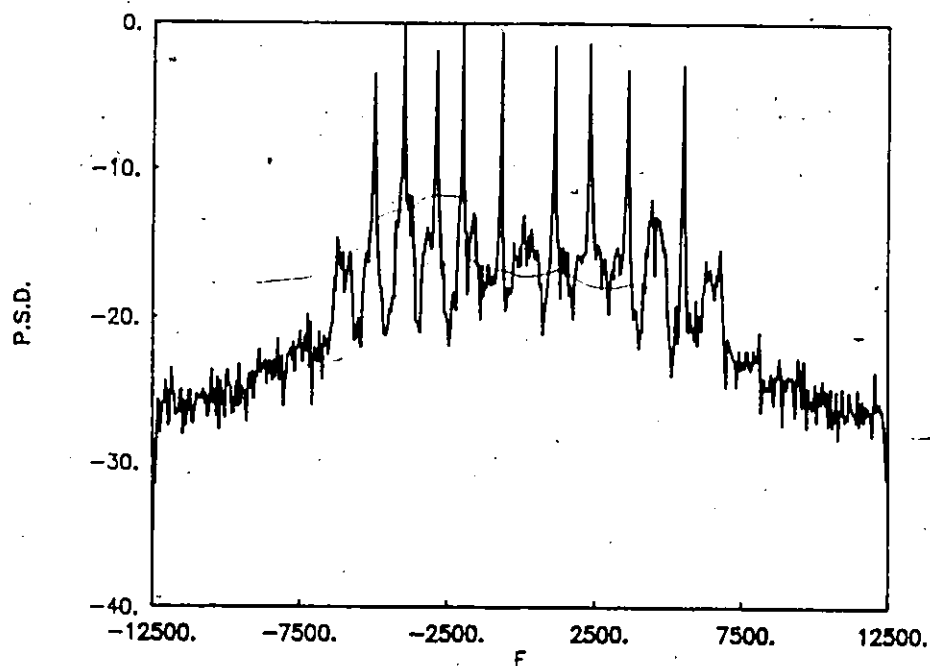
Fig. 5.30   Averaged periodogram spectrum for ten ELT signals with
P6/P1 = −20 dB.

described as the carrier components for all ten ELT signals. Then, all ten ELT signals can be detected easily. With P_6 at -15 dB and -20 dB level, the obtained spectrum is shown in Fig. 5.29 and 5.30 respectively. We note from these results that at the -10 dB threshold level, nine peaks are detected, these peaks described as the carrier components of the powerful ELT signals. The weak ELT signal overlaps with the other undesirable sidebands which reduces the probability of detection of this weak ELT signal. However, the baseband averaged periodogram spectral estimation method improves the detection of the single-shot weak ELT signal in the case of ten pulse modulated ELT signals. Further it is seen that the ratio between the power levels (P_1/P_6) at the input before processing equals the ratio $\{S_1 (f_{c1} - F_l)/S_6 (f_{c6} - F_l)\}$ at the ouput of the averaged periodogram processor.

5.4.3   Processing Results Using the Maximum Entropy Method

The use of MEM in the processing of multiple ELT signals with different power levels using the baseband processor is investigated in this section.

5.4.3.1   Three ELT Signals

The baseband MEM spectral estimates for the same three pulse modulated ELT signals $s_1(t), s_2(t)$ and $s_3(t)$ are examined in this section using MEM filter order 50. We choose the average power P_1 of $s_1(t)$ equal to the average power P_3 of $s_3(t)$, but the average power P_2 of $s_2(t)$ is reduced from -5 dB to -20 dB in 5 dB steps as compared to P_1. The results for all these four cases are given in Fig 5.31 to 5.34, respectively. Figures 5.31 illustrates the MEM spectra when the average power level P_2 is reduced 5 dB below the level of P_1. From this figure we note that seven peaks are observed at the -10 dB threshold level, six of these peaks belonging to the powerful ELT signals $s_1(t)$ and $s_3(t)$ and the remaining peak being the carrier component peak of the weak ELT signal $s_2(t)$. Thus, it can be seen that we can identify and

Fig. 5.31   MEM = 50 spectrum for three ELT signals with P2/P1 = − 5 dB.

Fig. 5.32   MEM = 50 spectrum for three ELT signals with P2/P1 = − 10 dB.

Fig. 5.33   MEM = 50 spectrum for three ELT signals with P2/P1 = − 15 dB.

Fig. 5.34 ·   MEM = 50 spectrum for three ELT signals with P2/P1 = − 20 dB.

detect all the three ELT signals. Reducing the average power P_2 by 10 dB gives the MEM spectra depicted in Fig. 5.32. From this figure it is clear that at the -10 dB threshold level, six peaks are observed, these peaks described as three peaks for each ELT signal $s_1(t)$ and $s_3(t)$. However, the weak ELT signal $s_2(t)$ cannot be detected. At the -15 dB threshold level, the carrier component peak of the weak ELT signal $s_2(t)$ starts to appear with seven peaks being observed, six of these peaks belonging to $s_1(t)$ and $s_3(t)$, and the remaining peak being due to $s_2(t)$. As shown from this figure, we can also identify and detect all the three ELT signals. Reducing the average power level P_2 by amounts of 15 dB and 20 dB as compared to the power level P_1, gives the MEM spectra illustrated in Figures 5.33 and 5.34 respectively. These results indicates that it is difficult to identify and detect the weak ELT signal $s_2(t)$.

Thus, by processing these three ELT signals using the non-linear (MEM) spectral estimation method it is seen that, the ratio between the power levels of the spectrum $\{S_1 (f_{c1} - F_I)/S_2(f_{c2} - F_I)\}$ at the output of the MEM processor are not equal to the ratio of the power levels (P_1/P_2) at the input before processing. From the analysis, we find that as P_2 at the input is reduced by 5 dB, the spectrum peak $S_2 (f_{c2} - F_I)$ at the output is reduced by 8 dB. When P_2 is reduced by 10 dB, $S_2 (f_{c2} - F_I)$ reduced by 14 dB. . This is due to the non-linearity of the spectral estimation method.

5.4.3.2   Ten ELT Signals

The detection of the presence of ten pulse modualted ELT signals $s_1(t)$, $s_2(t)$, $s_3(t)$,........., $s_{10}(t)$ with the same mixed carrier frequencies as before using the baseband MEM technique with MEM filter order 100 is studied here. All ELT signals having the same average power, except the ELT signal $s_6(t)$ with mixed carrier frequency 100 Hz, which has different power level. The average power P_6 of $s_6(t)$ is reduced from -5 dB to -20 dB in 5 dB steps as discussed before. The MEM spectral estimation results are given in Fig. 5.35 to 5.38
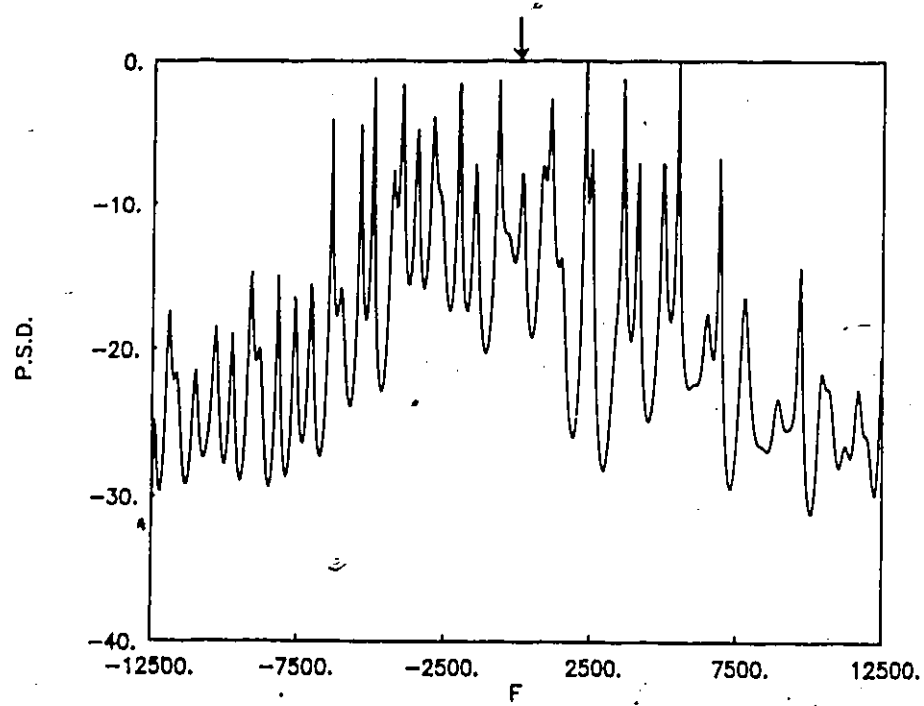
Fig. 5.35   MEM = 100 spectrum for ten ELT signals with P6/P1 = −5 dB.

Fig. 5.36   MEM = 100 spectrum for ten ELT signals with P6/P1 = −10 dB.
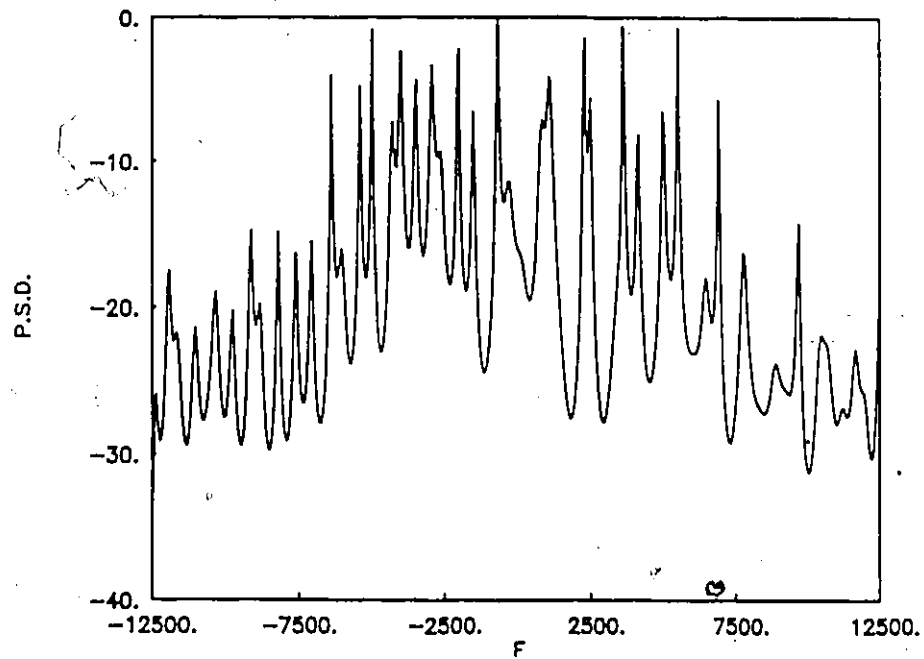
Fig. 5.37   MEM = 100 spectrum for ten ELT signals with P6/P1 = − 15 dB.
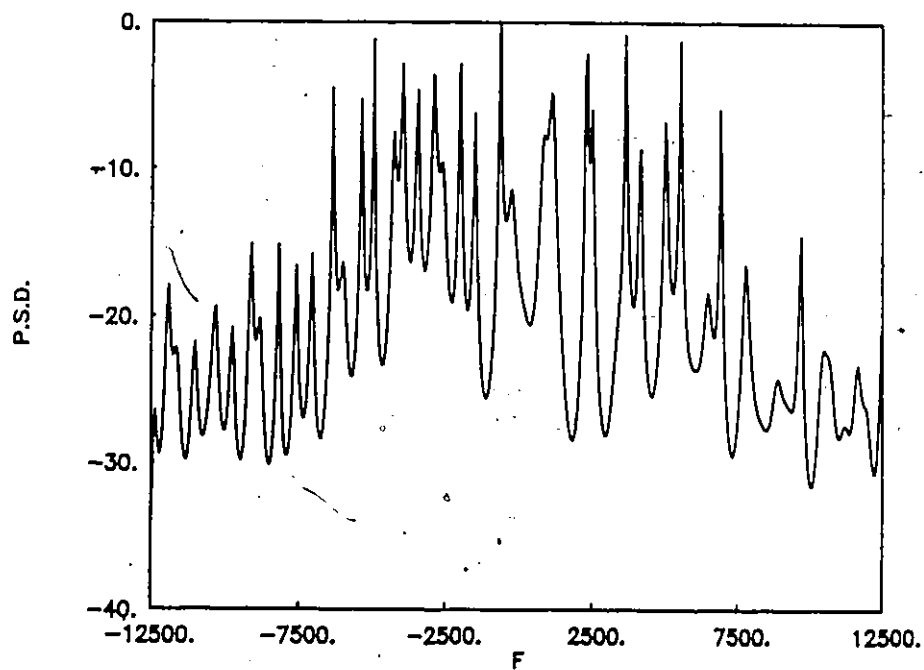
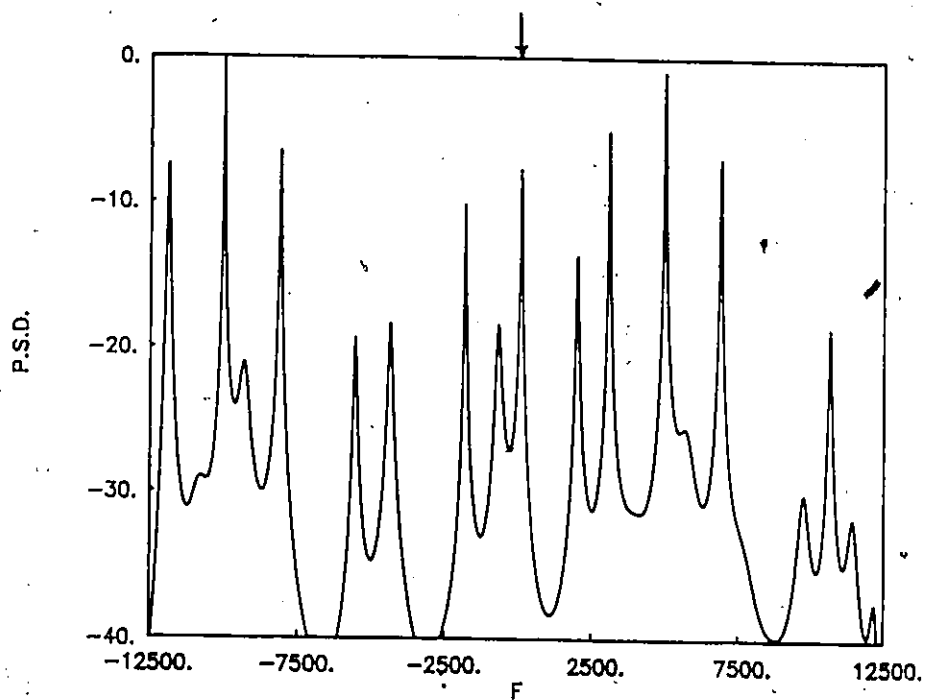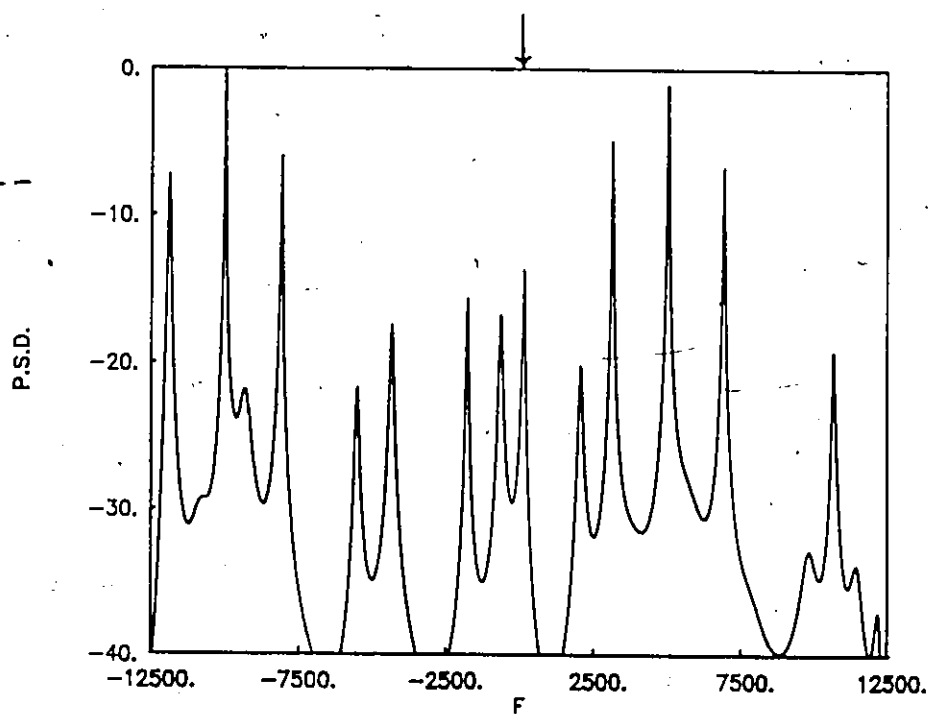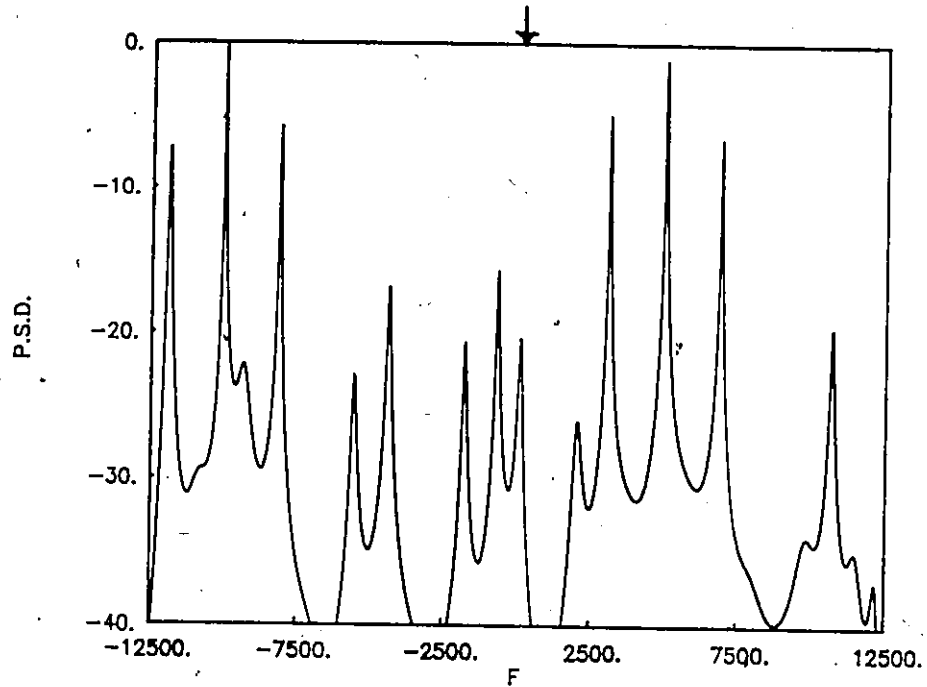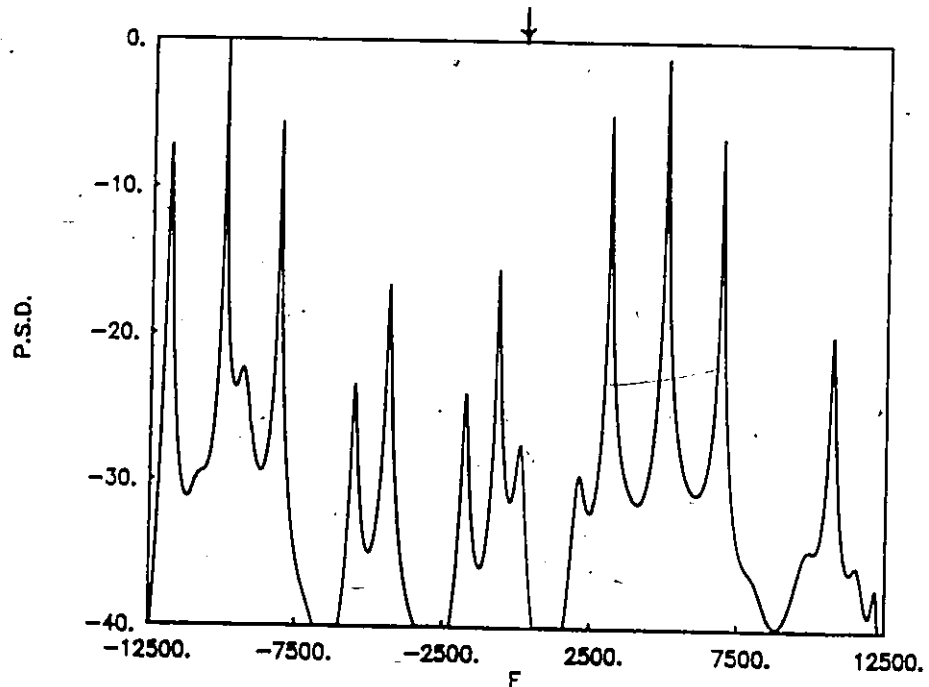Fig. 5.38   MEM = 100 spectrum for ten ELT signals with P6/P1 = − 20 dB.

for all the four cases respectively. Figure 5.35 illustrates the MEM spectra when the average power level P_6 is reduced by 5 dB below the level of all other ELT signals. From these results it is seen that, at the -10 dB threshold level, there are 20 peaks observed. Ten of these peaks are the desired peaks which occur at the proper frequency; but these peaks are shadowed by other undesirable sideband peaks. The carrier component peak of the weak ELT signal $s_6(t)$ is overlaped with these undesirable peaks which makes the detection of this ELT signal difficult.

Reducing the power level P_6 by 10 dB, 15 dB, and 20 dB below the average power level of all other ELT signals gives the MEM spectra plotted in Fig. 5.36, 5.37 and 5.38, respectively. These results indicate that the weak ELT signal $s_6(t)$ disappears with into the undesirable sidebands which reduces the probability of the detection of this weak ELT signal due to numerous peaks near the carrier frequency of this weak ELT signal.

Again, it is seen that the ratio of the power spectrum level $\{S_1 (f_{c1} - F_I)/S_6 (f_{c6} - F_I)\}$ at the output of the processor varies non-linearly as compared to the the power level ratio (P_1/P_6) at the input before processing.

5.4.4 Processing Results using the Averaged MEM

In this section, we study the spectral estimation results using the averaged MEM for the multiple ELT signals having different power levels. As described before, the averaged MEM reduces the effect of undesirable sidebands on the spectral estimation and consequently improves the detection of the weak ELT signal.

5.4.4.1 Three ELT Signal

The same three pulse modulated ELT signals are examined here using the averaged MEM with MEM filter order 50. The power level P_2 of $s_2(t)$ is reduced from -5 dB to -

20 dB in 5 dB steps. The spectral estimation results are given in Fig.5.39 to 5.42 for all four cases, respectively. Figures 5.39 and 5.40 illustrate the MEM averaging spectral estimation results for the first two cases in which the power level P_2 is reduced by 5 dB and 10 dB as compared to the power level P_1 of $s_1(t)$. From these results, we note that we can easily identify and detect all the transmitted ELT signals. With P_2 at -15 dB and -20 dB, we obtain the spectral estimation results shown in Figs. 5.41 and 5.42. Thus, it is seen from these results that the detection of the weak ELT signal $s_2(t)$ becomes difficult since the carrier component peak of this ELT signal must compete with other undesirable sidebands. However, the baseband averaged MEM spectral estimation technique improves the detection of the single-shot weak ELT signal due to the reduction of the level of undesirable sidebands in the case of three ELT signals.

5.4.4.2   Ten ELT Signals

The ten pulse modulated ELT signals with the same mixed carrier frequencies as before are examined here using the averaged MEM with MEM filter order 100. The power level P_6 of the signal $s_6(t)$ with mixed carrier frequency 100 Hz is varied in level from -5 dB to -20 dB in 5 dB steps while the power levels of all other ELT signals are kept constant. The spectral estimation results computed using the averaged MEM for all four cases are plotted in Fig. 5.43 to 5.46 respectively. Figure 5.43 shows the result when the the power level P_6 is reduced by 5 dB. From these results we can detect all ten ELT signals. With P_6 at -10 dB, -15 dB and -20 dB as illustrated in Figures 5.44, 5.45 and 5.46 respectively, we note that the detection of the weak ELT signal becomes difficult because the carrier component peak of this weak ELT signal is congested by other undesirable sidebands. In addition, all the above results indicate that the spectrum power level ratio $\{S_1 (f_{c1} - F_l)/S_6 (f_{c6} - F_l)\}$ at the output of
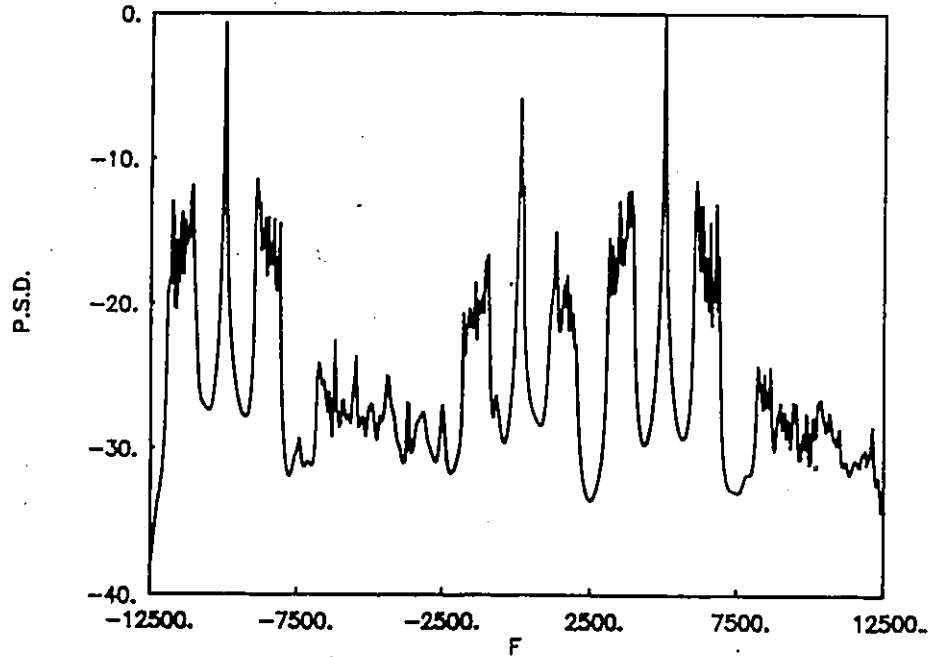
Fig. 5.39   Averaged MEM = 50 spectrum for three ELT signals with P2/P1 = −5 dB.
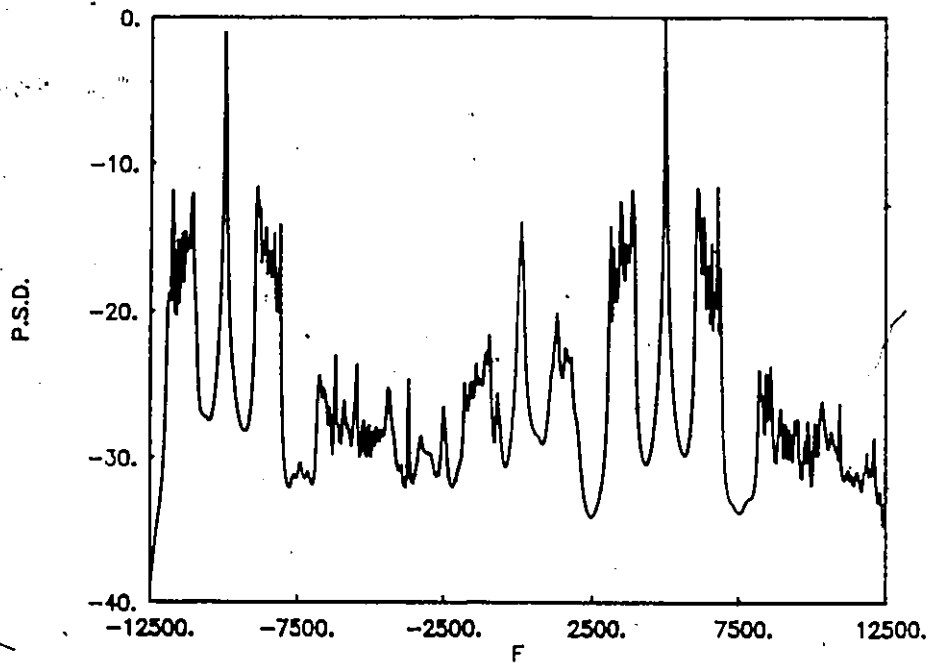
Fig. 5.40   Averaged MEM = 50 spectrum for three ELT signals with P2/P1 = −10 dB.
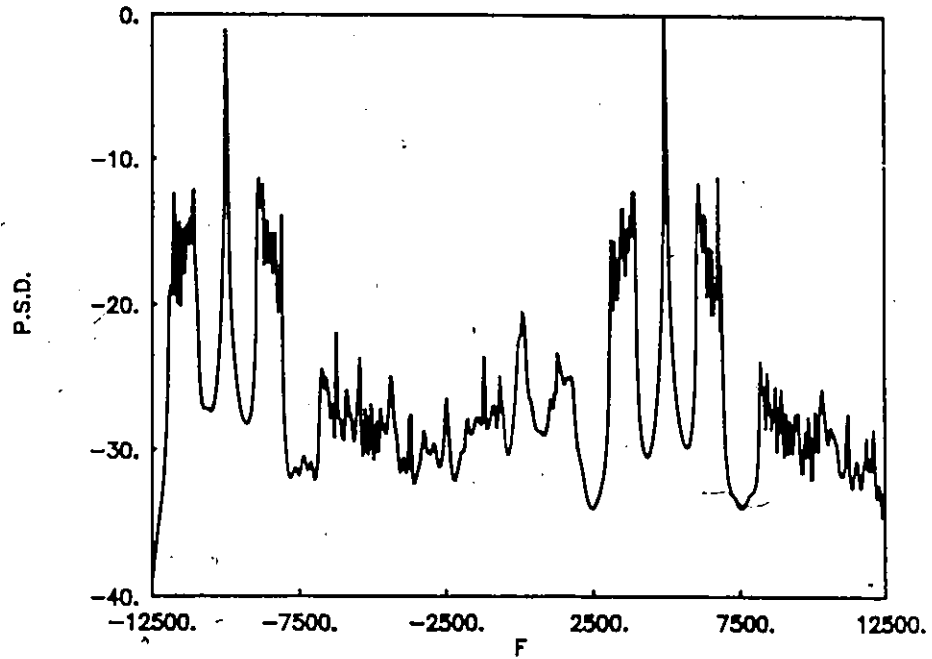
Fig. 5.41   Averaged MEM = 50 spectrum for three ELT signals with
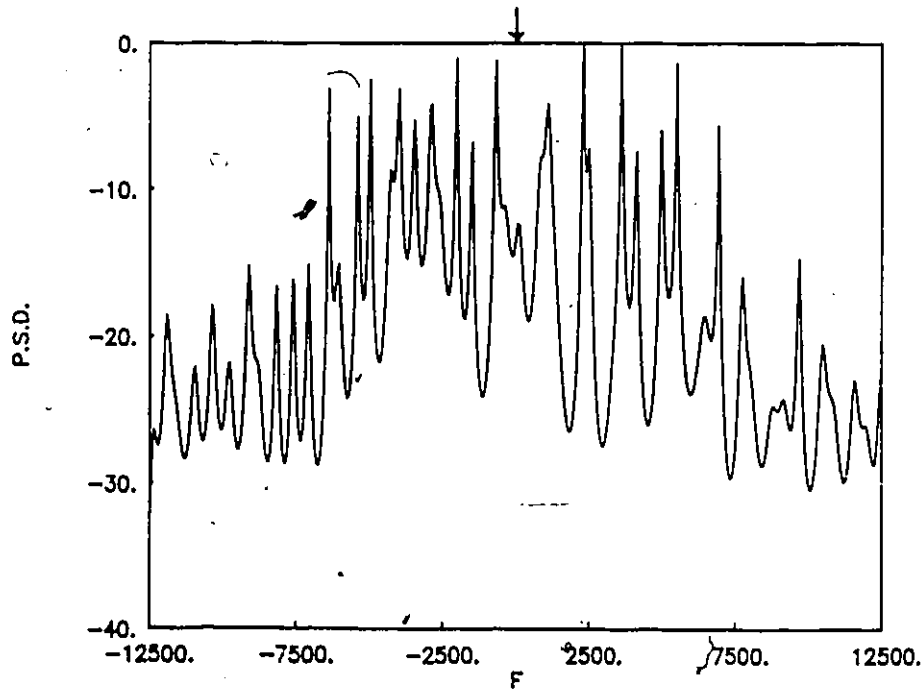P2/P1 = − 15 dB.
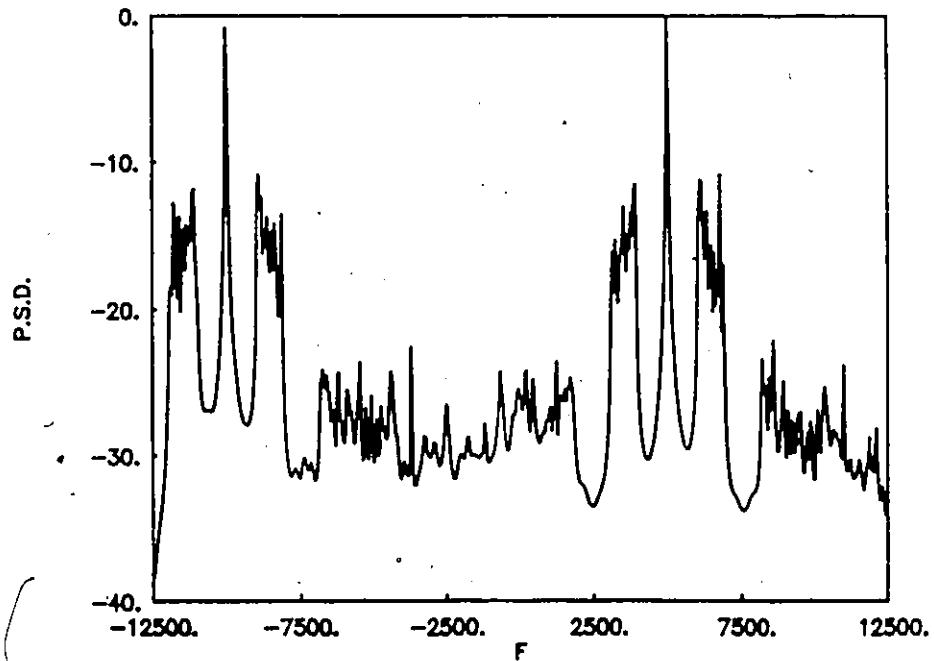
Fig. 5.42   Averaged MEM = 50 spectrum for three ELT signals with
P2/P1 = − 20 dB.
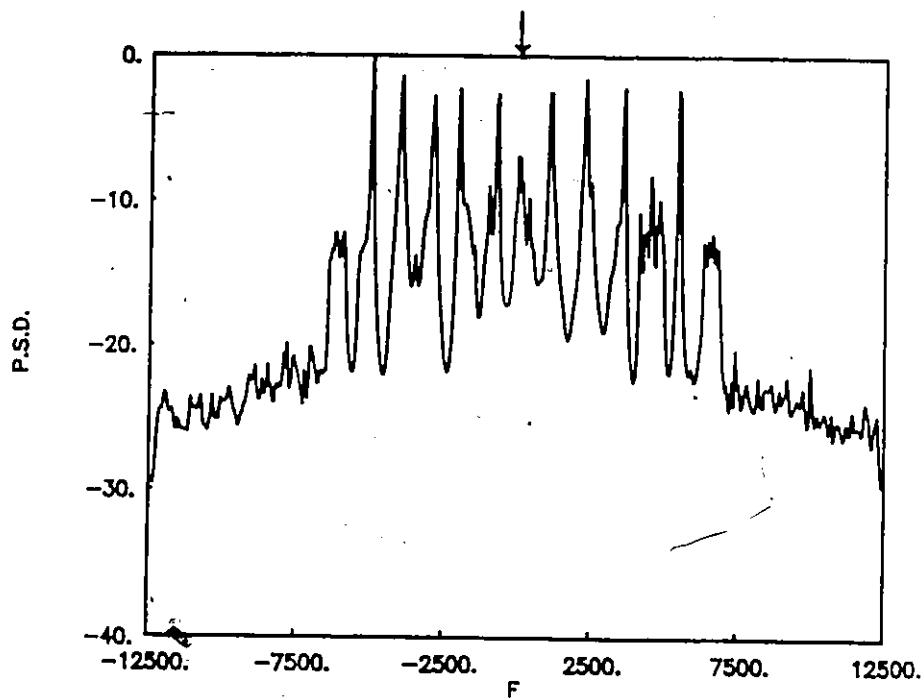
Fig. 5.43   Averaged MEM = 100 spectrum for ten ELT signals with
             P6/P1 = −5 dB.
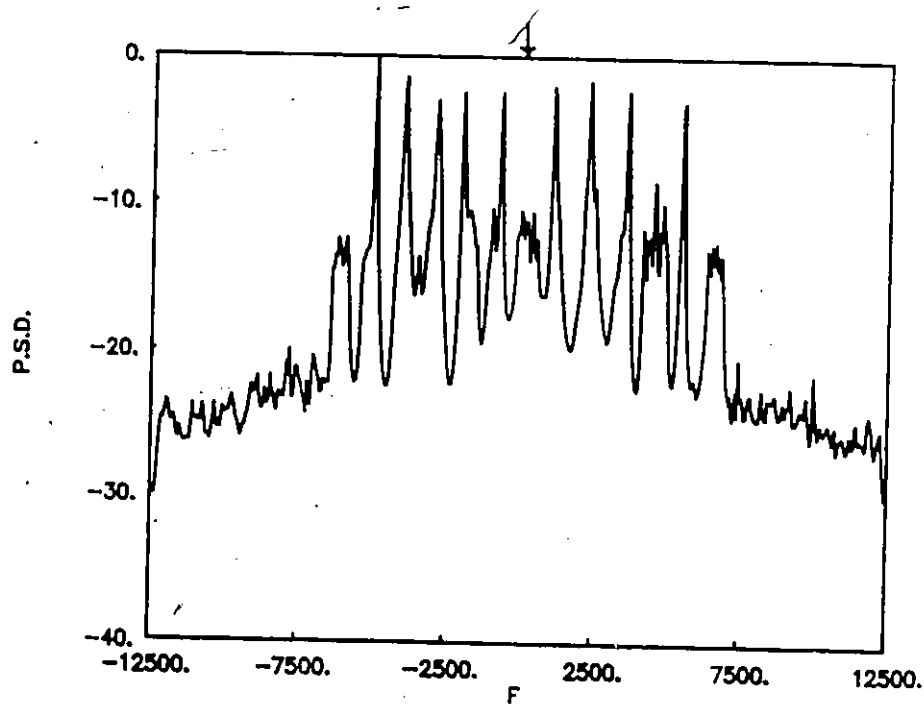
Fig. 5.44   Averaged MEM = 100 spectrum for ten ELT signals with
             P6/P1 = −10 dB.
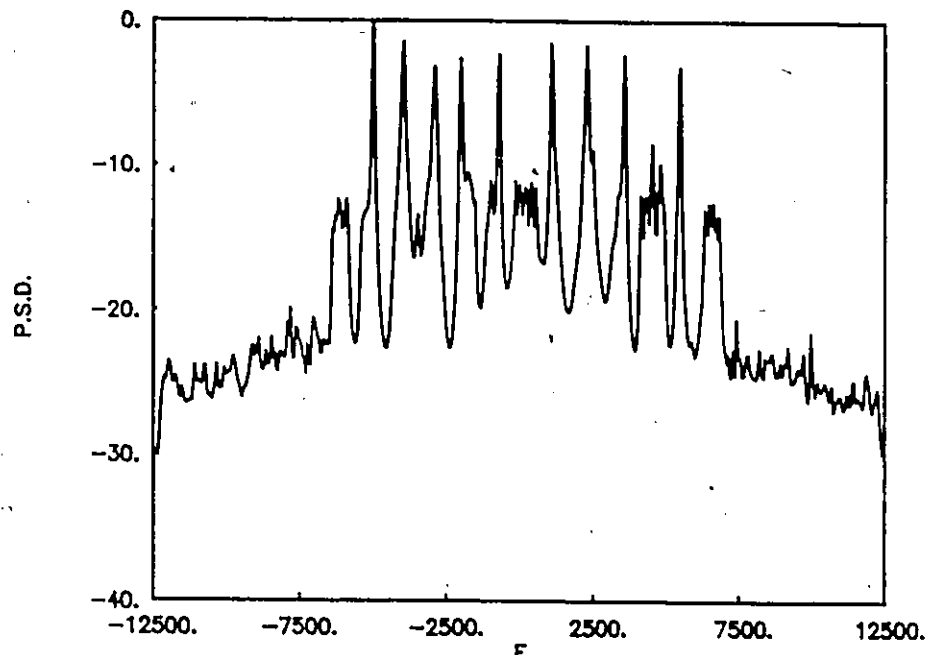
Fig. 5.45   Averaged MEM = 100 spectrum for ten ELT signals with
P6/P1 = −15 dB.
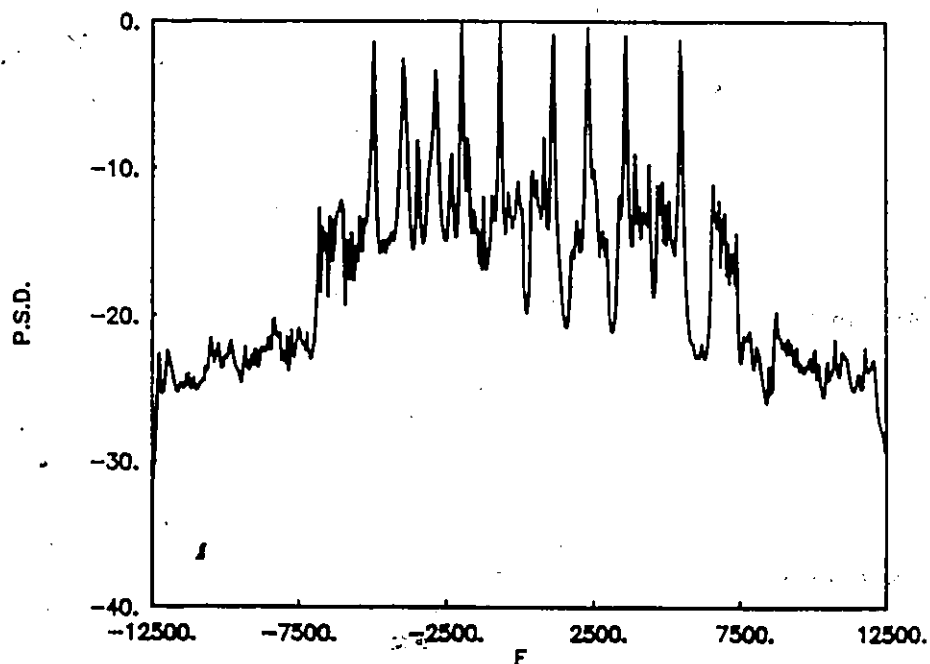
Fig. 5.46   Averaged MEM = 100 spectrum for ten ELT signals with
P6/P1 = −20 dB.

the processor varies non-linearly compared to the power level ratio (P_1/P_6) at the input of the processor.

Comparing these results with those obtained using the baseband MEM we note that, the averaged MEM improves the detection as compared to the single-shot weak ELT signal.

5.5   Detection of the Weak ELT Signal Using Rate Reduction Filtering

This section is devoted to an examination of the results of processing multiple pulse-amplitude modulated ELT signals with different power levels in the presence of additive white Gaussian noise, processed by the baseband periodogram and baseband MEM techniques using rate reduction filtering.

In this section, the same three pulse modulated ELT signals $s_1(t)$, $s_2(t)$ and $s_3(t)$ are used to study the performance of the periodogram and MEM using the rate reduction filtering method. These ELT signals are processed with mixed carrier frequencies -10 kHz, 100 Hz and 5 kHz, and carrier to noise density ratio (CNDR) level equal 39 dB-Hz. The power levels P_1 and P_3 of the ELT signals $s_1(t)$ and $s_3(t)$ are kept equal, but the power level P_2 of $s_2(t)$ is reduced by 10 dB below the power level P_1. These pulse modulated ELT signals are tested using 512 complex points for the baseband periodogram and MEM with averaging steps, $\ell = 1,2,4$ and 8.

5.5.1   Rate Reduction Filtering Using the Baseband Periodogram

First, all the three ELT signals are processed with equal power level, and with no rate reduction. The FFT spectral result for this case is given in Fig.5.47. From this figure, it is seen that at the -10 dB threshold level, there are nine peaks for the three ELT signals with three peaks for each ELT signal occur, these comprising the carrier component peak and two
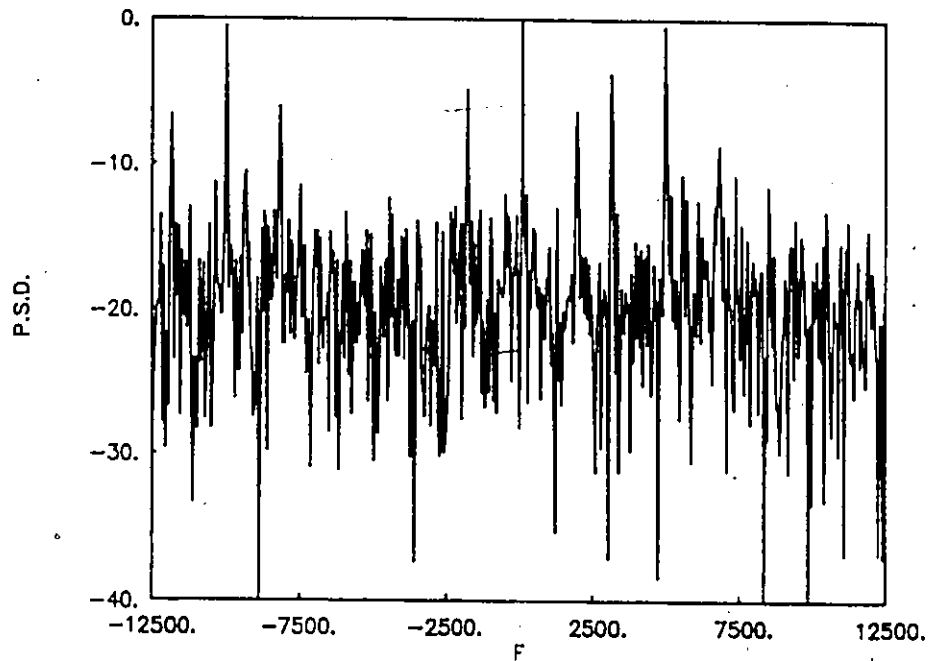
Fig. 5.47   Periodogram spectrum for three ELT signals with CNDR = 39 dB-Hz.

Fig. 5.48   Periodogram spectrum for two ELT signals with
             CNDR = 39 dB-Hz and one ELT signal at 29 dB-Hz. No rate reduction.

major sidebands. Reducing the power level P_2 of $s_2(t)$ by 10 dB below the power level P_1 of $s_1(t)$ gives the FFT spectral result illustrated in Fig.5.48. From this figure, it is seen that at the -10 dB threshold level, six peaks occur, these peaks described as three peaks for each of $s_1(t)$ and $s_3(t)$; but, the weak ELT signal $s_2(t)$ has disappeared with the other undesirable sidebands which makes the detection of this weak ELT signal difficult. These results indicate that only two ELT signals are present. Figure 5.49 shows the results in the case of averaging by 2. From this figure it is clear that, at the -10 dB threshold level, two peaks are detected. These peaks described as the carrier peak component of $s_3(t)$ and the weak ELT signal $s_2(t)$. Also, in this figure, the level of the background side peaks are reduced by 3 dB which improves the detection of the carrier component peak of the weak ELT signal $s_2(t)$. Figure 5.50 depicts the FFT spectral estimation result in the case of averaging by 4. From this figure it is shown that the weak ELT signal is the only one which can be detected and observed, since the carrier component peak of this weak ELT signal can be detected above the -5 dB threshold level. Increasing the averaging steps to 8 gives the periodogram spectral estimation result shown in Fig. 5.51. From this figure, it is clear that the level of the side peaks is reduced by 3 dB and only one peak is detected easily above the threshold level of -10 dB, this peak being the carrier component of the weak ELT signal $s_2(t)$.

From the above analysis, we note that rate reduction by 8 gives an improvement in signal-to-noise ratio by 9 dB which consequently improves the detection of the weak ELT signal when using the baseband periodogram.

5.5.2   Rate Reduction Filtering Using MEM

In this section we study the baseband MEM specrta of a three pulse modulated ELT signals in the presence of noise using rate reduction filtering. The same three ELT signals are processed using this method with MEM filter order 50. First, all the three ELT signals
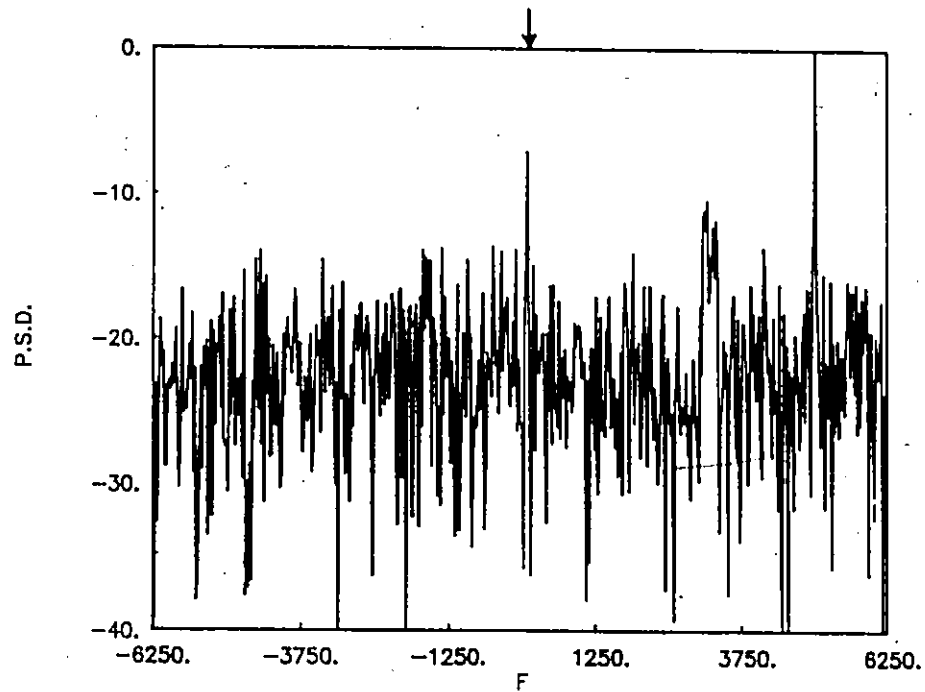
Fig. 5.49   Periodogram spectrum for two ELT signals with
            CNDR=39 dB-Hz and one ELT signal at 29 dB-Hz. Rate reduction = 2.

Fig. 5.50   Periodogram spectrum for two ELT signals with
            CNDR=39 dB-Hz and one ELT signal at 29 dB-Hz. Rate reduction = 4.

Fig. 5.51   Periodogram spectrum for two ELT signals with
CNDR = 39 dB-Hz and one ELT signal at 29 dB-Hz. Rate reduction = 8.

are tested with equal power level, and the MEM spectral estimation result for this case with no rate reduction is given in Fig.5.52. From this figure it is clear that at the -10 dB threshold level, nine peaks are detected, these peaks described as three peaks for each ELT signal, which comprising the carrier component and the two major sideband. It is seen that we can easily detect and identify all three ELT signals. Reducing the power level P_2 of $s_2(t)$ by 10 dB below the power level P_1 of $s_1(t)$ gives the MEM spectral results shown in Fig.5.53, in the case of no averaging. From this figure we note that, at the -10 dB threshold level six peaks are detected, these peaks described as three peaks for each strong signal $s_1(t)$ and $s_3(t)$, but the weak ELT signal $s_2(t)$ disappears with the other undesirable peaks which makes the detection of this ELT signal $s_2(t)$ difficult. Increasing the averaging steps ℓ to 2, gives the MEM spectral estimation result depicted in Fig. 5.54. From this figure, it is shown that at the -10 dB threshold level only two peaks are detected, these peaks described as the carrier component of $s_3(t)$ and one of its two major sidebands while the other sideband is rejected. Figure 5.55 illustrates the MEM specrtal result using $\ell = 4$. From this figure it is clear that, at the -5 dB threshold level, only one peak is detected. This peak being the carrier component of the weak ELT signal $s_2(t)$, which makes the detection of this weak ELT signal easy. Increasing the averaging steps ℓ to 8, gives the MEM spectral estimation result depicted in Fig. 5.56. From these result it is seen that only one peak is detected above the threshold level of -10 dB, this peak being the carrier component of the weak ELT sigal $s_2(t)$.

Thus, from the above analysis we conclude that, increasing the rate reduction (averaging) steps ℓ to 8 improves the signal-to-noise ratio by about 10 dB, producing a sharp carrier component peak and improving the frequency resolution. This consequently improves the detection of the weak ELT signal in the presence of noise.
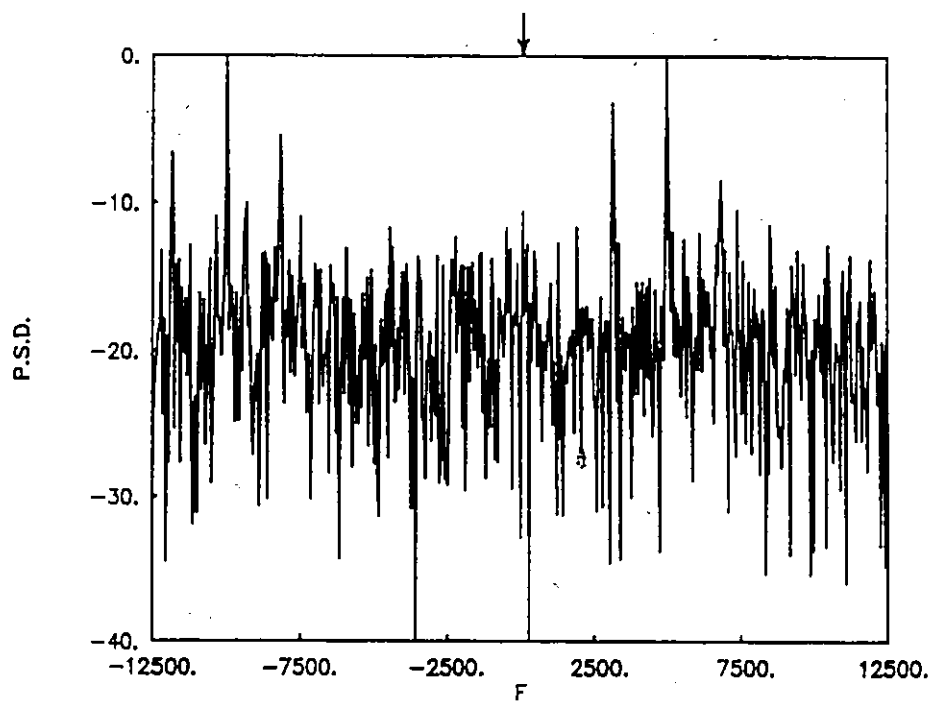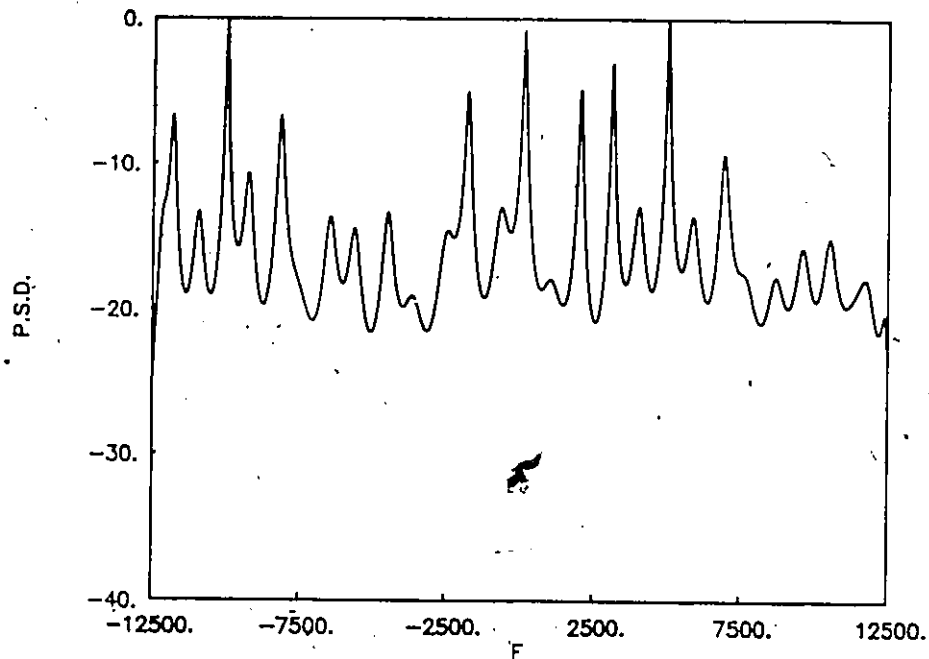
Fig. 5.52   MEM = 50 spectrum for three ELT signals with CNDR = 39 dB- Hz.
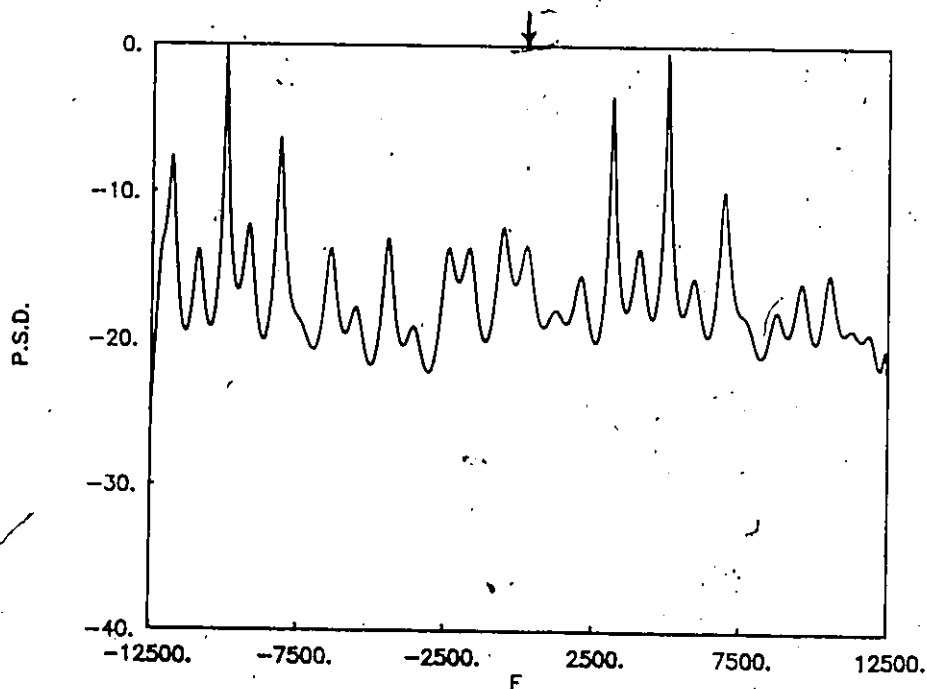
Fig. 5.53   MEM = 50 spectrum for two ELT signals with
CNDR = 39 dB-Hz and one ELT signal at 29 dB-Hz. No Rate reduction.
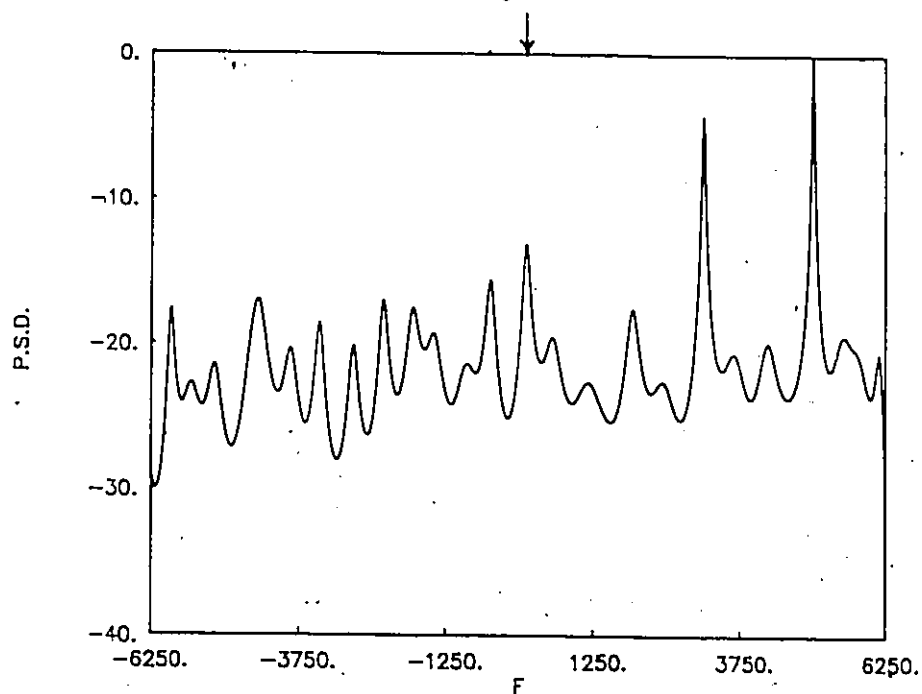
Fig. 5.54　　　　MEM = 50 spectrum for two ELT signals with
CNDR = 39 dB-Hz and one ELT signal at 29 dB-Hz. Rate reduction = 2.
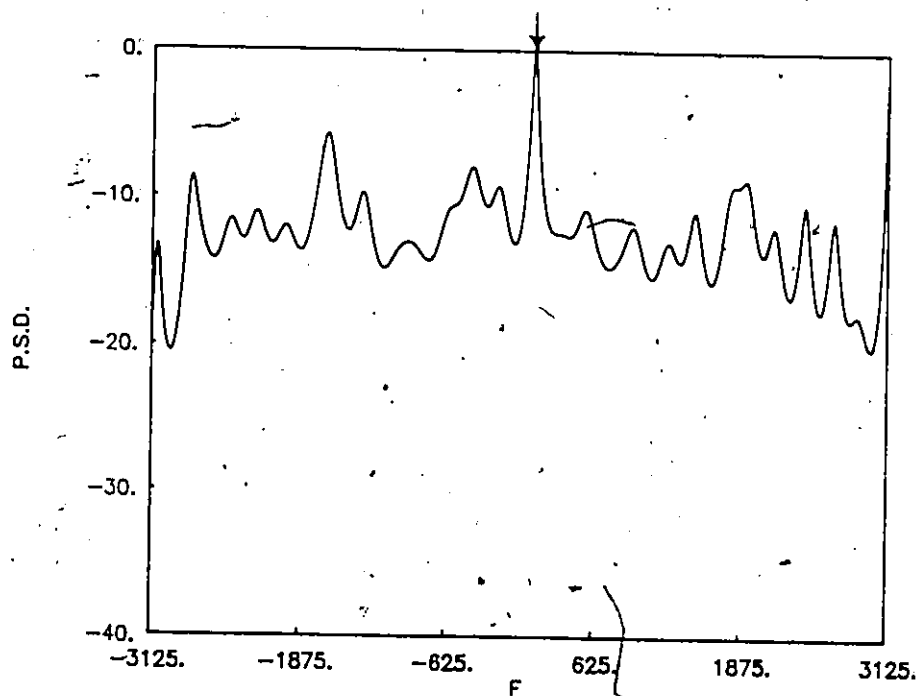
Fig. 5.55　　　　MEM = 50 spectrum for two ELT signals with
CNDR = 39 dB-Hz and one ELT signal at 29 dB-Hz. Rate reduction = 4.
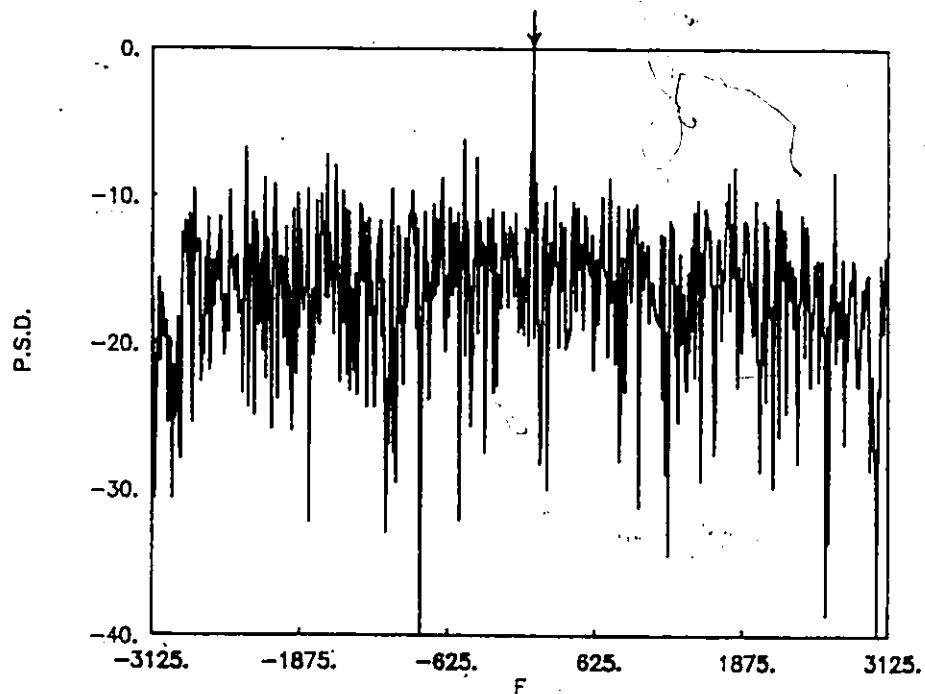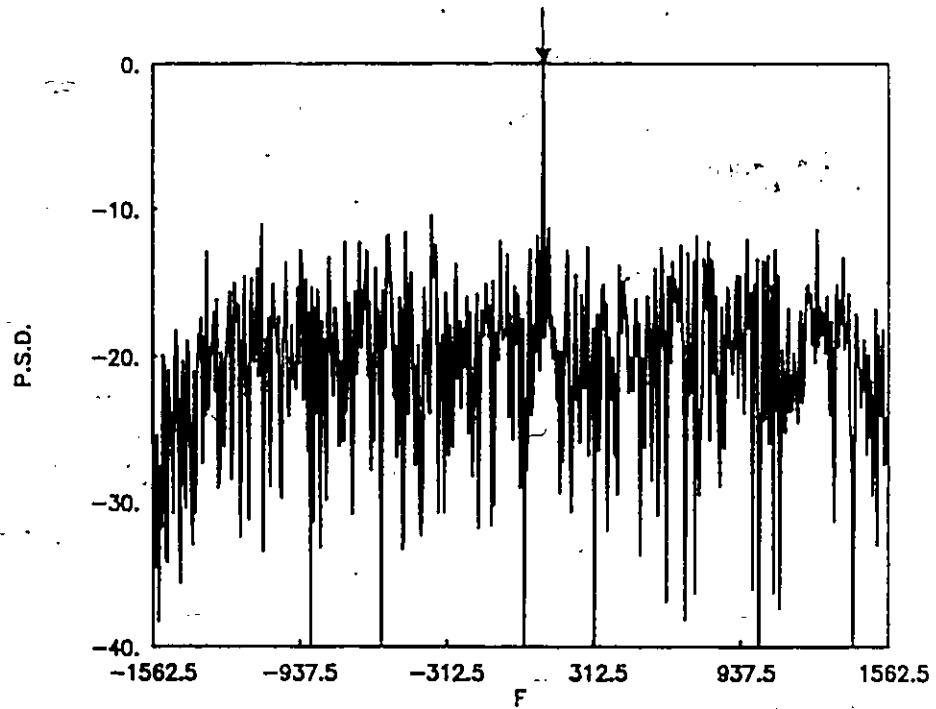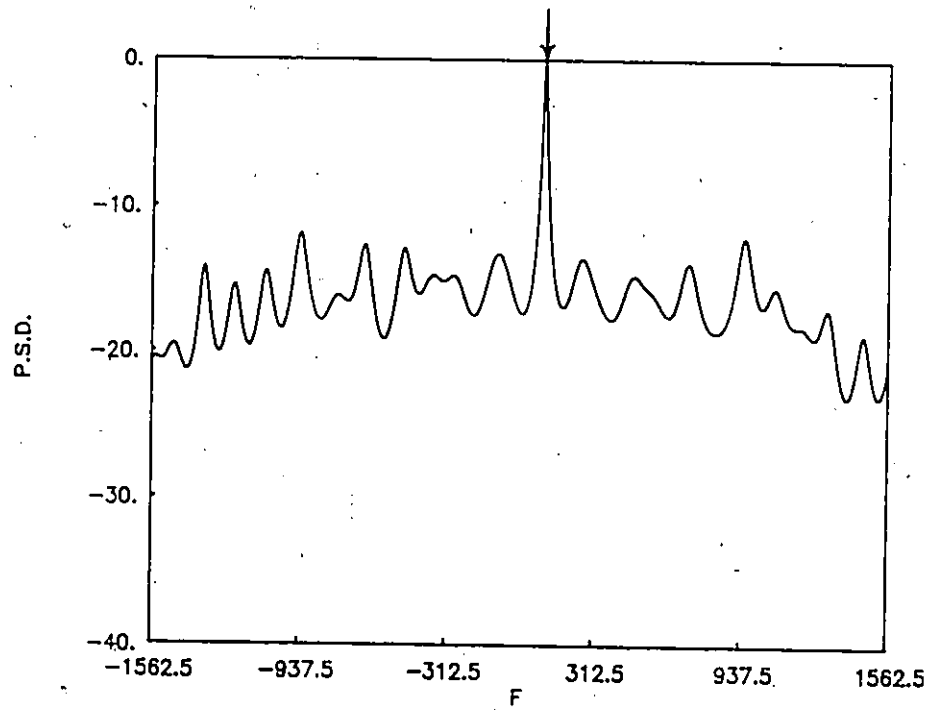
Fig. 5.56   . MEM = 50 spectrum for two ELT signals with
CNDR = 39 dB-Hz and one ELT signal at 29 dB-Hz. Rate reduction = 8.

5.6   Summary

A baseband processor for multiple ELT signals has been described and tested using computer generated signals. These multiple ELT signals can have either equal or unequal strength. Linear and non-linear spectral estimation methods have been employed.

From the above detailed analysis we conclude the following:

(A)   *For Multiple ELT Signals with Equal Power Levels*

1.   The periodogram technique performs satisfactory for three ELT signals. However, for ten ELT signals, the spectrum obtained using this method is crowded. This degrades the detection of the ten ELT signals.

2.   The averaged periodogram reduces the level of undesirable sidebands and smoothes the spectrum. The level of these sidebands appears at a level below the level of the carrier component peaks by usually 10 dB, which consequently improves the detection of the present ELT signals.

3.   A low order of prediction error filter produces a broad peak with large RMS frequency error for the analysis of the multiple ELT signals. High MEM filter order reduces the RMS frequency error and produces a sharp carrier peaks.

4.   The averaged MEM reduces the level of undesirable sidebands and improves the detection of the multiple ELT signals.

(B)   *For Multiple ELT Signals with Different Power Levels*

1.   Strong ELT signals which have strong sidebands can sweep through the band of a weak ELT signal, which makes the detection of this weak ELT signal difficult.

2.   The processing results using the baseband periodogram or MEM technique (single-shot) for three ELT signals indicate that, we can identify and detect all three ELT

signals, if the difference of the power levels is within 10 dB. The detection of the weak ELT signal becomes difficult if the power difference is reduced by more than 10 dB.

3.   When ten ELT signals are processed using the periodogram technique with one ELT signal at a lower power level, the detection of this weak ELT signal is difficult due to spectral overlap.

4.   For three ELT signals, if the power level of the weak ELT signal is reduced by no more than 15 dB below the power level of the powerful ELT signals, we can detect all the ELT signals using the averaged periodogram, assuming adequate frequency separation.

5.   Using the averaged periodogram technique, we can detect the weak ELT signal, for ten ELT signals when the power level of the ELT signals is within 10 dB.

6.   Using the averaged MEM, the weak ELT signal can be detected if its power level is reduced by no more than 10 dB below the level of the powerful ELT signals for the case of three ELT signals. But for the case of ten ELT signals, the power level of the weak ELT signal must be no more than 5 dB below the power level of the powerful ELT signal for detection.

7.   The detection of the weak ELT signal in the presence of noise is improved using the single-shot periodogrm or MEM method with rate reduction filtering because this technique improves the frequency resolution and increase the signal-to-noise ratio.

CHAPTER 6

BASEBAND PROCESSOR FOR REAL SARSAT SIGNALS

6.1 Introduction

In the preceding chapters we have studied the baseband processing of computer generated ELT signals. In this chapter, the signal processing of real ELT signals is studied using the periodogram and maximum-entropy method. In order to enhance the signal detectability, spectral averaging is employed. These real ELT signals (described later) were recorded at the Communication Research Centre (CRC) in Ottawa and include individual ELT signals and combinations of ELT signals. A complete discussion of the results for these cases is covered. Further, the Rate Reduction Filtering technique is applied with the periodogram and the MEM for detection and identification of the weak carrier frequency component ELT signals.

6.2 Real ELT Signals

The CRC in Ottawa has supplied tape recordings of several real ELT signals. These recordings were made from an ELT testbed capable of combining the signals of up to 20 real ELT signals [39,40]. The signals include: those from individual ELT units; and those from combinations of ELT units. These tapes were digitized using an 8-bit analog to digital converter at a sampling rate of 100 kHz. The reference numbers, manufacturers, models and power output of the testbed ELT units are listed in Table 6.1.

Individual signals include : Pointer ELT01 and ELT07; Garrett ELT12 and ELT15;

TABLE 6.1

DESCRIPTION OF ELT SIGNALS

Reference Number	Manufacturer	Model Number	Power Output (mW) 121.5 MHz Band
ELT01	Pointer	Sentry C-4000	417
ELT07	Pointer	Sentry C-4000	303
ELT12	Garrett	Rescu 88C	132
ELT14	Garrett	Rescu 88C	118
ELT15	Garrett	Rescu 88C	121
ELT17	Narco	ELT10	340
ELT19	Narco	ELT10	277

and, Narco ELT17 and ELT19. Signals in combination include: two ELT units (ELT01 and ELT19); three ELT units (ELT01, ELT12 and ELT19) and (ELT01, ELT14 and ELT19); and five ELT units (ELT01, ELT07, ELT12, ELT17 and ELT19).

6.3   Processing of Individual Real ELT Signals

In this section, we examine the processing of one real ELT signal using linear and non-linear spectral estimation methods. The post-processing technique (spectral averaging) is also used in order to enhance the spectral performances. These single real ELT signals are processed using the baseband processor with mixing frequency F_I and the lowpass filter cutoff frequency equal to 12.5 kHz. The number of points used in this analysis is 512 complex points for all cases. Results are now presented for Pointer (ELT01 and ELT07), Garrett (ELT12 and ELT15) and Narco (ELT17 and ELT19) ELT signals.

6.3.1   Processing Results Using the Periodogram

6.3.1.1   Pointer ELT Signals

We examine the spectral estimation performance using the baseband periodogram for the Pointer Sentry C4000 ELT units ELT01 and ELT07. The spectral densities for these two ELT units are given in Figs.6.1 and 6.2 respectively. From these results and detailed results presented in [41] we note the following: 1) three peaks are detected above the threshold level of -10 dB; these peaks comprising the carrier component and the first upper and lower sidebands; 2) the carrier peak occurs at mixed carrier frequency of 3400 Hz for Pointer ELT01 and about 4800 Hz for Pointer ELT07; and 3) the levels of the sidebands are not symmetrical about the carrier frequency, with the lower sideband being stronger than the upper sideband. These Pointer ELT signals can be classified as non-ideal coherent.
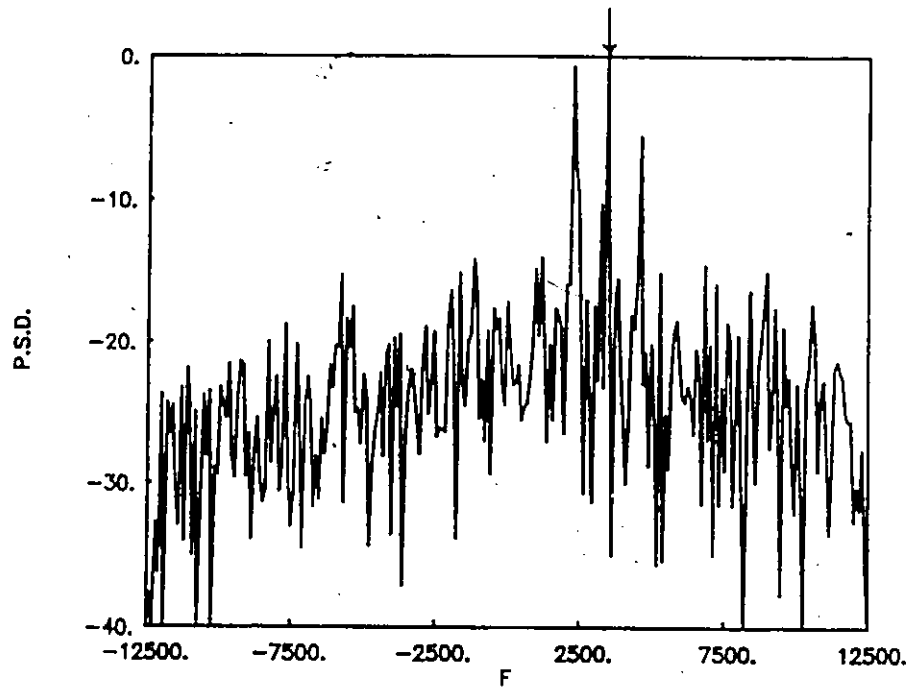
Fig. 6.1   Periodogram spectrum of Pointer ELT signal (ELT01).
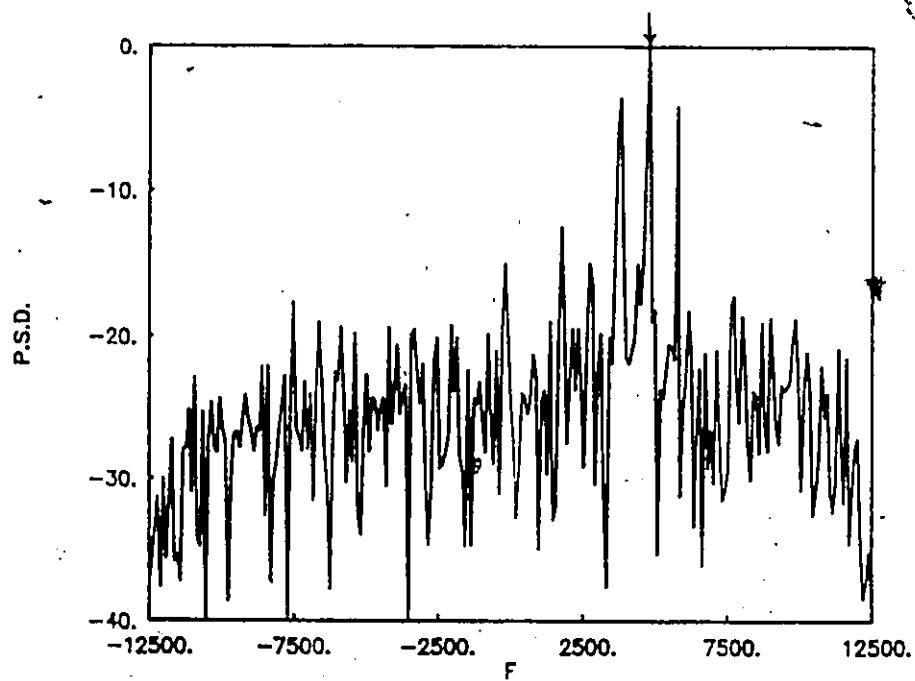
Fig. 6.2   Periodogram spectrum of Pointer ELT signal (ELT07).

6.3.1.2 Garrett ELT Signals

Next, we examine the spectral estimation performance using the periodogram for a Garrett Rescu 88C ELT units ELT12 and ELT15. Figures 6.3 and 6.4 show the periodograms for these two ELT signals. In this case, we see that; 1) at the -10 threshold level three peaks are detected, these peaks being the carrier component and the first upper and lower sidebands; 2) the carrier component peak occurs at mixed carrier frequency equal about 4300 Hz for ELT12 and at about 1900 Hz for ELT15; and 3) the levels of the sidebands are not symmetrical about the carrier frequency. Again these ELT signal can be classified as non-ideal coherent.

6.3.1.3 Narco ELT Signals

Now, we consider Narco ELT10 units ELT17 and ELT19. The spectral estimation results for these two ELT signals are shown in Fig. 6.5 and 6.6, respectively. For ELT17, we note that; 1) the relative levels of the sidebands change during the sweep and these levels of sidebands are not symmetrical about the carrier frequency.; 2) the lower sidebands are much stronger than the upper sidebands.; and 3) the detection for the carrier component peak.is not easy using single-shot periodogram. Narco ELT17 can be classified as non-ideal coherent.

For Narco ELT19 it is seen that there are several peaks; consequently this ELT signal can be classified as non-coherent (random phase) signal.

6.3.2 Processing Results Using the Averaged Periodogram

As discussed in Chapters 3 and 5, the averaged periodogram technique reduces the variance and makes the spectrum estimate smooth. In this section, we study the spectral estimation performance for single real ELT signals using the baseband averaged periodogram. As described in Chapter 3, the data record is divided into K blocks covering
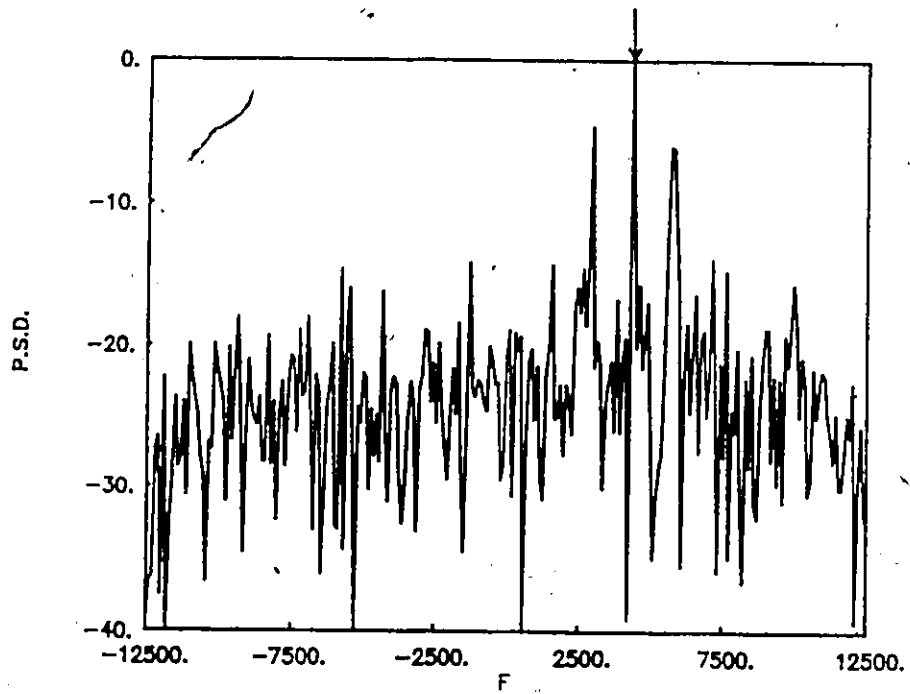
Fig. 6.3   Periodogram spectrum of Garrett ELT signal (ELT12).
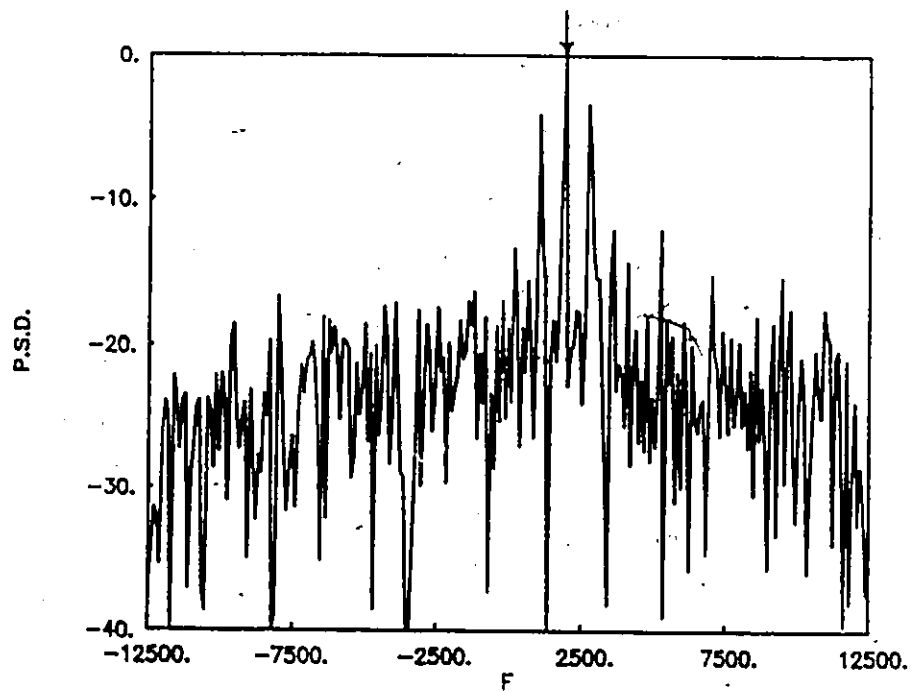
Fig. 6.4   Periodogram spectrum of Garrett ELT signal (ELT15).
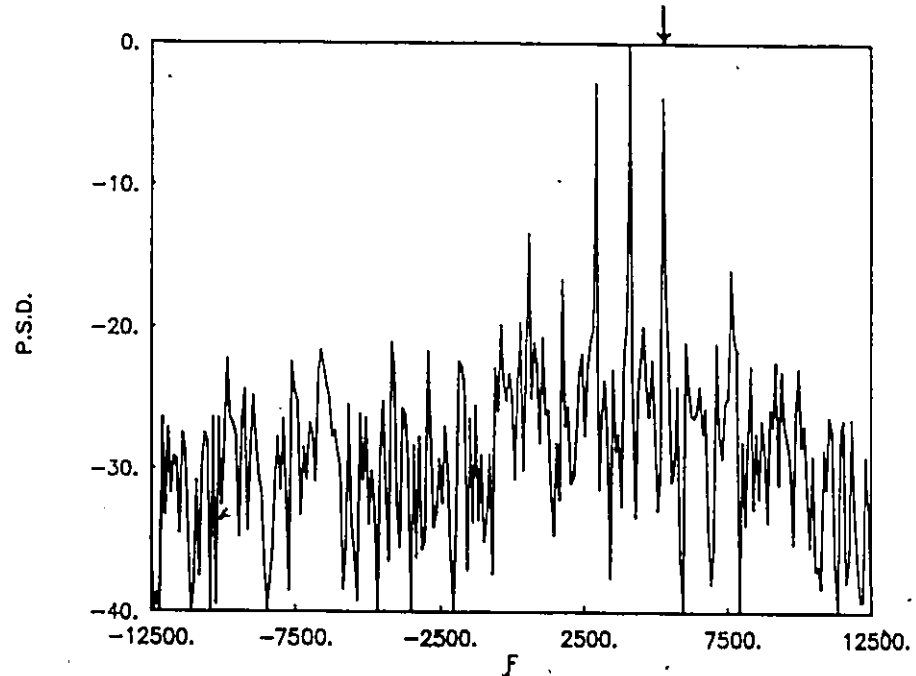
Fig. 6.5   Periodogram spectrum of Narco ELT signal (ELT17).
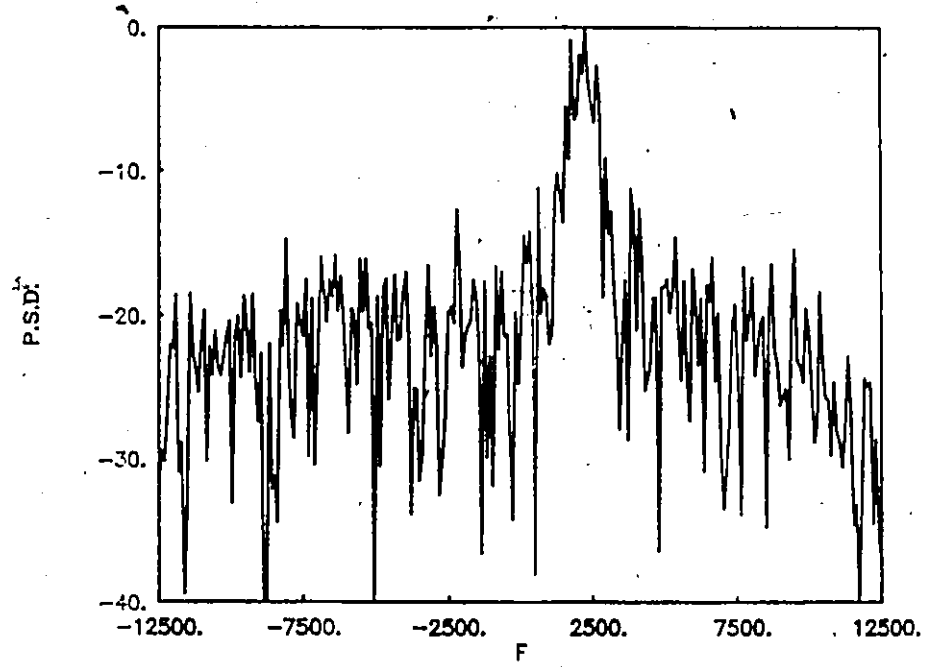
Fig. 6.6   Periodogram spectrum of Narco ELT signal (ELT19).

different time intervals with each block containing P complex points. In this section, we choose K = 50 and P = 512 complex points.

6.3.2.1   Pointer ELT Signals

For Pointer ELT signals ELT01 and ELT07, the spectral estimation results are given in Fig. 6.7 and 6.8, respectively. From these results we note that; 1) the averaged periodogram reduces the level of the first upper and lower sidebands by about 7 dB or more as compared to the results obtained using single-shot periodogram for the same ELT signals illustrated in Fig. 6.1 and 6.2 respectively.; 2) the carrier component peak for each ELT signal can be detected easily above the -10 dB threshold level.; 3) the carrier component peak occurs at constant mixed carrier frequency (at about 3400 Hz for ELT01 and at about 4800 Hz for ELT07).; and 4) the lower sideband is stronger than the upper sideband as shown for both ELT01 and ELT07 spectral plots. Furthermore, it is seen that the averaged sidebands are well defined as shown in these figures. Since the lower and upper sideband bandwidths may be unequal, we designate them with W1 and W2. Thus, signal identification is furthered by noting the relative amplitude between the carrier peak and first upper and lower sidebands.

6.3.2.2   Garrett ELT Signals

The spectral estimation results for Garrett ELT signals are plotted in Fig. 6.9 and 6.10 for ELT12 and ELT15, respectively. These results indicate that; the levels of the first upper and lower sidebands are reduced by about 7 dB as compared to the results shown in Fig. 6.2 and 6.3 for the same ELT signals using the single-shot periodogram. the carrier component peak for each ELT signal can be detected easily above the -10 dB threshold level. Again the carrier component peaks are located at mixed carrier frequencies of 4300 Hz and 1900 Hz for ELT12 and ELT15, respectively. It is also seen that the relative heights of the
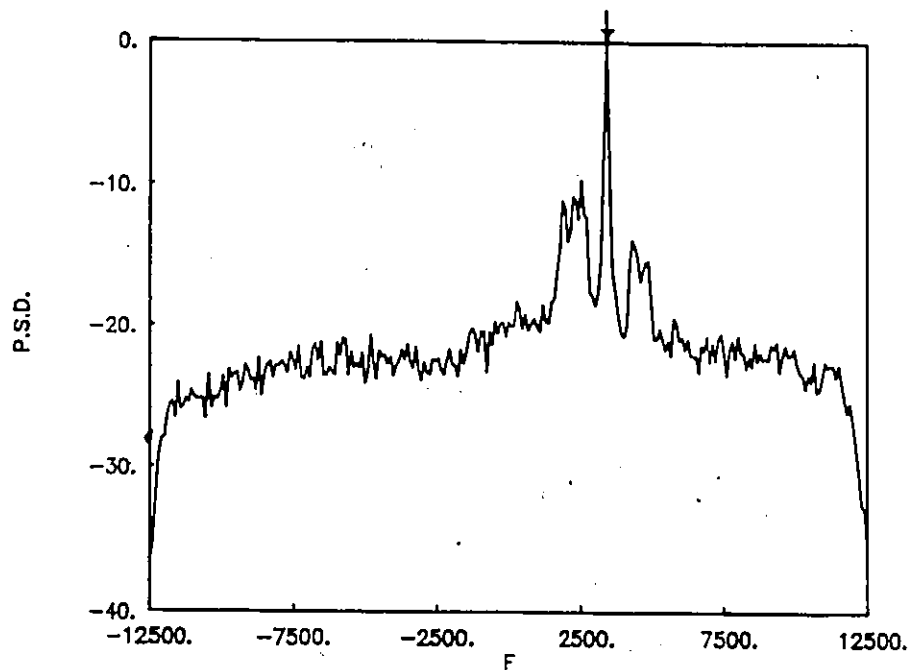
Fig. 6.7   The averaged periodogram spectrum of Pointer ELT01.
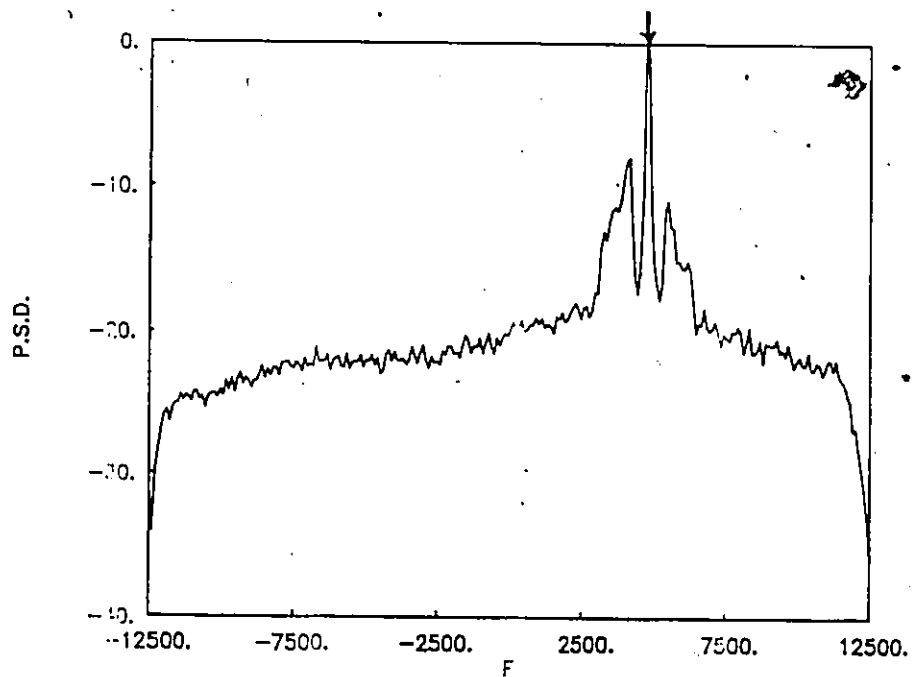
Fig. 6.8   The averaged periodogram spectrum of Pointer ELT07.
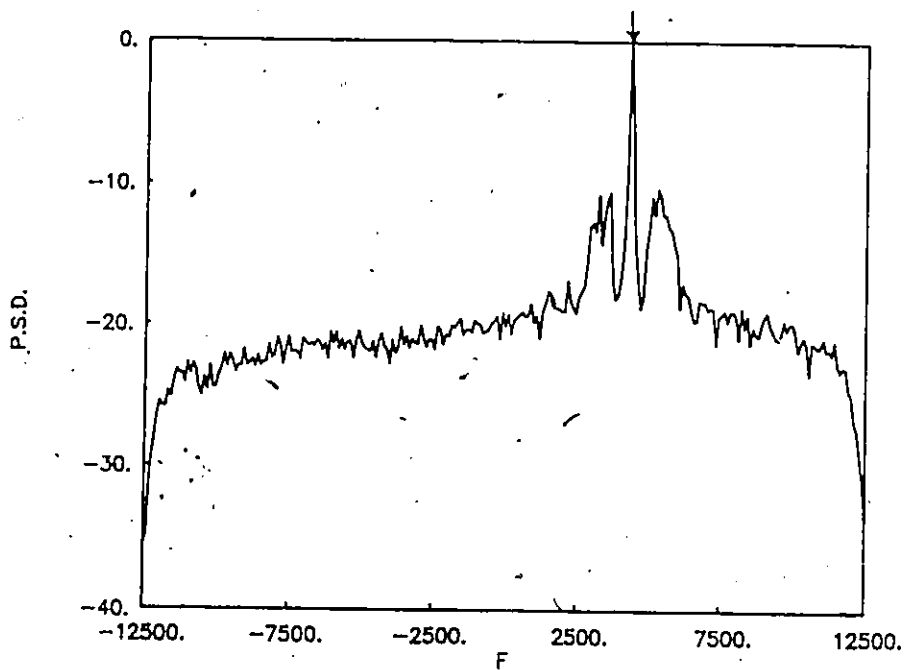
Fig. 6.9   The averaged periodogram spectrum of Garrett ELT12.
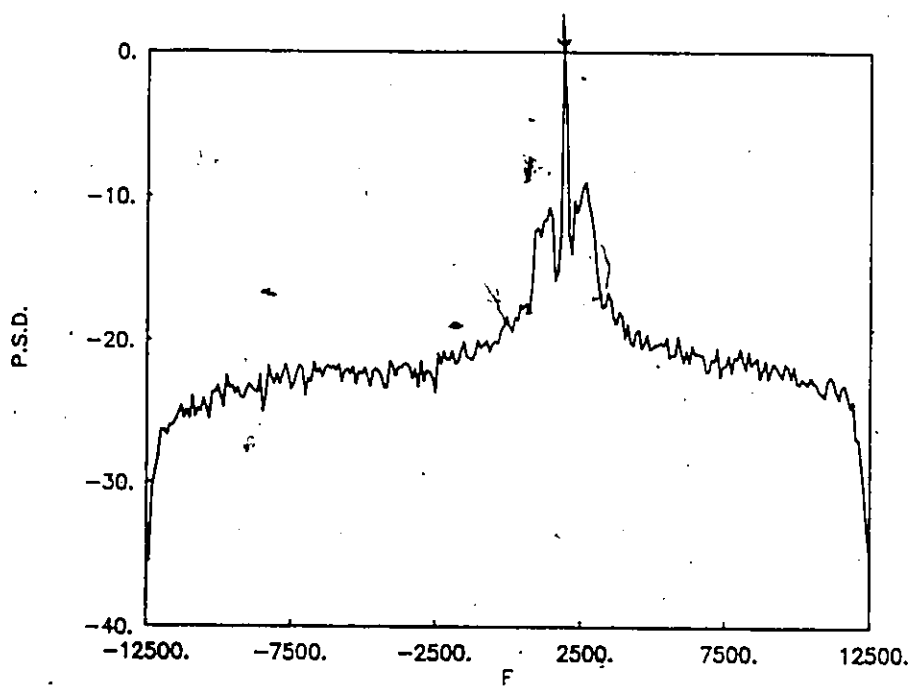
Fig. 6.10   The averaged periodogram spectrum of Garrett ELT15.

sidebands with respect to the center carrier peak are different, this should prove to be an effective identifer of an ELT signal.

6.3.2.3   Narco ELT Signals

The spectral estimation results for the Narco ELT signals are illustrated in Fig. 6.11 and 6.12. From these results we note the following: 1) the averaged spectrum indicates a large amount of the power contained in the lower sideband and this averaged spectrum for these sidebands is far broader than the carrier peak.; 2) the carrier component peak is very sharp and located at the end of this broadband spectrum. This provides an effective identifier for this weak carrier component Narco ELT signal.; and 3) the carrier component peak for Narco ELT17 is located at about 5.3 kHz. For Narco ELT19, the carrier frequency is not well defined.

6.3.3   Processing Results Using the MEM

The same individual real ELT signals are now examined using the MEM. Since the MEM filter order is not known a priori, the MEM = 100 estimator is chosen. Previous spectral estimates on computer generated signals indicate that MEM = 100 gives good results.

6.3.3.1   Pointer ELT Signals

The spectral estimation performance using the baseband MEM on Pointer ELT signals ELT01 and ELT07 are examined here. The MEM = 100 power spectral density results are given in Figures 6.13 and 6.14 for these two ELT signals, respectively. From these results and detailed analysis given in [41] we see that; 1) three peaks are detected above the threshold level of -10 dB. These peaks are described as the carrier component peak and the first upper and lower sidebands; 2) the levels of these sidebands are not symmeterical about
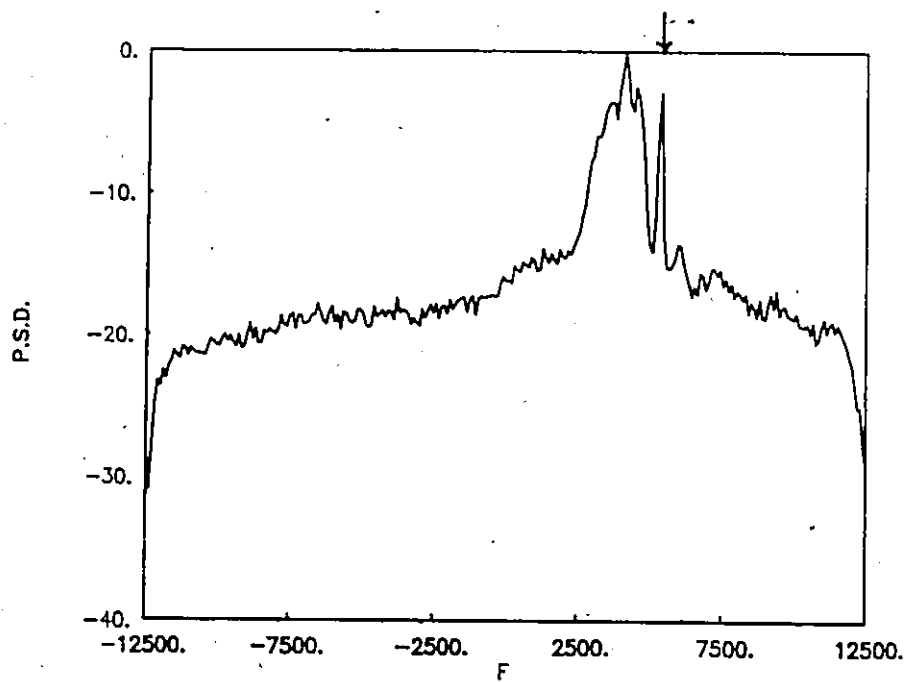
Fig. 6.11   The averaged periodogram spectrum of Narco ELT17.
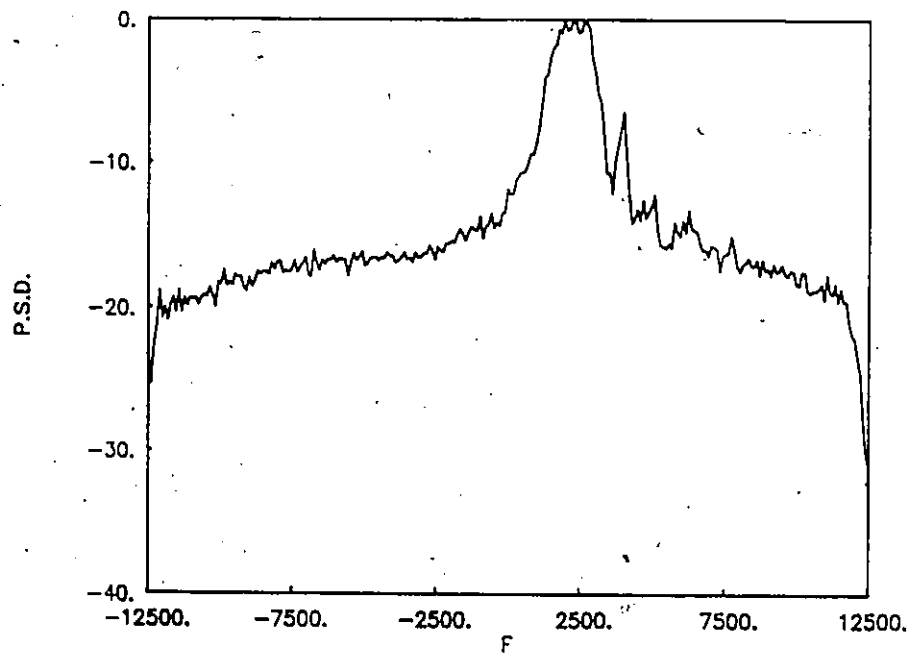
Fig. 6.12   The averaged periodogram spectrum of Narco ELT19.
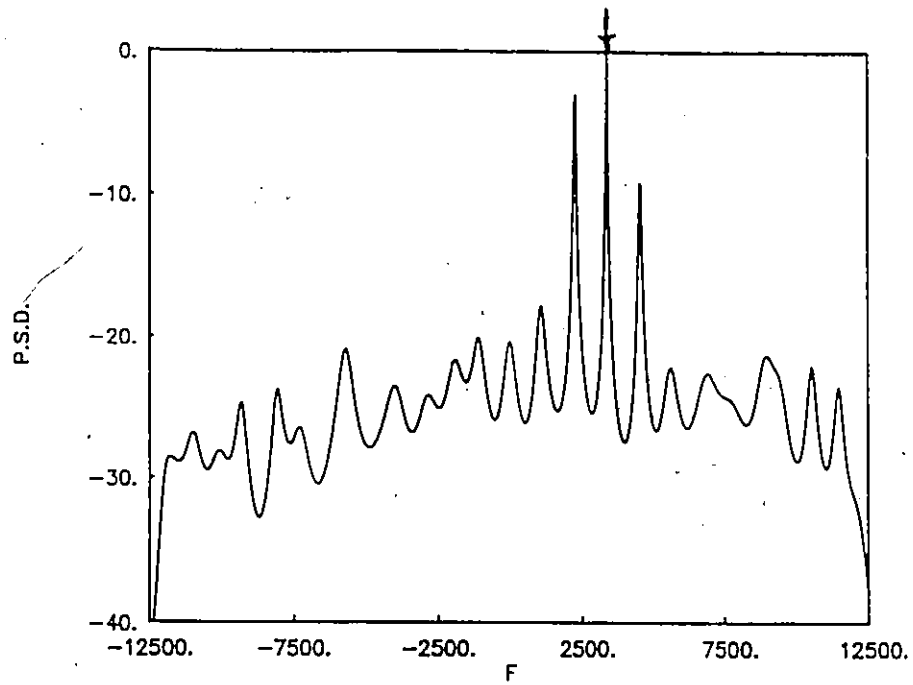
Fig. 6.13   MEM = 100 spectrum of Pointer ELT signal (ELT01).
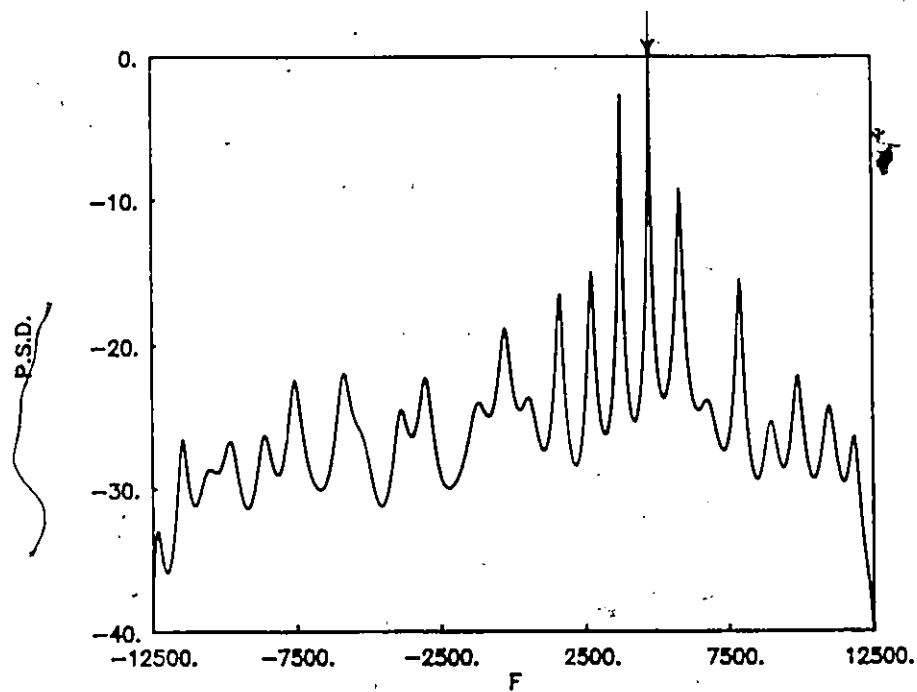
Fig. 6.14   MEM = 100 spectrum of Pointer ELT signal (ELT07).

the carrier frequency; and 3) the carrier component peak for ELT01 occurs at the constant mixed carrier frequency of about 3400 Hz while for ELT07 the carrier peak is located at about 4800 Hz.

6.3.3.2 Garrett ELT Signals

The Garrett ELT signals ELT12 and ELT15 are tested in this section using the baseband MEM processing technique. The MEM = 100 spectral estimation results for these two ELT units are illustrated in Fig. 6.15 and 6.16, respectively. These results indicate that: the carrier component peak and the first upper and lower sidebands are detected above the -10 dB threshold level; the first upper sideband is stronger than the first lower sideband; and, the carrier component peak for ELT12 occurs at mixed carrier frequency equal about 4300 Hz while for ELT15 the carrier peak is located at about 1900 Hz.

6.3.3.3 Narco ELT Signals

Figures 6.17 and 6.18 illustrate the MEM spectral estimation results for ELT17 and ELT19 signals using MEM filter order 100. For ELT17, we see that; the first and second lower sideband peaks are stronger than the carrier component peak; this ELT signal has a weak carrier component. For Narco ELT19, the MEM resolves a single carrier frequency component peak which is not resolved using the periodogram as shown in Fig. 6.6. Thus, detection of this Narco ELT signal using single-shot MEM is improved as compared to the periodogram spectral estimator result.

6.3.4 Processing Results Using the Averaged MEM

Now, we study the spectral estimation performance for the same individual ELT signals using the baseband averaged MEM. The data record is divided into K blocks with
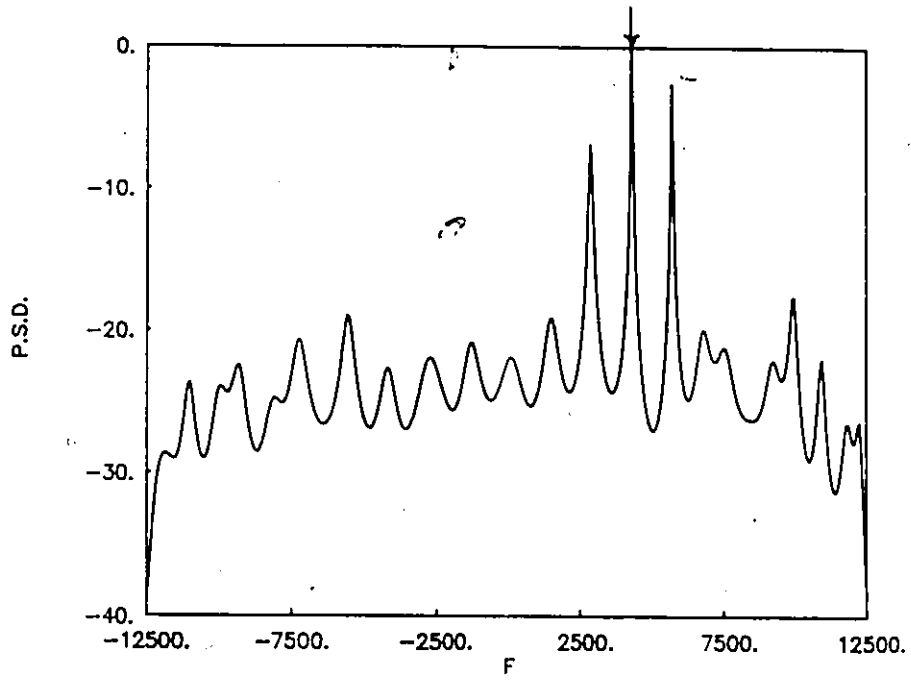
Fig. 6.15   MEM = 100 spectrum of Garrett ELT signal (ELT12).
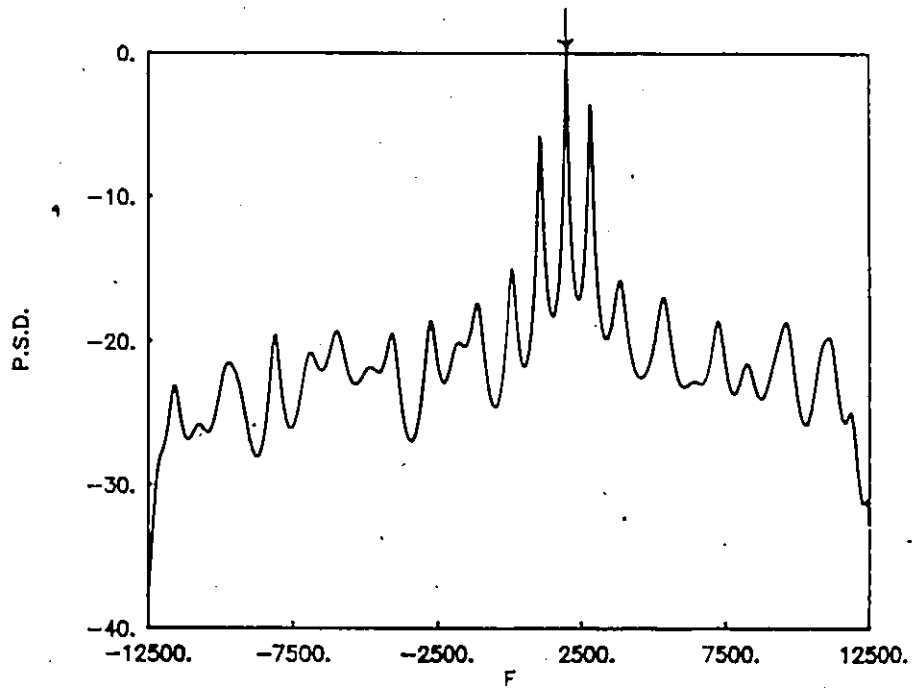
Fig. 6.16   MEM = 100 spectrum of Garrett ELT signal (ELT15).
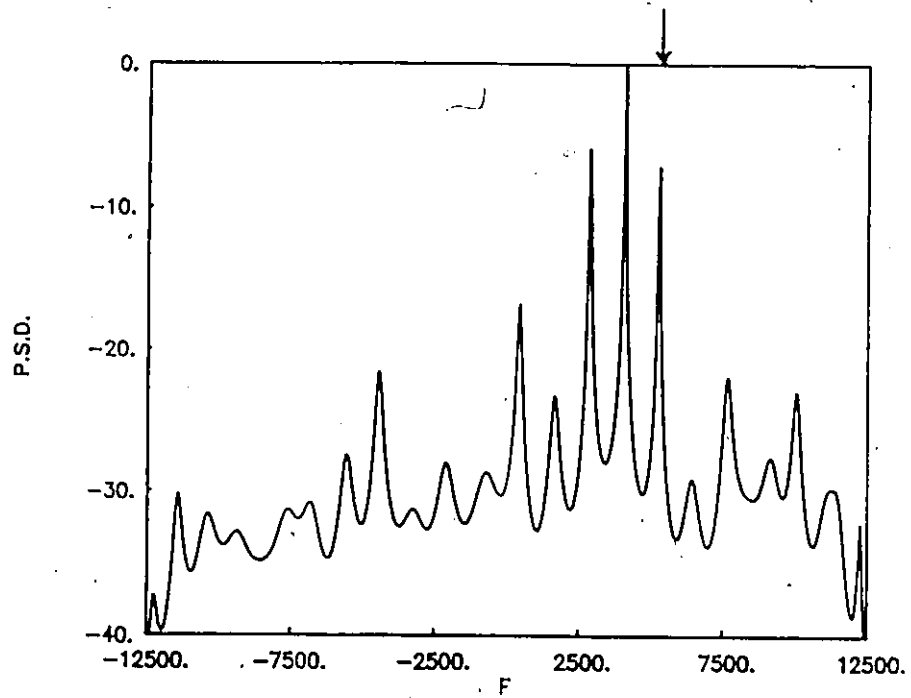
Fig. 6.17   MEM = 100 spectrum of Narco ELT signal (ELT17).
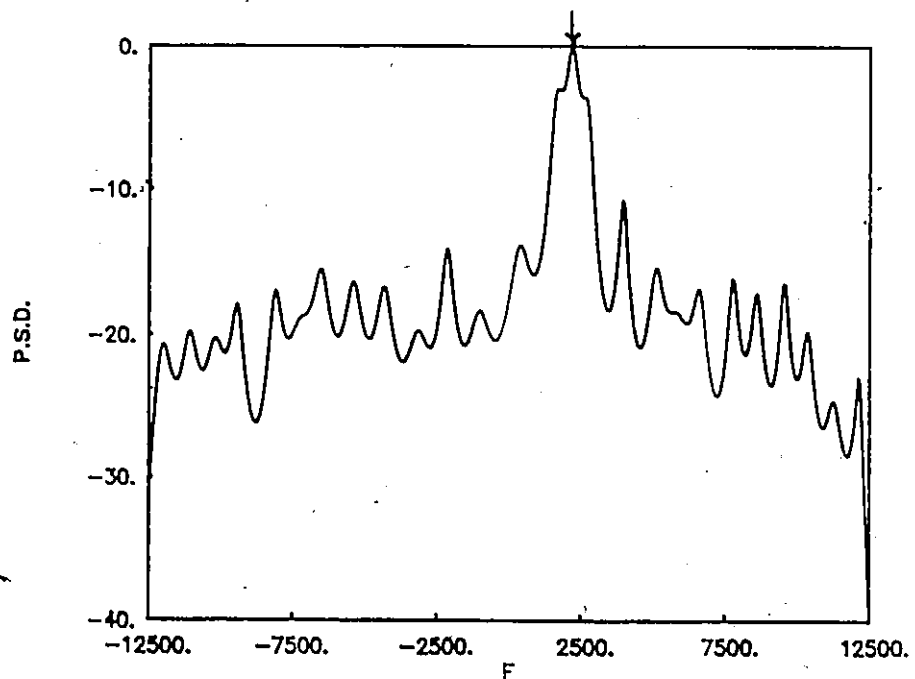
Fig. 6.18   MEM = 100 spectrum of Narco ELT signal (ELT19).

each block containing P complex points. In this section we choose K = 50, P = 512 complex

points and the MEM filter order equal 100 for this analysis.

6.3.4.1   Pointer ELT Signals

The spectral estimation results for ELT01 and ELT07 are given in Fig. 6.19 and

6.20 for these two ELT units. From these results we note the following ; 1) the averaged MEM

reduces the level of the undesirable sidebands by about 5 dB which improve the detection of

the carrier component peak of the ELT signal; 2) a sharp peak is detected and located at mixed

carrier frequency of about 3400 Hz for ELT01 and about 4800 Hz for ELT07; and 3) for both

ELT units the lower sidebands are stronger than the upper sidebands. Thus, measuring the

bandwidths W1 and W2 and the relative heights of the sidebands and compared it with the

height of the carrier peak provides an effective identifier of the ELT signal.

6.3.4.2   Garrett ELT Signals

Figures 6.21 and 6.22 depict the averaged MEM spectra for ELT12 and ELT15

signals, respectively. In this case, it is seen that, the averaged MEM reduces the level of

undesirable sidebands by about 5 dB which improves the detection of the carrier component

peak of the Garrett ELT signals. The upper sideband for both ELT units is much stronger

than the lower sideband and the relative heights of the carrier peak are different. The carrier

peak for ELT12 is located at about 4300 Hz while for ELT15 this carrier peak is located at

about 1900 Hz.

6.3.4.3   Narco ELT Signals

Figures 6.23 and 6.24 illustrate the averaged MEM spectral estimation results for

ELT17 and ELT19. From these figures we note that; 1) for ELT17, the carrier component
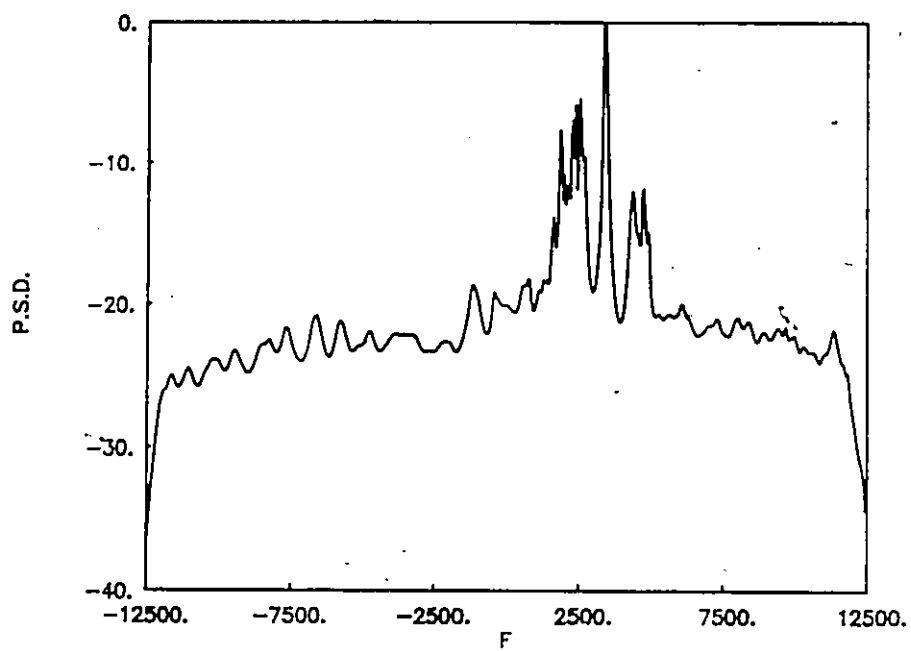
Fig. 6.19   The averaged MEM = 100 spectrum of Pointer ELT01 signal.
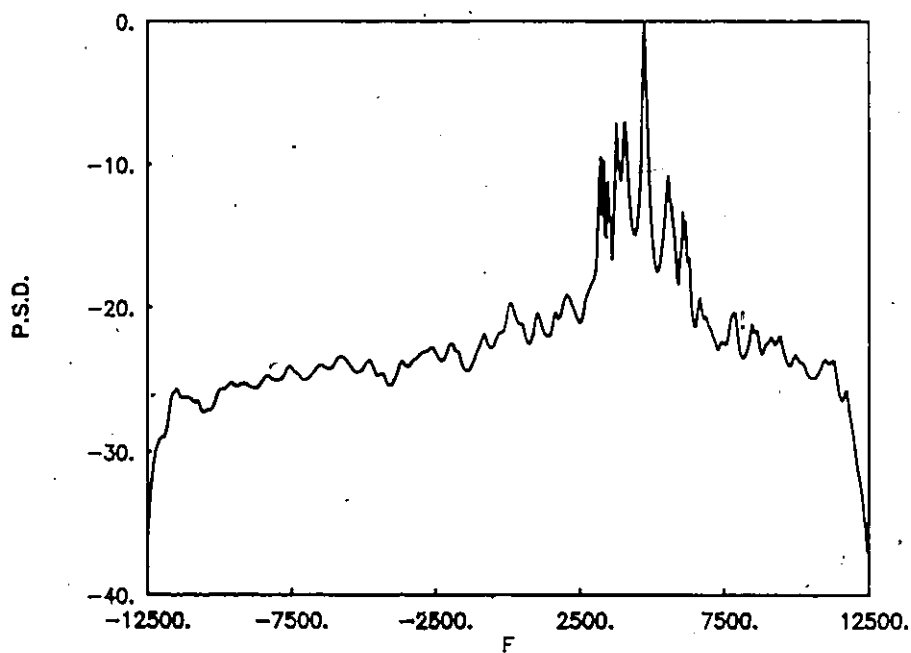
Fig. 6.20   The averaged MEM = 100 spectrum of Pointer ELT07 signal.
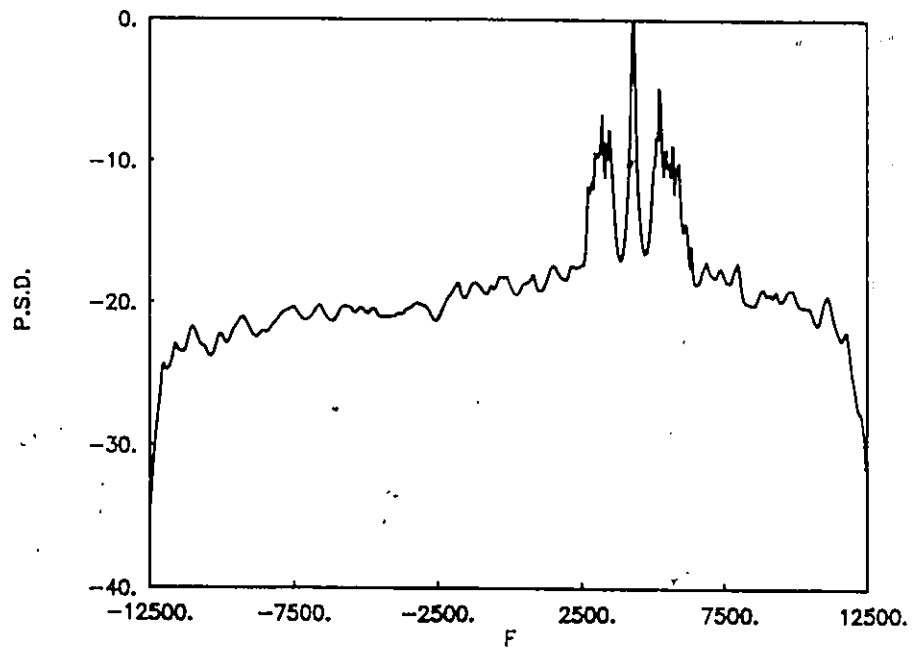
Fig. 6.21   The averaged MEM = 100 spectrum of Garrett ELT12 signal.
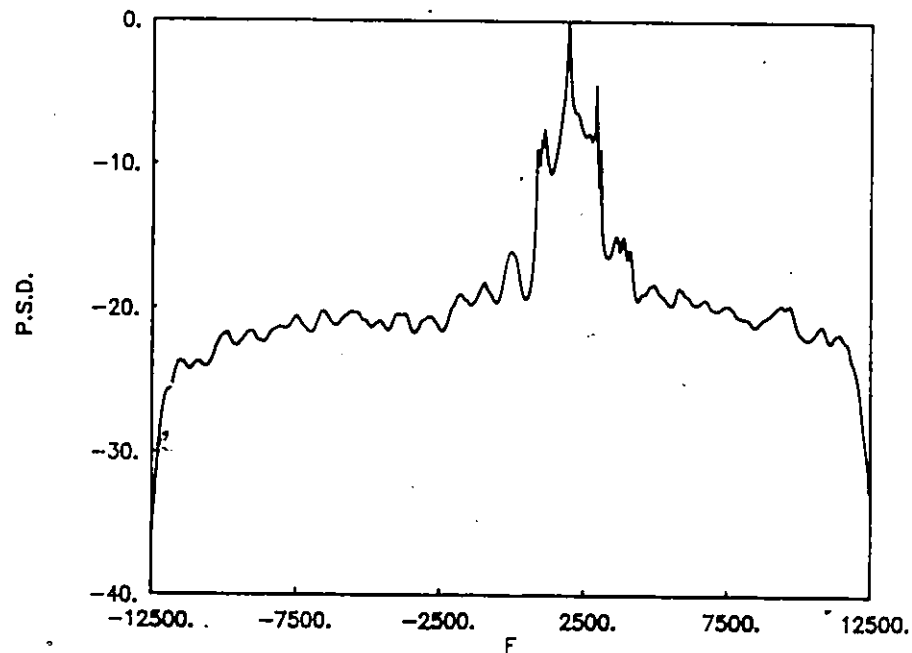
Fig. 6.22   The averaged MEM = 100 spectrum of Garrett ELT15 signal.
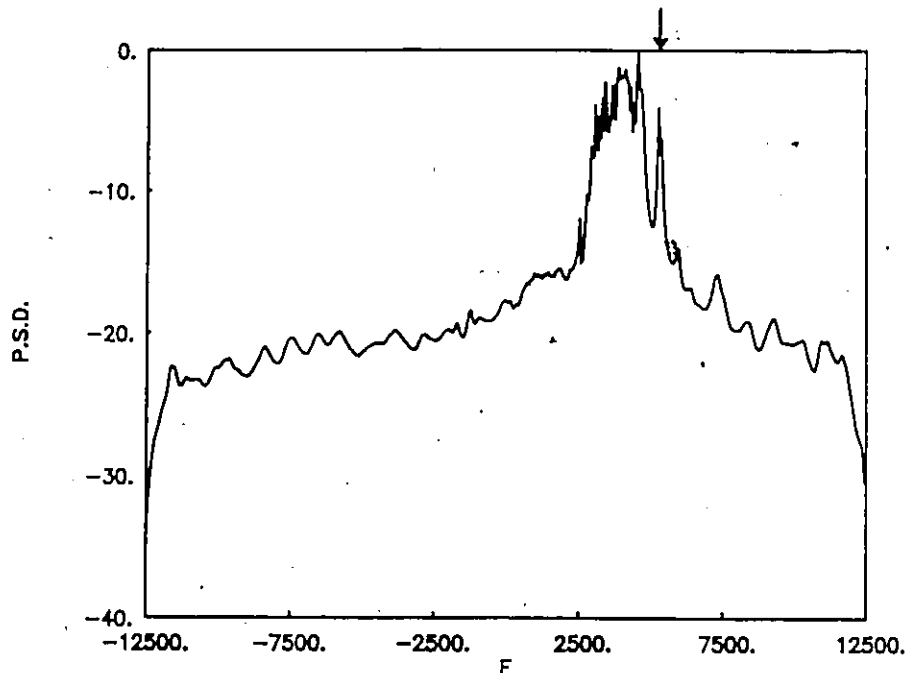
Fig. 6.23   The averaged MEM = 100 spectrum of Narco ELT17 signal.
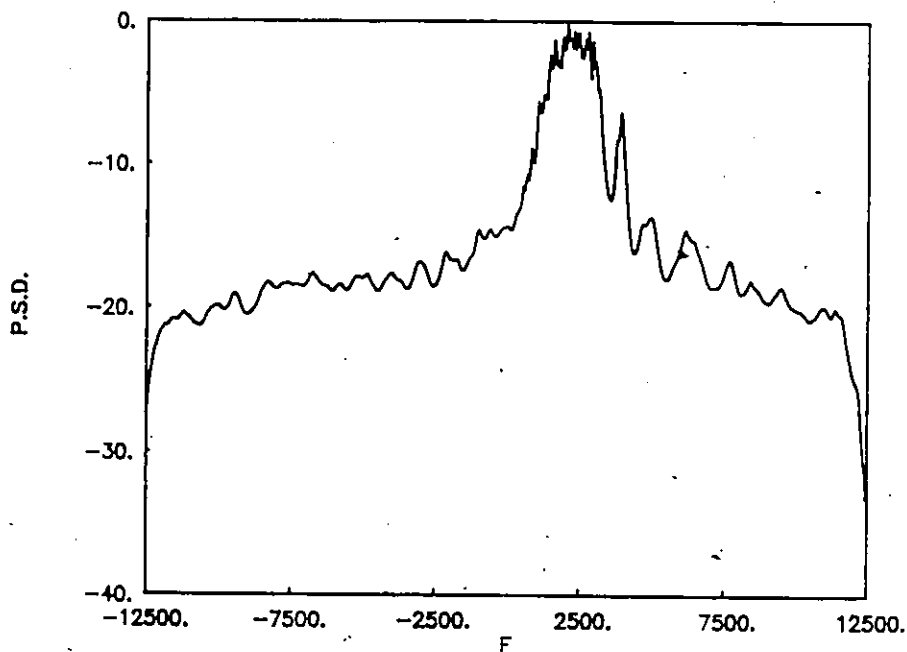
Fig. 6.24   The averaged MEM = 100 spectrum of Narco ELT19 signal.

peak is very sharp and occurs at mixed carrier frequency equal about 5300 Hz. For ELT19, the carrier frequency is not well defined; 2) the lower sideband for ELT17 becomes broad as compared to the carrier component peak; and 3) Narco ELT17 signal has most of its power in its lower sidebands.

6.3.5   Comparison between Linear and Non-Linear Spectral Estimation Results

The processing results using linear and non-linear spectral estimation methods for individual real ELT signals indicate that:

(A)   *Pointer ELT Signals*

Single-shot periodogram, averaged periodogram, single-shot MEM and averaged MEM spectral estimation methods perform well for processing the Pointer ELT signals ELT01 and ELT07. Thus, we conclude the following:

1.   This type of ELT signal can be classified as non-ideal coherent.

2.   The signal has constant carrier frequency. The Pointer ELT01 has mixed carrier frequency of about 3400 Hz and ELT07 has mixed carrier frequency of about 4800 Hz.

3.   The first lower sideband is stronger than the first upper sideband.

(B)   *Garrett ELT Signals*

Single-shot periodogram, averaged periodogram, single-shot MEM and averaged MEM perform satsfactorily for processing the Garrett ELT signals. Also:

1.   These ELT signals can be classified as non-ideal coherent signals.

2.   The carrier frequency of Garrett ELT signals remains stationary. Garrett ELT12 has mixed carrier frequency equal about 4300 Hz while for Garrett ELT15 the mixed carrier frequency equal about 1900 Hz.

3.   The levels of the first upper and lower sidebands are not symmetrical about the carrier frequency.

(C)   Narco ELT Signals

The processing results of the Narco ELT signals indicate that;

1.   The detection of Narco ELT signal ELT19 using single-shot periodogram is difficult, but single-shot MEM tends to resolve the carrier component peak.

2.   Narco ELT17 can be classified as a non-ideal coherent ELT signal while Narco ELT19 can be classified as a non-coherent.

3.   Narco ELT17 has weak carrier frequency component with mixed carrier frequency equal to about 5300 Hz. For Narco ELT19 the carrier frequency is not well defined.

4.   Averaged periodogram or averaged MEM enhances the detection and identification of Narco ELT17. For Narco ELT19 no more information about the carrier frequency is obtained because the averaged spectra produces a broad peak for this Narco ELT signal.

6.4   Processing of Combinations Real ELT Signals

In this section, we discuss the processing of multiple real ELT signals using the baseband processing technique. The analysis which is given here includes two, three, and five real ELT signals. The spectral estimation performance degrades somewhat as a result of increasing the number of signals. These combinations of real ELT signals are examined using the baseband processor system with the same format as described earlier.

In [41] we examined these combinations of real ELT signals through different positions on the tape recording. In this section, we present typical results and summarize the main conclusions given in [41].

6.4.1   Processing Results Using the Periodogram

This section discusses the spectral estimation performance for combinations of two, three, and five real ELT signals using the baseband periodogram. As described earlier in Chapter 5 and in [37,41] we found that the detection of the multiple ELT signals using single-shot periodogram is difficult and restricted in some cases because the FFT spectrum suffers from numerous peaks.

6.4.1.1   Combination of Two Real ELT Signals

The power spectral density result is given in Fig. 6.25 for Pointer ELT01 and Narco ELT19. We note the following; 1) numerous peaks are detected above the threshold of -10 dB; 2) a carrier peak on the right of the spectrum, located at mixed carrier frequency of about 9800 Hz, with first lower sideband being stronger than the first upper sideband. This is characteristics of a coherent ELT signal and belongs to the Pointer ELT01; and 3) the second ELT signal contained in the spectrum (which is Narco ELT19) produces a broad FFT spectrum. The carrier frequency for Narco ELT19 is not well defined, however. Thus, measurement of the carrier frequency of this Narco ELT signal using single-shot periodogram is difficult.

6.4.1.2   Combinations of Three Real ELT Signals

First, the spectral estimation result for the combination of Pointer ELT01 and Garrett ELT12 overlapped by Narco ELT19 is given in Fig. 6.26. In this case we note that; ten

Fig. 6.25   Periodogram spectrum of two ELT signals (ELT01 and ELT19).
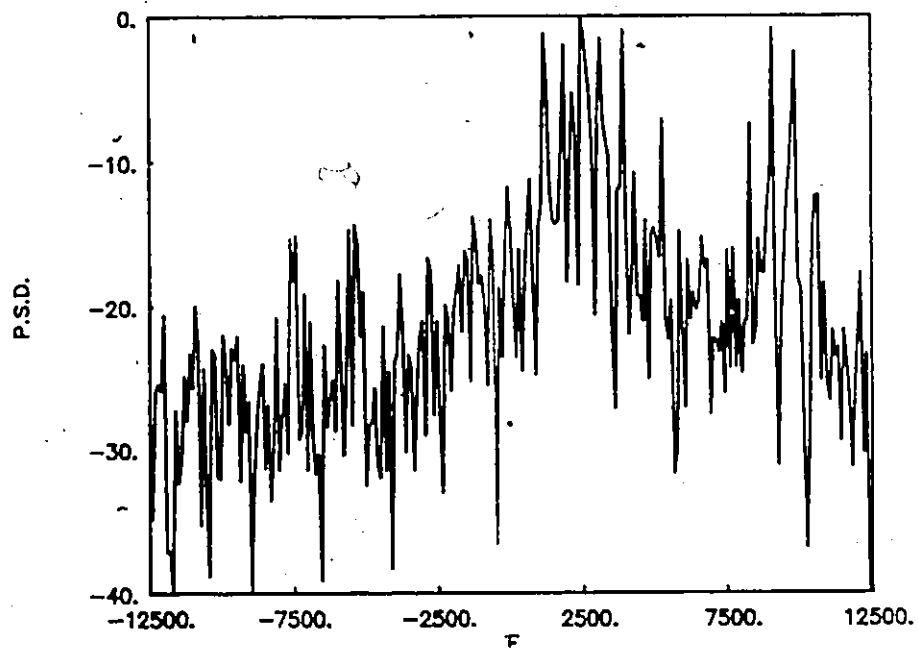
Fig. 6.26   Periodogram spectrum of three ELT signals (ELT01 - ELT12 and ELT19).

peaks are detected above the -10 dB threshold level for these three ELT signals. The carrier component peak on the right of the spectrum, located at mixed carrier frequency of about 9800 Hz, is related to a coherent ELT signal. In addition, we see that no measure of carrier frequency is possible for the case of the overlapped signals.

Second is another combination of three real ELT signals which comprises Pointer ELT01, and Garrett ELT14 overlapped by Narco ELT19. The spectral estimation result for this case using the periodogram is given in Fig. 6.27. From this result it is clear that coherent ELT signal produces a peak on the right of the spectrum. Again, measurment of the carrier frequency components for the Narco ELT19 and Garrett ELT14 (overlapped case) is difficult.

6.4.1.3   Combination of Five Real ELT Signals

Here, we study the spectral estimation performance of combination of five real ELT signals including Pointer (ELT01 and ELT07), Garrett (ELT12) and Narco (ELT17 and ELT19) processed using the baseband periodogram. The FFT spectrum result is plotted in Fig. 6.28. From this result, it is seen that 14 peaks are detected above the -10 dB threshold level. The Pointer and Garrett ELT signals have stationary carrier frequencies while the Narco ELT17 signal has a weak carrier component. For Narco ELT19, the carrier frequency is not well defined. Thus, we note that detection of the ELT signals using single-shot periodogram is difficult due to numerous peaks which create many false alarms.

6.4.2   Processing Results Using The Averaged Periodogram

This section is concerned with studying the spectral estimation performance for combinations of real ELT signals using the averaged periodogram. As described before, we

Fig. 6.27   Periodogram spectrum of three ELT signals (ELT01 - ELT14 and ELT19).
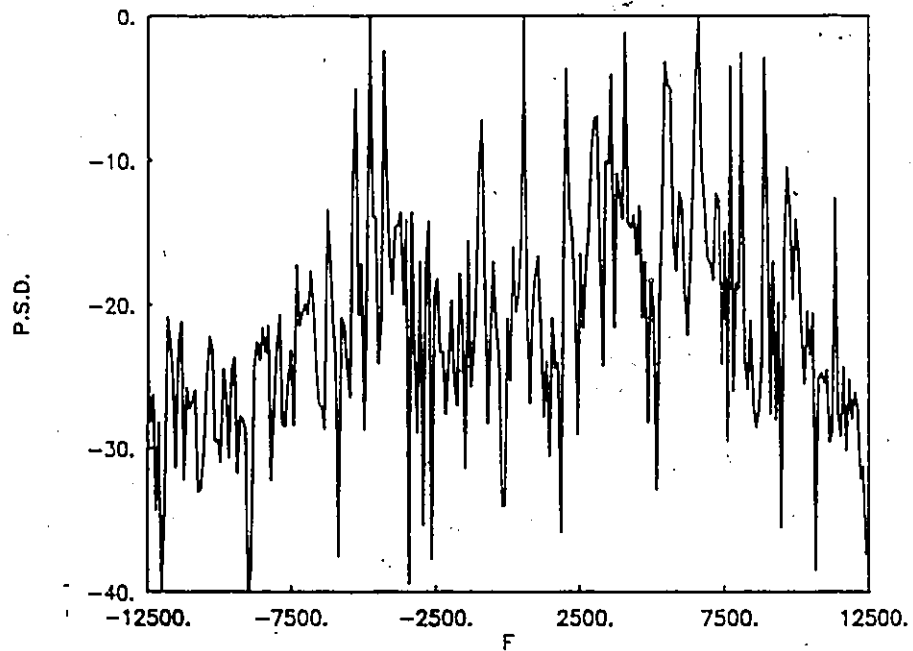
Fig. 6.28   Periodogram spectrum of five ELT signals (ELT01 - ELT07 - ELT12 - ELT17 and ELT19).

choose $K = 50$ with each block containing 512 complex points and average the periodograms over all blocks.

6.4.2.1 Combination of Two Real ELT Signals

The combination of Pointer ELT01 and Narco ELT19 ELT units are depicted in Fig. 6.29, which illustrates the spectral estimation results for this case. It is seen from these results that the averaged periodogram reduces the variance and the level of the undesirable sidebands which enables us to identify and detect both of the ELT signals. The Pointer ELT signal ELT01 has a sharp carrier peak which is located at mixed carrier frequency of about 9800 Hz. The Narco ELT19 produces a broad peak spectrum and the carrier frequency of this Narco ELT signal is not well defined. Again, it is indicated that the Narco signal is random phase ELT signal.

6.4.2.2 Combinations of Three ELT Signals

Now, we discuss the power spectral density for the combinations of three ELT units using the averaged periodogram. First, the spectral estimation result for the combination of Pointer ELT01, Garrett ELT12 and Narco ELT19 is given in Fig. 6.30. The Garrett ELT12 is overlapped by the Narco ELT19 signal. The spectrum result contains two sharp peaks and one broad peak above the -10 dB threshold level. The sharp peak at frequency 9800 Hz is related to the coherent ELT signal (ELT01) and the second sharp peak at 2700 Hz belongs to the second coherent ELT signal (ELT12). The broad peak is related to the noncoherent Narco ELT signal (ELT19) and no information about the carrier frequency for this Narco ELT19 is obtained.

The second example examined here is for another combination of three ELT units, namely Pointer ELT signal (ELT01) and Garrett (ELT14) overlapped by the Narco (ELT19).
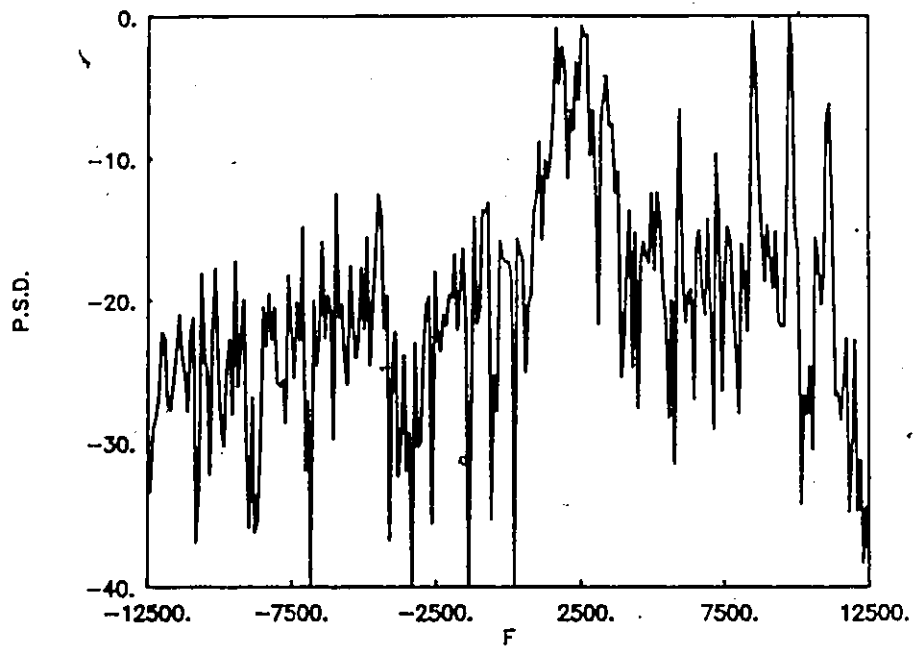
Fig. 6.29   The averaged periodogram spectrum of two ELT signals (ELT01 and ELT19).

Fig. 6.30   The averaged periodogram spectrum of three ELT signals (ELT01 - ELT12 and ELT19).

The averaged periodogram spectral estimation result for this case is depicted in Fig. 6.31. From this result, we find that the coherent signals (Pointer ELT01 and Garrett ELT14) produce sharp peaks at frequencies 3500 Hz and 80 Hz respectively. The Narco ELT19 produces a broad peak which is located on the left of the spectrum. However, no measure of carrier frequency is possible for this signal.

6.4.2.3   Combination of Five Real ELT Signals

The combination of five real ELT signals containing Pointer (ELT01 and ELT07), Garrett (ELT12) and Narco (ELT17 and ELT19) is examined in Fig. 6.32. This result indicates that three sharp strong peaks and two broad peaks are present in the spectrum. These three topmost sharp peaks are described as being related to the Pointer ELT signals (ELT01 and ELT07) with the third sharp peak belonging to the Garrett ELT signal (ELT12). The two broad peaks are related to the Narco ELT signals (ELT17 and ELT19), with the Narco ELT17 having a weak carrier component which produces a sharp peak at the end of its spectrum as depicted in this figure. The carrier frequency for Narco ELT19 is not well defined.

Comparing these results obtained using the averaged periodogram with those using the single-shot periodogram, we note that the averaged periodogram reduces the level of the undesirable sidebands and improves the detection of the ELT signals which have strong carrier frequency component. However, detection of the Narco ELT signals, which have weak carrier frequency components, is not greatly improved as a result of using the averaged periodogram.
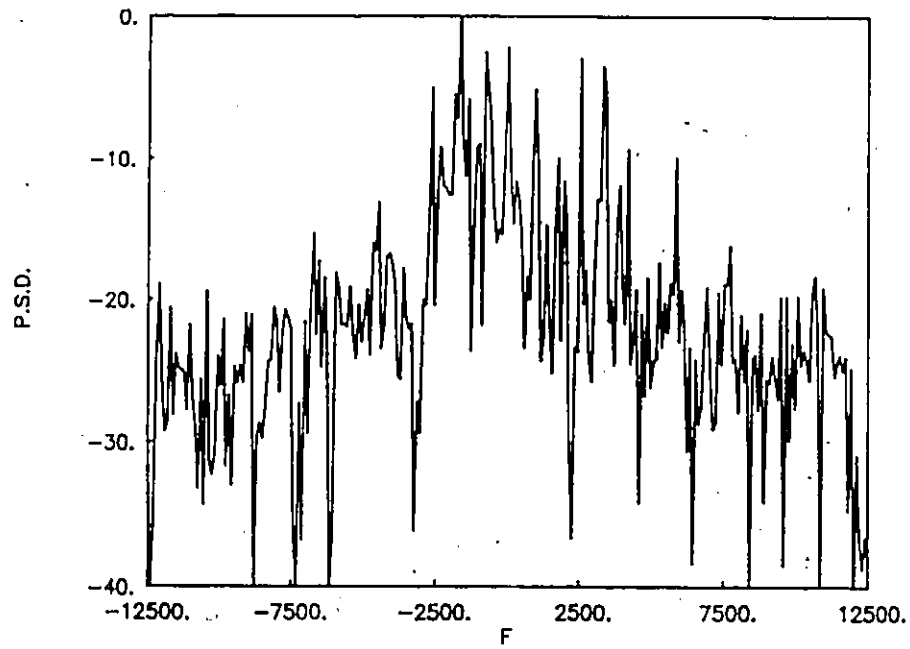
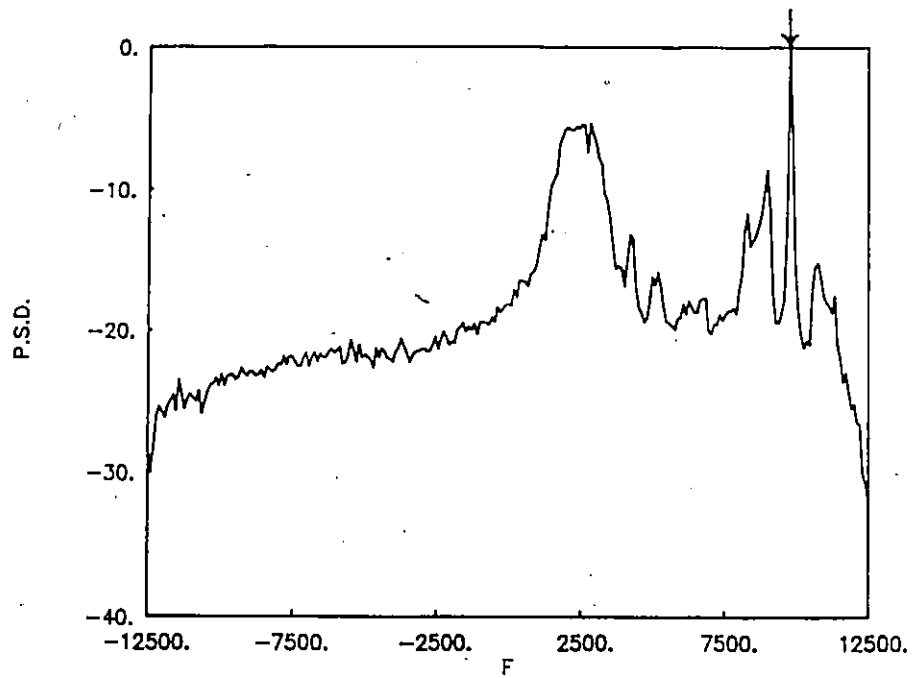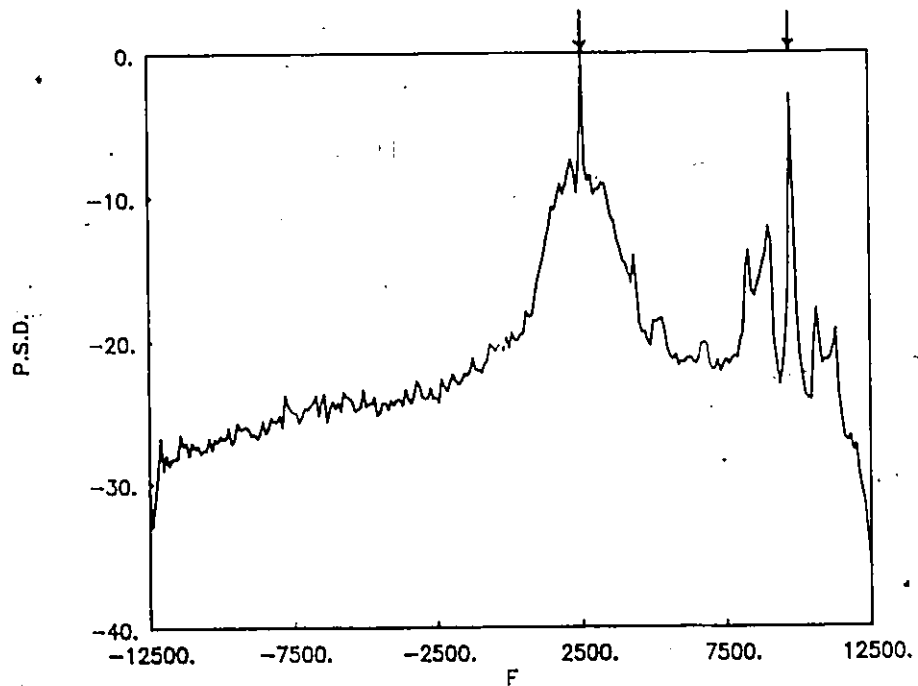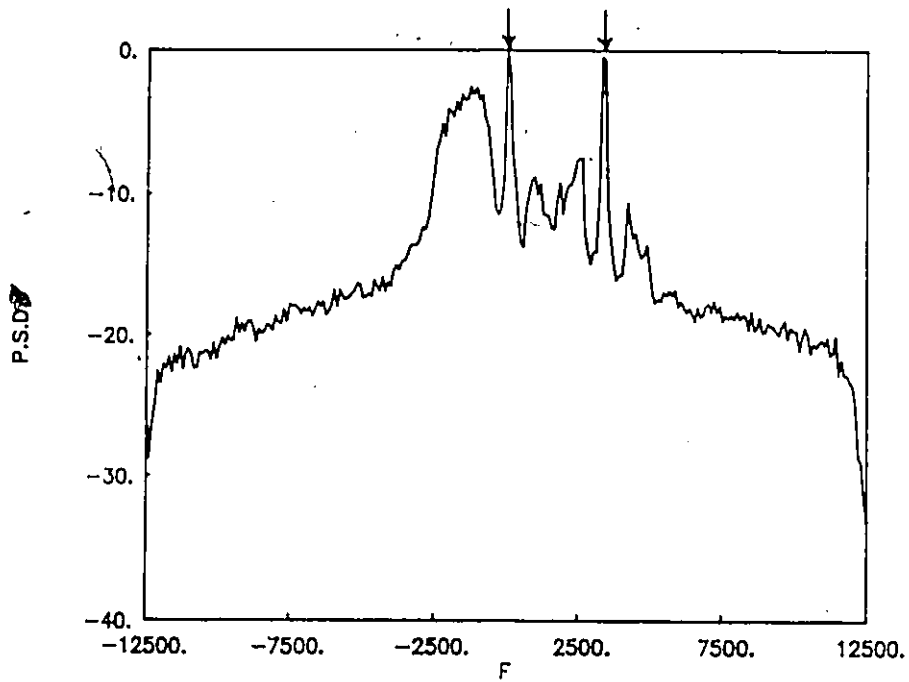Fig. 6.31   The averaged periodogram spectrum of three ELT signals (ELT01 - ELT14 and ELT19).
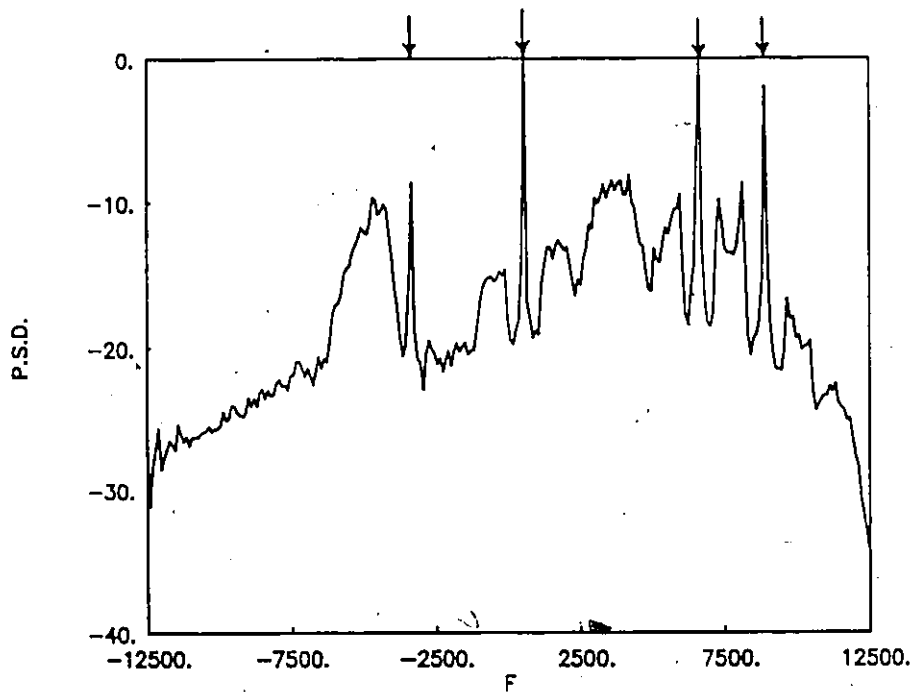
Fig. 6.32   The averaged periodogram spectrum of five ELT signals (ELT01 - ELT07 - ELT12 - ELT17 and ELT19).

6.4.3   Processing Results Using the MEM

The detection of the combinations of real ELT signals using the baseband MEM is investigated in this section. The prediction error filter (MEM filter order) used for this analysis is 100.

6.4.3.1   Combination of Two Real ELT Signals

The combination of two real ELT signals containing the Pointer ELT01 and the Narco ELT19 is analyzed here using the baseband MEM and the results is given in Fig. 6.33. We note that, a sharp peak on the right of the spectrum is detected which belongs to coherent ELT signal (Pointer ELT01) and located at a mixed carrier frequency of 9800 Hz. Further, we note that the lower sideband of this ELT signal is stronger than the upper sideband. The second ELT signal which is Narco ELT19 produces a broader peak but the carrier peak of this Narco ELT signal can be detected using the baseband MEM as shown in Fig. 6.33. This carrier peak can not be detected using the periodogram as illustrated in Fig. 6.25.

6.4.3.2   Combinations of Three ELT Signals

Now, we study the spectral estimation performance for the same combination of three ELT units described earlier using the baseband MEM. The MEM = 100 spectral result is given in Fig. 6.34 for the combination of Pointer ELT01, and Garrett ELT12 overlapped by Narco ELT19. We observe a sharp peak on the right of the spectrum, located at mixed carrier frequency of about 9800 Hz, which belongs to the coherent ELT signal. The broad peak belongs to the overlapped Garrett and Narco ELT signals. Thus, the measurment of the carrier frequencies for the overlapped case of Garrett (ELT12) and Narco (ELT19) is difficult which degrades the detection of these two ELT signals.

Fig. 6.33   MEM = 100 spectrum of two ELT signals (ELT01 and ELT19).
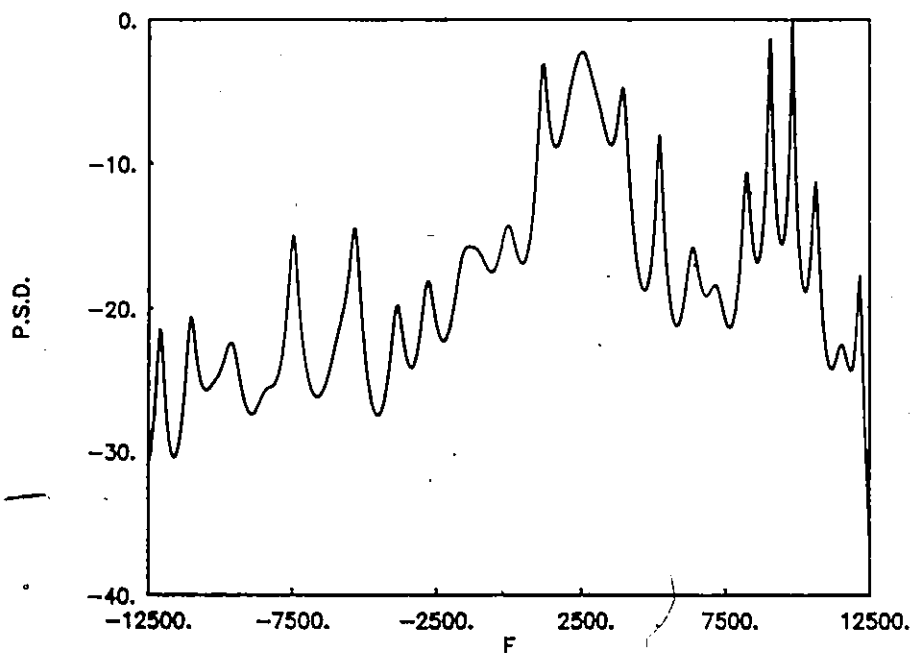
Fig. 6.34   MEM = 100 spectrum of three ELT signals (ELT01 - ELT12 and ELT19).

The second example is for another combination of three real ELT signals. The MEM = 100 spectral estimation result for this case is plotted in Fig. 6.35. From this figure it is clear that the peak which is located on the right of the spectrum with the first lower sideband stronger than the first upper sideband belongs to coherent ELT signal. The Garrett (ELT14) overlaps the the Narco ELT signal (ELT19). Both the Pointer and the Garrett ELT signals produce sharp peaks while the Narco ELT signal produces a broad peak as shown in this figure.

6.4.3.3 Combination of Five ELT Signals

The same combination of five real ELT signals described before is examined in this section using the baseband MEM and given in Fig. 6.36. From this result, it is clear that numerous peaks are detected above the -10 dB threshold level. Some of these peaks marked by the arrows are the carrier component peaks of the present ELT signals while the other peaks are undesirable sidebands which create false alarms. As shown in this figure the baseband MEM technique resolves the carrier peak for the Narco ELT19.

6.4.4 Processing Results Using the Averaged MEM

In this section, the spectral estimation performance for the combination of real ELT signals using the averaged MEM is studied. As discussed before, we find that the spectral estimation performance degrades as a result of increasing the number of ELT signals due to the overlapping sidebands problem. The averaged MEM reduces the level of the undesirable sidebands and consequently improves the detection of the ELT signals. The results presented here are for the same combinations of two, three and five real ELT units as before. Again, we choose the number of blocks K = 50 with each block containing 512 complex points. The MEM filter order selected is 100 for this analysis.

Fig. 6.35   MEM = 100 spectrum of three ELT signals (ELT01 - ELT14 and ELT19).
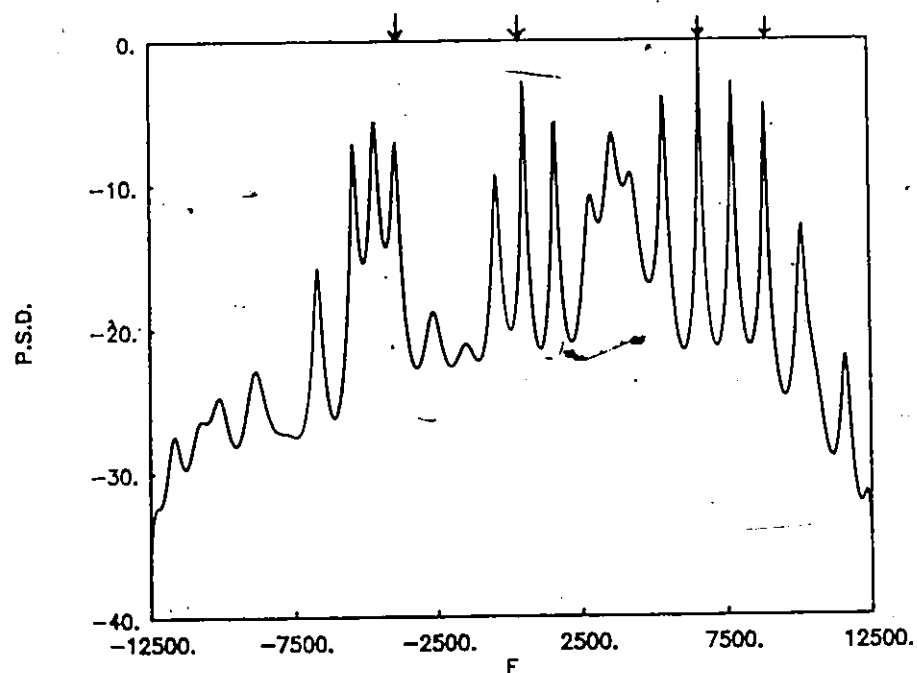
Fig. 6.36   MEM = 100 spectrum of five ELT signals (ELT01 - ELT07 - ELT12 - ELT17 and ELT19).

6.4.4.1   Combination of Two Real ELT Signals

The spectral estimation result for the combination of two real ELT signals Pointer ELT01 and Narco ELT19 using the averaged MEM is given in Fig. 6.37. In this case we see, a sharp peak on the right of the spectrum located at a mixed carrier frequency of about 9800 Hz which belongs to Pointer ELT signal (ELT01). In addition, the lower sideband of this Pointer ELT signal is stronger than the upper sideband. Another broadband peak is obtained in the centre of the spectrum. This broad peak is related to the Narco ELT signal ELT19 and it is seen that the carrier frequency of this ELT signal is not well defined.

6.4.4.2   Combinations of Three Real ELT Signals

The combination of three real ELT signals which are Pointer ELT01 and Garrett ELT12 overlapped by Narco ELT19 is now examined in Fig. 6.38. From this figure it is clear that one sharp peak is detected on the right of the spectrum. This peak is located at a mixed carrier frequency of about 9800 Hz, and belongs to a coherent ELT signal (Pointer ELT01). Furthermore, it is seen that the carrier peak of the Garrett ELT12 can be detected. The Narco ELT signal ELT19 produces a broad peak spectrum and the measurment of the carrier frequency for the Narco ELT signal is not possible, however.

The second plot, illustrated in Fig. 6.39, depicts another combination of three real ELT signals. From these results, we note that the Pointer ELT01 and the Garrett ELT14 are located at two different mixed carrier frequencies. The Garrett overlaps the Narco ELT signal ELT19. The spectrum contains two topmost sharp peaks and one broad band of signal. The two sharp peaks belong to the coherent ELT signals (Pointer ELT01 and the Garrett ELT signal ELT14) while the broad peak belongs to the Narco ELT19. Again, we note that the
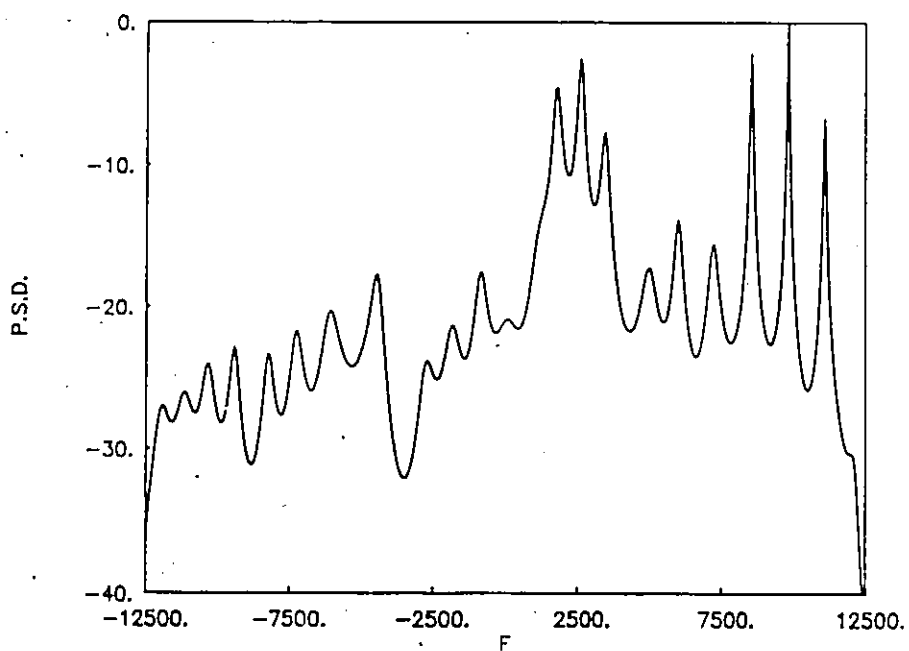
Fig. 6.37   The averaged MEM = 100 spectrum of two ELT signals (ELT01 and ELT19).
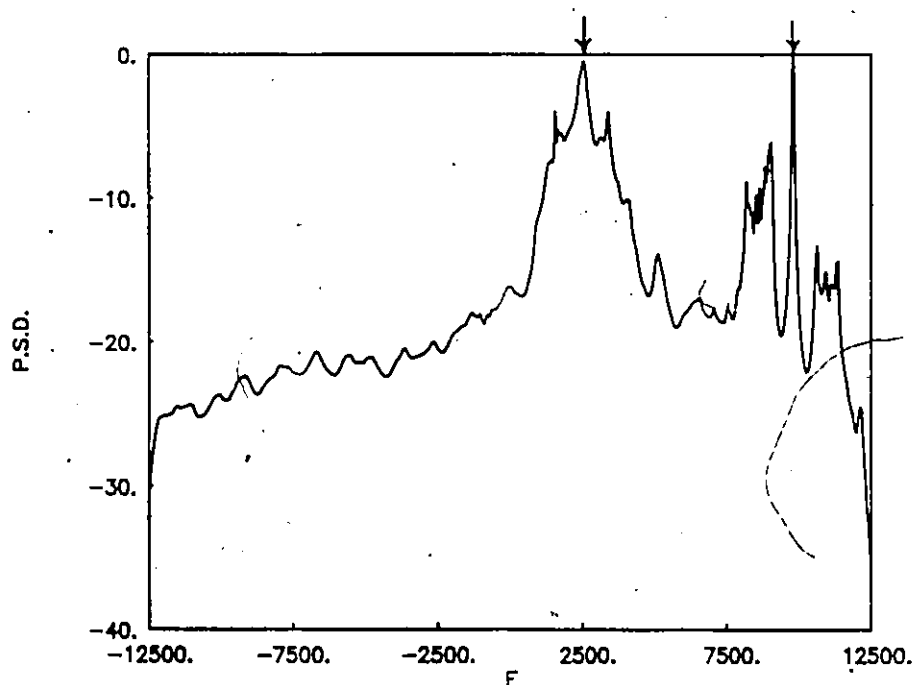
Fig. 6.38   The averaged MEM = 100 spectrum of three ELT signals (ELT01 - ELT12 and ELT19).

carrier frequency for the Narco ELT signal ELT19 is not well defined which reduces the possibility of detecting this Narco ELT signal.

6.4.4.3   Combination of Five Real ELT Signals

Finally, we examine the combination of five real ELT signals using the averaged MEM with MEM filter order equal 100. The spectral estimation result depicted in Fig. 6.40, contains five ELT signals, three with strong constant carrier frequencies and two Narco ELT signals which have weak carrier frequencies. From these results, it is seen that the three topmost sharp peaks belong to the coherent ELT signals represented by Pointer ELT signals ELT01 and ELT07, and Garrett ELT12. The Narco ELT signals produce broad peak with a sharp carrier component peak detected for Narco ELT17; however, for Narco ELT19 the carrier frequency is not well defined.

6.4.5   Comparison of the Processing Results Using Linear and Non-Linear Spectral Estimation Methods

(A)   *Combination of Two Real ELT Signals (ELT01 and ELT19)*

1.   Single-shot periodogram performs well for detecting the Pointer ELT01 but does not resolve the carrier peak for the Narco ELT19.

2.   The averaged periodogram enhance the detection of the Pointer ELT signal ELT01 by reducing the level of undesirable sidebands relative to the carrier peak level, but no more information about the carrier frequency for the Narco ELT signal is obtained using the averaged periodogram. The Pointer ELT signal ELT01 gives sharp peak and located at mixed carrier frequency of about 9800 Hz, while the carrier frequency for the Narco ELT signal ELT19 is not defined.
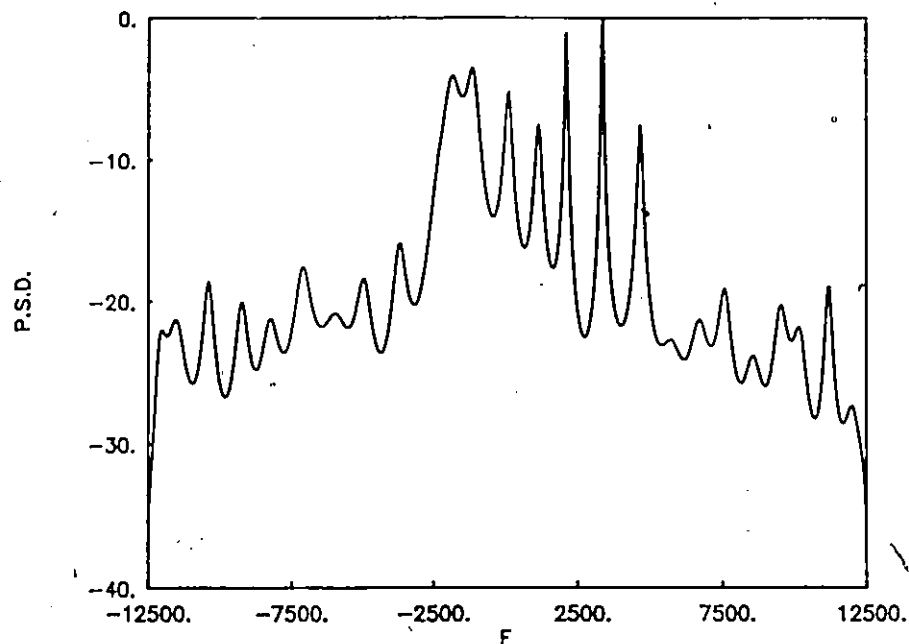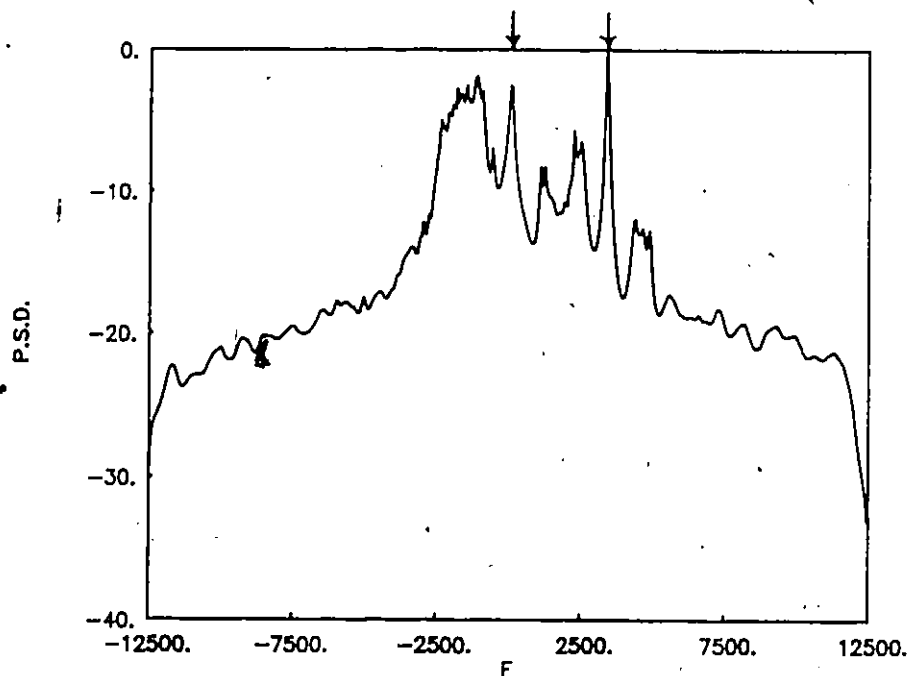
Fig. 6.39   The averaged MEM=100 spectrum of three ELT signals (ELT01 - ELT14 and ELT19).

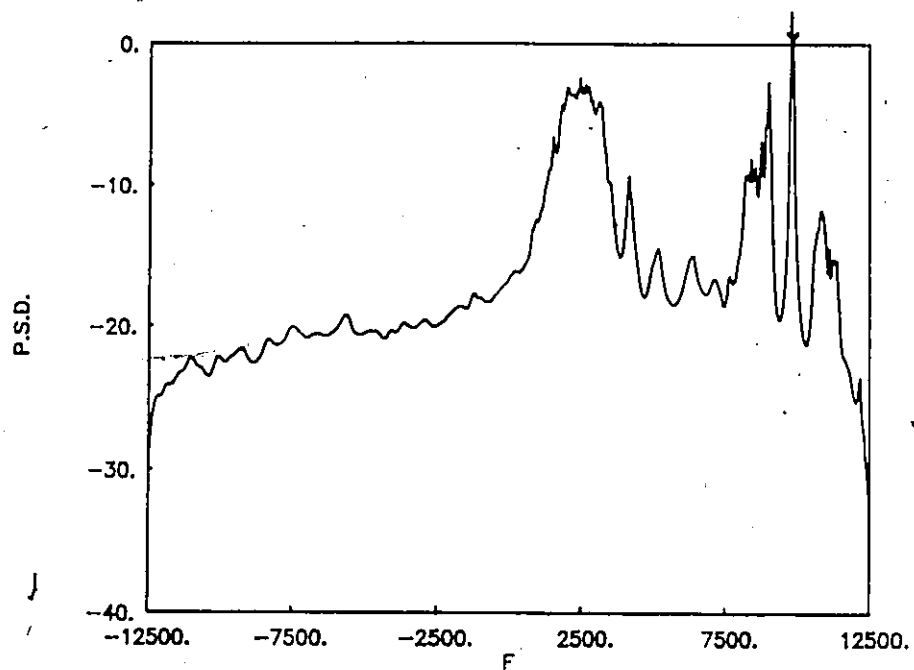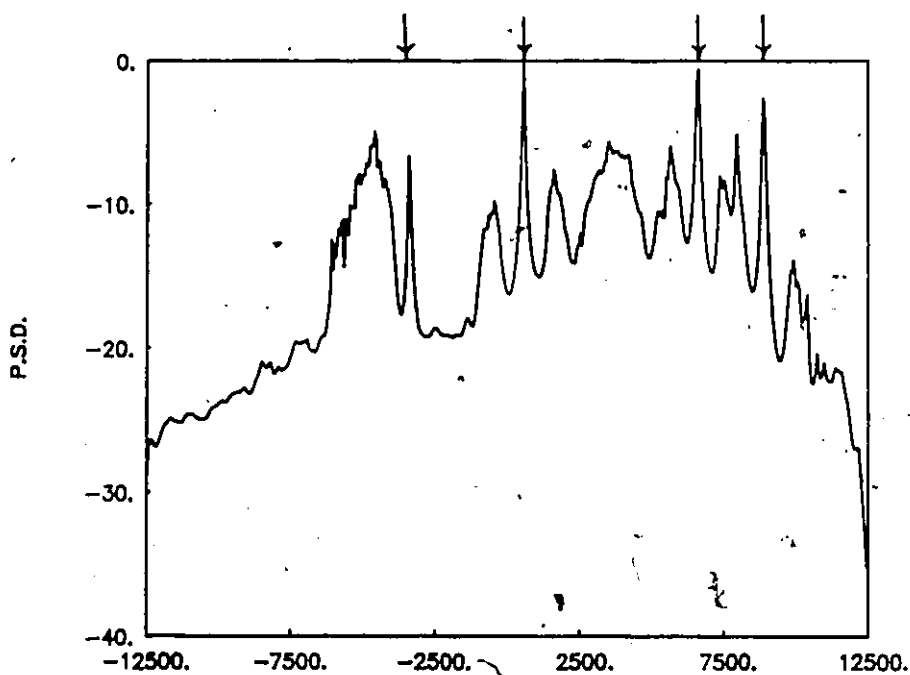Fig. 6.40   The averaged MEM=100 spectrum of five signals (ELT01 - ELT07 - ELT12 - ELT17 and ELT19).

3. Single-shot MEM performs well for detecting the carrier component peaks for these two real ELT signals.

4. The averaged MEM reduces the level of undesirable sidebands and enhances the detection of Pointer ELT01. For Narco ELT19 a broad peak is obtained using the averaged MEM and no more information about the carrier frequency is obtained.

(B)   *Combinations of Three Real ELT Signals*

For the combination of (Pointer ELT01 and Garrett ELT12 overlapped by Narco ELT19) the spectral estimation results indicate that the Pointer ELT01 and the Garrett ELT12 have constant carrier frequency while for Narco ELT19 no measure of carrier frequency is possible.

2. For the combination of (Pointer ELT01 and Garrett ELT14 overlapped by Narco ELT19) we found that, the carrier component peak for Pointer ELT01 and Garrett ELT14 can be detected, however the carrier frequency for the Narco ELT19 is not well defined which degrades the signal detectability.

(C)   *Combination of Five Real ELT Signals*

1. Neither the single-shot periodogram nor the single-shot MEM performs well for detecting all the ELT signals due to the overlapping sidebands problem.

2. The averaged periodogram and the averaged MEM improve the detection of the ELT signals which have a stationary carrier frequency component, i.e. Pointer ELT signals ELT01 and ELT07 and Garrett ELT12. No measure of carrier frequency is possible for the Narco ELT signal ELT19, but for Narco ELT17 the carrier frequency can be estimated.

3.   The Pointer ELT signals (ELT01 and ELT07) and the Garrett ELT signal ELT12 produce sharp distinct peaks which can be detected and identified easily.

4.   Narco ELT signal ELT17 produces a broad band spectrum and at the end of this broad band spectrum a sharp peak is oberved. This sharp peak being the carrier component of this Narco ELT signal. It is further seen that this Narco ELT signal has most of the power in its lower sidebands.

5.   Narco ELT signal ELT19 produces a broad peak and no more information about the carrier frequency is obtained using the averaged spectrum.

6.5   ELT Identification Using Rate Reduction Filtering

An important advantage of using the baseband processing technique is the ease in implementing the rate reduction filtering technique. By using this technique, the resolution of the spectrum improves due to increasing the data length.

In Section 6.3 we discussed the processing of single real ELT signal using the baseband periodogram, averaged periodogram, MEM and averaged MEM methods. We conclude that the Narco ELT signal (ELT17) has a weak carrier frequency component and note that the averaged spectrum indicates a large amount of the power contained in the lower sidebands. The identification and the detection of this Narco ELT signal using single-shot periodogram or MEM is not easy. In this section we discuss the processing of this Narco ELT signal ELT17 using rate reduction filtering and show how we can identify, detect and estimate the exact mixed carrier frequency of this Narco signal.

6.5.1   Rate Reduction Filtering Using the Periodogram

In Section 6.3.1.3 and Section 6.3.2.3 we examined the Narco ELT signal ELT17 using the periodogram and averaged periodogram and we found that, processing this ELT

signal using the baseband processor with mixing frequency F_I equal to 121.5 MHz we estimate the carrier peak is located at mixed carrier frequency of about 5300 Hz.

In this section we discuss the processing of the Narco ELT signal ELT17 using the periodogram with rate reduction filtering. Increasing the mixing frequency F_I by 4 kHz and processing this Narco ELT signal ELT17 using the baseband periodogram with rate reduction filtering gives the spectral estimation results shown in Fig. 6.41 to 6.44 for the averaging steps ℓ equal 1, 2, 4 and 8. From Fig. 6.41 and 6.42, it is difficult to detect the carrier frequency component peak because the strongest peak is a false peak which masks the carrier frequency and creates a false indication. Increasing the averaging steps to 4 gives the periodogram spectrum illustrated in Fig. 6.43. From this figure it is seen that the carrier frequency component has a sharp peak located at the mixed carrier frequency of about 1270 Hz. Furthermore, we note that the first and second lower sidebands become broad as compared to the carrier frequency component peak. Figure 6.44 depicts the result in the case of rate reduction by 8. In this figure it is clear that the carrier peak is located at mixed carrier frequency equal about 1270 Hz. In addition, it is seen that the carrier peak is very sharp and the level of the first and second lower sidebands is reduced relative to the carrier peak level. The widths of these sidebands becomes broadened as compared to the width of the carrier frequency component. This provides an effective identifier for the Narco ELT signal.

Comparing these obtained result using the periodogram with rate reduction filtering by 8 (Fig. 6.44) with those using the averaged periodogram (Fig. 6.11) we note the following; 1) Processing the Narco ELT signal (ELT17) by the periodogram and using rate reduction filtering with averaging steps $\ell = 8$, reduces the level of the lower sidebands by amounts of 2 to 7 dB as shown in Fig. 6.44; 2) This method improves the detection of the carrier component peak by about 5 dB relative to the level of the lower sidebands; and 3) It reduces the computation time as compared to the averaged periodogram.
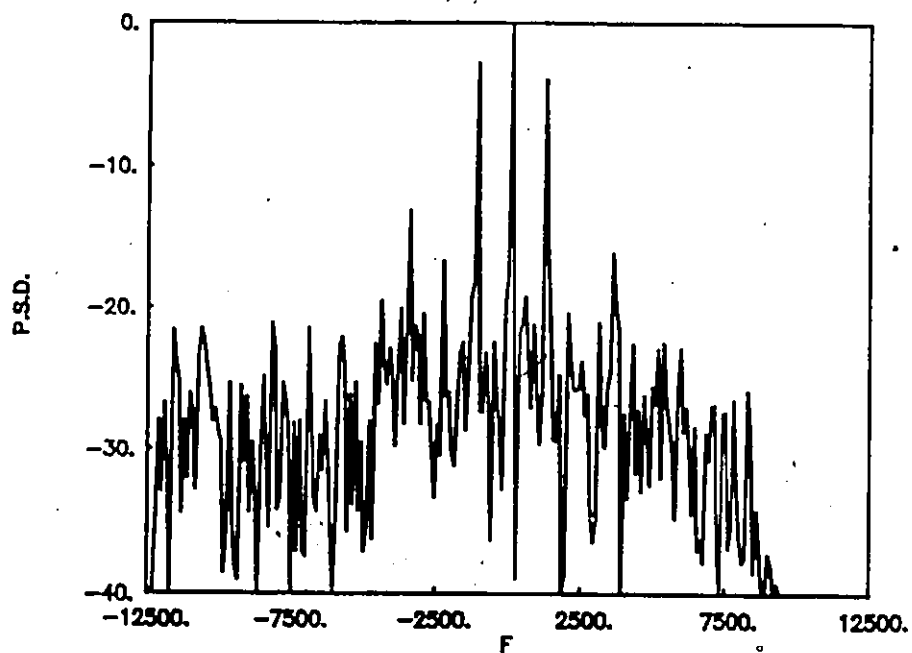
Fig. 6.41   The periodogram spectrum of Narco ELT17. No rate reduction.

Fig. 6.42   The periodogram spectrum of Narco ELT17. Rate reduction = 2.

Fig. 6.43   The periodogram spectrum of Narco ELT17. Rate reduction = 4.

Fig. 6.44   The periodogram spectrum of Narco ELT17. Rate reduction = 8.

Now, we will test the tracking algorithm and the frequency error across the band. In order to test the tracking, we increase the mixing frequency by 1 kHz as compared to the previous case in order to get the carrier peak near the mid band region to reduce the frequency error as discussed earlier in Chapter 4. Processing the Narco ELT signal ELT17 by the baseband periodogram using rate reduction filtering with this new mixing frequency and with averaging steps $\ell = 4$ and 8 gives the spectra illustrated in Fig. 6.45 to 6.46 respectively. The results here are the same as in Fig. 6.43 and Fig. 6.44 with the exception that the mixed carrier frequency is now 269 Hz.

In order to further see how the rate reduction filtering technique gives a good estimate of the mixed carrier frequency of this Narco ELT signal ELT17 and reduces the frequency error, we consider two examples of mixing frequency F_I. First, the Narco ELT signal (ELT17) is processed by the baseband periodogram using rate reduction filtering with averaging steps $\ell = 8$. This time the mixing frequency is increased by 1 kHz as compared to the previous case or increased by 6 kHz. The spectral estimation result for this case is plotted in Fig. 6.47. From this figure it is clear that only one sharp peak is detected above the -10 dB threshold level, this peak being the carrier component, located at mixed carrier frequency of -732 Hz. It is seen the undesirable sidebands are rejected.

The second mixing frequency chosen for this test is increased by 500 Hz compared to the previous one, i.e. over the original mixing frequency by 6500 Hz. Figure 6.48 illustrates the spectral estimation result for the case of rate reduction by 8. Once again one sharp peak is detected above threshold level of -10 dB. This peak described as the carrier component of this Narco ELT17, which occurs at the mixed carrier frequency equal about -1232 Hz.
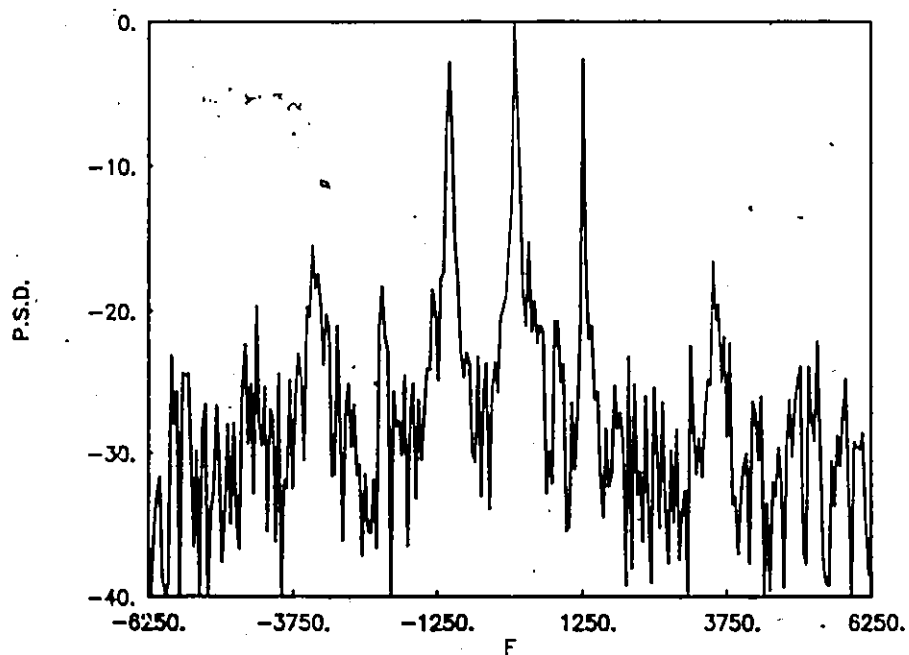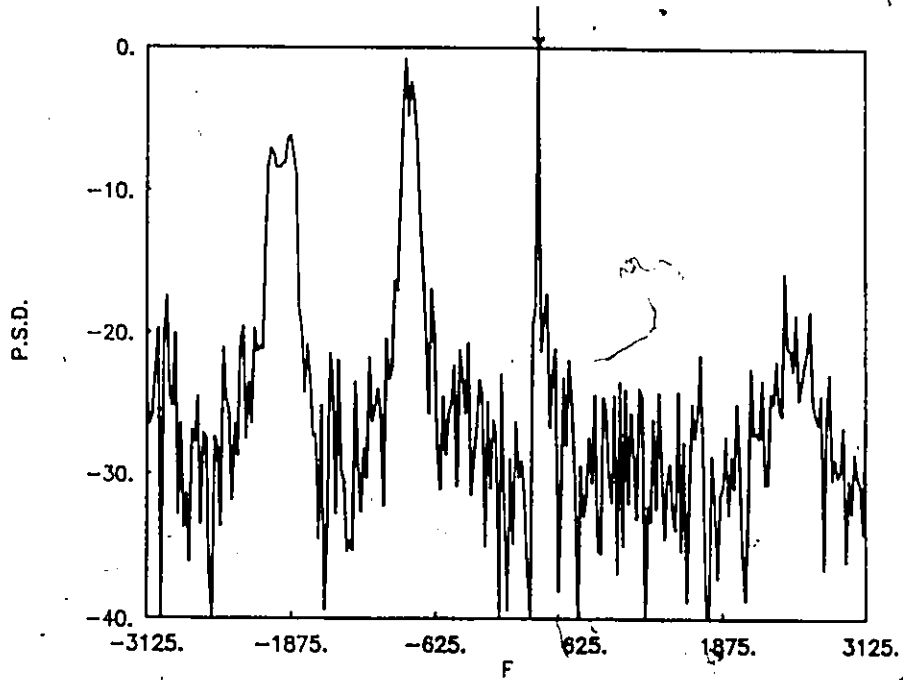
Fig. 6.45   The periodogram spectrum of Narco ELT17. Rate reduction = 4.
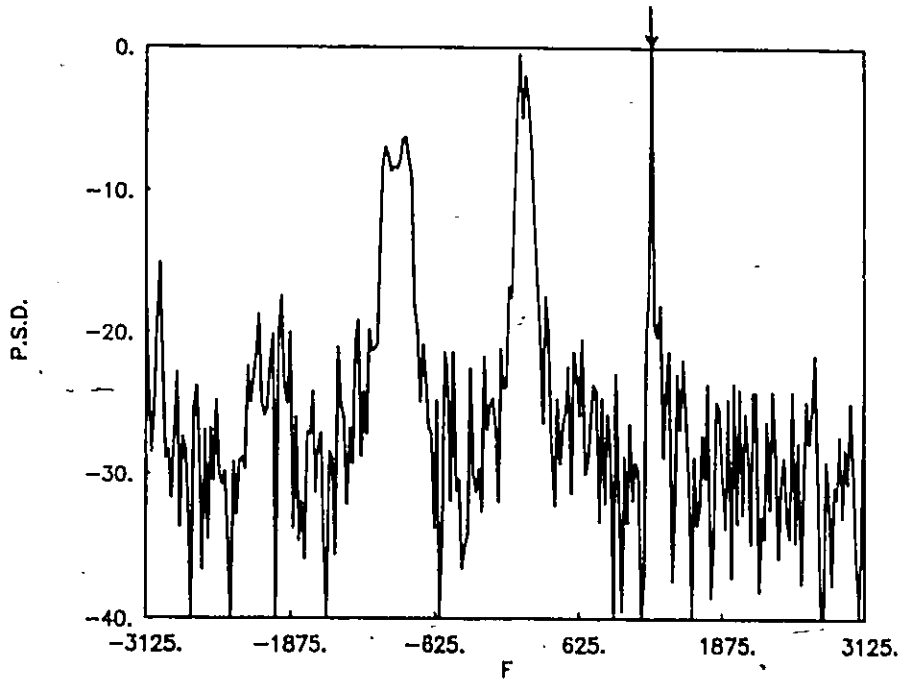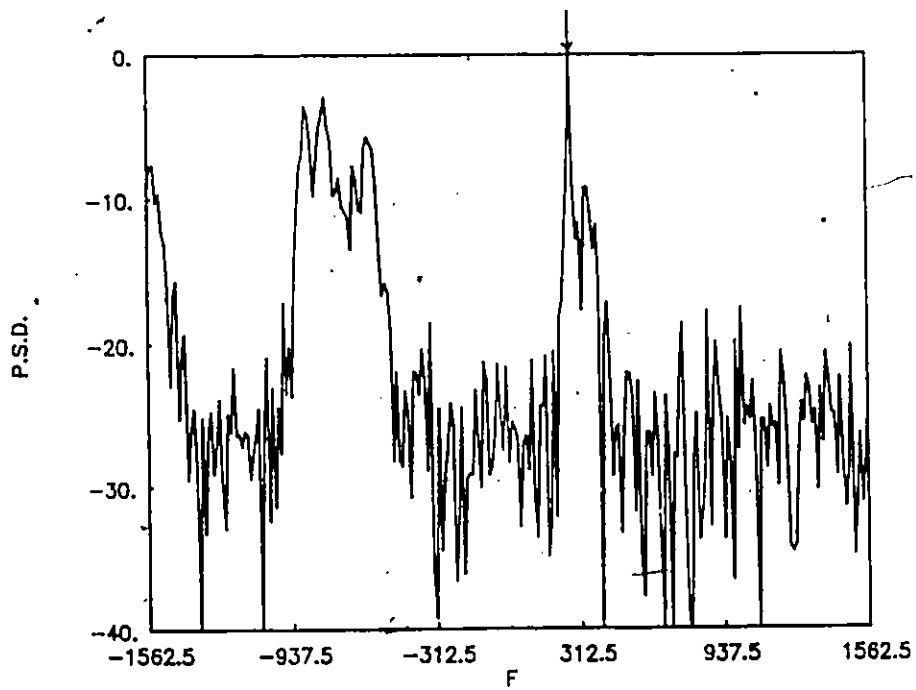

Fig. 6.46   The periodogram spectrum of Narco ELT17. Rate reduction = 8.

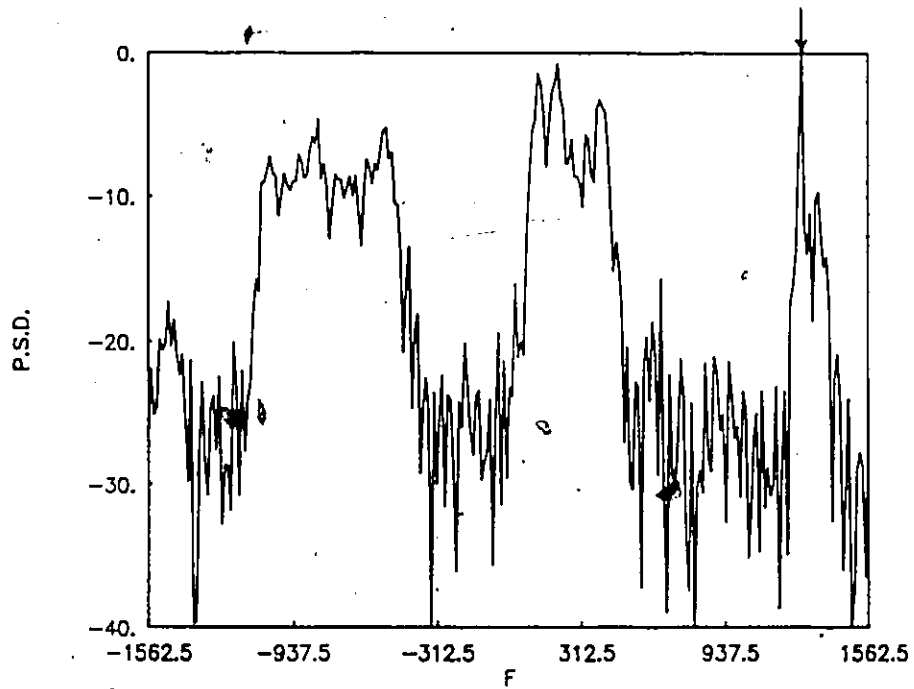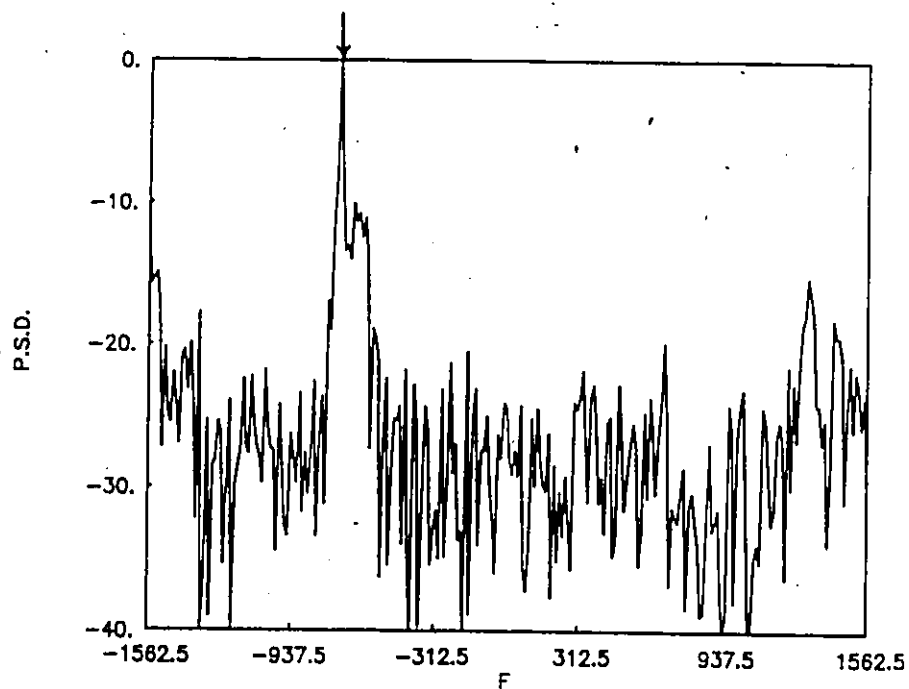Fig. 6.47   The periodogram spectrum of Narco ELT17. Rate reduction = 8.
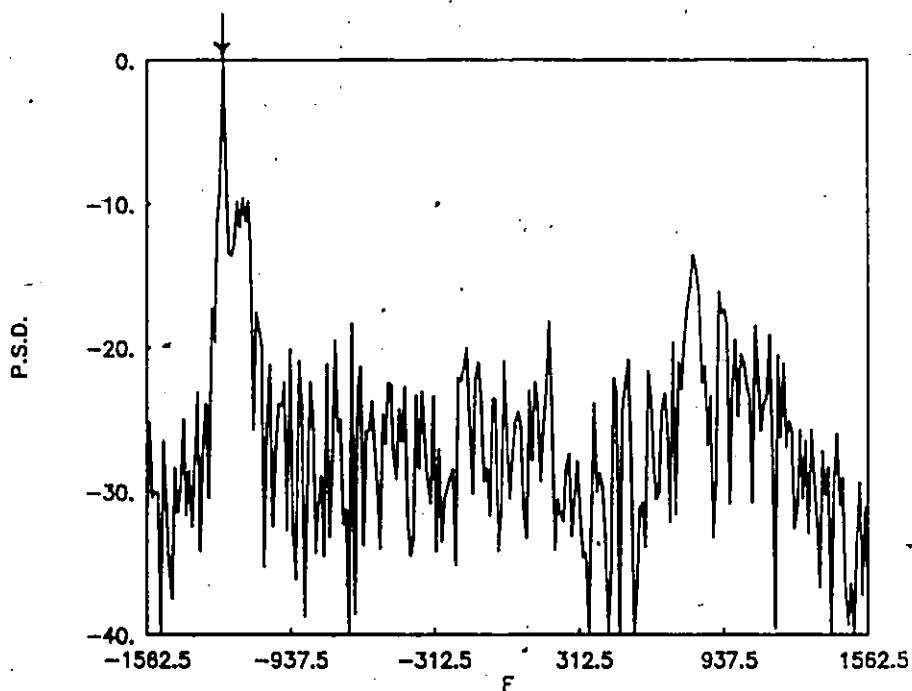
Fig. 6.48   The periodogram spectrum of Narco ELT17. Rate reduction = 8.

As a result of the above studied cases, we conclude the carrier frequency component of this Narco ELT signal (ELT17) can be measured with frequency error uniformly distributed over the range ±12 Hz using the baseband periodogram.

In order to ensure that the mixed carrier frequency for a Narco ELT signal (ELT17) equals 5270 Hz, the Narco ELT signal is processed by the baseband periodogram using rate reduction filtering with averaging steps $\ell = 8$ and this time the original mixing frequency F_I is increased by 5270 Hz in order to estimate the carrier peak at 0 Hz. The periodogram spectral estimation result is plotted in Fig. 6.49. From this figure it is seen that, one sharp peak and the first lower sideband of the signal are detected above the -10 dB threshold level. This sharp peak is the carrier component, located at the mixed carrier frequency equal 0 Hz as expected.

Thus, from the above analysis, we conclude that; processing the Narco ELT17 signal using the periodogram with rate reduction filtering and with averaging steps equal to 8 improves the detection, reduces the frequency error and reduces the level of the undesirable sidebands. As well, the width of these sidebands becomes broadened as compared to the width of the carrier component which is very sharp. This provides an effective identifier for this signal.

6.5.2 Rate Reduction Filtering Using the MEM

This section is concerned with studying the MEM performance of a Narco ELT signal (ELT17) using the rate reduction filtering technique.

First, the signal is processed using the baseband MEM with mixing frequency 121.5 MHz and MEM filter order 100. The MEM spectral estimation result for this case is given in Fig. 6.17. Increasing the mixing frequency by 4 kHz and processing the signal using the baseband MEM with MEM filter order 100 gives the spectral estimation result depicted in
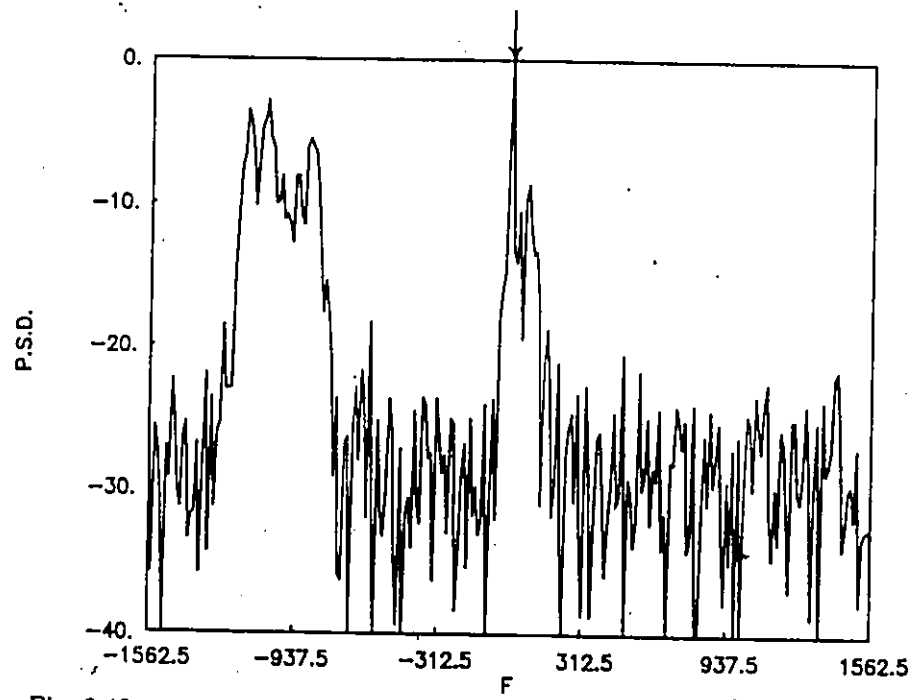
Fig. 6.49   The periodogram spectrum of Narco ELT17. Rate reduction = 8.

Fig. 6.50. In these two figures, we note that the center topmost peak is a false peak, i.e. not the carrier frequency component. This peak creates a false indication when detecting the carrier frequency component of this signal.

Now, we discuss the processing of the Narco signal using the baseband MEM with rate reduction filtering and with averaging steps $\ell = 1, 2, 4$ and 8. The ELT signal is processed using the same mixing frequency as before, but this time we choose the MEM filter order equal 50 in order to show that with rate reduction filtering, the order of prediction error filter can be reduced.

Figures 6.51 to 6.54 illustrate the MEM performance with no averaging, averaging by 2, averaging by 4 and averaging by 8. From these results, it is clear that in the case of no averaging, averaging by 2 and averaging by 4, it is difficult to identify the carrier frequency component. For these three figures, the center peak is not the carrier peak, it is a false peak which masks the carrier component of the signal creating a false indication. Increasing the averaging steps ℓ to 8 produces one sharp peak and several broad bands respresenting sidebands. This sharp peak occurs at mixed carrier frequency, of about 1270 Hz. It is seen that the level of the first lower sideband is reduced and the bandwidth of this lower sideband becomes broadened as compared to the width of the carrier frequency component which is very sharp as shown in Fig. 6.54. This provides an effective identifier for the Narco signal.

Now, we test the tracking and frequency error across the band using the baseband MEM with rate reduction filtering. We increase the mixing frequency by 1 kHz as compared to the previous case, i.e. by 5 kHz over the original mixing frequency, and process the Narco signal using MEM filter order 50 with rate reduction filtering with averaging steps $\ell = 8$. The spectrum, illustrated in Fig. 6.55, has one sharp peak above the -10 dB threshold level (on the right of the spectrum) and some other broad band peaks belonging to the lower sidebands. The carrier component occurs at mixed carrier frequency equal about 269 Hz.

Fig. 6.50   MEM = 100 spectrum of Narco ELT17. No rate reduction.

Fig. 6.51   MEM = 50 spectrum of Narco ELT17. No rate reduction.

Fig. 6.52   MEM = 50 spectrum of Narco ELT17. Rate reduction = 2.

Fig. 6.53   MEM = 50 spectrum of Narco ELT17. Rate reduction = 4.
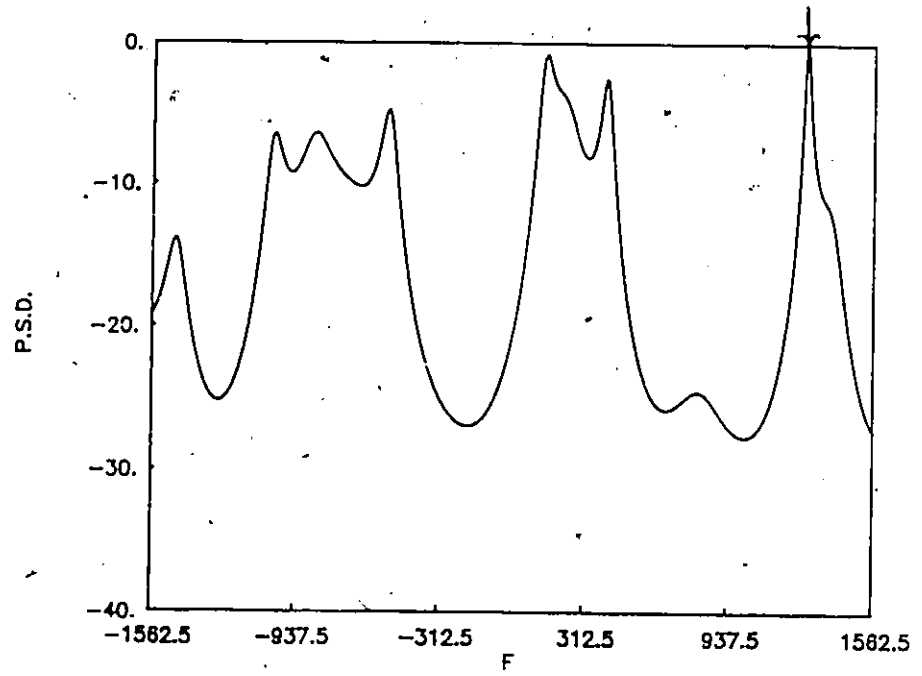
Fig. 6.54   MEM = 50 spectrum of Narco ELT17. Rate reduction = 8.
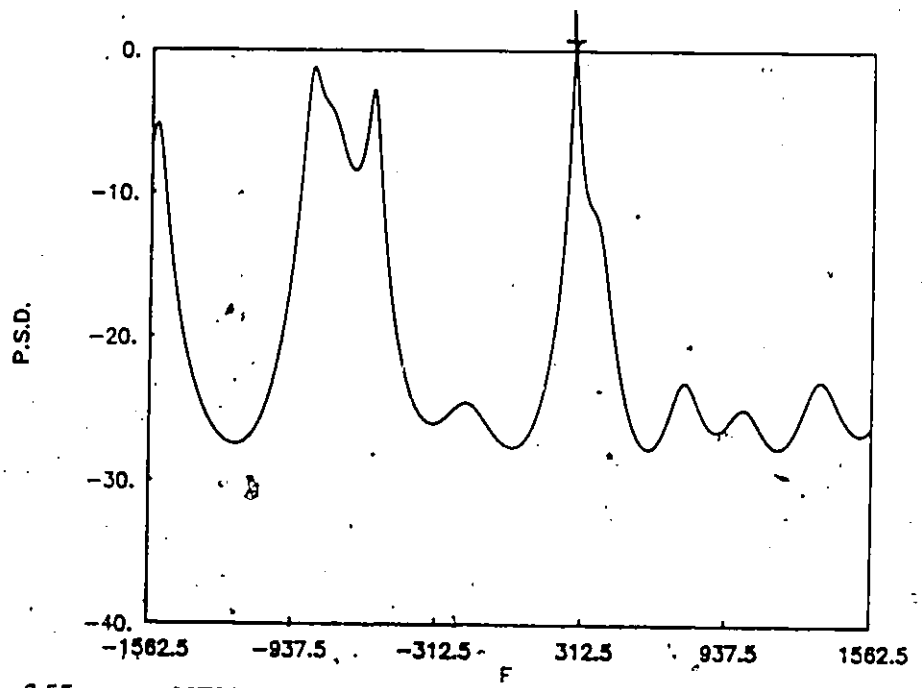
Fig. 6.55   MEM = 50 spectrum of Narco ELT17. Rate reduction = 8.

In order to obtain a good estimate of the mixed carrier frequency for this Narco ELT signal and test the frequency error across the band using the baseband MEM with rate reduction filtering, we consider processing the Narco ELT signal using two different mixing frequencies for F_I. First, the mixing frequency is increased by 1 kHz as compared to the previous case or by 6 kHz. Then the Narco ELT signal (ELT17) is processed by the baseband MEM using rate reduction filtering with averaging steps $\ell = 8$ and MEM filter order equal 50. The MEM spectral estimation result for this case is given in Fig. 6.56. From this figure it is shown that one sharp peak is detected above the -10 dB threshold level. The carrier component peak located at mixed carrier frequency of about -732 Hz.

Figure 6.57 illustrates the MEM = 50 spectral estimation result, but this time the mixing frequency is increased by amount of 500 Hz as compared to the previous case, or increased by 6500 Hz over the original mixing frequency. In this figure we note that the spectrum has one sharp peak detected above the -10 dB threshold level belonging to the carrier component peak and occurs at mixed carrier frequency of about -1232 Hz.

Thus, from the above analysis we found that the Narco ELT17 has mixed carrier frequency equal about 5270 Hz if it is processed using the original mixing frequency.

To verify that the mixed carrier frequency for the Narco ELT signal equals 5270 Hz, the signal is processed by the baseband MEM using rate reduction filtering with averaging steps $\ell = 8$ and MEM filter order equal 50. The mixing frequency chosen for this test is increased by 5270 Hz over the original mixing frequency. The MEM = 50 spectral estimation result for this case is depicted in Fig. 6.58. The spectrum shown in this figure has one sharp peak (on the right of the spectrum) and a lower sideband above the -10 dB threshold level. The carrier frequency component occurs at mixed carrier frequency equal 0 Hz as expected.
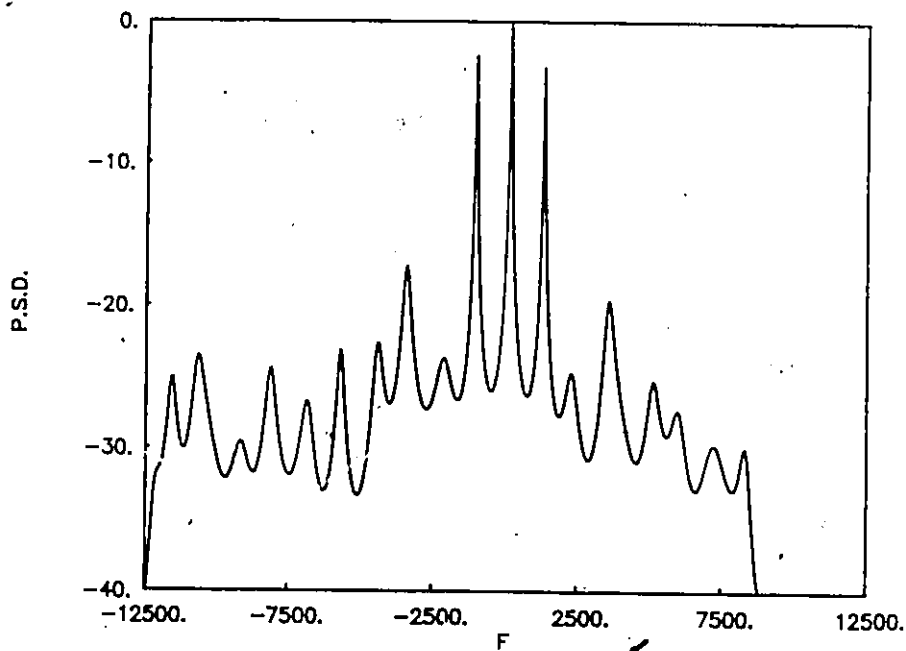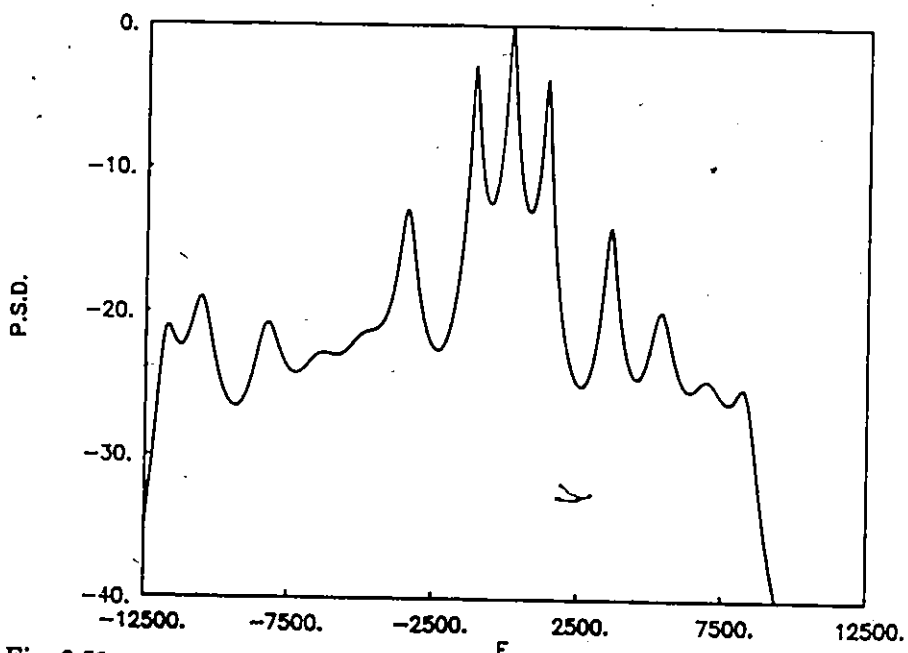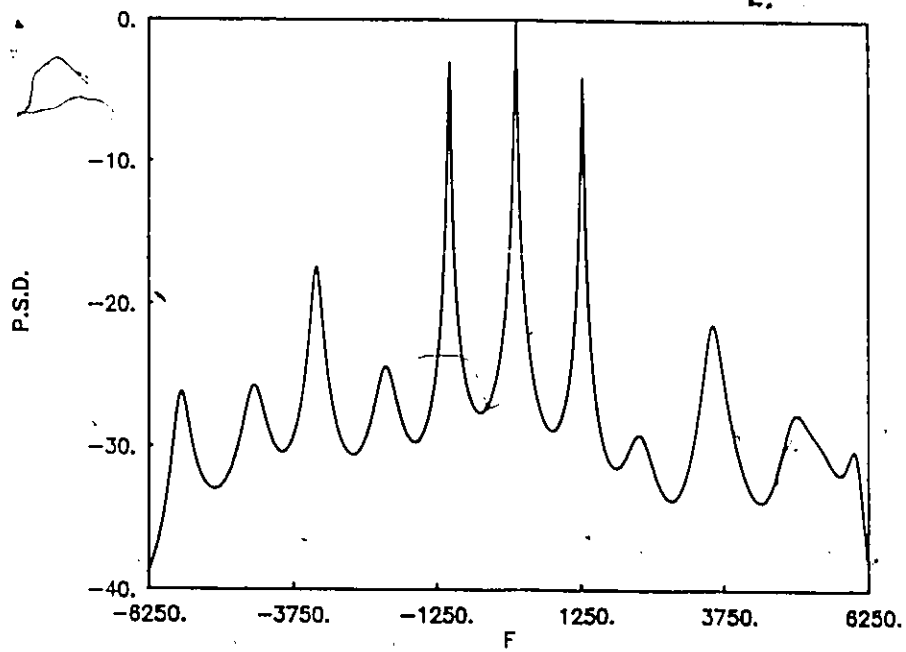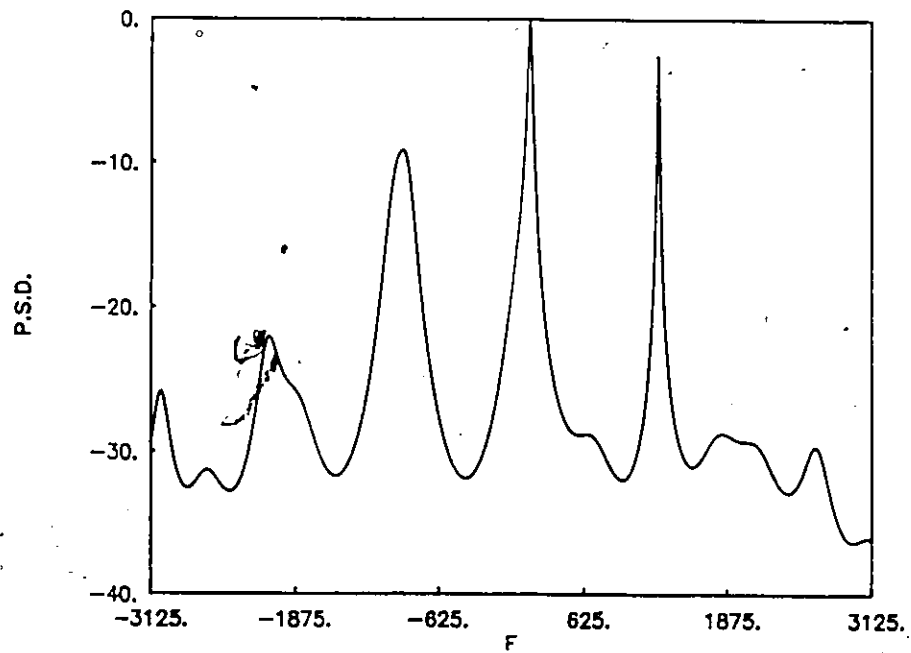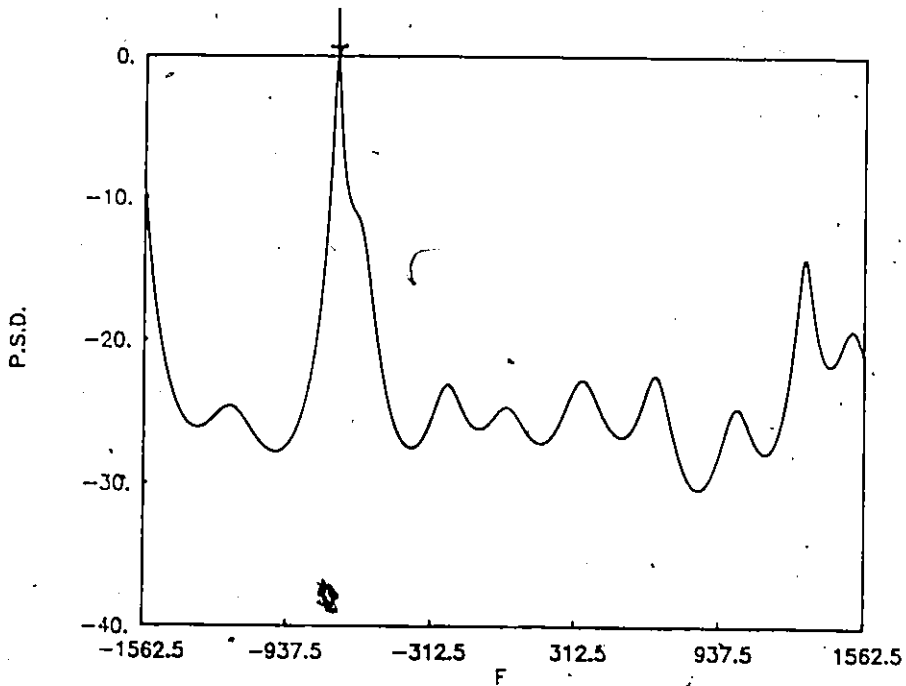
Fig. 6.56   MEM = 50 spectrum of Narco ELT17. Rate reduction = 8.
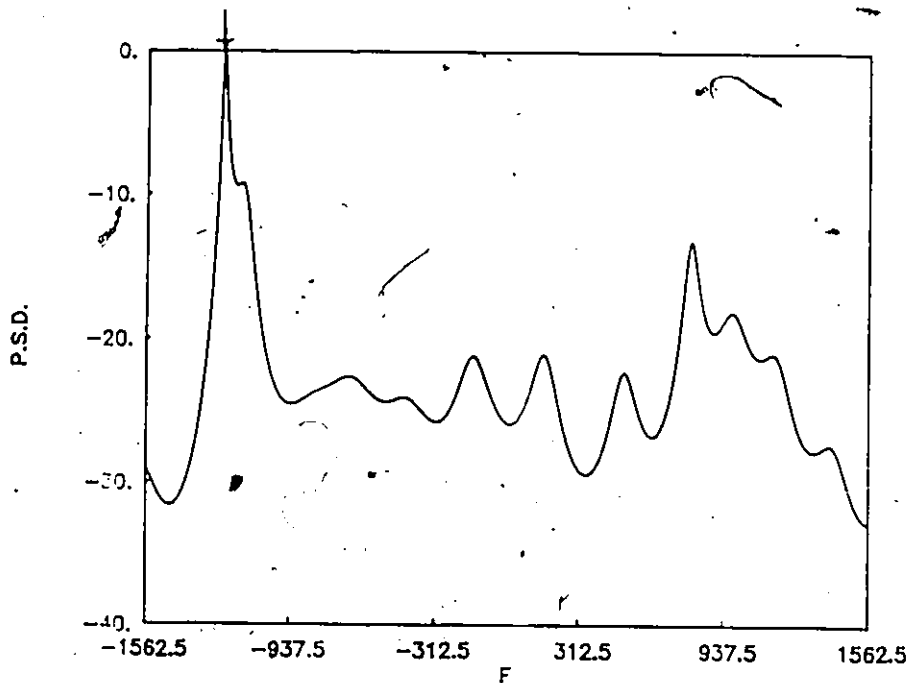
Fig. 6.57   MEM = 50 spectrum of Narco ELT17. Rate reduction = 8.
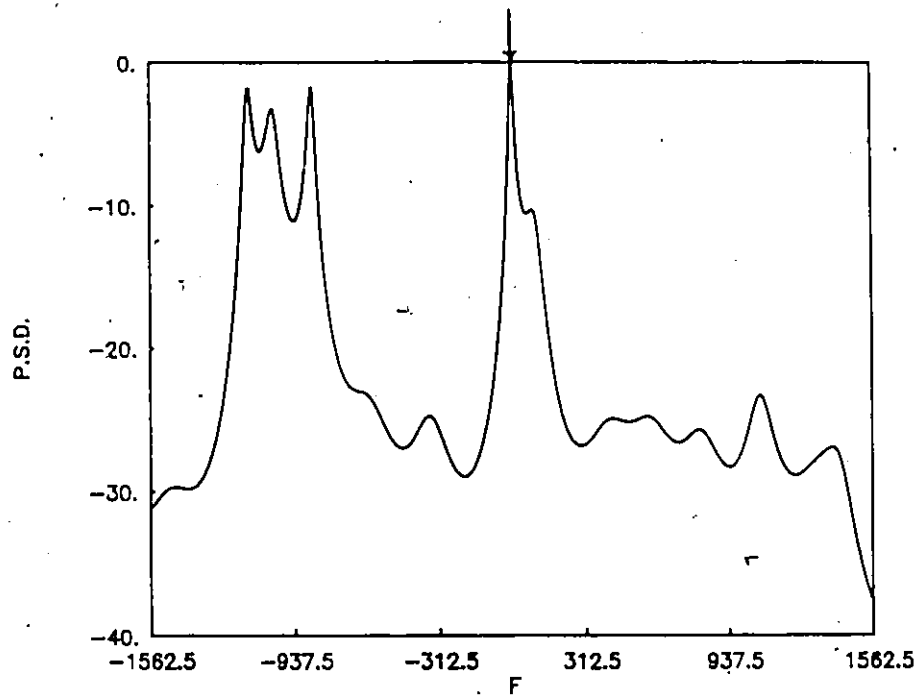
Fig. 6.58   MEM = 50 spectrum of Narco ELT17. Rate reduction = 8.

Comparing these results using the baseband MEM with those obtained using the baseband periodogram using rate reduction filtering with averaging steps ℓ equals 8, we observe the agreement is good in that as the averaging steps ℓ increases to 8, the carrier frequency component becomes very sharp while the width of the lower sidebands becomes broadened as compared to the width of the carrier frequency component. Furthermore, the relative heights of the undesirable sidebands are reduced relative to the level of the carrier component peak. This provides an effective identifier for the Narco ELT signal.

By adjusting the mixing frequency F_I and using the rate reduction filtering with averaging steps ℓ equals 8, we can easily track the carrier component of this Narco ELT signal and estimate the mixed carrier frequency of the signal which simplifies detection of this Narco ELT signal.

6.6   Summary

A baseband processor for processing the real ELT signals has been described and tested using individual and combinations of real ELT signals. The signal processing methods employed here include linear and non-linear spectral estimation methods. Post-processing using spectral averaging is employed to enhance the maximum signal detectability.

From the above analysis we conclude that:

(A)   *Individual Real ELT Signals*

1.   The processing results using linear and non-linear spectral estimation methods (single-shot) performs satisfactorily for the analysis of the Pointer (ELT01 and ELT07) and Garrett (ELT12 and ELT15) ELT signals. But for Narco ELT signal (ELT19), the single-shot periodogram spectral estimation result is not good and the detection of the Narco ELT signals is difficult. Single-shot MEM spectral estimator resolves the carrier peak for Narco ELT19.

2.   The baseband averaged periodogram and averaged MEM reduce the level of the undesirable sidebands which enhance the signal detectability for Pointer (ELT01 and ELT07), Garrett (ELT12 and ELT15) and Narco ELT17. But for Narco ELT19 no more information about the carrier frequency obtained using the averaged spectra.

(B)   *Combinations of Real ELT Signals*

1.   For the combination of two real ELT signals (ELT01 and ELT19), the single - shot periodogram or MEM perform well for detecting the Pointer ELT01. The single-shot peridogram fails to resolve the carrier peak for Narco ELT19; however, the single-shot MEM does provide a resolution.

2.   For two combinations of the three real ELT signals (Pointer and Garrett overlapped by the Narco), the single-shot periodogram can detect the carrier peak for Pointer ELT signal but no measure of the carrier frequency is possible for the case of the overlapped signals. Single-shot MEM resolves the carrier peaks for the Pointer and the Garrett ELT signals.

3.   As the number of ELT signals increases to five, the detection of the present ELT signals becomes difficult due to overlapping sidebands.

4.   The averaged periodogram and averaged MEM improve the detection of the ELT signals which have stationary carrier frequency components for the case of multiple real ELT signals due to reducing the level of undesirable sidebands relative to the carrier component peaks. In addition, the averaged spectra improve the detection of the carrier peak for the Narco ELT signal (ELT17) but for Narco ELT19 no information about the carrier frequency is obtained.

The processing results by single-shot periodogram or MEM using rate reduction filtering with averaging steps $\ell = 8$ gives excellent spectral estimation results for detecting the carrier component peak of the Narco ELT signal (ELT17) which has a weak carrier frequency component relative to its lower sidebands. Rate reduction filtering technique can be used as an effective identification method for the real ELT signals.

CHAPTER 7

BASEBAND PROCESSOR FOR SATELLITE PASS DATA

7.1　　Introduction

In this chapter the analysis concentrates on processing real SARSAT signals relayed from satellite passes. The signals are received from COSPAS satellite C1, orbits 860 and 861. Due to the satellite motion, there is a Doppler frequency shift in the signal up to a maximum of approximately ± 3 kHz. The analog tape supplied by the CRC was digitized at a sampling rate of 100 kHz.

These real signals are processed and tested using the linear and non-linear spectral estimation methods. The signal processing procedure is depicted in Fig.7.1. Specifically, the spectral estimation results for data lengths of 512, 1024 and 2048 complex points are presented using the baseband processing system with cut off frequency of the baseband lowpass filter B_c equal 12.5 kHz.

7.2　　Processing Signals Received from COSPAS Orbit 860

In this analysis, the data selected from the the tapes starts at the fifth minute of the satellite pass. Two comparisons are made among the spectral estimation methods. These are:

1. Linear spectral method (periodogram) and non-linear spectral method MEM.

2. Averaged periodogram and averaged MEM.

input ELT
signal

Baseband

processor

Periodogram

MEM

Averaging

Output

Post-processor
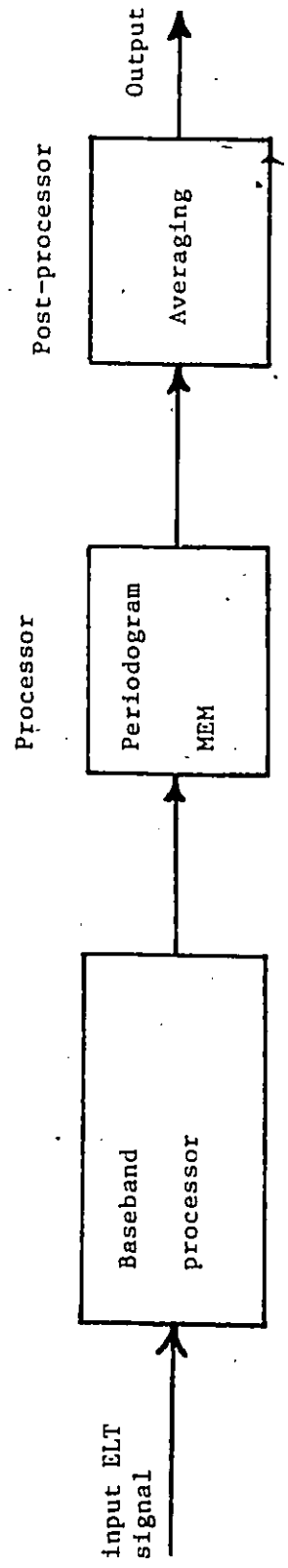
Processor

Fig. 7.1   ELT signal processor

7.2.1 Processing Results Using the Periodogram

512 - complex points

Figure 7.2 illustrates the periodogram spectra using 512 complex points. From these results it is seen that only one peak is detected and located at mixed carrier frequency equal about 1000 Hz. In addition, we note that the background noise level for this set of data is high and therefore detection of any signal is difficult.

1024 - Complex points

Figure 7.3 shows the periodogram spectra for the same set of data. Increasing the signal length to 1024 complex points does not decrease the variance using the periodogram method. From these results, we note that two peaks are detected. These two peaks are located at mixed carrier frequencies equal to about - 500 Hz and 1000 Hz respectively. Again, it is clear that the background level of noise is high.

2048 - Complex points

Figure 7.4 illustrates the periodogram spectrum using 2048 complex points. From this figure we note that; three peaks are located at mixed carrier frequencies of about -3750 Hz, -500 Hz and 1000 Hz. The detection of a signal is difficult due to high variance of this set of real signals.

7.2.2 Processing Results Using the Averaged Periodogram

Now, we employ the averaged periodogram technique which reduces the variance of the power spectrum estimate. For this set of signals, a one second data length is being analysed starting at the fifth minute point of the pass.

Fig. 7.2   Periodogram spectrum using 512 - complex points (orbit # 860).

Fig. 7.3   Periodogram spectrum using 1024 - complex points (orbit # 860).

Fig. 7.4   Periodogram spectrum using 2048 - complex points (orbit # 860).
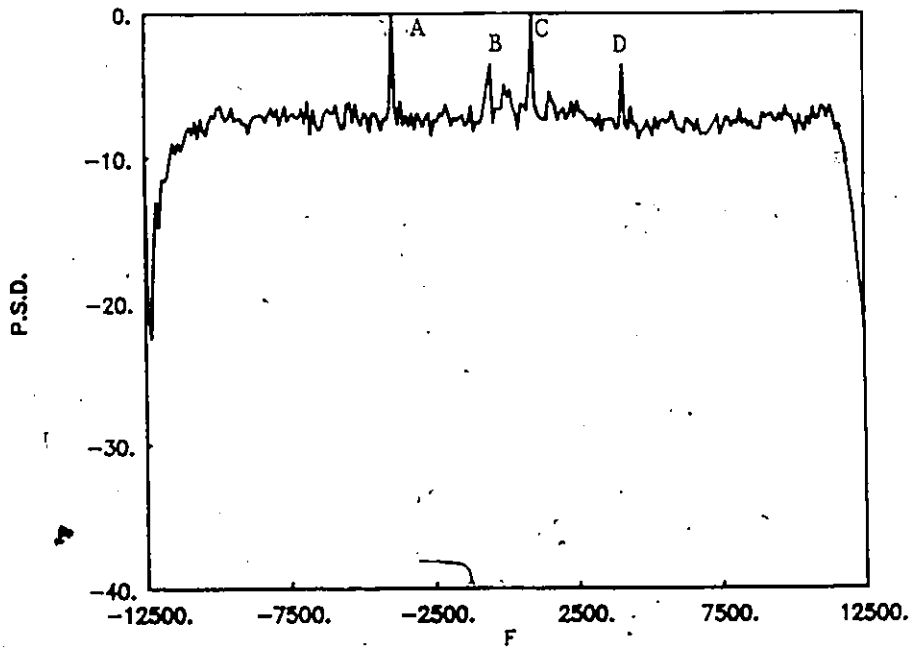
Fig. 7.5   Averaged periodogram spectra of 100 blocks 512 - complex points FFT (orbit # 860).
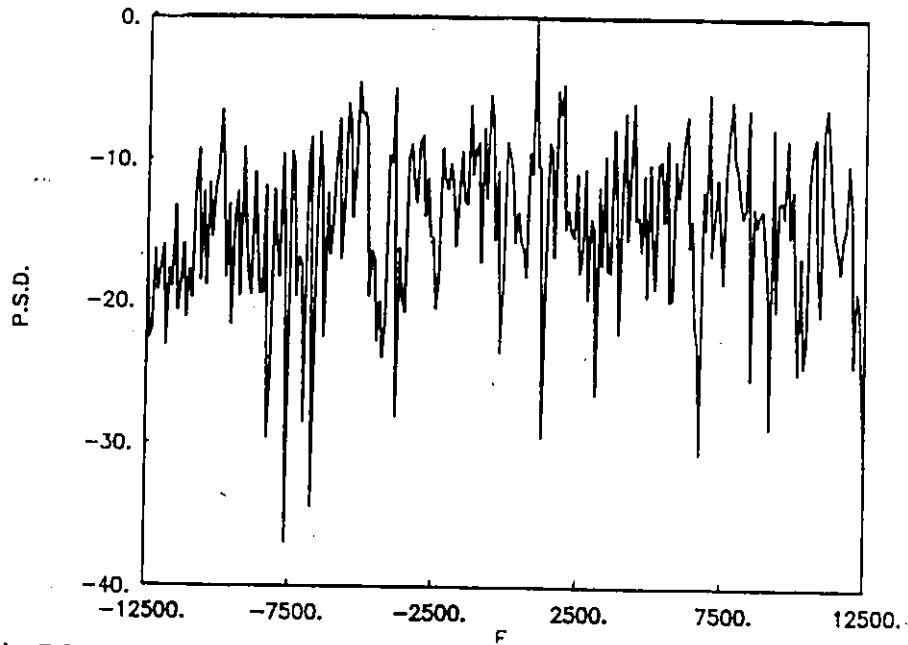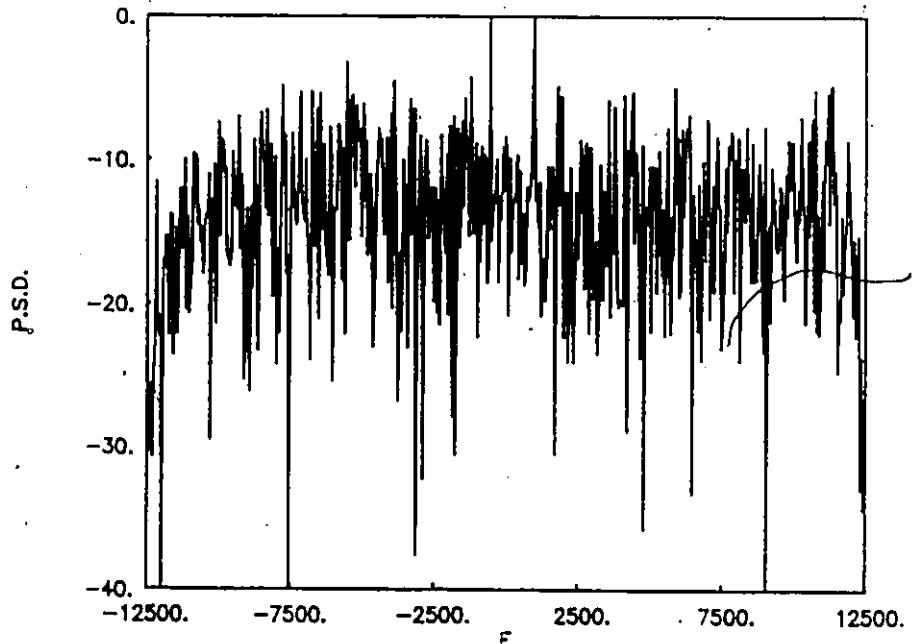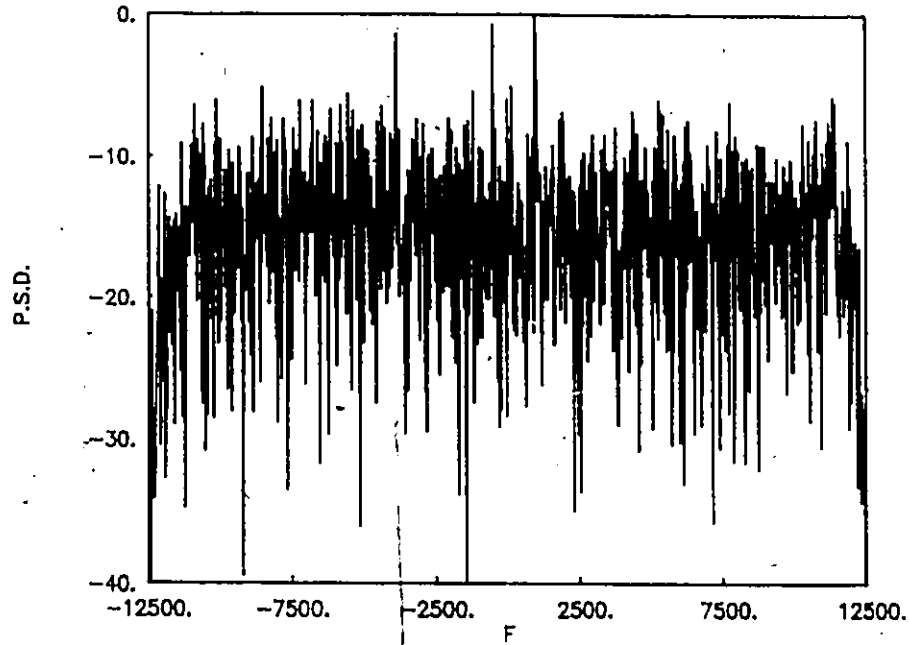
512 - Complex points

Figure 7.5 depicts the averaged periodogram spectra of 100 blocks with each block contains 512 complex points. From these results we note that, four distinct peaks can be identified and detected. These peaks denoted by A, B, C and D are located at mixed carrier frequencies -3750 Hz , -500 Hz , 1000 Hz and 4200 Hz respectively. It is seen that, the background noise level is about 7 dB below the highest carrier peak level.

1024 - Complex points

Figure 7.6 illustrates the averaged periodogram spectra of 50 blocks of data using 1024 - complex points for each periodogram. Comparing these results with those given in Fig.7.5 , we note that the background noise level is reduced by 1.5 dB. From this figure it is clear that, the four prominent peaks previously detected are still present at mixed carrier frequencies of -3750 Hz, -500 Hz, 1000 Hz and 4200 Hz.

2048 - Complex points

Figure 7.7 shows the averaged periodogram spectra for 25 sets of data using 2048 - complex points for each periodogram. This result shows that the noise background is further reduced by 1.5 dB, as compared to the result given in Fig.7.6. The four peaks previously detected are considerably enhanced. However, we note that peak C now exhibits line splitting. From the above analysis we note that the averaged periodogram smoothes the spectral estimation spectra and reduces the level of undesirable sidebands which improves the detection of the signals. The signal-to-noise ratio is improved by processing fewer blocks of longer records. This consequently improves the detection of the signals.

It appears that the four peaks indicated by A, B, C and D are not ELT signals, but peaks due to interference received by the satellite.
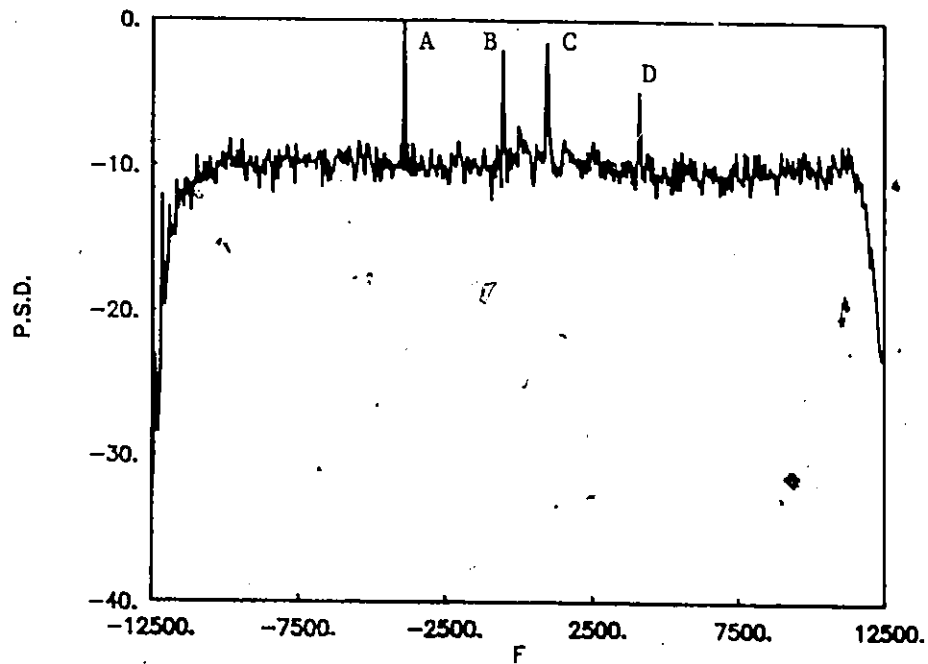
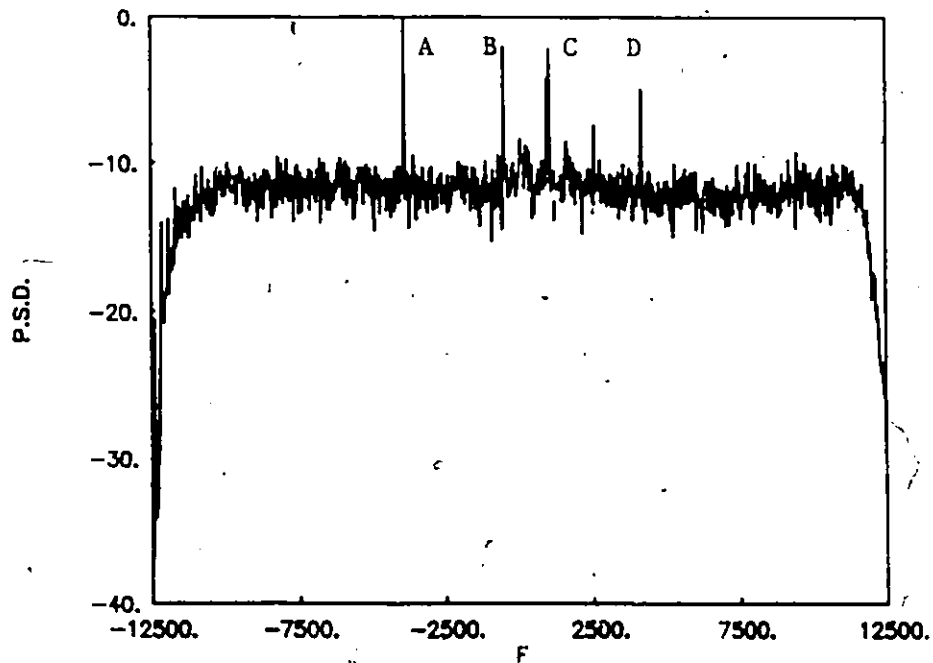Fig. 7.6   Averaged Periodogram spectrum of 50 blocks 1024 - complex point FFT (orbit # 860).

Fig. 7.7   Averaged periodogram spectrum of 25 blocks 2048 - complex point FFT (orbit # 860).

7.2.3 Processing Results using the MEM

Figure 7.8 illustrates the spectral estimation result for this set of data using an MEM filter order of 100 with 1024 complex points. From this figure it is seen that, one peak can be detected. This peak occurs at mixed carrier frequency 1000 Hz. These results indicate that this set of data contains a high noise level. Therefore, the detection of a signal is difficult.

Using the MEM, there is no significant change in processing various lengths of the signal using the same MEM filter order. Since the MEM is a parametric spectral estimation technique, it is possible to adjust the number of filter coefficients of prediction error filter in order to produce good frequency resolution. Higher MEM filter orders reduce the frequency error and improve the frequency resolution which consequently enhance the detection of the signals. However, higher MEM filter orders are time consuming and also generate spurious peaks which may be undesirable.

Now, we examine the same data set and increase the MEM filter order to 200 and then 300. Figure 7.9 depicts the MEM filter order 200 spectra for this set of data using 1024 - complex points. It is seen that one peak can be detected. This peak occurs at mixed carrier frequency 1000 Hz. Comparing these results with those given in Fig.7.8, we note that increasing the MEM filter order to 200 improve the frequency resolution and produces a sharp distinct peak.

Increasing the MEM filter order to 300 gives the spectra shown in Fig.7.10 for the same set of real signals. From these results, it is seen that more peaks are obtained and there is no indication of how many signals are present. Therefore, detection of the signals is difficult.

Comparing the results using the MEM (Fig.7.8) with those obtained from the periodogram (Fig.7.3) we note that, direct frequency measurment using either the
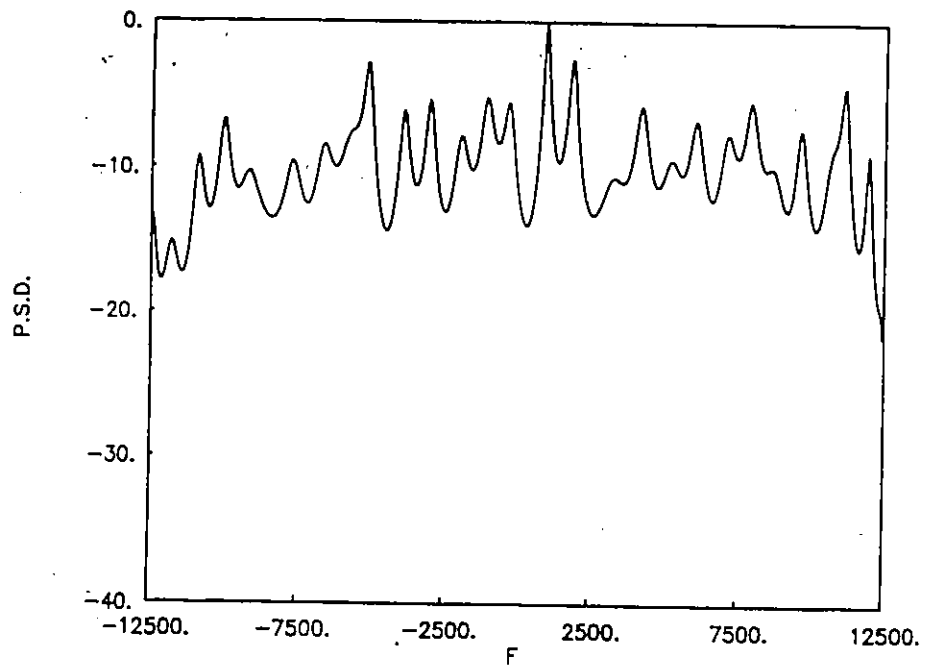
Fig. 7.8   MEM = 100 spectrum using 1024 - complex points (orbit #860)
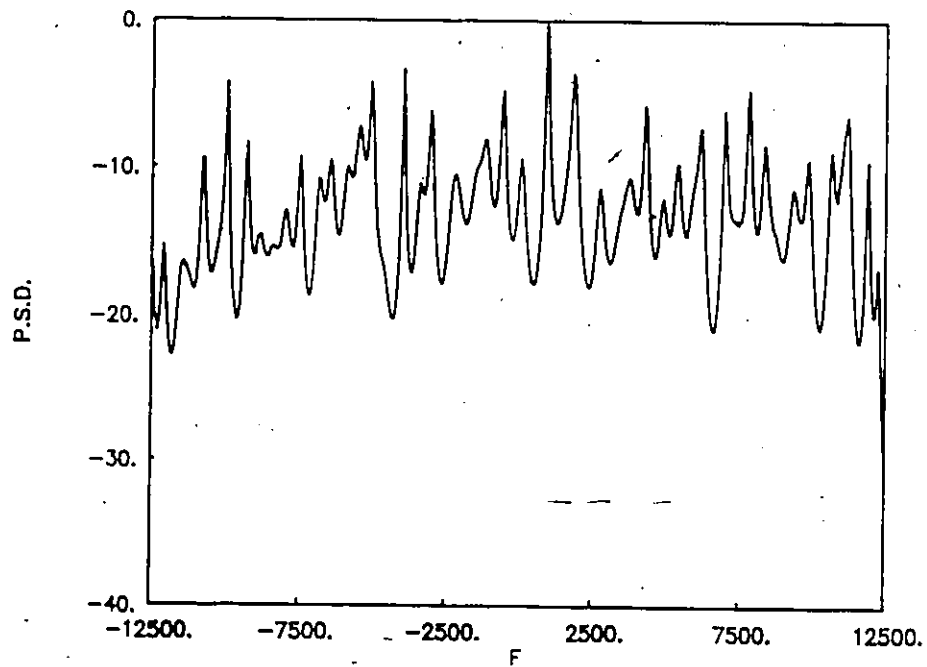

Fig. 7.9   MEM = 200 spectrum using 1024 - complex points (orbit #860)

Fig. 7.10   MEM = 300 spectrum using 1024 - complex points (orbit #860)
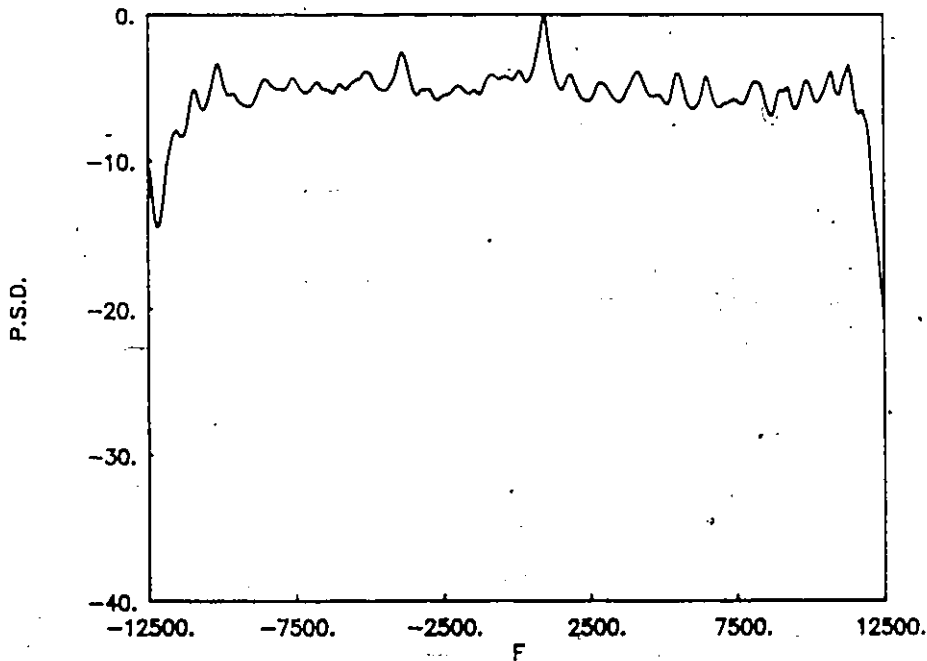
Fig. 7.11   Averaged MEM = 100 spectrum of 50 blocks 1024 - complex
                 points each (orbit # 860).

periodogram or the MEM (order 100) is not easy. In addition, it is seen that the number of spectral peaks obtained using the periodogram exceed those resolved by the MEM and the MEM spectrum is smoother than the periodogram spectrum. Both variance and frequency biases make frequency estimation difficult. Thus, it is seen that there is no indication of how many signals are present.

7.2.4.   Processing Results Using the Averaged MEM

We now consider the processing of this set of real signals using the baseband averaged MEM technique. This set of data is divided into 50 blocks with each block containing 1024 - complex points.

Figure 7.11 illustrates the spectral estimation result for this set of data using MEM filter order 100. From this figure we note that, the background noise level for this set of data is high. This level appears at about -5 dB threshold level.

The averaged MEM spectra for this set of data using MEM filter order equal 200 is given in Fig.7.12. From this figure it is clear that the spectrum improves as the MEM filter order increases to 200, as compared to the spectrum obtained using MEM filter order 100 shown in Fig. 7.11.

Figure 7.13 shows the averaged MEM spectra for this set of data using MEM filter order 300. From this figure we note that, the four peaks labeled (A, B, C and D) can be identified. Again, these four peaks are not considered to be ELT signals, but more likely interference signals received by the satellite.

Comparing all the results given in Fig.7.11, Fig.7.12 and Fig.7.13 for MEM filter order 100, 200 and 300 respectively, we conclude that, the MEM filter order plays a major role in the spectral estimation and higher MEM filter order gives a better spectral estimate.
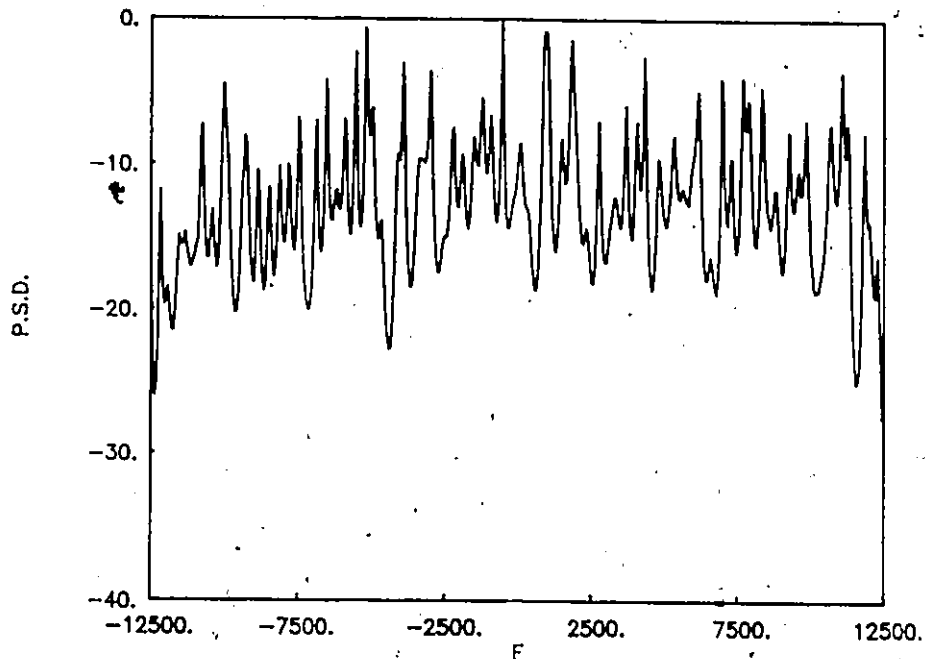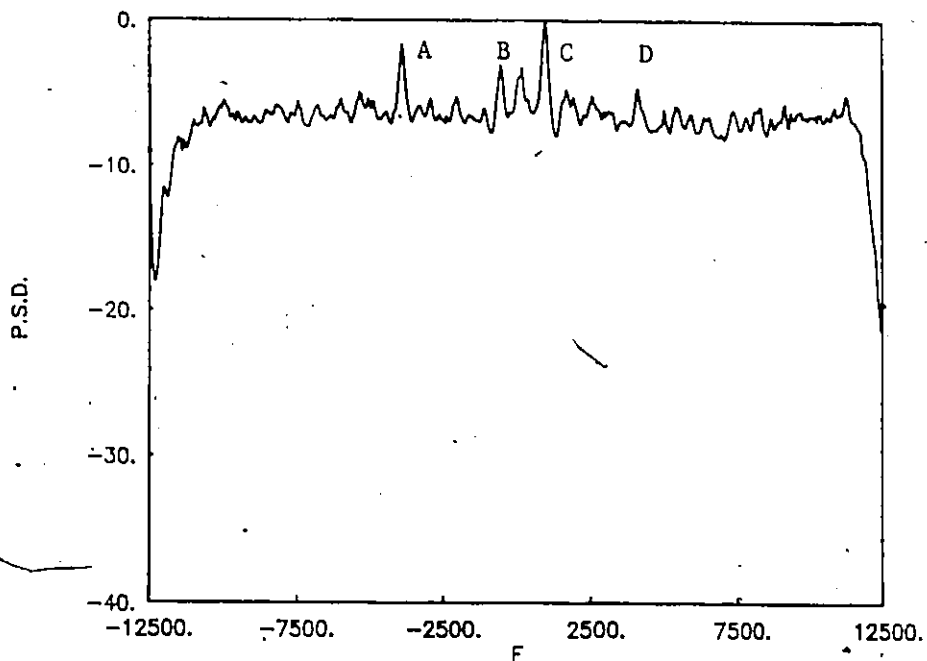
Fig. 7.12　　Averaged MEM = 200 spectrum of 50 blocks 1024 - complex
points each (orbit # 860).
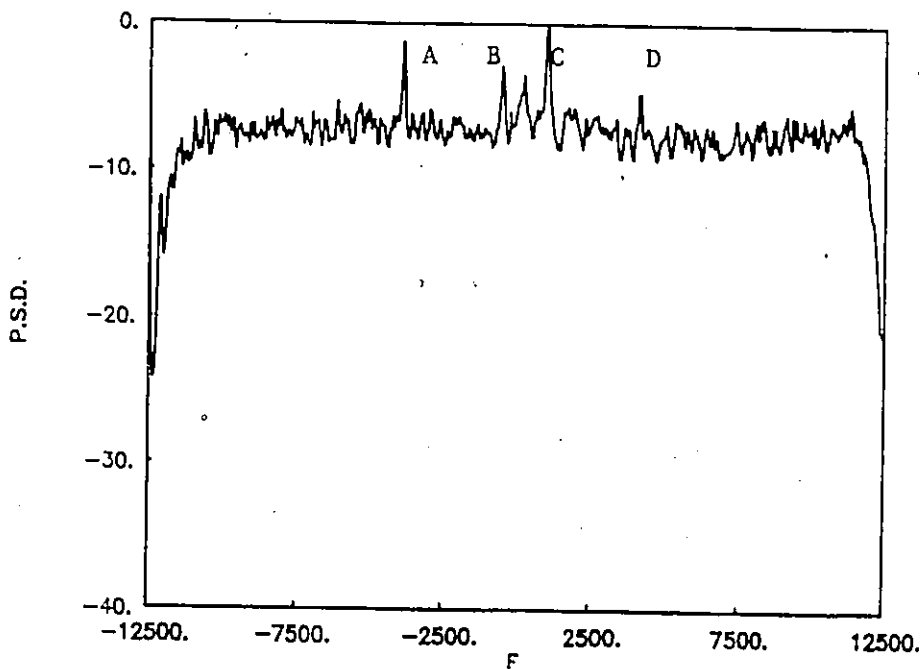
Fig. 7.13　　Averaged MEM = 300 spectrum of 50 blocks 1024 - complex
points each (orbit # 860).

Comparing these results using the averaged MEM with those obtained using the averaged periodogram we note that, the averaged periodogram gives much sharper peaks and has about 3 dB improvement in spectral performance over the averaged MEM. Furthermore, the longer data sequence benefits the averaged periodogram while for averaged MEM, the spectral estimation is improved as the prediction error filter order increases.

7.3   Processing Signals Received from COSPAS Orbit 861

This section discuss the processing of another set of real SARSAT signals received from COSPAS orbit 861. This set of data is selected from tapes starting at the fifth minute of the satellite pass.

7.3.1   Processing Results Using the Periodogram

512 - Complex points

Figure 7.14 illustrates the periodogram spectra for this set of data using 512 - complex points. From these results it is clear that there is a strong indication of carrier components at mixed carrier frequencies of about -2300 Hz and -750 Hz.

1024 - Complex Points

Increasing the number of data points to 1024 complex points gives the periodogram spectra depicted in Fig.7.15. From this spectral estimation result, we note that two peaks occur at mixed carrier frequencies equal about -2300 Hz and -750 Hz. Furthermore, there is an indication that a non-coherent ELT signal can be identified in the mixed carrier frequency range of 2000 Hz and 6000 Hz. Comparing these results with those shown in Fig.7.14, we note that the background noise level is reduced by amounts of 3 dB as the number of data points increases to 1024 - complex points.
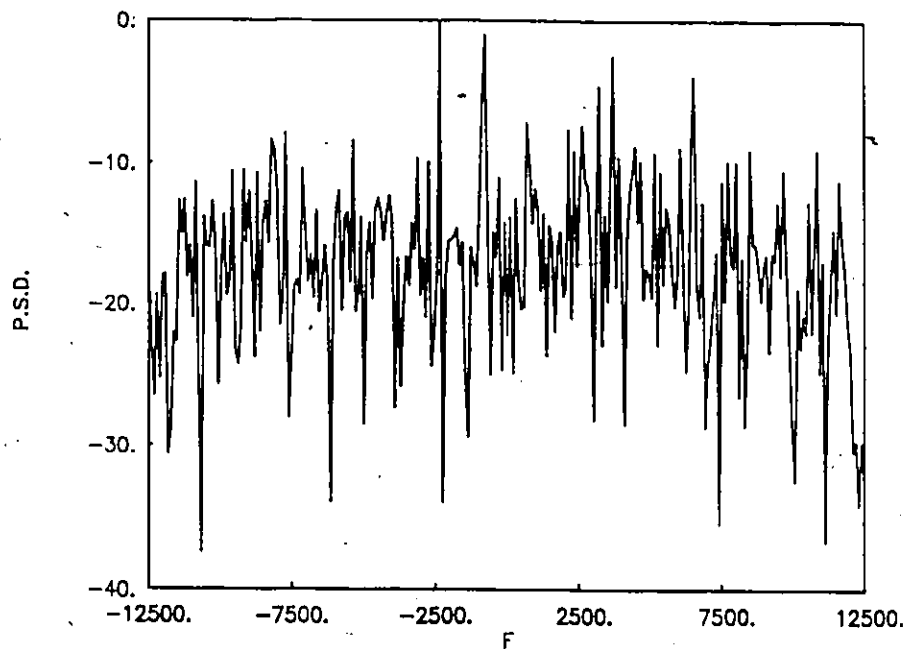
Fig. 7.14   Periodogram spectrum using 512 - complex points (orbit #861).
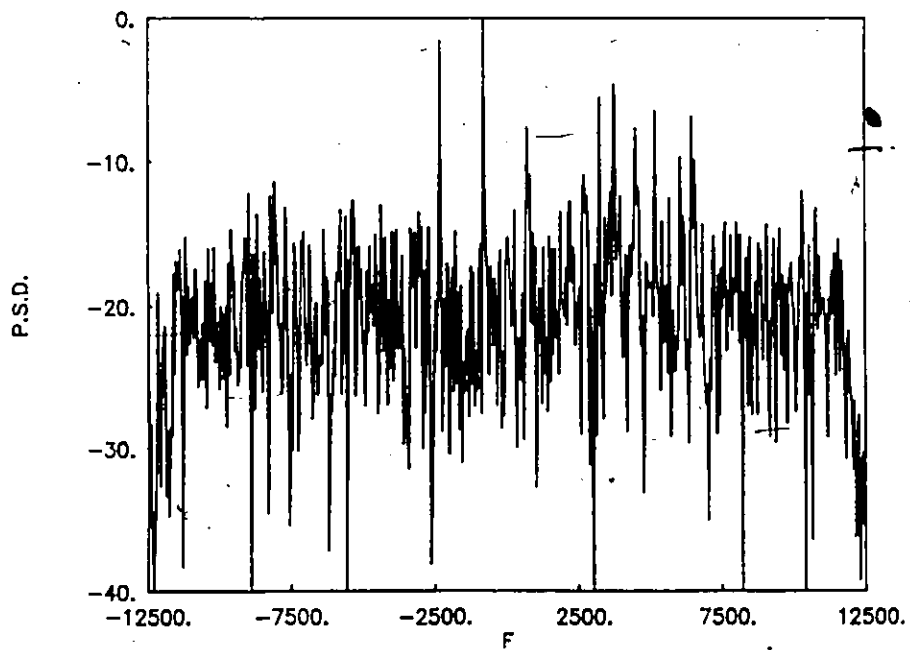
Fig. 7.15   Periodogram spectrum using 1024 - complex points (orbit # 861).

2048 - Complex Points

Figure 7:16 depicts the periodogram spectra using 2048 - complex points. From these results we observe that , the variance does not decrease as the number of data points increase , but the background noise level is reduced by 3 dB as compared with the result shown in Fig.7.15. The presence of a non-coherent ELT signal is probably indicated in the frequency range of 2000 Hz and 6000 Hz.

7.3.2   Processing Results Using the Averaged Periodogram

In this section, we study the spectral estimation characteristics of this set of real SARSAT signals using the averaged periodogram with 512 , 1024 and 2048 complex points for one second of data starting at the 5 minute point of the satellite pass.

512 - complex points

Figure 7.17 illustrates the averaged periodogram spectrum of 100 blocks with each block contains 512 complex points. From this figure, we observe that the averaged periodogram smoothes the spectra. As shown in this figure a broad peak in the mixed carrier frequency range of 2000 Hz and 6000 Hz is detected. This broad peak probably belongs to a non-coherent ELT signal. The background noise level appears at about -17 dB threshold level.

1024 - complex points

Figure 7.18 depicts the averaged periodogram spectra of 50 blocks with each block contains 1024 complex points. From these results we note that the peaks previously detected are further enhanced.. These peaks are sharper as compared to Fig.7.17. Furthermore, we

Fig. 7.16   Periodogram spectrum using 2048 - complex points (orbit # 861).

Fig. 7.17   Averaged periodogram spectra of 100 blocks 512 - complex points FFT (orbit # 861).
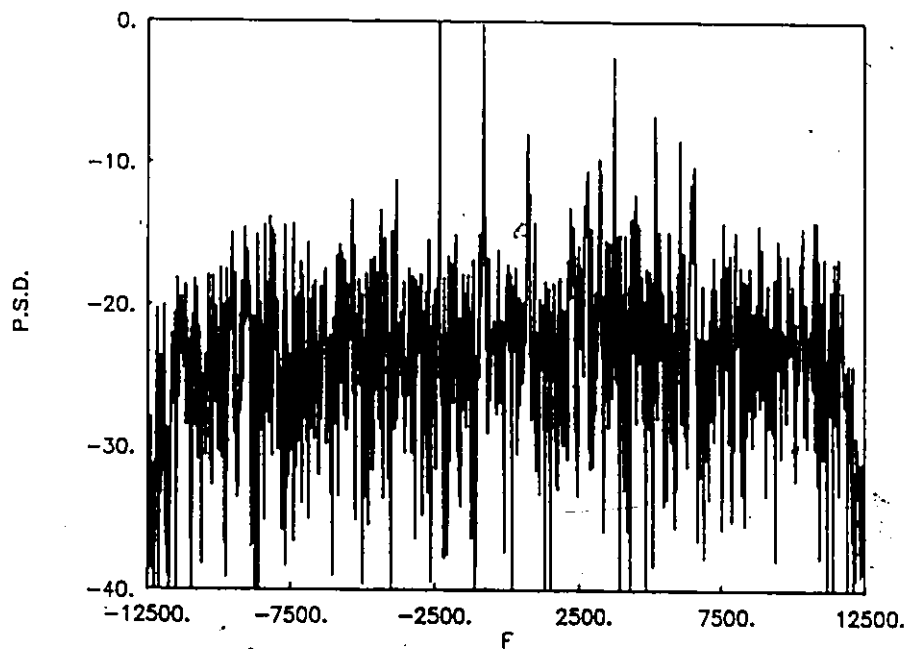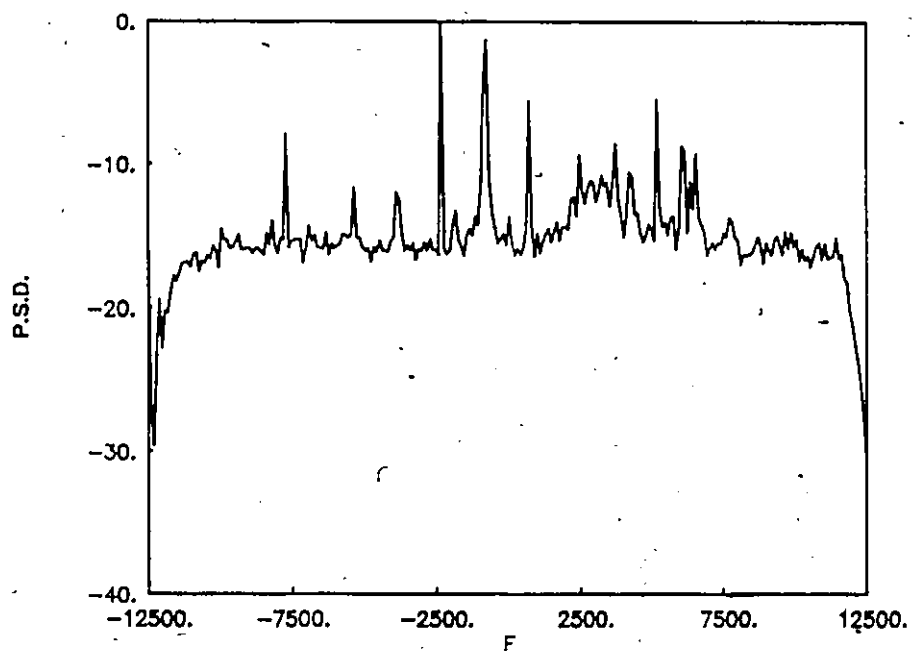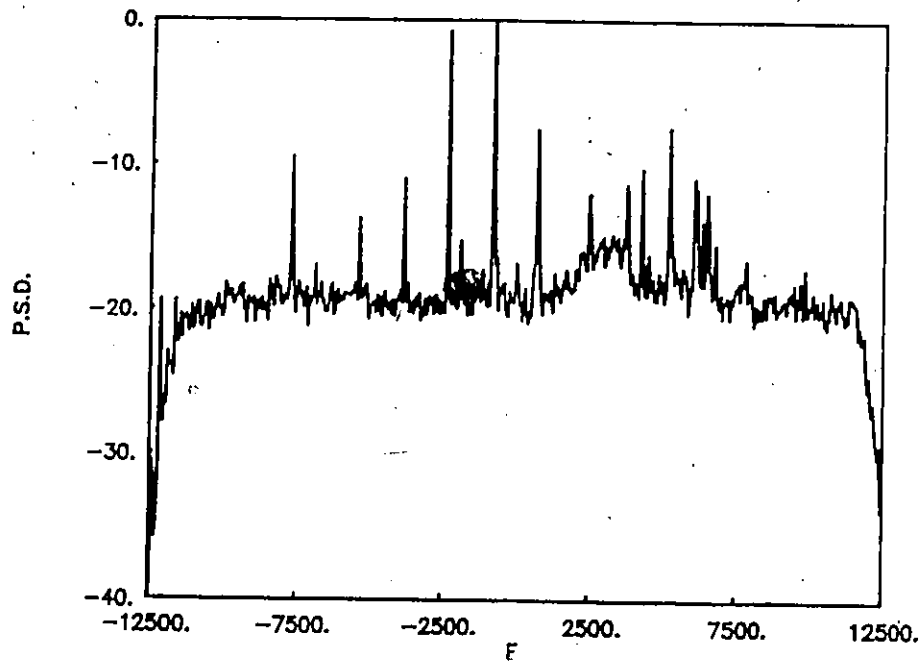
Fig. 7.18　　　Averaged periodogram spectrum of 50 blocks 1024 - complex point FFT (orbit # 861).
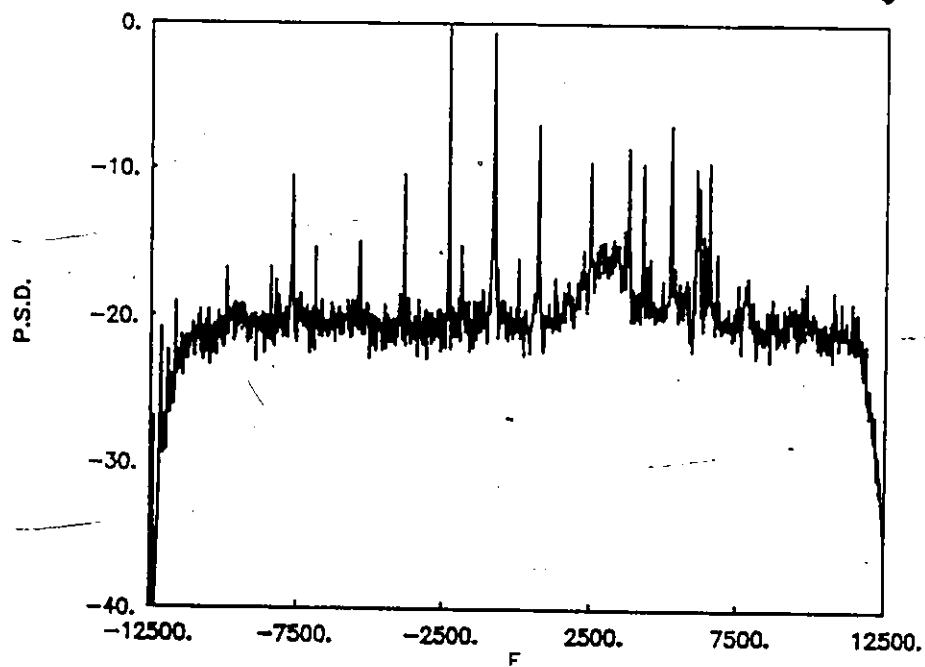
Fig. 7.19　　　Averaged periodogram spectrum of 25 blocks 2048 - complex point FFT (orbit # 861).

note that, the signal-to-noise ratio is improved by 1.5 dB. A broad peak is generated over the same frequency range as detected before indicating the non-coherent ELT signal.

2048 - Complex Points

The averaged spectra using the periodogram of 25 blocks with each block contains 2048 - complex points is given in Fig.7.19. From this figure it is clear that, an improvement of 1.5 dB (in terms of SNR) from 1024 complex points or 3 dB from 512 complex points is achieved using the averaged periodogram. The presence of a non-coherent ELT signal is indicated in the frequency range from 2000 Hz to 6000 Hz.

Thus, from the previous analysis we conclude that, increasing the number of data points improves the signal-to-noise ratio and averaged spectra reduces the variance and smoothes the spectrum. This, consequently, improves the detection of the carrier component peaks of the present ELT signals.

7.3.3   Processing Results using the MEM

In this section we are concerned with the study of spectral estimation performance of this set of data received from orbit 861 satellite C1 using the baseband MEM technique. This set of data examined using 1024 - complex points and MEM filter orders of 100 , 200 and 300 respectively.

Figure 7.20 illustrates the MEM spectra for this set of data using MEM filter order 100. From this figure we observe a strong indication of carrier components at mixed carrier frequencies of approximately -2300 Hz and -750 Hz. Thus, even if the signal is processed using MEM filter order of only 100 the detection of the carrier component peaks of the present signals is still feasible.
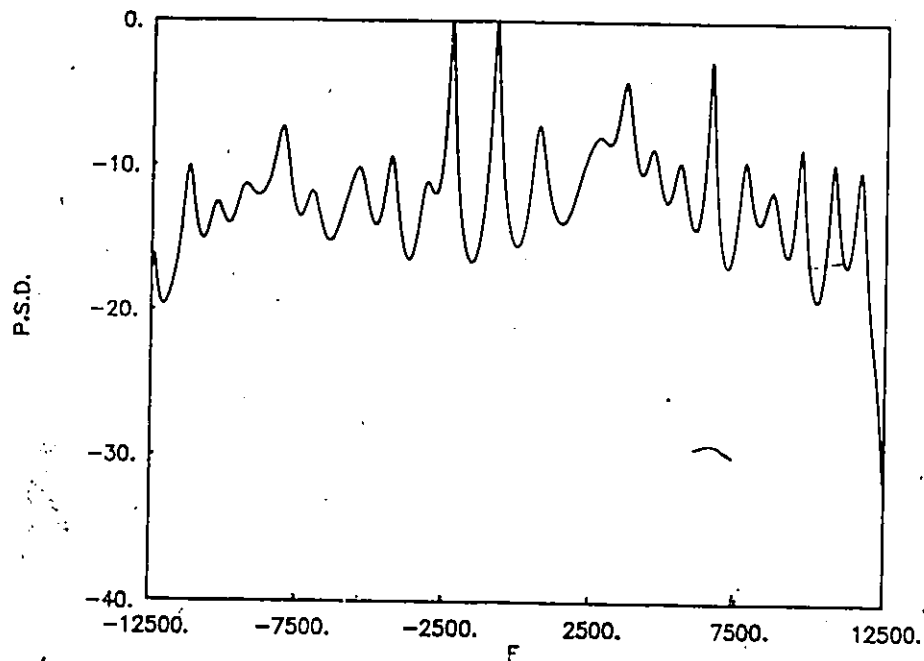
Fig. 7.20   MEM = 100 spectrum using 1024 - complex points (orbit # 861).
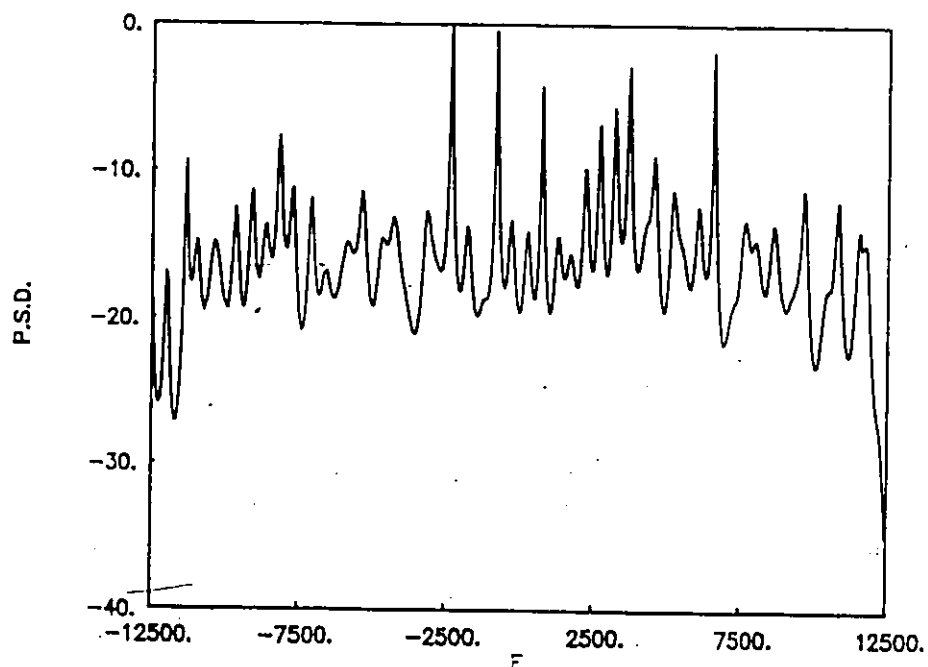
Fig. 7.21   MEM = 200 spectrum using 1024 - complex points (orbit # 861).

Increasing the MEM filter order to 200 gives the spectral estimation result shown in Fig.7.21. From this figure it is seen that a non-coherent ELT signal can be identified between frequencies of 2000 Hz and 6000 Hz. Comparing these results with those given in Fig.7.20 using MEM filter order 100 we note that, increasing the MEM filter order produces sharper peaks and good frequency resolution.

Figure 7.22 shows the MEM spectra computed using MEM filter order 300 for the same set of data. It can be seen from this figure that the presence of a non-coherent ELT signal is indicated in the frequency range from 2000 Hz to 6000 Hz. MEM = 300, produces sharper peaks as compared to the MEM spectra depicted in Fig.7.20 using MEM filter order 100.

7.3.4   Processing Results using using the Averaged MEM

Now, we consider the processing of this set of real data using the averaged MEM with 50 blocks, each block containing 1024 complex points.

Figure 7.23 illustrates the averaged MEM spectra using MEM filter order 100. Comparing these results with those obtained using the averaged periodogram for the same set of data we note that, the numbers of spectral peaks resolved by the averaged periodogram are more than that obtained using the averaged MEM. Nevertheless, the locations of the spectral peaks using the averaged MEM and the averaged periodogram are similar.

Figure 7.24 depicts the averaged MEM spectra using MEM filter order 200. From this figure it is clear that as the MEM filter order increases, the frequency resolution is improved. A broad peak can be identified between the mixed carrier frequency range of 2000 Hz and 6000 Hz. This broad peak belongs to the non- coherent ELT signal.

Increasing the MEM filter order to 300 and processing the same set of data using the averaged MEM method gives the spectral estimation results depicted in Fig. 7.25. It is
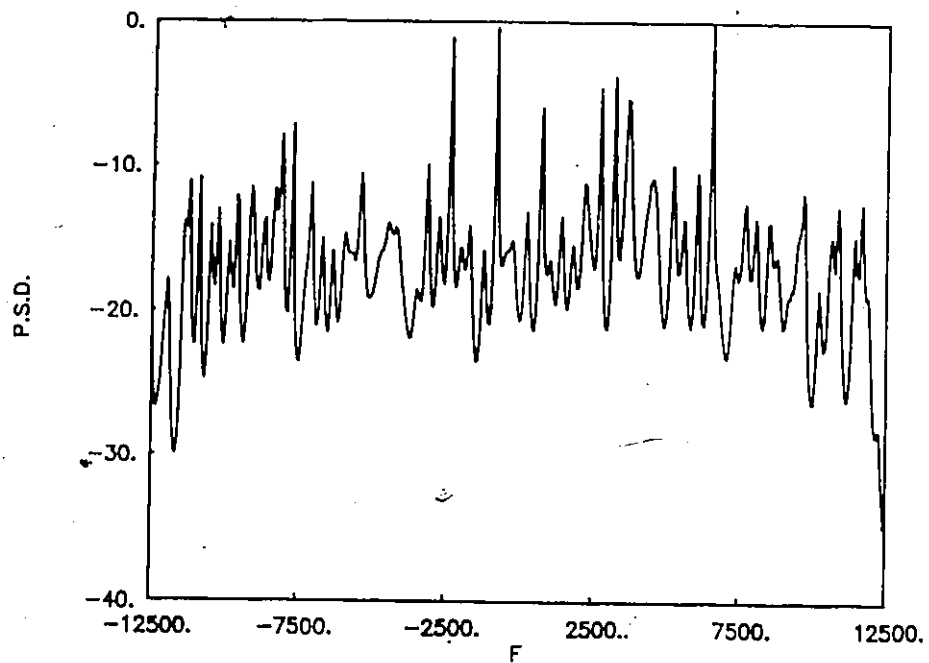
Fig. 7.22   MEM = 300 spectrum using 1024 - complex points (orbit # 861).
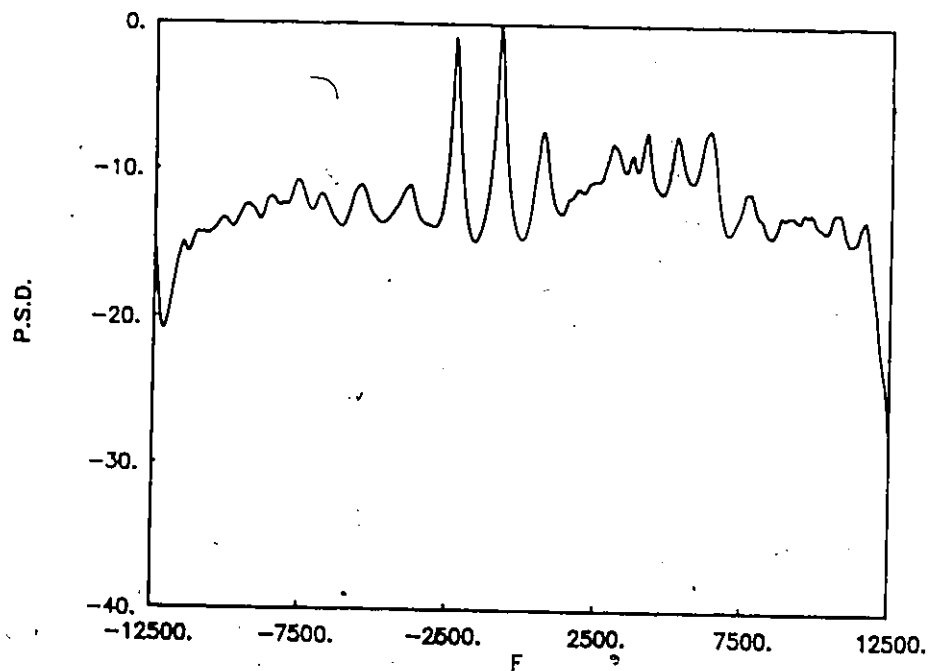
Fig. 7.23   Averaged MEM = 100 spectrum of 50 blocks 1024 - complex points each (orbit # 861).
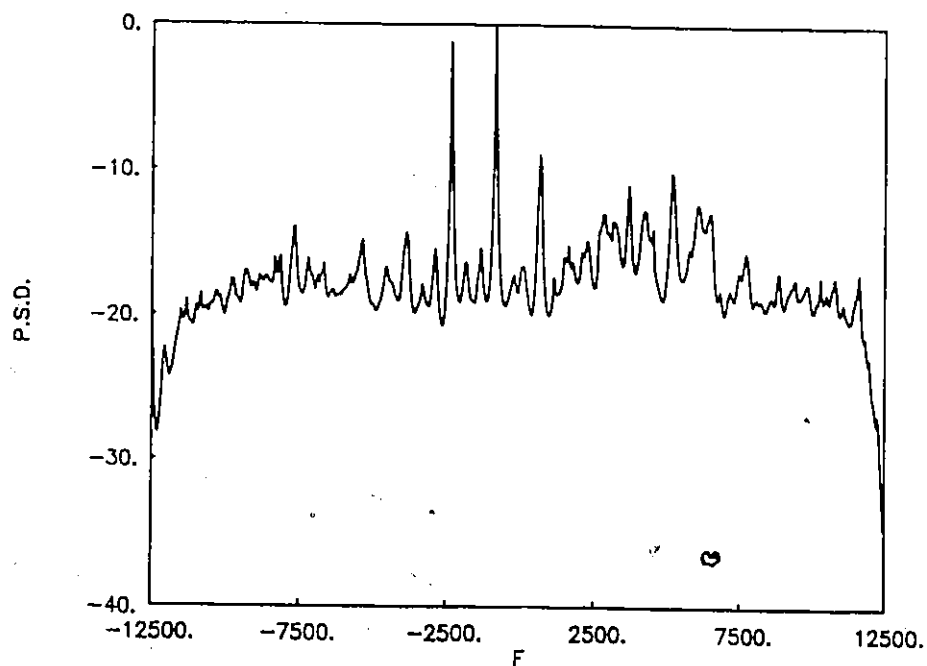
Fig. 7.24   Averaged MEM = 200 spectrum of 50 blocks 1024 - complex points
   each (orbit # 861).
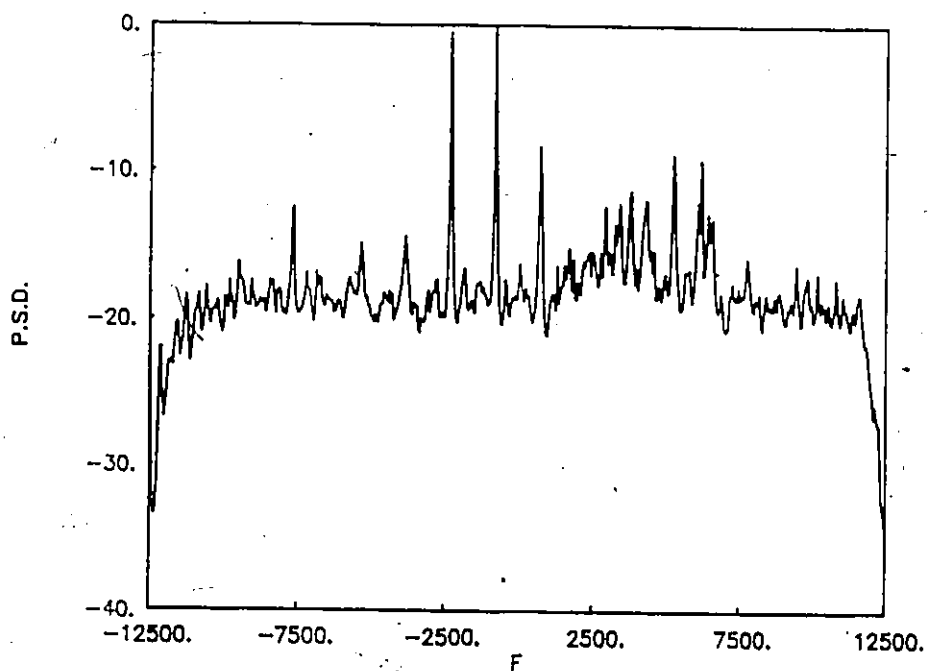
Fig. 7.25   Averaged MEM = 300 spectrum of 50 blocks 1024 - complex points
                 each (orbit # 861).

seen from this result that, the averaged MEM has an improvement of almost 7 dB when a higher MEM filter order is used, i.e. MEM = 300, as compared to the spectrum shown in Fig.7.23 using MEM order 100.

7.4   Summary

This chapter focused on studing the spectral estimation characteristics of real ELT signals received from two different satellite passes. The linear (periodogram) and non-linear (MEM) methods are the two spectral estimators being employed in the analysis. Specifically , we studied the effect of various data lengths of the signals on the linear spectral estimation method. In addition , the effect of using various MEM filters order has been studied.

The above simulation analysis indicates that, the periodogram performance can be improved by processing a longer sequence of data. However, the MEM provides a smoother spectrum. The MEM spectral estimator is more sensitive to the filter order than to the data length. The post-processing technique is also used in order to enhance the spectral performances. Spectral averaging is seen to improve the detectability of ELT signals which have stationary carrier frequency component.

CHAPTER 8

CONCLUSIONS

8.1   Contributions of The Thesis

The major contributions of the thesis may be summarized as follows:

1.   A theoretical expression for calculating the variation of the pulse duration across the sweep period for an ELT signal has been developed. The predictions are shown to have close agreement with measured values for real ELT signals.

2.   The ELT signal spectra for ideal coherent, non-ideal coherent and non-coherent models have been investigated. It has been found that the ideal coherent model gives an idealized spectrum while for random phase model it is difficult to detect the carrier component peak. New models have been proposed with nearly ideal spectral properties. These new modulation schemes for ELT signals provide signal with greatly improved spectral characteristics.

3.   A new complex baseband system for processing ELT signals has been developed. The baseband implementation offers flexibilty not found in the bandpass processor and has certain advantages over bandpass processing. Some of these advantages are:

(A)   Rate Reduction Filtering can easily be implemented which leads to increased signal-to-noise ratio (SNR).

(B)   Tracking of an ELT-signal is possible by adjusting the mixing frequency.

4.   The matched filter performance for optimum detection of ELT signals has been derived theoretically and the performance of the periodogram has been evaluated.

This comparison indicates that the periodogram performance is within 2.6 to 4.8 dB of that provided by a matched filter.

5. A theoretical bound for minimum detectable carrier-to-noise density ratio (CNDR) has been evaluated and verified by computer simulation. It has been also shown theoretically and by computer simulation that the minimum detectable CNDR is approximately 21 dB-Hz when the 512 complex point FFT is applied to 50 blocks comprising one second of data.

6. The performance of the baseband processor can be considerably improved by using a new approach called Rate Reduction Filtering method. It has been shown that the rate reduction filtering technique reduces the frequency error, improves the frequency resolution and increases the SNR. This consequently improves the detection of the carrier component peak of the ELT signal.

With rate reduction filtering technique, it was possible to use a lower MEM filter order which consequently reduces the computation time and gives good signal detection.

7. It has been found that the frequency error for MEM is less if the mixed carrier frequency of the ELT signal lies near the mid-band range. This observation allows us to use a new method called "ELT Tracking Method". This method based on using the MEM with rate reduction filtering technique using lower MEM filter order. By using this method we can easily track the signal and estimate its mixed carrier frequency which consequently simplifies the detection of the carrier component peak of this ELT signal.

8. An expression has been developed for estimating the location of the carrier component peak of the spectrum. This has been verified by simulation using the

ELT Tracking algorithm. The numerical results were found to be in good agreement with the theoretical analysis.

9.   The baseband processor developed in this thesis was extensively tested with the following ELT signals:

(a)   Computer generated ELT signals.

(b)   Real ELT signals.

(c)   Actual satellite pass data received from the COSPAS satellite orbits 860 and 861.

8.2   Suggestion for Further Research

1.   Examine methods of processing using a combined "Autoregressive - Moving Average" (ARMA) model at baseband.

2.   A theoretical analysis for the averaged MEM should be performed to provide an indication as to how to enhance the signal detectability and improve its performance.

3.   From the results obtained (in Chapter 7), we have shown that the signal length has a direct effect on the performances of the linear spectral estimation method. It is, therefore, necessary to investigate the optimum signal data length for the FFT processor.

REFERENCES

1.   T.E. McGunigal, " COSPAS/SARSAT: An International Joint Venture in Satellite-Aided Search and Rescue", Presented at the AGARD Symposium on Operational Modelling of the Aerospace Environment, Ottawa, Canada, 24-28, April 1978.

2.   "SARSAT System Summary", Unpublished Report.

3.   J.D. Lambert and A.E. Winter, "A Search and Rescue Satellite System (SARSAT) Experiment", Presented at Communications 1976 Conference, 8-11 June 1976, Brighton, England, and Published in IEE Publication 139, p. 351-355.

4.   A.E. Winter, J.D. Lambert, J.L. Pearce and H.L. Werstiuk, "Satellite-Aided Search and Rescue", IEEE Conference, Montreal, Canada, 20-22 October, 1976.

5.   H.L. Werstiuk and A.E. Winter, "The Search and Rescue Satellite (SARSAT) System Project", Presented at the AGARD Symposium on Operational Modelling of the Aerospace Environment, Ottawa, Canada, April 1978.

6.   H.L. Werstiuk, "COSPAS-SARSAT A System Overview". Paper No.83071. Proceeding IEEE International Electrical, Electronics Conference and Exposition 1983, pp. 168-171.

7.   M.A. Stott, "Design of the SARSAT Ground Stations", Paper No.83072, Proceedings IEEE International Electrical, Electronic Conference and Exposition 1983, pp. 172-175.

8.   J.V. King, E.J. Hayes and G.J. Jutras, "Results of COSPAS - SARSAT System Performance Testing," Paper No.83074, Proceeding IEEE International Electrical, Electronic Conference and Exposition 1983 (Toronto), pp.180-183.

9.   A. Premji, "Processing of ELT Signals and Rescue Satellite Aided Tracking (SARSAT) Using the MEM and FFT", M.Eng. Thesis, McMaster University, March 1982.

10.   T. Chung, "Digital Bandpass Processors for SARSAT Signals using the MEM and FFT", M.Eng. Thesis, McMaster University, August 1982.

11.   M.I. Dessouky and C.R. Carter, "Spectral Analysis of ELT Signals for SARSAT", Submitted to IEEE Transactions on Aerospace and Electronic Systems.

12.   C.R. Carter, E. Casas and T. Chung, "Emergency Locator Transmitter (ELT) Signal Models for SARSAT Signals", Canadian Electral Engineering Journal, Vol. 11 No.2, April 1986.

13.   S. Haykin, Communication Systems, Wiley and Sons, N.Y., 1982.

14.   V. Mangulis, "Handbook of Series for Scientists and Engineers", p.85, Eq. No. 5, Academic Press New York and London, 1965.

15.   J.M. Wozencraft and I.M. Jacobs "Principles of Communication Engineering", pp.234-237 (John Wiley and Sons, 1965).

16.   L.R. Rabiner and B. Gold, "Theory and Application of Digital Signal Processing" Prentice-Hall Inc., Englewood Cliffs, N.J., 1975.

17.   A.V. Oppenheim and R.W. Schafer, "Digital Signal Processing", Prentice-hall, Englewood Cliffs, N.J., 1975.

18.   E.O. Brigham, "The Fast Fourier Transform", Prentice-Hall Inc., 1974.

19.   J.P. Burg, "Maximum Entropy Spectral Analysis", Presented at 37th International SEG Meeting, Oklahoma City, OK, October 31, 1967.

20.   S. Haykin and S.B. Kesler, "Prediction-error Filtering and Maximum-Entropy Spectral Estimation", in Non-linear Methods of Spectral Analysis, ed., S. Haykin, Springer Verlag, Berlin, 1979, ch. 2.

21.   S.M. Kay and S.L. Marple, "Spectral Analysis- A Modern Perspective", Proc. of the IEEE, Vol. 69, No. 11, November 1981.

22.   N.O. Andersen, "On the Calculation of Filter Coefficients for Maximum Entropy Spectral Analysis", Geophys., Vol.39, pp.69- 72, Feb. 1974.

23.   S. Haykin and S. Kesler, "The Complex Form of the Maximum Entropy Method for Spectral Estimation", Proc. IEEE, Vol.64, pp.822-823, May 1976.

24.   H.C. Chan and S. Haykin, "Application of the Maximum Entropy Method in Radar Signal Processing", CRL-62, Communication Research Laboratory, Faculty of Engineering, McMaster University, Hamilton, Ontario, March 1979.

25.   S. Haykin and H.C. Chan, "Computer Simulation Study of a Radar Doppler Processor Using the Maximum-Entropy Method", IEE. Proc., Vol.127, Pt. F, No.6, December 1980.

26.   M.I. Dessouky and C.R. Carter, " A Baseband Processor for SARSAT Signals", Accepted for publication in Canadian Electrical Engineering Journal.

27.   E. Casas and C.R. Carter, "Two Methods of Spectral Estimation for SARSAT Signals", IEEE Transactions on Aerospace and Electronic Systems, AES-21, July 1985, pp.559-568.

28.   C.R. Carter and T. Chung, "Interference in the 121.5/243 MHz SARSAT Frequency Bands", IEEE Transactions on Aerospace and Electronic Systems, AES-21, Nov. 1985, pp.804-817.

29. M.I. Dessouky and C.R. Carter, "Baseband Spectral Estimator for SARSAT Signals", CRL Report No. 125 Communication Research Laboratory, Faculty of Engineering, McMaster University, April 1984.

30. M.I. Dessouky and C.R. Carter, "A Baseband Processor for SARSAT Signals Using Decimation in Time", CRL Report No. 129, Communication Research Laboratory, Faculty of Engineering, McMaster University, October 1984.

31. M.I. Skolnik, "Introduction to Radar Systems", McGraw-hill, 1962.

32. M.I. Skolnik, "Radar Handbook", McGraw-Hill, 1970, Ch.2.

33. C.E. Cook and M.Bernfeld, "Radar Signals", Academic Press, New York, 1967 p.22.

34. C.R. Carter, "A Theoretical Bound for Processing of SARSAT Signals", CEEJ, Vol.11, n.1, 1986, pp.23-27.

35. R.W. Schafer and L.R. Rabiner, "A Digital Signal Processing Approach to Interpolation", Proc. IEEE, Vol.61, No.6, pp.692-702, June 1973.

36. R.E Grochier and L.R. Rabiner, "Optimum FIR Digital Filter Implementations for Decimation, Interpolation, and Narrow-Band Filtering", IEEE Trans., Acoust., Speech, Signal Processing, Vol. Assp-23, pp.444-456, Oct. 1975.

37. M.I. Dessouky and C.R. Carter, "Baseband Processor for Multiple SARSAT Signals", CRL Report No.140, Communication Research Laboratory, Faculty of Engineering, McMaster University, April 1985.

38. M.I. Dessouky and C.R. Carter, "Baseband Processing for Multiple ELT SARSAT Environment", In Preparation.

39. E. Casas, "Emergency Locator Transmitter (ELT Signal Models and Frequency Estimation for the Search and Rescue Satellite (SARSAT)", M.Eng. Thesis, McMaster University, August 1983.

40. C.R. Carter, "Data Recordings of the ELT Signals for Spectral Analysis", CRL Report No. 110, Communication Research Laboratory, McMaster University, August 1983.

41. M.I. Dessouky and C.R. Carter, "Baseband Processor for Real SARSAT Signals", CRL Report No.144, Communication Research Laboratory, Faculty of Engineering, McMaster University, July 1985.

42. M.I. Dessouky and C.R. Carter, "A Baseband Processor for Real ELT Signals for SARSAT", In Preparation.